Modeling of Multiphase Reactors

A thesis submitted to

University of Pune

for the degree of

DOCTOR OF PHILOSOPHY

In

Chemical Engineering

By

Amit S. Chaudhari

Under guidance of

Dr. Vivek V. Ranade

At

Chemical Engineering and Process Development Division

National Chemical Laboratory (NCL)

Pune-411 008. INDIA

April 2010

राष्ट्रीय रासायनिक प्रयोगशाला
(वैज्ञानिक तथा औद्योगिक अनुसंधान परिषद)
डॉ. होमी भाभा मार्ग पुणे – 411 008. भारत
NATIONAL CHEMICAL LABORATORY
(Council of Scientific & Industrial Research)
Dr. Homi Bhabha Road, Pune - 411 008. India.

CERTIFICATE

This is to certify that the work incorporated in the thesis, **"Modeling of Multiphase Reactors"** submitted by **Mr. Amit S. Chaudhari,** for the Degree of **Doctor of Philosophy,** was carried out by the candidate under my supervision in Chemical Engineering and Process Development Division, National Chemical Laboratory, Pune – 411 008, India. Such material as has been obtained from other sources has been duly acknowledged in the thesis.

Dr. V. V. Ranade
(Research Supervisor)

DECLARATION

I hereby declare that the thesis entitled "**Modeling of Multiphase Reactors**", submitted for the Degree of Doctor of Philosophy to the University of Pune, has been carried out by me at the National Chemical Laboratory (NCL), Pune under the supervision of Dr. V. V. Ranade. The work is original and has not been submitted in part or full by me for any other degree or diploma to this or any other University.

Date: (Amit S. Chaudhari)

Place:

Dedicated to

My Father (Late)

Shri. Suresh D. Chaudhari

Acknowledgement

Acknowledgement - The most difficult job in research documentation

A long time ago, someone told me that the Acknowledgements were the most important part to write in a thesis. May be that person was right... This is a fair opportunity to say "THANKS" to everybody involved in this work process. I am talking about a process that not only implied an academic and educational perspective, but also a personal growing. Mentioning all people who deserve my gratitude without leaving someone out is quite a difficult task, but I will try to do my best.

First, in expressing my intangible gratitude to two iconic research supervisors – Dr. V. V. Ranade (VVR) and Dr. R. V. Chaudhari (RVC) of National Chemical Laboratory (NCL) in tangible words, I realize the full meaning of couplet of Sant Kabir:

सब धरती कारज करूँ, लेखनी सब बनराय ।
सात समुद्र की मसि करूँ गुरुगुन लिखा न जाय ॥

I find it difficult to acknowledge my research supervisors, VVR and RVC so briefly, though I feel deeply indebted to their immense contribution in the making of this thesis. I wish to express my sincere gratitude for their constant encouragement, thoughtful guidance, constructive criticism and friendship to shape up the researcher in me during the course of this work. Their insightful comments, invaluable suggestions and guidance, the research work wouldn't have taken the shape of a dissertation thesis. They bestowed sound technical knowledge and imparted all requisite skills to handle the research facility. I take this opportunity to salute their supporting attitude that has always led me to think and work independently, and follow them in the proper perspectives. My deepest regards and reverence are always due for their wonderful personality.

I would like to express my sincere gratitude to Dr. R. Jaganathan, who is responsible for helping me to complete the thesis. He was always there to meet and talk about the ideas and to ask me good questions to help me think through my problems. I am grateful for his valuable help, suggestions, teaching, guidance and friendship during my research work.

I am grateful to Council of Scientific and Industrial Research (CSIR), India for the research fellowship and also to NCL Research Foundation for providing me the travel grant to present my part of research work at international conference ISCRE-20, Japan. I am thankful to Dr. S. Sivaram, Director, NCL and Dr. B.D. Kulkarni, Dy. Director, NCL for allowing me to carry out research work and extending me all the possible infrastructural facilities during my research stay in NCL.

I sincerely acknowledge all the scientific staff of our division especially, Dr. A. A. Kelkar, Dr. R.M. Deshpande, Dr. C.V. Rode, Dr. V. H. Rane, Dr. S.P.Gupte, Mr. Sunil Joshi, Mr. P.B. Jadkar, Dr. Sayam, Dr. Venkat, Dr. Amol Kulkarni and Dr. Grover, for their valuable help and co-operation in several capacities for my build-up.

I would like to thank to my research colleagues and moreover my friends Narendra Patil, Debdut Roy, Dev Gupta, and Mohan Rampure for helping me all possible ways they can and for cheerful attitude during my stay at NCL. Special thanks to one of my colleague as well as a

friend, Naren, for helping me several times during my work. Interacting with Naren has always helped me in getting some new ideas to tackle the modeling problems.

I would like to thank all my colleagues and labmates and moreover I should say friends (Past and Present) for their helpful hand and cheerful attitude that had made my working very easy and enjoyable. I take this golden opportunity to acknowledge them all. First, I should mention my seniors: –Yogesh Borole, Charu, Rashmi, Abhishek, Nitin, Sunil Tonde, Sunil Shinde, Sangeeta, Makarand, Nandu, Anand, Manisha, Kapil, Mahesh, Gunjal, Ranjit; and friends Pippalad, Lalita, Savita, Chandan, Shailesh, Jayprakash (JP), Vikas, Amit Deshmukh, Ajit, Mahesh Bhure, Indresh etc. I shall specially thank our PP-I labmates for their presence in all aspects of my Ph.D. career –the list goes like: Shashi, Bibhas, Ajay, Latif, Chandrashekhar, Ganesh, Yogesh, Chaitanya, Amit Kanshetty, Madhavi, Vikrant, Atul, Munshi, Naina, Swapna etc. Apart from my own labmates, my stay at NCL is made pleasant by the good association that I enjoyed with many other friends from other research groups:– Malvi, Debabrata, Debasis, Mrityunjoy, Anal, Suman, Umesh, Lakha, Pallavi, Anandita, Sushma, Munmun, Suyana, Ajeet, Javed, Deepika, Nivedita, Ashish, Rameez and the list is incomplete as well. I am also thankful for the friendship of Soumitra, Pradip, Prabhas, Kaushik, Roopa, Sujeet, Sumantra (mama), Aniruddha, Bhalchandra, Sandip K., Yogesh C., Gyanprakash, Prasad, Abasaheb, Prakash, Dipak and many more in NCL, who made my stay colorful and are worth mentioning here.

Outcome of Ph.D. research also needs good rapport from the technical and administrative support system. I am fortunate to have good supportive staff. Specifically, I am thankful to Mr. Dure, Mr. Deepak, Mr. David and Mr. Borkar for their valuable help for troubleshooting of my experimental setup during my experimental part of the work and to Mr. Hasmukh Raheja for providing the necessary support from departmental office and exceptionally healthy working atmosphere. Also I wish to thank to Mr. Wanjale, Narwade, Murkute, Kambale, Patane, Kedari, Dorai, Khandekar, Radha, Subbu and associates for a very cooperative, friendly and cheerful working atmosphere.

It is my immense pleasure to mention that this thesis would not have been complete without the heartfelt wishes, blessings and love of my parents – "Aai and Pappa" and my brother "Jitendra" and sister in law "Neha". Needless to say it was because of the efforts and constant source of strength of my family today I stand where I am. I miss the ever-enthusiastic supportive touch from my Pappa today. No words would be enough in describing the affection and support of my brother "Jitendra"throughout my life in all aspects. I find this excellent opportunity to appreciate and acknowledge the immense support from "Aai & Pappa", brothers and sisters (my in-laws) and their unparallel belief and affection in me that has driven me to excel even under difficult situations.

Finally, nothing appropriate can describe the love and support of "Dipali", my dearest wife, whose constant encouragement and admiration sets new horizons for me to reach, in every facet of my life. I am thankful to her for standing by me at all times, may be good or bad. It's being the most colorful and glorious time of my life ever since our relation bloomed and that strengthens me everyday to achieve any goal with better ease and confidence.

April 2010 *Amit Suresh Chaudhari*
Pune

List of Contents

List of Figures

List of Tables

ABSTRACT OF THESIS

Multiphase reactors are used for large class of catalytic as well as non-catalytic reactions and are commonly encountered in many industrial chemical processes. Some of the important applications are found in oxidation, hydrogenation, carbonylation, hydroformylation, amination and combustion processes. These types of reactions are often highly exothermic and are accompanied by several side reactions.[1,2,3] In these applications, a multiphase chemical reactor is the heart of the process. The efficiency of the reactor operation dictates the design requirements and the load on all separation units and other unit operations that either precede or follow the reactor in the process. Hence, the efficiency of reactor design and operation has great impact on the total capital cost and manufacturing costs for the whole process.

The performance of any multiphase reactor is modeled as the development of quantitative relations which relate the volumetric productivity, conversion and selectivity to input and operating parameters. For this purpose, the equations for species mass balances and energy balance must be developed and solved for the reactor to understand the effects of various operating parameters on the overall reactor performance. The subject of modeling of multiphase reactors has been reviewed extensively in several notable texts and monographs.[4] The concept of multiphase reactor modeling was used in a rather broad sense for different purposes and can be used in both experimental research and engineering. The modeling is the method to translate the existing information and data to useful predictions for new conditions such as the scale up from laboratory reactor to large reactor, the effect of different reaction conditions on product distribution, optimization of steady state operating conditions and the better understanding of the system that may lead to process and design improvements. Therefore, the models can be used in designing equipment or in optimizing an existing production process.[4g]

Considering the wider applicability of modeling of multiphase reactors, investigations of more case studies of practical relevance will further establish the confidence in the use of predictive models for understanding multiphase reactor performances. It is in this context, the modeling of multiphase reactors has been investigated in this thesis by dividing it in two parts with the consideration of industrially important case studies as given below:

1) The phenomenological modeling of three phase (gas-liquid-solid) catalytic reactors by considering a case study of reductive alkylation of phenylenediamines
2) Computational Fluid Dynamic (CFD) modeling of a two phase (gas-solid) reactor by considering a case study of combustion of biomass

In this context, the following specific problems were chosen for the present work.

I) Kinetics and modeling of semi-batch slurry reactor for reductive alkylation of phenylenediamines with methyl ethyl ketone: Influence of substrates isomeric structures
II) Modeling of bubble column slurry reactor (BCSR) for reductive alkylation of *p*-phenylenediamine
III) Comparative modeling of fixed bed and slurry reactors for reductive alkylation of *p*-phenylenediamine
IV) CFD modeling of pulverized biomass combustion in an entrained flow reactor

The thesis is presented in five chapters, a brief summary of which is outlined here.

Chapter 1 presents a literature review on modeling of multiphase reactors relevant to the subject area of investigation. The literature on the development of reaction engineering and CFD models to improve the overall performance of multiphase reactors has also been presented with a special emphasis on three phase catalytic reactors (slurry and fixed bed) and a two phase gas-solid entrained flow reactor respectively. Moreover, a literature review on specific case studies selected has also been reviewed.

Considering the wider applicability of modeling of multiphase reactors, phenomenological modeling of three phase catalytic reactors and CFD modeling of a two phase gas-solid reactor was explored by considering the industrially important case studies. In this context, as a part of three phase catalytic system, the reductive alkylation of aromatic amine and a carbonyl compound in the presence of a supported transition metal catalyst was chosen for the present work. The first step in the synthesis is a non-catalytic homogeneous reaction, followed by hydrogenation in the second step to the desired *N*-alkylated product, which find applications as intermediates in fine chemicals and specialty

products.[5,6] The literature reports reveal that this is a unique class of reaction, which is a combination of non-catalytic and catalytic reactions. Though it has been practiced for decades in the industries and huge number of publications addressed the catalysts and substrates, there are only few reports[5,7,8] on the analysis of the reaction system from chemical engineering point of view. No detailed reports of kinetics of reductive alkylation of di-amines using ketones as alkylating agents for any of the catalysts have been published. The reaction engineering aspects, including analysis of external and intraparticle mass transfer effects, modeling of slurry and fixed bed reactors for reductive alkylation of di-amines have also been discussed. A detailed literature review on reductive alkylation reactions and phenomenological modeling of slurry and fixed bed reactors is presented as a part of this chapter.

Further, as a second part, CFD modeling of entrained flow reactor by considering a case study of combustion of biomass was explored. Biomass being an important renewable energy source is attracting increasing attention in order to improve understanding of their process characteristics during mass to energy conversion. Substantial progress has been made in the development and application of comprehensive multidimensional computational combustion models for fossil fuels. These models are now accessible as features in commercially available CFD computer codes.[9] There are few attempts to validate the devolatilization or char oxidation characteristics of pulverized biomass in an entrained flow reactor (EFR) by using CFD models.[10a-10c] Such studies have been reported for single operating conditions or at lower operating temperatures and concerns with CFD prediction validation focused on near complete devolatilization or char oxidation. Therefore, it is very important to develop a methodology for coupling CFD model and experimental measurements of biomass burnout data for providing valuable global kinetic parameters to large scale applications of biomass fuels (fast pyrolysis, co-combustion and gasification). In this chapter, an introduction on biomass combustion has been presented. The objective and scope of the present work also has been outlined.

Chapter 2 presents two parts in which Part-A describes the experimental study on reductive alkylation of *p*-phenylenediamine with methyl ethyl ketone using 3% Pt/Al_2O_3 catalyst as a model system. This is an industrially important example of reductive alkylation of di-amines, wherein two amine functionalities are available for the alkylation

reaction. The reaction goes through noncatalytic equilibrium condensation reaction to form two imine compounds, which is followed by hydrogenation over the metal surface. The kinetic experiments of the reaction were carried out in a slurry reactor. Due to unique combination of non-catalytic and catalytic reactions, the conventional approach for analysis of initial rates may be misleading for the present system. While, the initial rate data are useful for evaluation of mass transfer effects, the data is not directly useful for kinetic analysis, since the hydrogenation step in the reaction sequence comes after two homogeneous non-catalytic reactions, which could be rate limiting. Hence, the integral concentration-time data were considered for interpretation of the intrinsic kinetics. Therefore, a detailed analysis of initial rate based on quantitative criteria is presented to ensure that the experiments were carried out under kinetically controlled conditions. Several theoretical models considering non-catalytic as well as catalytic reaction steps have been presented to develop semi-batch slurry reactor models and the strategy to choose the appropriate model has been discussed. It was observed that a rate model considering dissociative adsorption of hydrogen followed by the reaction with liquid phase components represent the experimental data satisfactorily at different reaction conditions.

Part-B of Chapter-2 describes the experimental study on the effects of positions of amine groups in phenylenediamine isomers on their relative activities and selectivities in the reductive alkylation reaction using the same catalyst to understand the substrate structure activity correlation. It was observed that phenylenediamine isomers differ remarkably from each other in their activity in reductive alkylation and product distribution. The activity was found to decrease in the following order: *p*-phenylenediamine (PPDA) > *o*-phenylenediamine (OPDA) > *m*-phenylenediamine (MPDA). To understand the substrate structure activity correlation, the homogeneous equilibrium reactions involved in the alkylation step and the overall catalytic reactions were studied separately. Experimental concentration-time data for reductive alkylation of OPDA and MPDA with MEK in a slurry reactor at different sets of initial conditions were obtained to develop suitable semi batch slurry reactor models under isothermal conditions. The kinetic parameters of the individual steps were evaluated following the methodology used for PPDA and compared to understand the differences in the activity and selectivity patterns for OPDA, MPDA and PPDA substrates. It was observed that the rate model which was

suitable for PPDA also represented OPDA and MPDA for the range of operating conditions used.

Chapter 3 presents the modeling of bubble column slurry reactor (BCSR) for reductive alkylation of *p*-phenylenediamine (PPDA). A mixing cell model was developed using the kinetics presented in Chapter 2 (Part-A) to represent the BCSR. The changes in gas and liquid velocities influence the hydrodynamics of BCSRs and therefore alter degree of back mixing in liquid phase. Therefore, liquid phase back-mixing was accounted by including a backflow among mixing cells. The backflow stream was quantified using a CFD model. The model incorporates the contributions of gas-liquid and liquid-solid mass transfer, heat effects, and complex multi-step reaction kinetics. The effect of different operating parameters on the conversion, selectivity, global rate of hydrogenation and temperature rise is discussed. The comparison of the current approach with the traditional mixing cell model is discussed. The combination of mixing cell model coupled with CFD model for estimating degree of backmixing for a range of design and operating parameters was found to be useful for predicting reactor performance over a wide range of parameters. The use of radial baffles for reducing backmixing in bubble columns as proposed by Khare *et. al.*[11] was evaluated using the CFD model and was found to be useful for controlling and manipulating the degree of backmixing in BCSRs. The bubble column slurry reactor model proposed here will be useful to provide guidelines for designing and improving overall performance of bubble column reactors.

Chapter 4 presents comparative modeling of a fixed bed reactor (FBR) with downflow and upflow mode of operation and slurry reactors (CSTR and BCSR) for reductive alkylation of *p*-phenylenediamine (PPDA). The proposed FBR with downflow mode i.e. trickle bed reactor (TBR) model incorporates the contributions of axial mixing, partial wetting and stagnant liquid holdup effects in addition to external and intraparticle mass transfer resistances and heat effects under the consideration of the kinetics presented in Chapter 2 (Part-A). It was suitably modified to describe the behavior of upflow reactor. The effect of different operating parameters on the conversion, selectivity, global rate of hydrogenation and temperature rise is discussed. The comparison of fixed bed reactor with downflow and upflow mode of operation is discussed. It was found that the FBR with downflow mode outperforms the upflow mode under the reaction conditions studied.

Further, the BCSR model presented in Chapter 3 was used to develop continuous stirred tank reactor (CSTR) model with appropriate modifications of hydrodynamic, mass and heat transfer parameters. The fixed bed and slurry reactor models were used to evaluate the reactor performance for the selectivity and productivity towards the desired product and compared the salient features of reactor configuration. It was found that BCSR is the best choice when constant catalyst loading is taken as basis for comparison and the FBR with downflow mode is the best choice when constant volume of the reactor is taken as basis for comparison, under the reaction conditions studied. The reactor models developed will be useful to optimize the overall performance of multiphase reactors (FBR and slurry reactors) considered and will enhance the understanding to recommend a suitable reactor based on true intrinsic kinetics for the reaction system considered.

Chapter 5 presents CFD modeling of pulverized biomass combustion in an entrained flow reactor (EFR). For this purpose, the experimental results recently reported by Jimenez *et. al.* [12] were used. The one dimensional (1D) plug flow model and two dimensional (2D) axisymmetric CFD model were developed based on the experimental results available in Jimenez *et. al.*[12] The Eulerian - Lagrangian approach was used for modeling gas-solid two phase flow. Devolatilization was modeled as a single step Arrhenius type rate expression and char combustion was accounted by kinetic/diffusion controlled mechanism. The gas phase combustion was modeled by Arrhenius type rate expression. The radiative heat transfer was accounted by discrete ordinate (DO) model. The commercial CFD solver, FLUENT 6.3 (of Ansys Inc. USA)[13] was used to simulate the devolatilization and combustion characteristic of the biomass in an EFR at various operating conditions. Results predicted with the CFD model were compared with the published experimental data. The CFD model was then used to understand the influence of operating conditions and kinetic parameters (devolatilization and char combustion) on burning characteristics of biomass. The comparison between the predictions of 1D plug flow model and 2D axisymmetric CFD model is discussed. The sensitivity study on various model parameters was performed and their role in prediction of the devolatilization and char oxidation characteristics of biomass has been discussed. It was observed that the kinetic parameters cannot be obtained with the plug flow assumption; because 2D axisymmetric CFD simulations showed that the nature of gas flow was developing laminar flow rather than ideal plug flow. The flow profile

inside the EFR needs to be computed and the kinetic parameters should be evaluated based on this realistic information. The influence of inlet configuration on the flow profile is significant in EFR and hence any modeling effort should account the non uniformity at the inlet region and its effect on the flow profile. It is then possible to more confidently extrapolate the obtained information to large scale biomass combustors and gasifier. The developed model and presented results will be useful for enhancing our understanding on modeling of combustion characteristics of pulverized biomass.

REFERENCES

1. Duducovic, M. P.; Larachi, F.; Mills, P.L. Multiphase Catalytic Reactors: A perspective on current knowledge and future trends. *Catalysis Reviews*, **2002**, *44 (1)*, 123.
2. Chaidhari, R.V.; Mills, P.L. Multiphase catalysis and reaction engineering for emerging pharmaceutical processes. *Chem. Eng. Sci.*, **2004**, *59*, 5337.
3. Kelkar, V. V.; Ng, K. M. Screening multiphase reactors for non-isothermal multiple reactions. *A.I.Ch.E. Journal*, **2000**, *46(2)*, 389.
4. (a) Shah, Y. T. Gas-Liquid-Solid Reactor Design, McGraw Hill, New York. 1979. (b) Shah, Y. T. Design Parameters for Mechanically Agitated Reactors. *Adv. Chem. Eng.*, **1991**, *17*, 1. (c) Ramachandran, P. A.; Chaudhari, R. V. *Three Phase Catalytic Reactors*. Gordon & Breach: New York, **1983**. (d) Doraiswamy, L. K.; Sharma, M. M. Heterogeneous Reactions, Wiley, New York. **1984**, *vol-2*. (e) Gianetto, A.; Silveston, P.L. eds., Multiphase chemical reactors, Hemisphere, Washington, DC. **1986**. (f) Mills, P. L.; Ramachandran, P. A.; Chaudhari, R. V. Multiphase chemical reactors for fine chemicals and pharmaceuticals. *Rev.Chem. Eng.*, **1992**, *8*, 1. (g) Donati, G.; Paludetto, R. Scale up of multiphase reactors. *Catalysis Today*, **1997**, *34*, 483. (h) Thoenes, D. Current problems in modeling of chemical reactors. *Chem. Eng. Sci.*, **1980**, *35*, 1840.
5. Lehtonen, J.; Salmi, T.; Vaori, A.; Tirronen, E. On the principles of modeling of homogeneous-heterogeneous reactions it the production of fine chemicals. A case study: Reductive alkylation of aromatic amines. *Org. Pros. Res. Dev.*, **1998**, *2(2)*, 78.
6. Hayes, K. S. Industrial processes for manufacturing amines. *App. Cat. -A General*, **2001**, *221*, 187.
7. Salmi, T.; Lehtonen, J.; Kaplin, J.; Vuori, A.; Tirronen, E.; Haarrio, H. A homogeneoys-heterogeneously catalysed reaction system in a loop reactor. *Cat. Today*, **1999**, *48*, 139.
8. Roy, D.; Jaganathan, R.; Chaudhari, R. V. Kinetic modeling of aniline with acetone using 3% Pd/Al2O3 catalyst in a batch slurry reactor. *Ind. Eng. Chem. Res.*, **2005**, *44*, 5388.
9. Rostami, A.A.; Hajaligol, M.R.; Wrenn, S. E. A Biomass Pyrolysis Submodel for CFD Applications. *Fuel*, **2004**, *83*, 1519.
10. (a) Meesri, C.; Moghtaderi, B. Experimental and Numerical Analysis of Sawdust Char Combustion Reactivity in a Drop Tube Reactor. *Combust. Sci. and Tech.*, **2003**, *175*, 793. (b) Xiu, S.; Wang, N.; Yi, W.; Li, B.; Shahbazi, G. Validation of Kinetic Parameter Values for Prediction of Pyrolysis Behavior of Corn Stalks in a Horizontal Entrained Flow Reactor. *Biosystems Engineering*, **2008**, *100*, 79. (c) Jones, J.M.; Pourkashanian, M.; Williams, A.; Hainsworth, D. A Comprehensive biomass Combustion Model. Renewable Energy, **2000**, *19*, 229.
11. Khare, A. S.; Dharwadkar, S.V.; Joshi, J.B.; Sharma, M. M. Liquid- and solid-Phase mixing in sectionalized bubble column slurry reactor. *Ind. Eng. Chem. Res.*, **1990**, *29*, 1503.
12. Jimenez, S.; Remacha, P.; Ballesteros, J. C.; Gimenez, A.; Ballester, J. Kinetics of Devolatilization and Oxidation of a Pulverized Biomass in and Entrained flow Reactor under Realistic Combustion Conditions. *Combust. Flame*, **2008**, *152*, 588.
13. Ansys Fluent 6.3, Fluent Inc., 10 Cavendish Court, Lebanon, NH03766, U.S.A.

CHAPTER 1

Introduction & Literature Survey

1.1 GENERAL INTRODUCTION

Multiphase reactors are very common in chemical, petroleum, petrochemical and pharmaceutical industries. There are several definitions of multiphase reactors. In principle all reactors in which more than one phase is present is defined as a multiphase reactor. However, this specification is generally devoted to two fluid phases (gas-solid, gas-liquid, liquid-liquid) or three phase systems (gas-liquid-solid). Some commonly used types of reactors are shown in Figure 1.1. Although, the reactors included in Figure 1.1 show contacting modes in two phase systems (gas-liquid or gas-solid), similar reactors can also be used to carry out reactions involving more than two phases.[1]

The applications of multiphase reactors are found in diverse areas, some examples of which are manufacture of petroleum based products and fuels, the production of commodity and specialty chemicals, pharmaceuticals, production of polymers, pollution abatement, combustion processes etc. All such industrial chemical processes are designed to transform cheap raw materials to high value added products (via chemical reactions). A 'reactor' in which such chemical transformations takes place, has to carry out several functions such as bringing reactants into intimate contact (to allow chemical reactions to occur), providing an appropriate environment (temperature, concentration field, catalysts) for an adequate time and allowing for the removal of products and hence is the heart of any chemical process. Therefore, the study and development of multiphase reactors, for conversion of raw materials into products with high conversion and selectivity, play an important role in the innovation of chemical processes. The processes based on the multiphase reactions have a broad range of applications and form the basis for the manufacture of a large variety of intermediate and consumer end products. Some examples of multiphase reactors in industry are (1) the upgrading and conversion of petroleum feed stocks and intermediates; (2) the conversion of coal-derived chemicals or synthesis gas into fuels, hydrocarbons, and oxygenates; (3) the manufacture of bulk commodity chemicals that serve as monomers and other basic building blocks for higher chemicals and polymers; (4) the manufacture of chemicals for fine and specialty chemical markets as drugs or pharmaceuticals; (5) the conversion of undesired chemical or petroleum processing by-products into environmentally acceptable or recyclable products. An overview of the chemistry and process technology of these various application areas is provided in the

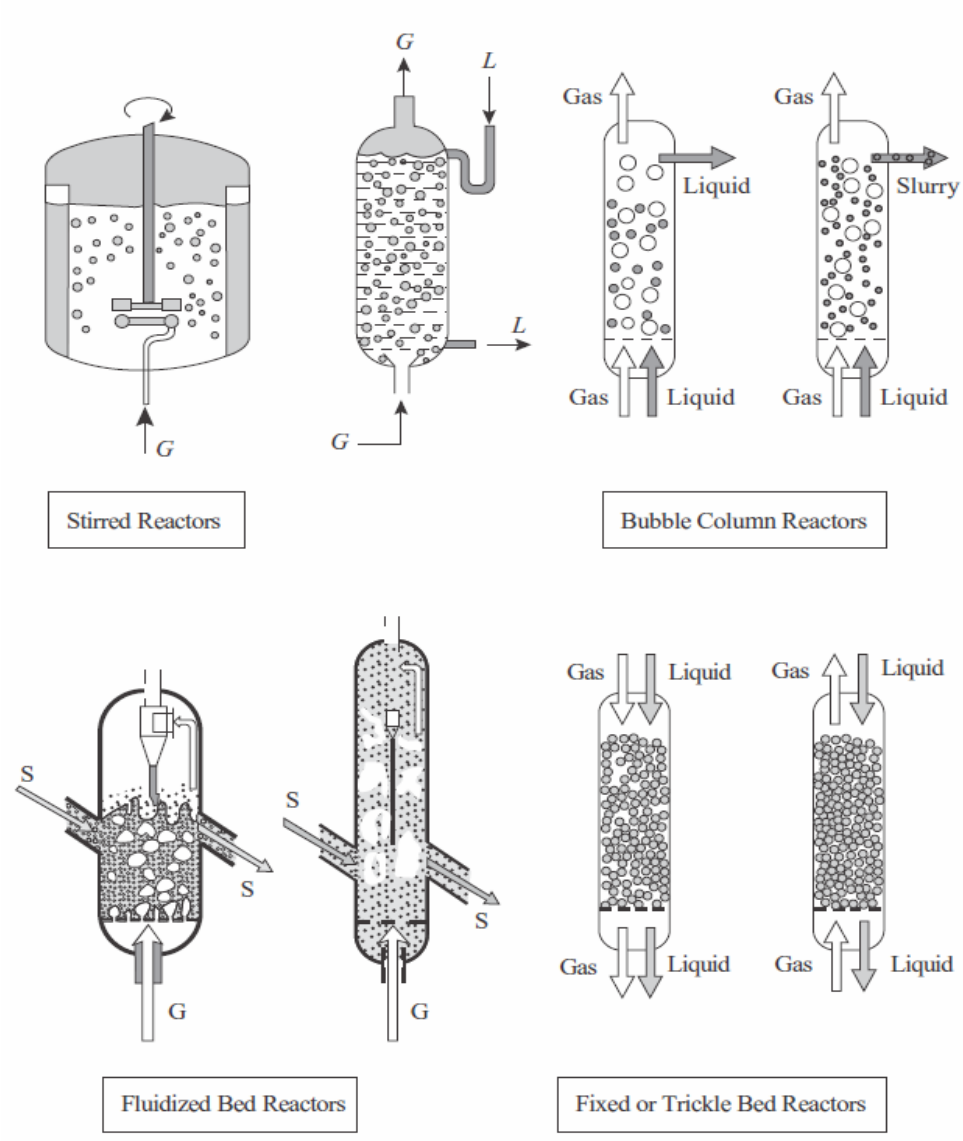

Figure 1.1. Commonly used reactor types[1]

monograph of Weissermel and Arpe.[2]

The overall performance of such processes depends on the type of catalyst used as well as interface/intraparticle mass transfer effects, reaction kinetics and mixing of fluid phases involved. It is of practical interest to understand the relative importance of these factors in any process. In this context, the modeling of multiphase chemical reactors is very important from the point of view of the process development and scale up of chemical processes. If one is to attempt the scale-up of any chemical process from laboratory scale to industrial scale, as the current economic climate increasingly demands, then one must have a

profound and detailed understanding of the performance of multiphase reactor that is being considered for scale-up. Hence, an improved understanding of the reaction engineering aspects, fluid dynamics and transport processes in frequently used multiphase reactors is more important for accomplishing large scale-up factors with confidence. Lack of thorough understanding of the phenomena occurring in multiphase reactors can lead to disasters in scale-up or design.[3] Therefore, the need to quantify the performance of any multiphase reactor leads to a need for modeling.

The subject of modeling of multiphase reactors has been reviewed extensively by several notable texts and monographs.[3,4] The reactor types used for multiphase reactions generally depend on the reaction class and type of phases involved. Therefore, considering the wider applicability of modeling of multiphase reactors, the thesis has been divided into two parts: Part-1, the phenomenological modeling of the three phase catalytic reactors and Part-2, computational fluid dynamic (CFD) modeling of a two phase gas-solid reactor. These two approaches of the modeling of multiphase reactors were used to study the industrially important examples to illustrate the usefulness of detailed models in understanding the reactor performance. Some of the important reaction types that are encountered in multiphase processes in chemical process industry with emphasis on gas-liquid-solid catalytic reactions and gas-solid reactions are summarized in Table 1.1 and Table 1.2 respectively.[3,5] This clearly shows the diverse products that can be produced using three phase catalytic as well as two phase gas-solid reactors.

Among the various types of gas-liquid-solid catalytic reactions shown in Table 1.1, catalytic hydrogenation of various organic functionalities is most commonly encountered with wide ranging applications in fine chemicals and pharmaceuticals. Some typical examples are shown in Table 1.3. Depending on the nature of the reactants and products and their volatility, the reactions are either carried out in vapor phase or liquid phase mode. Due to the advantage of easy catalyst-product separation, heterogeneous catalysts consisting of supported metal or composites of metal oxides are often used as catalyst precursors. Except the processes for low boiling commodity chemicals, most of the hydrogenation reactions are carried out in a liquid phase using either suspended solid catalysts or a fixed bed of catalyst. A detailed description of such multiphase reactions and their engineering analysis has been well developed as described in well known textbooks

Table 1.1. Types of Multiphase Gas-Liquid-Solid Catalytic Reactions

Reaction Type	General Stoichiometry
Acylation	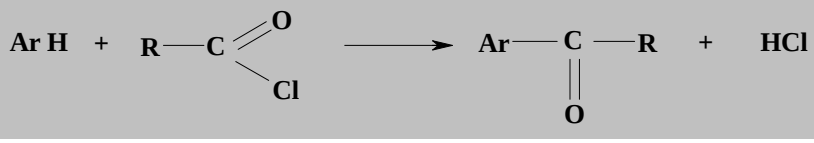
Carbonylation	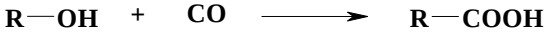
Oxidative carbonylation	
Dehydration	
Halogenation	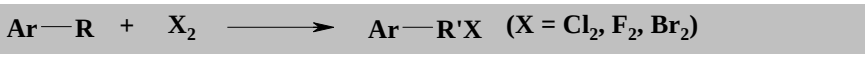
Hydroformylation	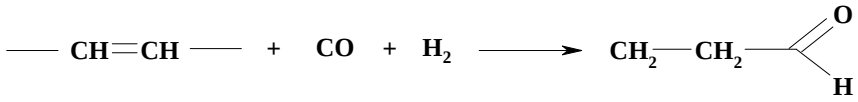
Hydrogenation	
Hydroxylation	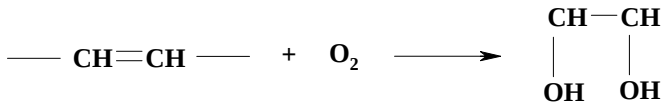
Nitration	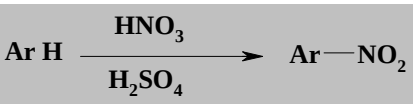
Oxidation	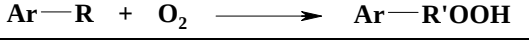

Table 1.2. Some Industrially Important Gas-Solid Reactions

Type	Physical state of reactants	Physical state of products	Examples
I	Solid + Gas	Solid + Gas	Roasting of sphalerite: $ZnS + 3/2O_2 \rightarrow ZnO + SO_2$ Sponge iron production: $Fe_2O_3 + 3H_2 \rightarrow 2Fe + 3H_2O$
II	Solid + Gas	Solid	SO_2 pollution abatement: $CaO + SO_2 + ½O_2 \rightarrow CaSO_4$ Manufacture of calcium cynamide: $CaC_2+N_2 \rightarrow CaCN_2+C$
III	Solid + Gas	Gas	Oxidation of UF4 by Fluorine: $UF_4 + F_2 \rightarrow UF_6$ Combustion of biomass: $CH_xO_y + O_2 \rightarrow CO_2 + H_2O$
IV	Solid	Solid + Gas	Calcination of limestone: $CaCO_3 \rightarrow CaO + CO_2$ Decomposition of $Al(OH)_3$: $2Al(OH)_3 \rightarrow Al_2O_3 + 3H_2O$
V	Gas	Solid + Gas	Thermal cracking of silane: $SiH_4 \rightarrow Si + 2H_2$ Production of metal oxide aerosol: $Ti(OC_3H_7)_4 \rightarrow TiO_2 + 4C_3H_6 + 2H_2O$
VI	Gas + Gas	Solid + Gas	Rutile preparation: $TiCl_4 + O_2 \rightarrow TiO_2 + 2Cl_2$ Silicon preparation: $SiHCl_3 + H_2 \rightarrow Si + 3HCl$

Table 1.3. Commercial Applications of Hydrogenation Reactions Using Heterogeneous Catalysts

No.	Process	Catalyst	Product	Application	Ref.
1	Selective hydrogenation of sorbic acid, hexyn-1-ol or hexadienols	Supported Pd colloids	Hexane-1-ols	Fruit, vegetable fragrances and flavors	6
2	Hydrogenation of methyl sorbate	Pd/C	Methyl-2-hexenoate	Flavors	7
3	Partial hydrogenation of cis-propenyl pyrethroids	Lindlar catalyst	Pyrethrins	Insecticides	8
4	Selective hydrogenation of dehydrolinalool	Pd-Bi catalyst	Citral, linalool	Perfumes and cosmetics	9
5	Production of 1,4-butanediol and THF	Fe promoted Raney-Ni, co-promoted with Cr, Mo, W, Co, Mn and Ti	1,4-butanediol and THF	Intermediate for polymers and solvent	10
6	Enantioselective carbonyl group hydrogenation of α-ketoester	Chinchona-modified Pt/Al_2O_3	Chiral α-hydroxyester	Intermediate for Benazepril®, a medicine for high blood pressure	11
7	Reductive amination of methanol	SiO_2-Al_2O_3 in the 1st step and mordenite in the 2nd step	Dimethyl-amine	Intermediate for pharmaceuticals, herbicides, rocket fuels. Dehairing agent in leather processing.	12
8	Hydrogenation of aromatic nitro compounds	Vandium doped precious metal powder	Aromatic amines	Intermediates for agrochemicals, dyes and fluorescent whitening agent	13
9	Hydrogenation of halonitro aromatics	Ir-Fe/C	Halo amino aromatics	Cosmetics	14
10	Partial hydrogenation of benzene	Supported Ru catalyst	Cyclohexene	Intermediates for polyamides and lysines	15
11	Dearomatization of aniline	5% Pd containing Deloxan® catalyst	Cyclohexyl-amine	Intermediates for rubber, food and pharmaceuticals	16
12	*N*-debenzylation to form Nebivolol®	Pd/C	Nebivolol®	Anti-depression drug	17

and reviews.[18,4c,4d] Though extensive work on theoretical as well as experimental multiphase reactors is reported previously, in most of these single step reactions with isothermal conditions have been considered. Only in a few cases, experimental studies on multistep multiphase hydrogenation reactions have been addressed.[19a-19d] In order to develop economically competitive processes, several new types of catalytic systems have been found to be advantageous. For example, reactions involving combinations of non-catalytic and catalytic reactions, complexities of equilibrium reactions with complex network where selective synthesis of an intermediate compound is desirable. Such reactions involve not only design of a selective catalyst but also the understanding of reaction engineering issues including the catalytic and noncatalytic steps in the overall reaction sequence. Further, Table 1.2 shows typical examples of gas-solid reactions in each category, covering systems of energy generation, pollution abatement, chemical synthesis, catalyst preparation, catalyst deactivation and regeneration, biomass combustion and pyrometallurgical operations such as reduction of ores and roasting of sulphided minerals. Thus, gas-solid reactions also play a vital role in producing materials for the electronic and space industries.

Considering the wider applicability of multiphase reactors, investigations of more case studies of practical relevance will further establish the confidence in the use of predictive models for understanding their performances. It is in this context, the following specific problems were chosen in the present work with the principal objective of understanding the reaction engineering aspects.

√ **Reductive Alkylation of Amines**

The manufacture of higher alkylated (secondary or tertiary) amine derivatives are important for dyes, fuels and rubber industries, which are synthesized by the reductive alkylation of aromatic amine and a carbonyl compound in the presence of supported transition metal catalysts. The reductive alkylation reaction goes through a condensation reaction between an amine compound and a carbonyl compound or an alcohol to form an imine intermediate, which undergoes hydrogenation in the presence of a metallic catalyst to *N*-alkylated products. An important example of this class of reaction is the reductive alkylation of phenylenediamines with methyl ethyl ketone (MEK) to *N*, *N*'-di-secondary-

alkyl-Phenylenediamines. This particular reaction system is commercially relevant and involves a combination of parallel and consecutive reactions comprising equilibrium non-catalytic (homogeneous) and catalytic (heterogeneous) steps. Therefore, proper analysis of the reaction engineering issues like mass and heat transfer parameters coupled with reaction kinetics is required to understand and select suitable reaction conditions to obtain improved selectivity of the product, *N*, *N'*-di-secondary-alkyl-Phenylenediamines. In this work, this particular reaction system was investigated from reaction engineering point of view.

√ **Combustion of Biomass**

The importance of biomass in combustion processes for the combined production of electric power and district heating systems is still rising. Biomass conversion technologies range from traditional direct fired biomass combustion systems designed to raise steam, to advanced integrated biomass gasification combined cycled systems with high projected efficiencies. The basic mechanism in combustion as well as gasification reactors is a fast pyrolysis with release of volatile species. The laminar entrained flow reactor is generally used for the fast pyrolysis of biomass fuels because it represents the conditions similar to those in practical combustion equipment. A reliable description of the global kinetics of biomass pyrolysis is the building block for accurately describing the high temperature chemistry that occurs in developing biomass thermochemical conversion systems and potentially can be used to optimize system design and performance. Moreover, experimental measurements in the reactor and predictions with computational fluid dynamic (CFD) computer codes can be used to accurately characterize the reactor as it is operated under laminar flow conditions. The computational models and experimental measurements facilitate the understanding of the system and allow detailed understanding and interpretation of experimental results. The ultimate goal of the modeling in bench scale experiments is to make accurate determination of fluid dynamic behavior, so that the results from simple bench scale combustion and pyrolysis experiments can be confidently extrapolated to large scale biomass combustors and gasifiers. While combustion models for coal are finding increasing applications in CFD studies, there is a need to develop specifically CFD models for the combustion processes of biomass. In this context, it was thought desirable to develop a procedure coupling the experimental measurements and

computational fluid dynamic modeling to provide better understanding of the combustion process and parameters useful for scale up.

In this chapter, a literature review on modeling of multiphase reactors relevant to the subject area of investigation is presented. The literature on the development of reaction engineering and CFD models to improve the overall performance of multiphase reactors has also been presented with a special emphasis on three phase catalytic reactors (slurry and fixed bed) and a two phase gas-solid entrained flow reactor respectively. Moreover, a literature review on specific case studies discussed earlier has also been reviewed.

1.2 MODELING OF MULTIPHASE REACTORS: GENERAL COMMENTS

The performance models for any type of multiphase reactor can be developed to evolve relations for volumetric productivity, conversion and selectivity in terms of operating parameters and system properties.[3] The generic conservation equations applied to any conserved property (e.g., species mass) for a particular phase i in a multiphase reactor is straightforward and described as:

$$\begin{aligned}&\left(Rate\ of\ \ output\ by\ \ phase\ i\right)-\left(Rate\ of\ \ input\ by\ \ phase\ i\right)\\&-\left(Net\ rate\ of\ \ interphase\ transport\ into\ \ phase\ i\right)\\&=\left(Net\ rate\ of\ \ generation\ in\ \ phase\ i\right)-\left(Rate\ of\ \ accumulation\ in\ \ phase\ i\right)\end{aligned} \qquad 1.1$$

The details of a reactor model depend on the level (i.e., to what size control volume) at which equation 1.1 is applied. The simplest models assume either perfect mixing of a phase or plug flow with no significant mass or heat transfer limitations (pseudo-homogeneous models). Deviations from such ideal models with respect to flow patterns are frequently accounted for using axial dispersion coefficients. The most sophisticated models are ones that resolve the fluid dynamics clearly by direct numerical solution (DNS) of the Navier–Stokes (N–S) equations and superimpose the kinetics and interphase mass transfer on it. In order to account for all the realistic physicochemical phenomena in a given reactor type, it is often required to consider an ensemble of N–S equations resulting in Euler–Euler interpenetrating multifluid models. Closure forms are required for interphase interaction

terms, turbulence parameters and kinetic rates. In between these, the approaches based on phenomenological models (also based on equation 1.1) and experimentally observed flow and mixing patterns are also used. The main objective here is to simply address the different levels of modeling as indicated in Table 1.4. As the degree of model sophistication increases, it becomes more time-consuming to develop both the rigorous models and to produce numerical solutions. The level of sophistication used in modeling the reactor flow pattern and mixing should be commensurate with the level of modeling used to understand the kinetics, i.e., the species generation rate. Whenever that is not the case, the modeling effort yields less than maximum benefits since kinetics ultimately dictates the overall reactor performance.[3]

The left hand side (LHS) of the equation 1.1 contains the information about fluid dynamics, flow pattern and phase contacting pattern (e.g., the input term describes convection and eddy transport into and out of the control volume, etc.). On the other hand, the first term on the right hand side (RHS), i.e., the generation term incorporates knowledge of chemical kinetics. The reactor production rate is obtained by appropriate volume averaging of the generation rate. Equation 1.1 is utilized primarily in the following three types of endeavors. First, in research and development, from the measured overall inputs and outputs at different compositions and temperatures, the form of the apparent kinetic rate of reaction, i.e., the generation term on the RHS of the equation 1.1 is evaluated. In order to properly establish such a kinetic form, a precise knowledge of the fluid dynamics and transport parameters in the experimental reactor is required, along with a quantitative relation between the overall input–output terms and local ones, i.e., a reactor model. Second, in reactor design efforts, the needed reactor size to meet the desired production rate and selectivity must be determined. Again, the knowledge of fluid dynamics and transport, i.e., the LHS of equation 1.1, as a function of reactor size and operating conditions is needed for proper design or scale-up. Third, in a manufacturing environment, the impact of changes in operating conditions that will yield the desired changes in the output is required. The knowledge of how the changes in operating parameters affect the fluid dynamics and transport parameters in the reactor is essential. Hence, the level of sophistication in the description of the generation term on the RHS of equation 1.1 increases, through the use of mechanistic models based on L-H type kinetics.

Table 1.4. Levels of Modeling of Multiphase Reactors[3]

Modern reaction engineering models requires handling of different phenomena over a multitude of scales • Molecular scale (micro-kinetics) • Eddy or particle scale (macro-local transport phenomena) • Reactor scale (meso-flow patterns, contacting and flow regime)			
Possible level of description			
Molecular scale (rate forms)			
Strictly empirical	Mechanism based	Fundamental elementary	
Eddy or particle scale transport			
Empirical	Micromixing models	DNS CFD	
Reactor scale			
Ideal reactors	Empirical models	Phenomenological models	CFD models

The rapid advances in available software for computational fluid dynamics (e.g., CFDLIB, FLUENT, PHOENICS, FLOW3D, and FIDAP) make it possible to simulate the gross flow patterns in large reactors. Kuipers and Swaaij[20] have presented a review of the role of CFD in chemical reaction engineering. It is clear from this review that those global system models, which typically provide the overall features of flow in large reactors, are sometimes tied with various degrees of empiricism in transport and kinetics to describe reactor performance. In absence of detailed models for most multiphase reactor types and chemistries, lower level models provide valuable tools in process development.

The above discussion leads to the perennial problem in multiphase reactors, namely, scale-up, and how to achieve the desired results in a large scale reactor based on observations made on the laboratory-scale unit. In this thesis, phenomenological and CFD modeling was explored by considering the industrially important case studies as discussed earlier (Section 1.1). For this purpose, the contribution to the modeling of multiphase reactors has been achieved for frequently used three phase catalytic reactors viz. agitated slurry, bubble column slurry and fixed bed reactors and a two phase gas solid entrained flow reactor. In this context, the following two sections (Section 1.3 and Section 1.4) present a brief review on modeling of three phase catalytic reactors with a special emphasis

on agitated slurry, bubble column slurry and fixed bed reactors and a two phase gas-solid entrained flow reactor respectively.

1.3 THREE PHASE CATALYTIC REACTORS

Three phase catalytic reactors with solid as a catalyst with gas and liquid reactants, are extensively used in chemical industries. Some important applications are shown in Table 1.1. Three phase reactors can be mainly divided into two main categories: (a) slurry reactors like mechanically agitated, bubble column, fluidized bed and loop recycle type, represent a class of reactors where the catalyst is suspended and (b) fixed bed reactors wherein the catalyst is stationary with cocurrent or countercurrent flow of gas or liquid phases. Some industrially important reactions practiced in these reactors are shown in Table 1.5. The choice of a reactor type is an important design factor and would depend on number of factors, which are summarized in Table 1.6.

Table 1.5. Important Industrial Applications of Three Phase Reactors

Reaction type	Gas phase reactant	Liquid reactant	Catalyst	Reactor type	Ref
Hydrodesulphurization	H_2	Sulphur compounds in crude oil	Co-Mo-on alumina	Trickle Bed	21
Hydrogenation	H_2	Fatty acids	Supported Ni	Slurry	22
	H_2	2-Butyne-1,4-diol	Supported Cu-Ni	Trickle Bed	23
Reductive Alkylation	H_2	*p*-nitroaniline or *p*-Phenylenediamine	Pt/Al_2O_3	Trickle Bed or Slurry	24
	H_2	*p*-aminodiphenylamine	63% Ni on kieselguhr	Slurry	25
Oxidation	O_2, C_2H_4	Inert	PdCl2-carbon	Slurry	26
	O_2, SO_2	Water (inert)	Activated carbon	Slurry or Trickle Bed	27
Hydroformylation	H_2, CO	Higher olefins	Co or Rh complex bound to polymers	Slurry	28
Ethynylation	C_2H_2	Formaldehyde	Cu_2C_2 supported	Trickle Bed or Slurry	23, 29

Table 1.6. Comparison of Trickle Bed and Slurry Reactors

Factors Influencing selection	Fixed Bed	Slurry
External mass transfer and intraparticle diffusion rate	Average	Best (high speed of agitation and small particles can be used)
Effects due to liquid mixing side reactions/selectivity	Good (close to plug flow)	Poor (back mixed flow)
Heat removal/ temperature control	Poor	Best (large liquid holdup)
Separation of catalyst from reactants	Best	Poor (filtration required)
Frequent catalyst replacement	Poor (requires dismantling the column)	Good

The overall performance of these reactors depends on the inter phase mass transfer, intrinsic kinetics of reactions, physicochemical properties and mixing of the fluid phases. A theoretical analysis of the kinetic model, overall rate of reaction incorporating contribution of external and intraparticle mass transfer as well as reactor models has been extensively studied and the details are available in monographs by Ramachandran and Chaudhari[4c] and Shah[30] and in reviews by Chaudhari and Ramachandran,[31] Doraiswamy and Sharma[4d], Chaudhari *et. al.*[32], Mills *et. al.*[18a] and Mills and Chaudhari[33].

For the purpose of modeling of continuous reactors, in addition to chemical reaction and transport effects, the variation of the reactant/product concentration along the length of a reactor and the degree of mixing of the two phases have to be considered. Also, additional complexities can exist in trickle beds due to incomplete wetting of catalyst particles and exothermicity of reactions. Theoretical analysis for batch and continuous reactors for generalized as well as limiting cases has been described by Ramachandran and Chaudhari.[4c] These authors have developed equations for the calculation of the reactor efficiency for plug flow as well as back mixed case for co-current and counter current operations in continuous reactors. In this part, a brief review of the principal multiphase reactor types and current state of development on modeling of three phase slurry and fixed bed reactors has been presented.

1.3.1 Agitated Slurry Reactors

The agitated slurry reactors are most commonly used in industrial scales in liquid phase processes. In agitated reactors, the catalyst particles are used in a powder form and kept in suspension by means of mechanical agitation (Figure 1.2). Due to smaller catalyst particle size, intraparticle diffusional effects are negligible in these reactors. Also, the overall mass and heat transfer efficiency is better than the fixed bed reactors and these reactors are preferred for mass transfer limited reactions and those with high level of exothermicity.

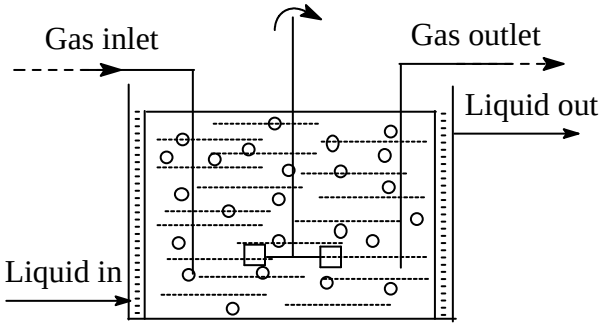

Figure 1.2. Mechanically agitated slurry reactor

The processes for small volume specialty chemicals are often operated in a batch mode. A dead-end operation with no discharge of gas phase is very common for safety reasons and convenience. The agitated slurry reactors can also be operated in a semi-batch or continuous mode depending on the process requirement. The important design parameters for agitated slurry reactors are selection of an agitator type, size, point of gas injection and the mode of heat removal, which have a direct influence on gas-liquid and liquid-solid mass transfer and overall heat transfer efficiencies. It is also important to ensure that the catalyst particles are kept in complete and uniform suspension. Several correlations have been proposed for the estimation of mass transfer and heat transfer parameters, the details of which have been reviewed by Chaudhari and Ramachandran[31] and Ramachandran and Chaudhari.[4c]

In continuous slurry reactors, in addition to mass transfer and kinetic steps, the variation of reactant concentration caused due to mixing of various phases needs to be considered. Goto and Smith,[34] Goto *et. al.*[35], Ramachandran and Smith,[36] Ramachandran and Chaudhari[4c] have described the approaches to model continuous slurry reactors.

1.3.1.1 Models for Semi-Batch Slurry Reactor

In a semi-batch operation of a three-phase reactor, the gas phase flows continuously through the system, while there is no net inflow or outflow of the liquid phase. These reactors find application in the manufacture of fine chemicals and pharmaceuticals where, small volume batch processes are involved. Also, these reactors are widely used for evaluating the catalyst performance of three phase catalytic reactions and to obtain reliable data on the kinetics of a particular reaction. The design problem in a semi-batch slurry reactor is to predict the conversion of the liquid phase reactant as a function of time, so that the batch time of operation of such reactors can be fixed. Theoretical analysis of semi-batch slurry reactors was earlier presented by Chaudhari and Ramachandran,[31] Ramachandran and Chaudhari[4c] for (1,0), (1,1) order kinetics and also in general for *m*-*n*th order kinetics. The equations for (1, 1) order are:

$$t_B = \frac{B_{l_i} X_B}{\nu A^*} \left[\frac{1}{k_L a_B} + \frac{1}{k_s a_p} \right] + \frac{B_{li} R^2 \rho_p I}{3 A^* w D_e} \qquad 1.2$$

where,

$$I = \frac{2}{\phi^2_{oi}} \ln \left[\frac{\phi_{oi} \cosh \phi_{oi} - \sinh \phi_{oi}}{\phi_{oi} \sqrt{1 - X_B} \cosh \phi_{oi} \sqrt{1 - X_B} - \sinh \phi_{oi} \sqrt{1 - X_B}} \right] \qquad 1.3$$

with ϕ_{oi}, the Thiele modulus based on the initial concentration of B is given as,

$$\phi_{oi} = R \left[\frac{\rho_p k_{11} B_{l_i}}{D_e} \right]^{1/2} \qquad 1.4$$

A few examples of previous work on semibatch slurry reactor modeling for hydrogenation reactions are summarized in Table 1.7 and some of these are discussed here.

Jaganathan *et. al.*[50] reported the intrinsic kinetics of hydrogenation of *p*-nitrocumene to *p*-cumidine over supported Pd catalysts in a mechanically agitated slurry reactor. Intraparticle diffusion effects were studied using pelleted catalysts and equations for overall effectiveness factor were derived for Langmuir-Hinshelwood type kinetics. To verify the applicability of the kinetic model experimentally, a semibatch slurry reactor model was developed for both isothermal and non-isothermal conditions.

Table 1.7. Reactor Modeling Studies in Semi Batch Slurry Reactors

Sr. No.	Reaction system	Catalyst	Remarks	Ref.
1.	Crotonaldehyde	Pd/Al_2O_3	Catalyst effectiveness factor determined	37
2.	Chlorobenzene	Pt/C	Gas-liquid mass transfer important	38
3.	Phenylacetylene	Pt/Al_2O_3	Reactor modeling with intraparticle diffusional effects	39
4.	Dimethylnitrobenzene	Pd/C	Kinetics and reactor modeling	40
5.	Butenediol	$Pd\text{-}Zn\text{-}CaCO_3$	Kinetics and batch reactor modeling	41
6.	Phenylacetylene	Pd/C	Kinetics and reactor modeling.	42
7.	Buytnediol	Pd/C	Kinetics and reactor modeling	43
8.	2-ethyl- 5,6,7,8 tetrahy - droanthraquinone	Pd/Al_2O_3	Reactor model incorporating both internal and external mass transfer resistance	44
9.	Furan amines	Rh/Al_2O_3	Kinetics and reactor design	45
10	Benzene	Ni	Kinetics, reactor modeling with intraparticle diffusion	46
11.	1,5,9-cyclododecatriene	Pd/Al_2O_3	Kinetic modeling taking into consideration all the parallel isomerization and consecutive reactions	47
12.	Acetophenone	Rh/C	Reactor modeling with intraparticle diffusional effects	48
13.	2,4-dinitrotoluene	Ni/HY	Intrinsic kinetics and reactor modeling	49

Sr. No.	Reaction system	Catalyst	Remarks	Ref.
14.	*p*-nitrocumene to *p*-cumidine	Pd/Al_2O_3	Methodology for development of slurry reactor model to predict isothermal and non-isothermal performances	50
15.	2, 4-dinitrotoluene to 2, 4-toluene-diamine	Pd/ Al_2O_3	Molecular level approach to kinetic modeling and non-isothermal effects	51
16.	Isooctenes to isooctane	Pt/Al_2O_3	Hydrogenation kinetics was combined with catalyst deactivation kinetics	52
17.	Cinnamaldehyde	Ru/ Al_2O_3	A L-H rate equation considering two-site model was used to describe the kinetic experiments.	53
18.	Benzene to cyclohexane	Ni/Al_2O_3	Kinetics and reactor modeling in presence of significant pore diffusion was proposed.	54
19.	Lactic acid to propylene glycol	Ru/C	Through mass transfer analysis showed that there was no transport limitations in the operating conditions.	55
20.	Reductive alkylation of aromatic amines	Pt/C	Kinetics and semibatch slurry reactor modeling	56
21.	Aniline to *N*-isopropylaniline	Pd/Al_2O_3	Langmuir-Hinshelwood type model was proposed considering the implications of catalytic and noncatalytic steps	57

Rajashekharam *et. al.* [51] studied the kinetics of hydrogenation of 2, 4-dinitrotoluene (2, 4-DNT) in a semibatch slurry reactor using a 5% Pd/Al_2O_3 catalyst at 323-363 K. A fundamental approach based on a molecular level description of the catalytic cycle was used to derive the rate models. It was found that the intraparticle diffusional effects were important for particle sizes (d_p) > 3×10^{-4} m, but the external mass-transfer (g-l and l-s) effects were unimportant. For the complex rate equation observed in this case, an approximate expression for the overall effectiveness factor was derived and the experimental data for different particle sizes were found to agree with the predictions of the model incorporating intraparticle diffusion effects. A mathematical model has also been proposed to predict the temperature and concentration profiles in a semibatch reactor under non-isothermal conditions.

Lehtonen *et. al.* [56] reported the reductive alkylation of an aromatic amine with one alkyl substituent and an aldehyde, which implies a combination of homogeneous and heterogeneous reactions. The rate equations (intrinsic kinetics) were derived starting from a probable catalytic reaction mechanisms and combined with a reactor model for the three phase semi-batch reactor incorporating gas-liquid mass transfer. The kinetic parameters were estimated for a model reductive alkylation reaction system and it was concluded that the number of adjustable parameters in the model could be considerably reduced without any decisive deterioration of the fit of the model on the laboratory scale.

Roy *et. al.*[57] reported the kinetics and semi-batch slurry reactor modeling of reductive alkylation of aniline to *N*-isopropylcyclohexylamine using $3\%Pd/Al_2O_3$ catalyst at 378-408K. The impact of homogeneous and heterogeneously catalyzed reactions (involved in overall reaction sequence) on overall reaction kinetics was addressed.

1.3.2 Bubble Column Slurry Reactor

In the case of bubble column slurry reactors the particles are suspended by gas-induced agitation and the reactant gas itself provides the required stirring action. The gas is dispersed through a deep pool of liquid containing finely suspended catalyst particles. The reactor may be operated in a semi-batch manner for conversion of a liquid reactant or for continuous reaction between gaseous and liquid reactant. The advantages of these reactors include absence of moving parts, minimum maintenance, smaller floor space compared to

agitated reactor and high liquid circulation rates leading to more efficient rates of heat transfer than in the fixed beds. In addition, power consumption required is less than agitated reactors. As small particle sizes can be used, the intraparticle diffusional resistance is minimized and hence maximum utilization of the catalyst is possible. The disadvantages include considerable back mixing of the liquid phase resulting in poorer reactor performance and when the gas is passed at atmospheric pressure, additional energy has to be spent to overcome the pressure drop in the column.[4c]

As the bubble column does not require any additional mechanical or mixing devices, the bubble column reactor can be considered as a standard simple industrial equipment for multiphase reactions, with high service life and operating safety. In industrial practice, because of special process engineering problems, a large number of bubble column types are in use differing in the fluid dynamics and special internal configurations. Some of the basic types are shown in Figure 1.3, showing several different modes of operation for the bubble column reactors. Gerstenberg[58] and Steiner[59] reported in detail the industrial use of bubble column reactors.

1.3.2.1 Modeling of Bubble Column Slurry Reactor

The mathematical description of bubble column reactor can be interpreted as two step process as given below:

i) Description of fluid dynamic flow conditions by considering liquid circulation and backmixing properties with an appropriate fluid dynamic model
ii) Development of reactor model by linking together the fluid dynamics, mass and heat balances under specific boundary conditions for a bubble column

The primary target quantity of interest in a reactor model is the conversion data of the reacting components. In many cases, the temperature profiles in the reactor can be of equal interest. In addition, a fully developed reactor model allows a process to be optimized by analyzing the influence of special adjustable parameters. The degree of progress that has been made in our understanding of modeling of bubble column reactors can be found in

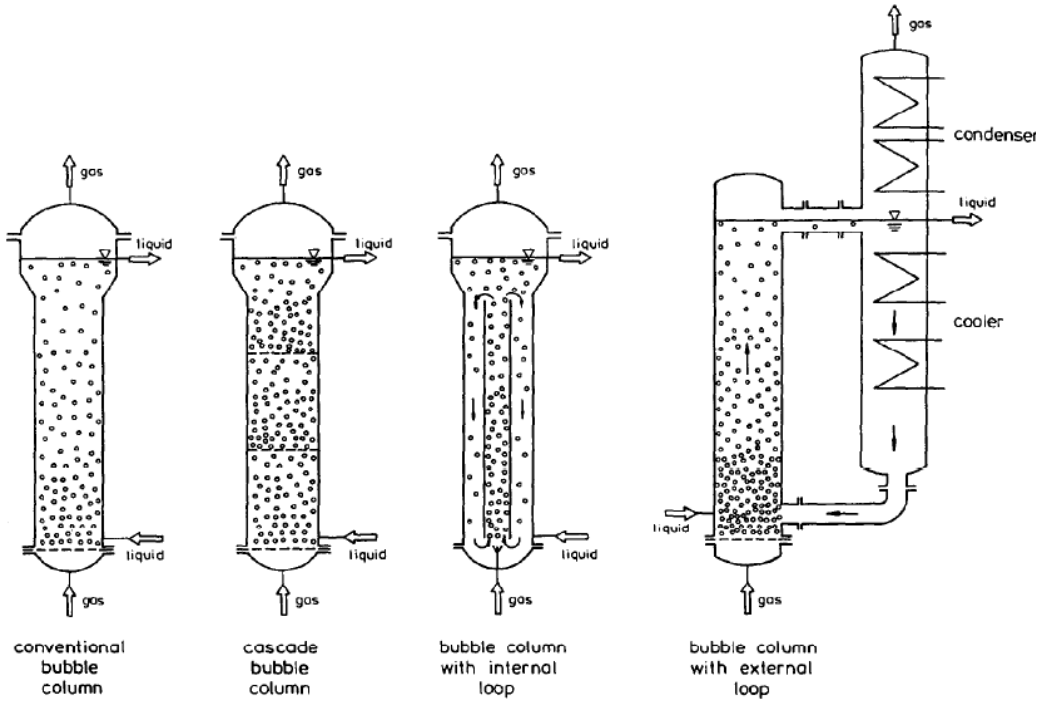

Figure 1.3. Basic bubble column types used in industrial practice

some recent reviews by Jakobsen *et. al.*,[60] Kantarci *et. al.*,[61] Ranade[1] and Joshi[62]. Some important literature on fluid dynamic and reactor models of bubble column reactors is discussed in the following two sections.

1.3.2.1.1 Fluid Dynamic Models

Some of the important fluid-dynamic models for describing gas and liquid flow patterns in bubble columns are summarized in Table 1.8. The basic physical approach and the target quantities are shown for comparison. The detailed information about the methods can be found in comprehensive review by Schluter.[63] The most important fluid-dynamic quantity is the liquid circulation velocity field in the bubble column. Several other process engineering variables like the axial backmixing properties or the heat and mass transfer coefficients can be correlated in relation to this value. So the circulation flow models of Ueyama and Miyauchi,[66,64] Joshi and Sharma[69,70] and Zehner[71,72] are widely used to estimate this velocity. The axial dispersion model (ADM) given at the head of Table 1.8 cannot be regarded as a model describing the special bubble column fluid dynamics on physical basis. From a physical point of view, the ADM is a fully empirical model giving

Table 1.8. Fluid Dynamic Models for Bubble Columns

Model	Main Target Quantity	Remarks	Ref.
Dispersion model	Axial and radial concentration profile of component in multiphase system	Approach analogous to Fick's law of molecular diffusion with dispersion coefficient as global model parameter	65
Recirculation flow models	Liquid velocity profile, axial dispersion coefficient	Starting point is force balance for differential cylindrical volume element and solution is given by introducing a special radial gas hold up distribution and integrating over column radius with boundary conditions	66, 67
Energy balance method	Liquid velocity profile	Overall balance considering 'hydraulic jump' at free liquid surface. Model equations are limited to columns	68
Circulation cell model	Mean circulation velocity of liquid phase: Axial dispersion coefficient and heat transfer coefficient	Enhanced energy balance method with multiple circulation cells arranged in axial direction; circulation cell height determined empirically	69, 70
Cylindrical vortex model	Mean circulation velocity of liquid phase: Axial dispersion coefficient, heat transfer coefficient, mean gas hold up	Liquid circulation is given by gas hold up difference between two circulation cells arranged in parallel.	71, 72
Bubble class models	Gas-phase residence time distribution	Two bubble classes are assumed; large bubble class in plug flow and small bubble class perfectly mixed; no interaction between small and large bubble strand; separated mass balances set up for both classes	73, 74
Tank in series model (cascade model)	Residence time distribution of gas and liquid phase	Perfectly mixed reactor cascade without backflow between neighboring cells; model assumes equal cell numbers (and therefore equal backmixing properties) for gas and liquid phases	65

Model	Main Target Quantity	Remarks	Ref.
Cell model with backflow	Residence time distribution of gas and liquid phase	Perfectly mixed reactor cascade with backflow between neighboring cells; the cell model with backflow is a finite difference equivalent of axial dispersion model	75, 76, 77, 78
Enhanced cell model	Various properties of gas and liquid phases	Several theoretical models for description of large and small bubble behavior considering coalescence and dispersion interaction between phases	79
Fluid mechanical model	Distribution of phase velocities and mass concentration of all components	Comprehensive fluid mechanical description of bubble column reactor; the partial differential equation systems are solved numerically by several complicated algorithms	80

the unknown fluid-dynamic properties of the multiphase system in the value of an ‘axial dispersion coefficient’ as a lumped parameter. Nevertheless, the dispersion model can predict gas- and liquid-phase residence time distributions with accuracy sufficient for most technical cases (for example, see Table 1.9).

Some more physically based models have been published by Gasche[81] and Torvik and Svendsen[80] which can predict the gas/liquid-phase holdup and the circulation velocity profile of both phases with good accuracy. However, the solution of partial differential equations arising from these approaches cause problems if the strong nonlinear temperature dependences of some model parameters are to be considered in the general non-isothermal case.

1.3.2.1.2 Reactor Models

A reactor model can be developed by linking the fluid-dynamic assumptions with the mass and energy balances of the multiphase system. Selected works on modeling bubble column reactors for industrial processes is summarized in Table 1.9. The fluid-dynamic models mentioned in the previous section have rarely been used to describe the chemical reaction engineering data of bubble column reactors. In particular, the very comprehensive multi-component models proposed for describing the Fischer-Tropsch and methanol synthesis in the slurry phase allow us to conclude that the axial dispersion model is a good pragmatic basis for the development of reactor models for industrial processes carried out in bubble column reactors. It should be noted here that the cell model with backflow, which is widely applied in industrial practice too (see Table 1.9), is a finite-difference equivalent of the axial dispersion model. Considering specific mathematical relations between the basic parameters of both models, the cell model with backflow leads to nearly the same numerical results if the number of mixing cells is assigned high enough. A main advantage of the cell model is its great flexibility in modeling processes with concentrated and unequally distributed mass and heat sources.

Table 1.9. Selected Papers on Modeling of Bubble Column Reactors

Chemical Reaction	**Backmixing Model (gas-liquid/solid)**	**Remarks**	**Ref**
Absorption of isobutene in sulfuric acid	CWB (cell model with backflow)/ CWB/-	Axial dependent superficial gas velocity	75, 76
Alkylation of benzene with ethylene	PFM (Plug flow model)/ CWB/-	N = 10 cells, multifeed	82
Fischer-Tropsch synthesis in liquid phase	ADM (Axial dispersion model) /ADM/ADM/-, PFM/TIS/TIS (tank in series model), TIS/TIS/TIS/-	Balanced component: H_2	83, 84
Methanol synthesis in liquid phase	TIS (Tank in series model) /CWB/CWB/-, Comprehensive fluid mechanical model, ADM/ADM/ADM/-	Experimental data: d_T = 60 cm, L = 5 m Heat balance integrated	80, 85, 86
Fischer-Tropsch synthesis in liquid phase	PFM/ADM-PFM/ADM/-	Balanced component: H_2 Balanced components:H_2, CO, CO_2, H_2O	87
Chlorination of ethylene	PFM/CWB/-	Reaction heat removal by direct vaporization of liquid product; model with integrated energy balance	64
Reaction of hydrogen, acetone, and 4-aminodiphenylamine	-/ADM/-	Dynamic model	88
Chlorination of toluene (slow reaction), Absorption of CO_2 in NaOH solution (fast reaction)	Two dimensional dispersion model with radial dependent circulation flow	Constant reaction temperature	81

1.3.3 Fixed Bed Reactors

Multiphase catalytic fixed-bed reactors (FBR) are operated either with a continuous gas and a distributed liquid phase (trickle operation), when the mass transfer resistance is mainly located in the gas phase or with a distributed gas and a continuous liquid phase (bubble operation). In this type of reactors, the gas and the liquid phase flow over a fixed bed of catalysts. The fixed bed reactors can be classified into mainly three types (i) co-current down-flow of both gas and liquid phases (ii) downward flow of liquid with gas in the countercurrent upward direction and (iii) co-current up-flow of gas and liquid phases. These reactors are schematically shown in Figure 1.4. Reactors with co-current down-flow of gas and liquid is called as trickle bed reactor (TBR) and the co-current up-flow reactors are also referred to as packed bubble bed reactors.

Trickle bed reactors, wherein, the liquid reactant trickles down concurrently along with the gaseous reactant, over a fixed bed of catalyst pellets, find applications in a wide variety of chemical, petrochemical and biochemical processes including waste water treatment. The examples of trickle bed reactors are given in detail in several monographs.[89,90,91,92] These include oxidation, hydrogenation, isomerization, hydrodesulfurization, hydroprocessing, decomposition of hydrogen peroxide, deuterium exchange between hydrogen and water to produce heavy water,[93] adsorption of benzene from water on activated carbon particles,[94] hydration, catalytic dewaxing of lube stock [95] etc.

Fixed bed up-flow reactors, wherein, gaseous and liquid reactants co-currently flow upwards over a fixed bed of solid catalysts find applications in many industrial processes. These include hydrodesulfurization of petroleum fractions, liquid phase hydrocracking, hydrogenation of nitro compounds, amination of alcohols, ethynylation of formaldehyde in butynediol synthesis, waste water treatment etc.[4c,96] This type of reactor is mainly used when comparatively small amount of gas has to be processed with large amount of liquid and when a higher residence time for the liquid phase is required. The fixed bed up-flow reactor has the advantage of completely wetted catalyst particles due to high liquid holdup. This can provide a better mass and heat transfer between the liquid phase and the solid catalyst though it has the disadvantage of enhanced external mass transfer resistance. Various parameters affecting the reactor performance of trickle bed reactors and fixed bed up-flow reactors and the details of reactor modeling are discussed in following sections.

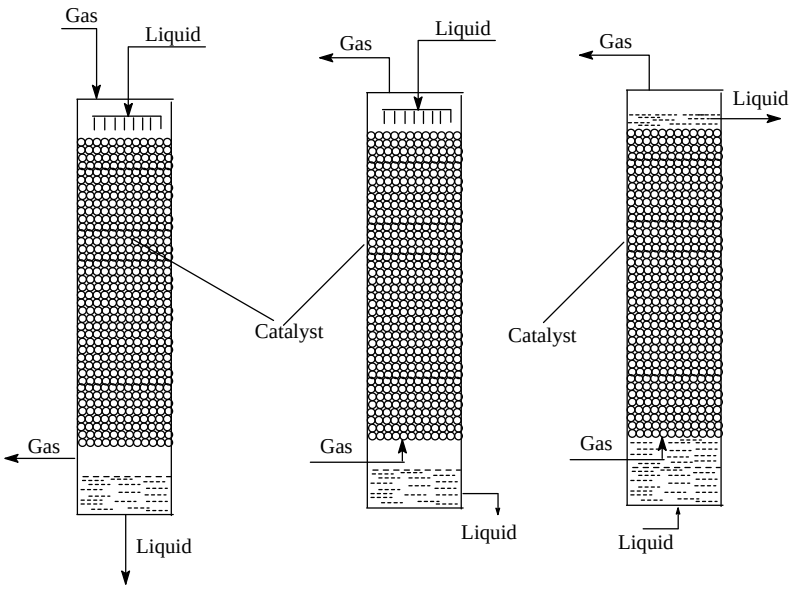

Figure 1.4. Fixed Bed Reactors (a) Trickle Bed Reactor (b) Countercurrent Reactor and (c) Up-flow or Packed Bubble Column Reactor

1.3.3.1 Important Design Parameters

The important design parameters which influence the reactor performance include, pressure drop, liquid holdup, gas-liquid mass transfer coefficient, liquid-solid mass transfer coefficient and the heat transfer parameters such as effective thermal conductivity and bed to wall heat transfer coefficient. Various correlations exist in the literature for calculating all these parameters and have been reviewed from time to time in various monographs by Satterfield,[89] Hofmann,[96] Shah,[90] Herskowitz and Smith,[97] Ramachandran and Chaudhari,[4c] Gianetto and Specchia,[98] Saroha and Nigam[92] and Al-Dahhan *et. al.*[91] Also, Lamine *et. al.*[99] have published a detailed report on the heat transfer properties of both up-flow and down-flow modes of operations.

Catalyst wetting efficiency is one of the most important parameters in the design of trickle bed reactors, since it represents the extent of utilization of the catalyst particles. Many correlations exist in the literature for the determination of wetting efficiency of the catalyst particles and have been reviewed by Julcour *et. al.*[100], Satterfield,[89] Shah,[90] Herskowitz and Smith,[97] Ramachandran and Chaudhari,[4c] Gianetto and Specchia,[98] Saroha and Nigam[92] and Al-Dahhan *et. al.*[91] Recent studies are focused on incorporating the effect

of pressure on the catalyst wetting efficiency. Al-Dahhan and Duducovic[101] investigated the effect of pressure on the wetting characteristics and developed a semi-empirical model, incorporating the effect of reactor pressure and gas velocity. A review of previous work on modeling of fixed bed reactor is presented in the following sections.

1.3.3.2 Reactor Performance Studies in FBR

Due to gas and liquid flowing co-currently through the catalyst-bed, fixed-bed reactor performance depends on a complex interaction of the intraparticle and interphase mass transport, reaction kinetics and hydrodynamics. Many reports on experimental and modeling studies involving fixed-bed reactors have been published with the aim of comparing the predictions with experimental data and understanding the interplay between overall reactor performance and various factors affecting it.[102] Many of the industrially important reactions involve complex reaction network and highly exothermic reactions. Investigation of TBR performance for important complex multi-step reactions is scarce in literature.[103,104,105,106] Some recent investigations into fixed bed reactor (with upflow and downflow mode) performance studies are presented in the Table 1.10.

Most of the previous studies were carried out under isothermal conditions and have considered pseudo-homogeneous models based on plug flow[107, 108] or heterogeneous models with plug flow of both gas and liquid phases.[103,135,109,110] Some models accounted for liquid flow non-uniformity and maldistribution by using an axial dispersion model.[111] The investigations deal with hydrogenation or oxidation in pure or moderately concentrated organic or aqueous solutions (large excess of liquid reactant). Liquid reactants/solvents were assumed to be non-volatile and gas phase assumed to be pure at constant partial pressure of the reacting gas. Thus, the primary model variables of interest have been the liquid phase concentrations of the dissolved gaseous reactant and the resulting conversion of the liquid phase reactant. The key effect that was incorporated in most recent models was that of partial wetting and transport of gaseous reactant to externally dry areas of the catalyst resulting in higher rates observed in most experimental data.[112,113] It was observed generally that under conditions of gas phase reactant limitation, the rates decreased with increase in liquid velocity due to higher catalyst wetting at higher liquid velocities and hence reduced direct gas-solid mass transfer contribution. Under conditions of liquid phase

Table 1.10. Investigations of TBR and Fixed Bed Up-Flow Reactor (UFR) Performance

S. No.	Reaction / Reactor	Rate Analysis	Model Assumptions	Ref.
1	H_2O_2 decomposition / TBR	Linear kinetics	Isothermal, partial wetting, 2-region cell model	114
2	Hydrogenation of C_4 olefins /UFR	L-H kinetics	Isothermal, plug flow	115
3	Hydrogenation of 3-hydroxypropanal /TBR	L-H kinetics	Isothermal, plug flow, partial wetting, heat balance	116
4	Hydrotreating of vacuum gas oil /TBR	L-H kinetics	Isothermal, plug flow, partial wetting	117
5	Hydrogenation of α-methyl styrene /TBR and UFR	L-H kinetics	Isothermal, plug flow, partial wetting, high pressure	118
6	Selective hydrogenation of 1,5,9-cyclododecatriene / UFR	Linear kinetics	Isothermal, axial dispersion, high pressure/temperature	119
7	SO_2 oxidation /TBR	L-H kinetics	Isothermal, full wetting	120
8	SO_2 oxidation/ TBR/ UFR	L-H kinetics	Isothermal, partial wetting, axial dispersion, static-dynamic	121
9	Phenol oxidation /TBR	L-H kinetics	Isothermal, full wetting, plug flow, high pressure/ temp.	122
10	Hydrogenation of α-methyl styrene /TBR	Linear kinetics	Isothermal, plug flow, partial wetting	123
11	Hydrogenation of acetophenone /TBR	L-H kinetics	Non-isothermal, plug flow, full wetting, high pressure/temp.	106
12	Hydrogenation of unsaturated ketones in supercritical CO_2 /TBR	Power law kinetics	Non-isothermal, plug flow, full wetting	124
13	Hydrogenation of 2,4-dinitrotoluene /TBR	L-H kinetics	Non-isothermal, plug flow, partial wetting, stagnant liquid	103
14	Hydrogenation of α-nitromethyl-2- furanmethanol /TBR	L-H kinetics	Isothermal, plug flow, partial wetting	125

S. No.	Reaction / Reactor	Rate Analysis	Model Assumptions	Ref.
15	Oxidation of substituted phenols /TBR	Linear kinetics	Isothermal, plug flow	126
16	Hydrogenation of maleic anhydride / UFR	L-H kinetics	Isothermal, axial dispersion, full wetting	127
17	Hydrogenation of 1,5,9-Cyclododecatriene/TBR and UFR	L-H kinetics	Non-isothermal, plug flow, partial wetting, stagnant liquid	128
18	Hydrogenation of 1,5,9-Cyclododecatriene/TBR	Eley-Riedal Kinetics	Nonisothermal heterogeneous model, partial wetting effect	129
19	Catalytic hydroprocessing of oil feedstock	L-H kinetics	Nonisothermal, homogeneous plug flow axial dispersion model	130
20	Hydrogenation of α-methyl styrene and phenol oxidation/ TBR and UFR	L-H kinetics	Axial dispersion model	131
21	Catalytic wet air oxidation/ TBR and UFR	L-H kinetics	Axial dispersion model for liquid phase coupled with cell stack model for gas phase	132
22	Wet air oxidation of phenol	Power law kinetics	Non-isothermal, plug flow model, partial wetting effect	133
23	Hydrotreating of benzene/TBR	L-H kinetics	Non-isothermal, 1D and 2D cell network Models, Radial liquid maldistribution, partial wetting effect	134
24	Hydrogenation of benzene/TBR	L-H kinetics	Nonisothermal-heterogeneous three phase model , Maxwell-Stefan mass transfer model and effective diffusivity model	135
25	Catalytic oxidation of phenol/TBR	L-H kinetics	Isothermal, Axial dispersion model, plug flow model	136

reactant limitation, the rates were found to decrease with lower wetting due to decrease in effective liquid-solid contacting. Al-Dahhan and Duducovic[137] achieved an improvement in the performance of trickle bed reactor operating under conditions where limiting reactant is in the liquid phase by the use of fines. The addition of fines improved the liquid-solid contacting efficiency and a corresponding increase in the rate was observed. Some models considered non-isothermal effects and used pseudo-homogeneous energy balance to solve for the temperature at any axial location.[138,139,103] Other variants include a cell model[140], a cross flow model[141], mixing cell model [142,143] and some other based on liquid flow maldistribution[144] or stagnant liquid zones in the reactor[103].

Among the reactor scale models, the plug flow model has been generally used for the modeling of TBR.[145] The axial dispersion model (ADM) is the simplest model describing differential mixing in fixed-bed reactors by superimposing axial dispersion on plug flow.[146] The ADM involves only one parameter, the axial dispersion coefficient, usually expressed as a Peclet number. The mixing cell model considers a flow through a series of mixing cells in the interstices of the packing, where the flow is characterized by the number of cells in series and the liquid holdup. However, this model does not adequately represent the actual flow in a fixed-bed.[147] The cross flow model has been suggested to account for the considerable liquid stagnancy. It assumes that liquid holdup can be split into two parts: stagnant pockets or films, and liquid in plug flow, with exchange between the two. The cross flow model requires three parameters: the fraction of the plug flow, the exchange coefficient, and the external liquid holdup.[148]

Enhancing the reactor performance by using various modeling techniques have been of great research interest in recent years. In some studies, cell network model has been applied for TBR modeling, in which, fixed bed of spheres was approximated as a cylindrically symmetrical network of perfectly stirred tank reactors.[134] The reactants were envisioned to enter any given stirred tank as a single phase from the two preceding tanks. Alternative rows were offset at half a tank to allow for radial mixing. The effluent from the stirred tank was then fed through subsequent stages.[149] Jaffe[150] applied this concept to the heat release of a single phase hydrogenation process, and simulated the occurrence of steady state hot spots due to flow maldistribution. Schnitzlein and Hofmann[151] developed an alternative cell network model in which the elementary unit consisted of an ideal mixer and a subsequent

plug flow unit. These fluid streams were split or merged in infinitesimally small adiabatic mixing cells (without reaction), located between the different layers of the elementary units. Kufner and Hofmann[152] incorporated the radial porosity distribution into the above cell model, which led to a better agreement of the predicted temperature profile with the experimental data. The cell network models mentioned above were examined for single phase flow with offset in alternative rows of cells. Recently, Guo *et. al.*[134] has developed a TBR model, which is capable of handling multiphase flow and reactions as well as temperature change due to the phase transition and flow maldistribution. The model serves as a guide to understand the reactor performance and optimization.

Pellet scale diffusion with reaction was studied by taking reactant limitation into account in simpler versions[153] and in general case, by considering both gas and liquid phase reaction zones and solution of gas liquid interface by considering liquid inhibition, pore filling and capillary condensation in a partially internally wetted pellet.[139] Approximate solutions from gas-solid catalyst level equations have also been verified by numerical solution for n^{th} order as well as Langmuir-Hinshelwood type kinetics.[154] Some selected studies and observations in trickle bed reactors where performance studies have been carried out are summarized below.

Khadilkar *et. al.*[118] has employed El-Hisnawi's plug-flow model[112] for the reaction of hydrogenation of α-methyl styrene at high pressure (1:5 MPa), where a numerical solution was demanded due to non-linear kinetics exhibited by the reaction. The pellet effectiveness factor in El-Hisnawi model was fitted at one space–time with the experimental observation. Then the effectiveness factor was used as a fitting parameter for the other space–time, which, however, in no way reflected the actual mass transfer resistance inside the pellet and the pellet external wetting contact with the liquid.

Hydrogenation of benzaldehyde to benzyl alcohol was studied in a slurry reactor using nickel catalysts by Herskowitz[155] and the Langmuir–Hinshelwood type of kinetic model developed was used to predict the performance of a trickle bed reactor for the above mentioned reaction. A completely wetted catalyst model was developed and all the mass transfer resistances were considered in the model assuming that hydrogen is the rate limiting reactant. The study was carried out for a varying range of gas velocity, temperature

and pressure. It was concluded that slurry reactor was a better choice than a trickle bed reactor for such high rate reactions.

A three-phase reactor model for hydrotreating reactions in a pilot trickle bed reactor was developed by Korsten and Hoffmann[117] The model based on the two-film theory, was tested with regard to the hydrodesulfurization of vacuum gas oil in a high pressure pilot plant reactor under isothermal conditions. The axial dispersion in both phases were found to be negligible and various mass transfer coefficients, gas solubility and other properties of the gas as well as the liquid phases were determined using various correlations. The kinetics of the reaction was represented by a Langmuir-Hinshelwood model and the intraparticle mass transfer within the catalyst pellets were represented by catalyst effectiveness factor. The poor conversion observed was explained with regard to the incomplete catalyst wetting properties.

Liquid phase hydrogenation of acetophenone using Rh/C catalyst was studied by Bergault *et. al.*[106] in trickle bed reactor and slurry airlift reactor and the performance of these two reactors were compared in terms of productivities and yields. For modeling trickle bed reactor performance, a non-isothermal plug flow reactor model incorporating the external and intraparticle mass transfer effects was developed. It was assumed that the catalyst was fully wetted and the mass and heat transfer correlations were estimated using various correlations available in the literature. It was concluded that the available correlations for gas-liquid mass transfer are not satisfactory and catalyst wetting is an important process that cannot be neglected in the modeling and intraparticle diffusional effects played an important role in determining the reactor efficiency.

Rajashekharam *et. al.*[103] reported the experimental verification for a non-isothermal trickle bed reactor model for the hydrogenation of 2, 4-dinitrotoluene using 5%Pd/Al_2O_3 catalyst, incorporating the partial wetting of the catalyst as well as the stagnant liquid hold up. It was assumed that the catalyst can be divided into three zones, where the catalyst is exposed to dynamic liquid flow, static liquid pockets and exposed to gas phase. The external mass transfer effects and intraparticle diffusional effects of the gaseous reactant hydrogen was taken into consideration in the model and a Langmuir-Hinshelwood type of rate model was used to describe the intrinsic kinetics of the reaction. The effect of various parameters like liquid velocity, gas velocity, temperature and catalyst particle size on rate

of hydrogenation, conversion and temperature rise inside the reactor was investigated. It was found that the importance of parameters in the descending order was gas-solid > gas-liquid > liquid-solid and also concluded that the contribution by stagnant liquid pockets was negligible.

Roininen *et. al.*[135] has developed a heterogeneous three phase reactor model to simulate the industrial TBR for benzene hydrogenation and simulated the temperature profiles were compared with the actual plant data. Analysis of the simulation results shows that the process is limited by hydrogen mass transfer through the gas-liquid interface. Therefore the mass transfer correlations, especially for k_La, must be carefully chosen. A completely wetted catalyst model was also developed and all the mass transfer resistances were considered in the model assuming that hydrogen is the rate limiting reactant. The study was carried out for a varying range of gas velocity, temperature and pressure. It was concluded that slurry reactor was a better choice than a trickle bed reactor for such high rate reactions.

Iliuta and Larachi[156] have discussed the design of reactors by exploring a parallel modeling framework in which the reactor and particle scales were considered. The reactor scale piston dispersion exchange (PDE) model was employed to capture both transient and space dependences of reactants in the dynamic and static liquid zone. The mass transfer processes between gas–liquid, gas–solid, and dynamic liquid–static liquid were integrated. Chemical reaction, as a sink to deplete the reactants, was coupled with the (PDE) model. At the pellet scale, they solved the general diffusion–reaction equation to supply the time and space distribution of the reactant concentrations. They employed a parallel solution strategy to simultaneously resolve the pellet and the reactor scale model for the catalytic wet oxidation of phenol in fixed-bed with MnO_2/CeO_2 catalyst pellets.

1.3.3.3 Reactor Performance Studies in FBR with Co-current Upflow

Due to increasing competition and environmental needs, alternative modes of operation such as fixed bed with up-flow of gas and liquid phases are gaining considerable attention.[157] The fixed bed up-flow reactor has the advantage of completely wetted catalysts due to its high liquid holdup, thus providing better mass transfer and heat transfer between the liquid phase and solid catalyst. But it has the disadvantage of enhanced external mass transfer resistance and significant liquid backmixing compared to that of

trickle bed reactor. The wetting efficiency of the catalysts in an up-flow reactor is assumed to be one. There are also reports where wetting efficiency of the catalyst was assumed less than one.[158] In such cases it was assumed that some part of the gas, which passes through the reactor, comes into direct contact with the catalyst particles and direct transfer of mass from the gas phase to the catalyst particle takes place. Reactor performance studies in fixed bed up-flow reactors are less compared to that of trickle bed reactor studies. Some of the studies carried out are enlisted in Table 1.10 and observations made are summarized below.

Al-Dahhan and Dudukovic[137] and Wu *et. al.*[159] has shown that under conditions of liquid phase reactant limitation up-flow reactor outperform trickle bed reactor due to its efficient liquid-solid contact. This higher liquid holdup and liquid-solid effective contact also results in a better heat dissipation in case of exothermic reactions and can be advantageous in reactions where temperature dependence of selectivity is sensitive.

For better catalyst life and cycle efficiency, up-flow reactor can be used in view of effective temperature control due to its better heat transfer properties as shown by Ragaini and Tine[160] for the hydrogenation of diolefin compounds in pyrolysis gasoline. Mochizuki and Matsui[161] studied the selective hydrogenation of phenyl acetylene and styrene in an up-flow reactor using supported palladium catalyst and also investigated the various parametric effects like substrate concentration, temperature and pressure on the reactor performance. It was found that hydrogen was rate controlling in most cases and diffusional effects of phenyl acetylene was also important at its lower concentrations. Stuber *et. al.*[119] studied the partial hydrogenation of 1, 5, 9-cyclododecatriene in a fixed bed up-flow reactor and found that by increasing the gas flow rate, increased gas-liquid mass transfer and also efficient heat transfer was possible. Higher reactor length was simulated by splitting up the process in two steps resulting in the significant improvement in selectivity. Van Gelder *et. al.*[162,163] described a reactor model for the hydrogenation of 2, 4, 6-trinitrotoluene in an up-flow reactor in the presence of an evaporating solvent to absorb the heat of reaction. It was shown that a model incorporating dispersion of gas phase represents the experimental data better compared to a plug flow model.

Design aspects of co-current up-flow reactors were reviewed by Hofmann,[164] Ramachandran and Chaudhari[4c] and Shah[90]. The generally used reactor model for fixed bed up-flow reactor is steady state, isothermal, heterogeneous, one dimensional model taking

into consideration the back mixing of the phases involved. Dynamic models, which can predict the startup and sudden changes in the reaction parameters on the performance of the reactors, applied for industrially important reactions are rare. Julcour *et. al.*[165] have investigated the dynamic aspects for the hydrogenation of 1,5,9-cyclododecatriene using a Pd/Al_2O_3 catalyst incorporating resistance to heat and mass transfer at the gas-liquid and liquid-solid interfaces and the model predictions were compared with the experimental observations under varying gas and liquid velocities. Visser *et. al.*[166] had investigated the influence of forced periodic oscillations of the gas phase component for the hydrogenation of phenyl acetylene based on a heterogeneous model considering both the transient mass balance over the reactor length as well as accumulation inside the catalyst pellets.

1.3.3.4 Comparison of Downflow and Upflow Mode of Operation

There are only few comparison studies on performances of up- and down-flow mode of operations applied to industrially important reactions. Goto *et. al.*[167, 168]studied successively the oxidation of ethanol and the hydration of an olefin at atmospheric pressure in the down-flow and up-flow modes. They concluded that the trickle-bed is more efficient at low gas and liquid velocities, because of the partial catalyst wetting leading to an enhanced transfer of the gaseous reactant. Wind *et. al.*[169] have evaluated the performance of hydrotreating catalysts in up- and down-flow fixed bed reactors. They found that the catalyst utilization was poor in bench scale reactors compared to commercial reactors, due to the lower mass velocities of liquid in the test reactors (bench scale). They also found that the up-flow operation resulted in a better utilization of the catalyst, comparable to those in commercial reactors. Larachi *et. al.*[170] have measured the liquid saturation operated under higher pressures in concurrent up-flow and down-flow fixed bed reactors. They found that for up-flow, the saturation was greater than for the down-flow regardless of the operating pressure. However, in the pulsing flow regime an asymptotic value was observed for both flows. For a given mass flow rate, the liquid saturation increased with pressure but decreased when the liquid viscosity was decreased independently of the direction of flow or operating pressure. Yang *et. al.*[171] have compared the hydrodynamics of up- and down-flow packed bed reactors and concluded that the hydrodynamic characteristics such as pressure drop, and liquid hold up are similar for both up- and down-flow reactors in the

high interaction regime. Vergel[172] investigated the selective hydrogenation of butadiene in a C_4 olefinic cut in trickle-bed and up-flow reactors of 5.5 cm diameter. The author noticed that the selectivity remains stable in the flooded-bed in a wide range of fluid velocities, but decreases in the trickle-bed at low liquid velocities. This low selectivity was explained by segregation phenomena inside the down-flow reactor.

Mills *et. al.*[173] examined the productivity of packed beds with down-flow, up-flow and countercurrent flow of gas and liquid for a gas-limited reaction (the hydrogenation of α-methylstyrene in hexane). They obtained similar conversions for cocurrent down-flow and countercurrent modes in the low interaction regime, while the cocurrent up-flow generally yielded lower values. For the same reaction system, Khadilkar *et. al.*[113]compared both reactors over a wide range of operating pressures (from 30 to 200 psig). They related the observed performance to the type of reaction system used (gas-limited or liquid-limited). When the reaction is gas-limited at low pressure and high liquid feed concentration, trickle-bed reactor outperforms the up-flow reactor due to ready access of the gas to the incompletely externally wetted catalyst. At high pressure and low liquid feed concentration, the reaction becomes liquid-limited and up-flow reactor performs better. In a recent report, Julcour *et. al.*[174] investigated the hydrogenation of 1,5,9–cyclododecatriene and observed that the rate of hydrogenation was higher for the up-flow mode compared to down-flow in contrast to earlier reports. This can be due to the bigger dimension of the reactor used, where in the down-flow mode of operation, the catalyst may not be completely wetted internally.

In many of the studies in trickle bed reactor, it was found that the partial wetting of the catalyst particle has a decisive role in determining the reactor efficiency. Catalyst bed dilution using fine particles was suggested by Al-Dahhan and Dudukovic[137] to improve the catalyst wetting efficiency in trickle bed reactor. Wu *et. al.*[159] investigated the performance of up and down-flow reactors with and without fines. Hydrogenation of α-methyl styrene to cumene with 2.5%Pd/Al_2O_3 as the catalyst and n-hexane as the solvent was chosen for this study. It was shown that trickle bed reactor outperform up-flow reactors under conditions of catalyst partial wetting and gas phase reactant limitation, due to elimination of external mass transfer resistances at the no-wetted catalyst portions. Under conditions of liquid phase reactant limitation, it was found that up-flow reactor gave a better performance

than the trickle bed reactor due to efficient catalyst wetting and hence availability of limiting reactant is enhanced. Performance of both the reactors at different pressures, liquid phase reactant feed concentrations and gas flow rates are compared and explained on the basis of shifting from the gas to liquid limitation. Experiments on dilution of bed with solid fines in both mode of operation gave identical reactor performances and showed that hydrodynamics and kinetics can be decoupled by the use of fines.

1.4 ENTRAINED FLOW REACTOR

The entrained flow reactor (EFR) systems are commonly used for the high temperature fast gas-solid reactions (viz. Biomass combustion, coal combustion) to study the kinetics due to their advantage of minimizing interparticle effects. In this type of reactor, the particles entrained in a carrier gas are injected along the axis of a hot furnace tube into a flowing preheated gas stream.[175,176,177,178,179] A schematic view of an entrained flow reactor is shown in Figure 1.5. The residence time is controlled by the positions of a water cooled injector and collector and by gas velocity. These reactors can be designed for complete collection and separation of the char, tar and gas products.[178,180,181] This technique has number of advantages such as high heating rates (~10^4 K/sec) to high temperatures (≤ 1900 K). Moreover, the particle velocities can be accurately calculated[178,182,183] and can be validated by in-situ measurements using Laser Doppler Velocimeter (LDV).[184,185,186] One disadvantage of this method is that the volatile products remain hot during the experiment and thus undergo secondary reactions. Their temperature history will generally not be the same as that of the particles. However, the major disadvantage of the method is that particle temperature histories are difficult to determine. The particle temperature history is usually calculated from heat transfer/fluid mechanics models. The exact details of mixing of fuel particles and carrier gas with the preheated gas, which are not generally known, are very important to a precise prediction of temperatures.

The design of an entrained flow gas-solid reactor is often difficult due to the need to fulfill the global kinetic study requirements. Because of the dramatic temperature effects on reactions, solid particles must be maintained at low temperature until injected into the reactor. Once injected, the particles should be heated to the reactor temperature and equilibrate with the gas phase in the reactor very rapidly. In addition, after a short period of

reaction, the collected particles have to be cooled rapidly in an inert gas environment to prevent any possible additional reactions. For high temperatures, isothermal conditions are difficult to obtain. Besides incomplete mixing of solid and gaseous reactants and problems in sampling the solid product may also compound the operational problem.[187]

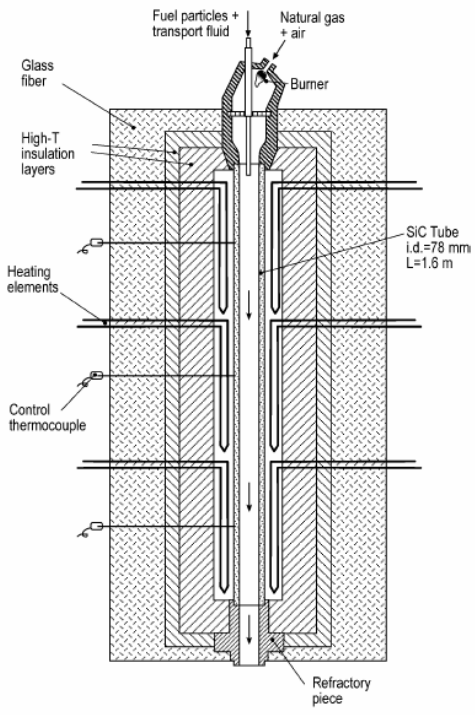

Figure 1.5. Schematic of entrained flow reactor[188]

In previous literatures, many mathematical models describing the EFR behavior with special emphasis to fluid dynamic aspects inside the tube were reported, which mainly include empirical,[189] Eulerian-Lagrangian[190] and Eulerian-Eulerian models.[191]

The following two sections presents a literature review on case studies selected for the purpose of modeling of multiphase reactors as discussed in earlier section (Section 1.1).

1.5 REDUCTIVE ALKYLATION OF AMINES

1.5.1 Reaction Pathway and Product Distribution

Reductive alkylation is a class of reaction, which involves the condensation of an amine or ammonia and a carbonyl compound followed by reduction of the intermediate imine

derivative to the desired amine. This reaction can also be termed as reductive amination when it is looked from the perspective of the carbonyl compound. Aromatic *N*-alkylated products have a wide variety of applications in dyestuff industries as intermediates, in petroleum and rubber industries as anti-oxidants and anti-ozonant, in agrochemical industries as intermediates.

Though, the mechanism of this reaction is well documented in the textbooks, only limited information is available on catalytic reaction mechanism on a molecular scale. The reaction occurs in three steps as shown in Figure 1.6 in which aniline and acetone are considered as the representative reactants of amine and carbonyl compound respectively. The condensation of amine and a carbonyl compound produces hemiaminal (I, also called carbinolamine), which may undergo dehydration reaction to form the imine intermediate (II, commonly termed as Schiff's base) or may undergo hydrogenolysis to produce the secondary amine (III). The imine compound may hydrogenate catalytically to III.

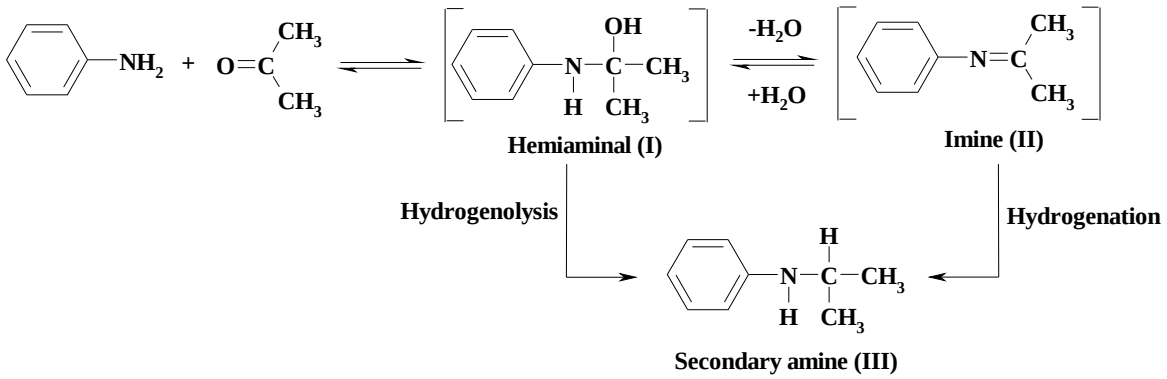

Figure 1.6. Mechanism of *N*-monoalkylation of aniline

The equilibrium-controlled formation of the Schiff's base [SB] is believed to be the slowest step in the consecutive reaction sequence. Acids and bases are reported to promote the formation of Schiff's base (II).[192] Continuous removal of water from the reaction mixture by azeotropic distillation[193] or using molecular sieves[194] can shift the equilibrium towards the right side and enhance the overall rate of reductive alkylation.

The secondary amine (III) may further condense with another molecule of a carbonyl compound to form hemiaminal (IV) that cannot dehydrate to an imine but Enamine (V) (Figure 1.7). Hydrogenolysis of IV or hydrogenation of V gives *N*-dialkylamine (VI). In

reality, due to the lower reactivity and bulkier size of ketones, the reaction stops at monoalkylamine.[195] *N*-dialkylation requires severe conditions and very selective catalysts.[196] On the other hand, alkylation continues for the aldehyde substrates to the *N*-dialkylated products. Due to the stepwise reaction mechanism, monoalkylated product can be formed with aldehyde by optimizing the reaction conditions.[197]

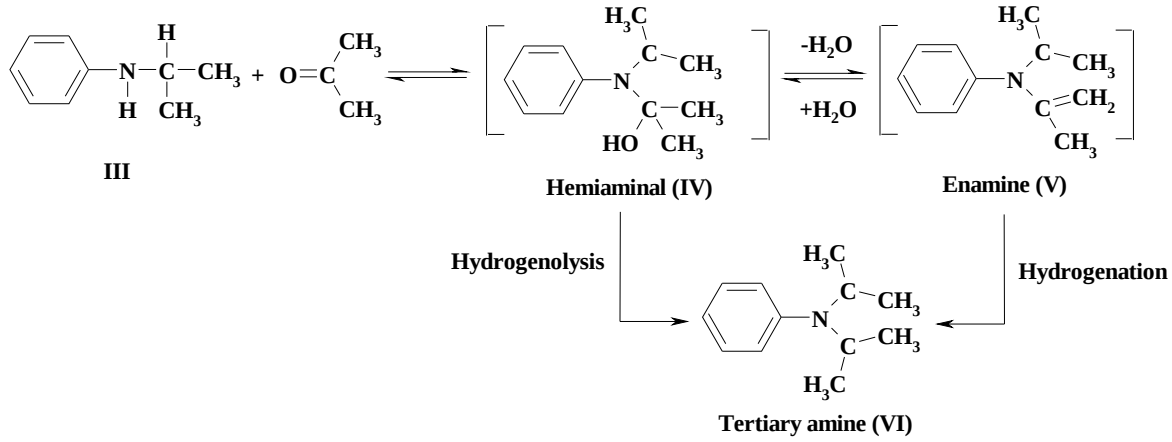

Figure 1.7. Reaction pathway of *N*-dialkylation of aniline

Alkylation of aromatic moiety is one more possibility in this reaction. This may be a probable side product in reductive *N*-alkylation reaction when acids are used as promoters for formation of II and V, because C-alkylation is reported to be catalyzed by acids and accelerated by *o*-, *p*- directing groups like –NH_2 or –OH in the aromatic moiety.[198] The reaction is a typical aromatic electrophilic substitution by the carbonium ion as shown in Figure 1.8.

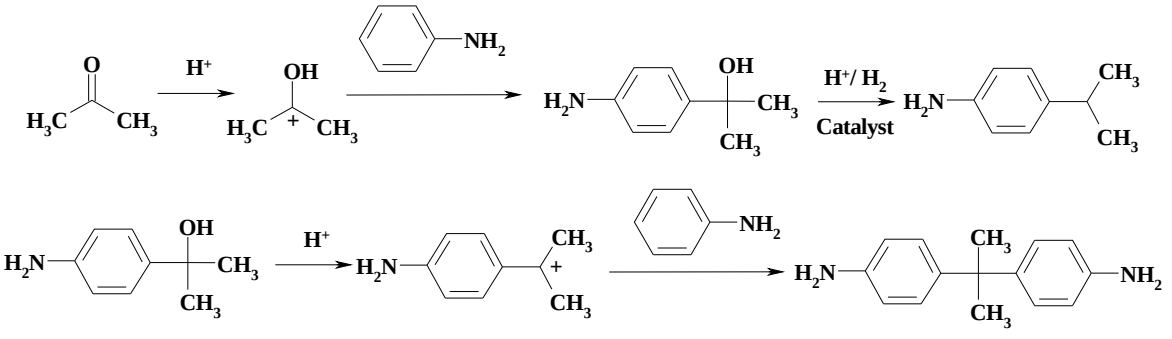

Figure 1.8. Ring alkylation of aromatic amines by carbonyl compounds

Aromatic ring hydrogenation and hydrogenation of the carbonyl functionality to the corresponding alcohol are also important side products in this class of reaction. The aromatic ring hydrogenated alicyclic products are much more basic than the aromatic species and may strongly adsorb on the catalyst, thereby causing the catalyst inhibition. Alcohol formation may be a crucial problem in a commercial process, because it utilizes the carbonyl compound and hydrogen, and leads to a problem in separating alcohol from the unreacted ketone. Archar *et.al.*[199] allowed the carbonyl compound to stand together overnight with the amine compound before hydrogenation in presence of Adams platinum oxide, so that the imines could be available on the catalyst surface with an appreciable concentration to hydrogenate and that could suppress the carbonyl hydrogenation. Emerson[200] isolated the imine from the reaction mixture before hydrogenation reaction to eliminate the formation of alcohol. The complex product distributions in reductive alkylation due to ring hydrogenation of aniline analogues have been reviewed by Stieber *et. al.* [201a] and Greenfield[201b]. Stieber *et.al.*[201a] suggested the use of highly pure starting materials and selective catalysts under controlled reaction conditions to reduce the impurities in the reaction mixture. According to Greenfield, [201b] reactions at lower temperature, high pressure, high catalyst loading and large excess of ketone can be a solution for minimizing side products.

1.5.2 Substrates and Catalysts

Reductive alkylation has been investigated previously using a wide range of alkylating agents and catalysts. Any type of amine precursors like nitro, nitroso or nitrile compounds, are suitable for this reaction, which hydrogenate in-situ to generate the amine.[202] Secondary amines like amides are also reported for reductive alkylation with aldehydes and ketones in good yield (>80%) without any O- or C- alkylated products.[203] Due to the lower cost and less toxicity compared to amines, nitro compounds are often used as the starting compounds in industrial processes.

The choice of a catalyst and reaction conditions are two strong factors in the performance of reductive alkylation reactions. In the early literature, Raney-Ni was reported as the preferred catalyst at elevated temperature and pressure, and seems to be a good choice for synthesis of primary amines. Supported Ni, Cu, Co, copper chromite

($2CuO.Cr_2O_3$) were also suggested as catalysts. Among the transition metals, palladium is the most preferred catalyst because,

- Pd is the most active metal for the saturation of double bonds in conjugation with aromatic ring,
- Pd is least active metal for hydrogenation of aromatic ring at lower temperatures (<423K)
- Pd has lower activity for hydrogenation of aliphatic aldehydes and ketones.

As an example, the performances of different transition metal catalysts for reductive alkylation of aniline with acetone at identical conditions are presented in Table 1.11.[201b]

Table 1.11. Comparison of Transition Metals for Reductive Alkylation of Aniline and Acetone

Catalyst	Temp. (K)	Time (h)	Conv. (%) Aniline	Sel. (%) N-IPA	Sel. (%) N-IPC	Low boiling amines	IPA[a] (%)
5% Pd/C	378	1	100	67	14	6	0
5% Pt/C	378	1	60	47	<2	>1	33
5% Rh/C	378	10	100	0	81	21	>90
5% Ru/C	378	1.8	100	0	74	23	100
5% Pd/C	378	4.7	>99	50	20	13	0
5% Pd/C	418	1	>98	40	39	18	0

Reaction conditions: aniline, 1 mol; acetone, 15 mole; catalyst, 6 g (all are procured from Engelhard Industries); P_{H2}, 400-600 psig; reaction taken in 1 gallon stirred autoclave.
[a]IPA formed w.r.t. excess acetone used.
N-IPA: N-isopropylaniline; N-IPC: N-isopropylcyclohexylamine; IPA: isopropylalcohol.

Table 1.12. Comparison of Pt and Pd metals for reductive alkylation of PAPD and MIBK

Catalyst	Temp (K)	Time (h)	Conversion (%)	Yield (%) based on conv.
5% Pd/C	393	12.5	76	78
5% Pt/C	373	10	92	93

Reaction conditions: PAPD, 0.40 mol; MIBK, 1.6 mol; catalyst, 3 g (procured from Engelhard Industries); P_{H2}, 150-300 psig; reaction done in 600 ml Magne Drive autoclave.
PAPD: *p*-amino diphenylamine; MIBK: methyl isobutyl ketone.

It is clear from Table 1.11 that Pd is far superior to the other catalysts for reductive alkylation of aniline and acetone. Pt showed less tendency for ring hydrogenation, but it

suffers from lower conversion, which may be due to severe catalyst poisoning by amines. But, interestingly, the activity and selectivity of Pt catalyst was reported to increase over Pd for higher molecular weight of ketones and amines as substrates such as *p*-aminodiphenylamine (PAPD) and methyl isobutyl ketone (MIBK) as shown in Table 1.12. Therefore, the nature of amine and ketone are also important in selecting a suitable catalyst for this class of reaction. A detailed literature report on reductive alkylation with specific examples of amines (or precursors), carbonyls (or alkylating agents), catalysts and reactors are presented in Table 1.13.

Rusek[204] reported *N*-monoalkylation of sterically hindered amines with secondary alcohols with Pt/SiO_2 catalyst in the presence of metallic promoters like Sn, Ge, Re etc. and found that $Pt\text{-}Sn/SiO_2$ pretreated with Ca^{2+} gave the best result (Figure 1.9 and Table 1.13). The authors proposed that alcohol dehydrogenates to the corresponding ketone, which reacts with the amine to form imine intermediate. In contrast to copper chromite catalyst, which is the active catalyst for primary alcohols only, this Pt based catalyst was active for secondary alcohols too.

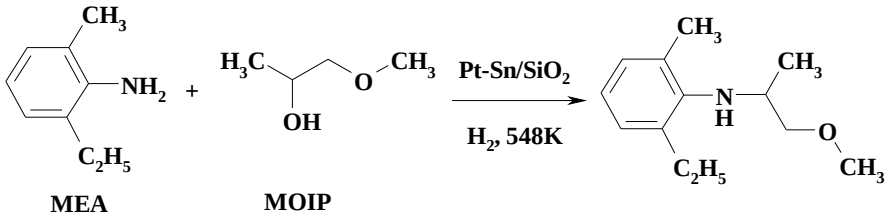

Figure 1.9. *N*-alkylation of sterically hindered amines with alcohols

The influence of acidity or basicity of faujasites and effect of temperature are discussed for gas phase alkylation of aniline with methanol. As proposed by Su *et. al.,* [205] the reaction starts with the formation of methyl carbocation (CH_3^+).

Table 1.13. Literature Survey on Reductive Alkylation of Aromatic Amines and Carbonyl Compounds (and their precursors)

No.	Substrates	Catalyst	Reaction conditions	Reactor	Remarks	Ref.
1	2-Methyl-6-ethylaniline (MEA) and methoxy-2-propanol (MOIP)	Pt-Sn/SiO_2 pretreated with Ca^{2+}	Feed: MEA: MIOP=0.5 (3ml/h); P_{H2}: 1 atm; H_2: 4.7 ml/min.; 548K	Microreactor quartz tube	Conversion (MEA): 36.4; selectivity (N-alkylated product): 76.2.	204
2	Aniline and methanol	LiY and NaY non-protic and non-basic zeolites	Aniline: MeOH, 3:1; 623-723K	Fixed bed Reactor	Conv. (aniline): 100; Sel. (N-methyl aniline, N, N-dimethyl aniline and toluidine): 60, 6 and 34 respectively.	205
3	2-Butoxy-5-tert-octylnitrobenzene and butanal p-alkoxy nitrobenzene and benzaldehyde	Pd/C Pd/C	353K; P_{H2}: 30kg/cm^2; solvent: EtOH; time: 5h	Stirred autoclave	N, N-dibutyl-2-butoxy-5-tert-octylaniline is the major product (yield 98.1%). N,N-dibenzyl compound (yield 91.4).	206
4	3-Aminobenzoic acid and aqueous HCHO	Pd/C	323K; P_{H2}: 5kg/cm^2; solvent: MeOH; time:1 h		3-dimethylamino benzoic acid is the major product (95.5%)	207
5	Aromatic amines and aldehydes	3-5% Pt/C	303-348K; P_{H2}: 15 bar; solvent: MeOH	Slurry reactor (2 lit)	Conv. (aniline): 100%, sel. (N-mono and di alkylated pdt.): 47 and 18% at 3.5 h at 314K. Conv (aniline): 100%, sel. (N-mono and di alkylated pdt.): 10 and 47% at 10 h at 314K.	208

No.	Substrates	Catalyst	Reaction conditions	Reactor	Remarks	Ref.
6	Aromatic amines and aldehydes	3-5% Pt/C	303-348K; P_{H2}: 15 bar; solvent: MeOH	Loop slurry reactor		209
7	*p*-Phynelenediamine and isobutyl ketone	63% Ni on kieselguhr; organic/inorganic acid; organic sulfur containing compound	438K; P_{H2}: 750-1000 ponds; 4h	Slurry reactor (1 lit)		210
8	3,4-$Me_2C_6H_3NH_2$ (3,4-xylidine) and 2-heptanone	5% Pt/C; 2-napthalene sulfonic acid	P_{H2}: 47 psi; 343K; 0.75 h	Slurry reactor	Conv. 100; yield and purity (N-2-heptyl-3,4-xylidine) 99 and 100.	211
9	$NH(C_6H_4NO_2)_2$ and methyl isobutylketone	Pt/C	353-383K; P_{H2}: 100 kg/cm^2	Slurry reactor	Sel. $NH(C_6H_4NHCH MeCH_2CHMe_2)$: 100.	212
10	Aniline and acetophenone	3% PtS_x/C (sulfided catalyst)	398K; 500-800 psig; 3.5h; solvent: aniline	Slurry reactor (1 lit)	Yield of N-phenyl-α-methylbenzylamine: 94%.	213
11	Amides and carbonyls	10% Pd/C; sodium sulfate	373K; 40 bar; solvent: ethyl acetate	Slurry reactor	Isolated yield: 81-98	203a
12	Nitro aromatics and α-ketoester	10% Pd/C; sodium sulfate	293K; 50 bar; solvent: cyclohexane	Slurry reactor	Isolated yield: ≥ 60	203b
13	L- α-Methyl benzylamine and α-ketobutanoicacid	10% Pd/C	303K; 50 psi; solvent: EtOH; 10h		L-2-aminobutanoic acid (after debenzoylation): yield 84.9, enantioselective excess: 81.4%.	214

No.	Substrates	Catalyst	Reaction conditions	Reactor	Remarks	Ref.
14	4-nitrodiphenylamine, methyl isoamyl ketone (MIAK); methyl isobutyl ketone (MIBK) (after the rx^n with MIAK)	1% Pd/C (63% water) and acidic carbon co-catalyst	393K; ~30 bars; 113 min. 423K; ~30 bars; 95 min	Slurry reactor	N-(1,4-dimethylamyl)-N'phenyl-*p*-phynelene diamine (50.8); N-(1,3-dimethylbutyl)-N'-phenyl-*p*-phynelene diamine (48.7)	215
15	2-methyl-5-ethyl-aniline (MEA) and methoxy acetone (MOA)	5%Pt/C, H_2SO_4	323K, 5 bar	Batch reactor	N-methoxy propyl-2-methyl-5-ethyl-aniline (intermediate for metolachlor)	216
16	Aliphatic amines and ketones	5% Pd/C, 5% Pt/C	320-473 K 23-54 bars 60-30 min.	Slurry Reactor	96% yield of tertiary amine; Slower reductive alkylation from secondary to tertiary than primary to secondary	217
17	2-ethyl-6-methyl-aniline (1.73 mol); Methoxyacetone (2.01 mol); Water (1.11mol)	5% Pt/C (3.7g) 96% H_2SO_4 (0.0438 mol)	313-318K 4.8-5 bars Time: 4.5 hrs.	Slurry Reactor	Conversion: 98.5-100% Selectivity: 97% Yield: 98.7% High turnover of Pt catalyst is achieved	218
18	Reductive isopropylation of benzene with acetone	Nano-Copper Chromite Loaded H-Mordenite	Benzene:Acetone (4:1), 403-523K	Fixed Bed Reactor	Conversion (Acetone):70%, Selectivity(Cumene):100%	219

Use of nitro compounds as precursors for amine compounds in the reductive alkylation reactions are reported by Kaneko *et.al.*[206] Aromatic nitro compounds containing alkyl, alkoxy, carboxylic, ester functionalities in *o*-, *m*-, *p*- positions are reductively alkylated with a wide range of aliphatic and aromatic aldehydes in presence of Pd or Pt catalysts. It was observed that lower homologues of aliphatic aldehydes (e.g., butyraldehyde or iso-butyraldehyde) give *N*, *N*-dialkylated products in good yields (>85%) even if there is an *o*-substitution in the nitro compound. Benzaldehyde was reported to produce *N*, *N*-dialkylated product with the nitro compound having no *o*-substituents (Figure 1.10).

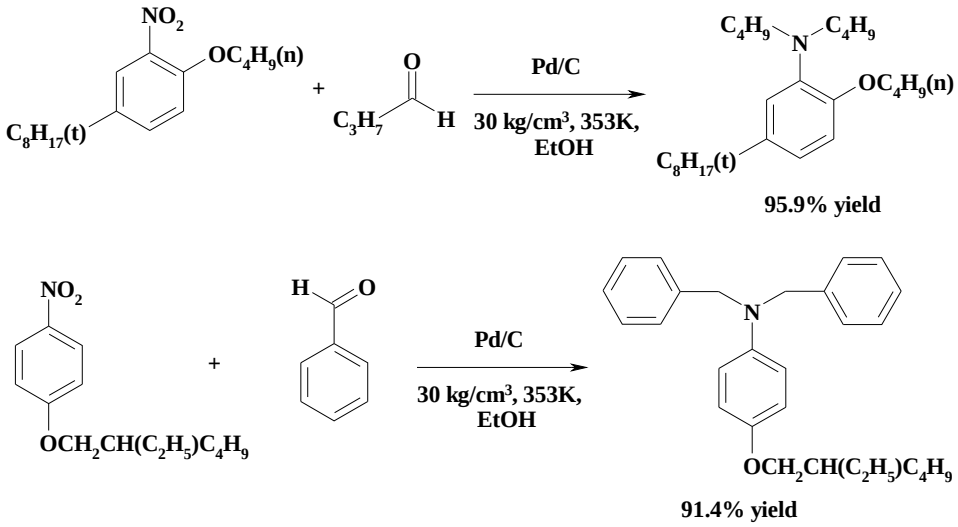

Figure 1.10. Reductive alkylation of nitro-compounds with aldehydes

Watanabe[212] reported reductive alkylation of di-nitro compounds with aliphatic ketones in the presence of Pt/C or copper-chromium bimetallic catalysts.

Malz *et. al.*[213] reported the *N*-alkylation of aniline using acetophenone as a carbonyl compound. The product, *N*-phenyl-α-methylbenzylamine is useful as an antioxidant in petroleum and synthetic industries. As reported by Rylander,[220] the main issue in using acetophenone is its hydrogenolysis to ethyl benzene in the presence of normal transition metal catalysts and hydrogen. Sulfur poisoned catalysts solved this problem and Pt was reported as the best catalyst (yield: 94%). 5% RuS_x/C and RhS_x/C gave *N*-phenyl-α-methylbenzylamine in 80% and 72% yields respectively.

Metolachlore is the active ingredient of Dual®, one of the most important grass herbicides for use in maize and a number of other crops. It is synthesized by the following transformations (Figure 1.11):[216] Ciba-Giegy Corporation introduced the product to the market in 1976 as a mixture of four stereoisomers. Later in 1982, it was found that only two isomers were active as herbicides. It was found that enantioselective hydrogenation of the imine (Schiff's Base) compound formed in the reductive alkylation gives the desired active metolachlors. In 1997, [Ir (cod) Cl]$_2$ with xyliphos ligand was reported as the catalyst for the imine hydrogenation at 80 bar and 323K.

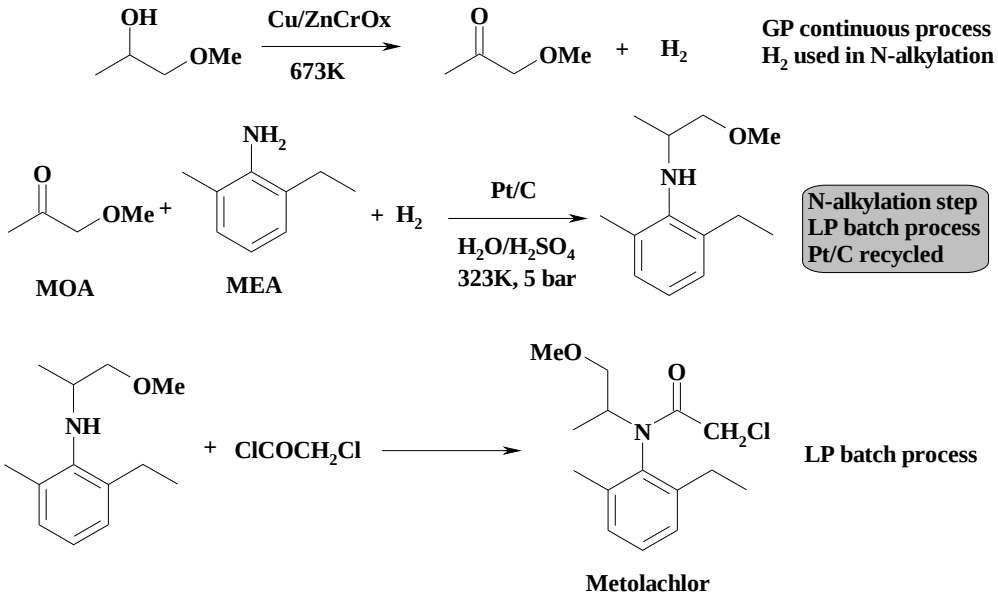

Figure 1.11. Synthesis of Metolachlor by reductive alkylation reaction

Lehtonen *et. al.*[208] have proposed a kinetic model for reductive alkylation of aromatic amine with alkyl substituents in the ring and a short chain aldehyde (having less than three carbon atoms), applicable for laboratory as well as industrial scale semibatch slurry reactor taking into account the mass transfer at the gas-liquid interface. Imine formation by homogeneous reaction was found to be non-catalytic. The imine reacts with hydrogen on the active Pt metal surface to produce the *N*-alkylated amine. Further, the catalytic three-phase reaction including homogeneous liquid-phase steps were simulated in a loop reactor by Salmi *et. al.*[209] The loop reactor was modeled using tanks-in series or alternatively, axial dispersion models. Kinetics of the reductive alkylation of aromatic amines, which was

determined from the experiments in a laboratory autoclave, was used for verifying the reactor model and for concentration profile simulations in the loop reactor.

Barman and Pradhan[219] have proposed a kinetic model for the commercially important cumene synthesis reaction by reductive isopropylation of benzene with acetone in the presence of nano-copper chromite loaded H-Mordenite (HM) catalyst. Experiments were carried out in a fixed bed reactor in a mass transfer resistance free zone by varying different parameters. The catalytic activity of the catalyst was found to increase with an increase in copper chromite content in the mordenite. The bifunctional catalyst system was found to be quite stable at an operating temperature of 443K. A detailed kinetic study was performed and various kinetic models were proposed based on Langmuir-Hinshelwood-Hougon-Watson approach. A reaction mechanism was proposed together with a rate expression for the disappearance of acetone. The kinetic and the adsorption constants of the rate equation were proposed by best fit.

Reductive alkylated derivatives of *p*-phenylene diamines, *N*, *N*'-disubstituted *p*-phenylenediamines (NNPPDA) are used as antidegradants of rubber, in particular effective in protecting vulcanized rubber from ozone attack. Blends of two or more NNPPDA are more useful in rubber industries and sold commercially after mixing them. This needs separate mixing and storage equipment. Merten *et. al.*[215] reported the synthesis of two NNPPDAs by sequential reaction of 4-nitrodiphenylamine (or its reduced forms) with two ketones. 4-nitrodiphenylamine, methyl isoamyl ketone (MIAK) was treated in a stirred reactor in the presence of Pt/C and acidic carbon co-catalysts to produce NNPPDA**1** [*N*-(1, 4-dimethylamyl)-N'phenyl-*p*-phynelenediamine]. After cooling the reaction mixture, methyl isobutyl ketone (MIBK) was added into the reaction mixture and conducted the reaction at similar conditions to react remaining unconverted 4-nitrodiphenylamine to form NNPPDA**2** [N-(1,3-dimethylbutyl)-*N*'-phenyl-*p*-phynelenediamine]. The final product constituted 50.8 and 48.7% of NNPPDA**1** and NNPPDA**2** respectively.

Malone and Merten[221] compared the reactor performance of laboratory scale (1 lit) stirred tank, Buss-Loop (50 lit) and industrial plant for reductive alkylation of 4-nitrodiphenylamine with ketone at similar conditions used by Merten *et. al.* [215] (with single ketone in contrary to the ref. 220). The authors concluded that Buss-Loop reactor improved the rate by about 100%. The efficient mixing and better heat exchange ability of the Buss-

Loop reactor was responsible for higher reaction rate and controlling the product selectivity.

1.6 BIOMASS COMBUSTION

The combustion of biomass is a chemical reaction between biomass as a fuel and an oxidizer that releases light and energy as heat. For millennia, humans have used this basic technology to create heat and later to generate power through steam. Since, biomass is the only carbon-based renewable fuel, its applications becomes more and more important for climate protection and can be considered environmental friendly for several reasons.[222] There is no net increase in CO_2 as a result of burning biomass fuel. Biomass consumes the same amount of CO_2 from the atmosphere during growth as is released during combustion. The alkaline ash from biomass also captures some of the SO_2 and CO_2 produced during combustion.[223,224]

Among the biomass thermo-chemical conversion technologies (i.e. pyrolysis, gasification and combustion), combustion is the only proven technology for heat and power production.[225] Combustion is responsible for over 97% of world's bio-energy production.[226] Biomass can be burned by direct combustion to produce steam, the steam turns a turbine and the turbine drives a generator, producing electricity. Gasifier can be used to convert the biomass into a combustible gas (biogas). The biogas is then used to drive a high efficiency combined cycle gas turbine.[227]

The direct combustion and co-firing with coal for electricity production from biomass has been found to be a promising method in the near future. Some processes such as pyrolysis, gasification, anaerobic digestion and alcohol production have widely been applied to biomass in order to obtain its energy content. Biomass can be directly fired in dedicated boilers. However, co-firing biomass and coal has technical, economical and environmental advantages over the other options. Co-firing biomass with coal, in comparison with single coal firing, helps to reduce the total emissions per unit energy produced. The biomass and the old original fuel of the industrial revolution, coal, are key to this move to a new mission. Technical issues about biomass co-firing with coal are being resolved through testing and experience.[228] Improvements with respect to efficiency, emissions and cost are needed for further exploitation. Although improvements to reduce

the emissions have been achieved by optimized furnace design including modeling, there is still a relevant potential of further optimization.[225]

A detailed literature survey relevant to the subject area of the investigation reported in the second part of the thesis on CFD modeling of biomass combustion in an entrained flow reactor is given in Chapter 5 (Section 5.1). Some important aspects of biomass combustion are reviewed in the following sections.

1.6.1 The Process of Biomass Combustion

The process of biomass combustion involves a number of complex physical/chemical aspects. The nature of the combustion process depends both on the fuel properties and the combustion application. The combustion process can be divided into following processes: drying, pyrolysis, gasification and combustion. Drying and pyrolysis will always be the first steps in a solid fuel combustion process. The relative importance of these steps will vary, depending on the combustion technology implemented, the fuel properties and the combustion process conditions. In large-scale biomass combustion applications with continuous fuel feeding, such as moving grates, these processes will occur in various sections of the grate. Figure 1.12 shows qualitatively the combustion process for a small biomass particle.[229] For large particles, there will be a certain degree of overlap between the phases.

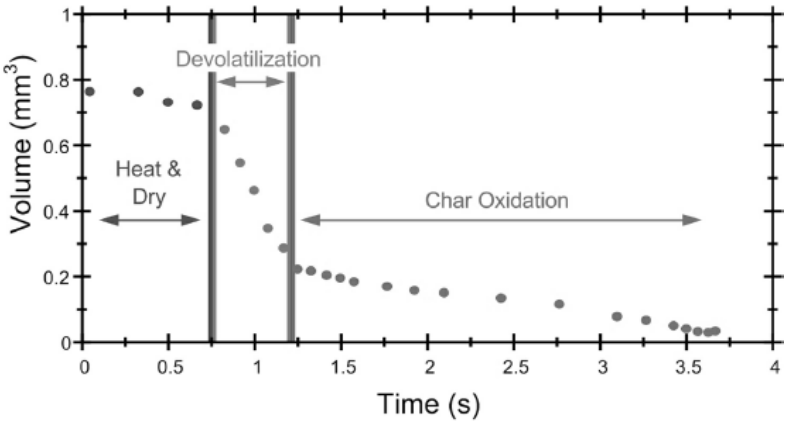

Figure 1.12. The combustion of small biomass particles proceeds in distinct stages[229]

By analogy to coal combustion, combustion of biomass can be considered as four steps: drying, devolatilization to char and volatiles and combustion of the volatiles and of the char. In most coal models, the process of drying is incorporated in the devolatilization

element. However in biomass combustion, water content is of significant importance and in some instances may dominate the combustion process. Consequently, the drying step is often treated as a separate process.[230] The steps involved in biomass combustion process are emphasized in the following sections.

1.6.1.1 Drying

Moisture will evaporate at low temperatures (< 100°C). Since vaporization uses energy released from the combustion process, it lowers the temperature in the combustion chamber, which slows down the combustion process. In wood-fired boilers, for example, the wet wood requires much energy to evaporate the contained moisture, and subsequently to heat the water vapor, which reduces the temperature below the minimum temperature required to sustain combustion. Consequently, moisture content is an important fuel variable.

1.6.1.2 Pyrolysis

Pyrolysis can be defined as thermal degradation (devolatilization) in the absence of an externally supplied oxidizing agent. The pyrolysis products are mainly tar and carbonaceous charcoal, and low molecular weight gases. In addition, CO and CO_2 can be formed in considerable quantities, especially from oxygen-rich fuels, such as biomass. The important variables that affect the amounts and properties of the products formed are fuel type, temperature, pressure, heating rate and reaction time.

The pyrolysis products can be used in a variety of ways. The char can be upgraded to activated carbon, which can be used in the metallurgical industry, as domestic cooking fuel. Pyrolysis gas can be used for heat production or power generation, or synthesized to produce methanol or ammonia.

1.6.1.3 Gasification

Gasification can be defined as thermal degradation (devolatilization) in the presence of an externally supplied oxidizing agent. However, the term gasification is also used for char oxidation reactions (for example, with CO_2 or H2O). While pyrolysis is usually optimized with respect to maximum char or tar yield and gasification is optimized with respect to

maximum gas yield. The gas contains mainly CO, CO_2, H_2O, H_2, CH_4 and other hydrocarbons. Gasification can be carried out with air and oxygen as oxidizing agents.

1.6.1.4 Combustion

Combustion can ideally be defined as a complete oxidation of the fuel. The hot gases from the combustion may be used for direct heating purposes in small combustion units, for example, water heating in small central heating boilers, to heat water in a boiler for electricity generation in larger units, or as a source of process heat. Drying and pyrolysis will always be the first steps in a solid fuel combustion process.

1.6.2 The Chemistry of Biomass Combustion

Biomass combustion is a series of chemical reactions by which carbon is oxidized to carbon dioxide, and hydrogen is oxidized to water. Oxygen deficiency leads to incomplete combustion and the formation of many products of incomplete combustion. Excess air cools the system. The air requirements depend on the chemical and physical characteristics of the fuel. The combustion of the biomass relates to the fuel burn rate, the combustion products, the required excess air for complete combustion, and the fire temperatures.[231]

The chemical and physical compositions of fuel are important determining factors in the characteristics of combustion. Biomass can be analyzed by breaking it down into structural components (called as proximate analysis) or into chemical elements (called as ultimate analysis). In general, combustion properties of biomass can be classified as macroscopic or microscopic. The macroscopic properties of biomass fuels are given for macroscopic analysis, such as ultimate analysis, heating value, moisture content, particle size, bulk density, and ash fusion temperature. Properties for microscopic analysis include thermal, chemical kinetic and mineral data.[232] Fuel characteristics such as ultimate analysis, heating value, moisture content, particle size, bulk density, and ash fusion temperature of wood fuels have been reviewed by Bushnell *et. al.*[233] Fuel characteristics include proximate analysis, ultimate analysis, chlorine content, higher heating value, ash elemental analysis, and trace metal content on a selective basis.[234]

Physical property values vary greatly and properties such as density, porosity, and internal surface area are related to biomass species whereas bulk density, particle size, and shape distribution are related to fuel preparation methods.

Important chemical properties for combustion are the elemental analysis, proximate analysis, analysis of pyrolysis products, higher heating value, heat of pyrolysis, heating value of the volatiles, and heating value of the char.

Thermal property values such as specific heat, thermal conductivity, and emissivity vary with moisture content, temperature, and degree of thermal degradation by one order of magnitude. Thermal degradation products of biomass fuels consist of moisture, volatiles, char and ash.

Main combustion reactions are:

Non-reacting solid →Heat, drying → Pyrolysis (Volatiles) → Pre-combustion reactions → Primary gas phase combustion → Secondary combustion → Effluent stack gas

Figure 1.13 shows the simple combustion model. The biomass fuels are thermally degradable and under the influence of sufficiently strong energy source, they break down into volatiles and carbonaceous char. The two modes of combustion (solid char and gaseous volatiles) have completely different chemical mechanisms and kinetics.

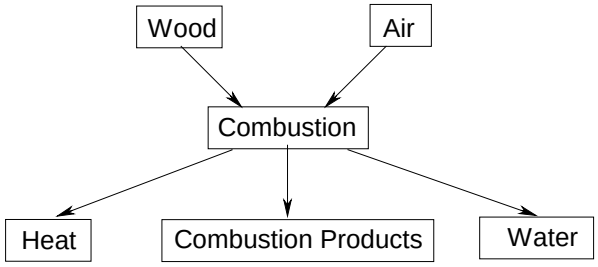

Figure 1.13. A simple model for biomass combustion

1.6.3 Solid Fuel Kinetics and Gas Phase Interaction

The main controlling factor in the combustion process is the heterogeneous combustion of the char remaining after drying and pyrolysis has occurred. Combustion of the char, which contains mainly carbon, requires that oxygen/oxidant is transported into the char surface by diffusion/convection, where it is adsorbed. The oxygen/oxidant then reacts heterogeneously on the surface with carbon; hereafter the product formed in the reaction

desorbs, and is carried away from the particle by diffusion/convection. The product is mainly CO_2 or CO. Final burnout of CO takes place in the gas phase, controlled by gas-phase chemical kinetics. The surface reaction is controlled by heterogeneous chemical kinetics, while the other steps are controlled by physical processes. Compared to gas phase combustion, heterogeneous combustion is usually slow. This has major implications e.g. for entrained flow combustion applications for pulverized fuels. Here it is essential to allow for a total residence time in the combustion application that satisfies the time requirements for drying, pyrolysis, gas phase combustion and heterogeneous combustion. Hence, the particle size must be small. Unburned carbon reduces the heat release and therefore the combustion efficiency.[235]

1.6.4 Scope of Modeling of Biomass Combustion

Modeling, together with experiments, enables a cost-effective approach for future biomass combustion application design, and can improve the competitiveness of biomass combustion for heat and electricity generation. Various types of modeling tools exist, from simple heat and mass balance models to high user level and time-consuming computational fluid dynamics (CFD) tools, as illustrated in Figure 1.14.

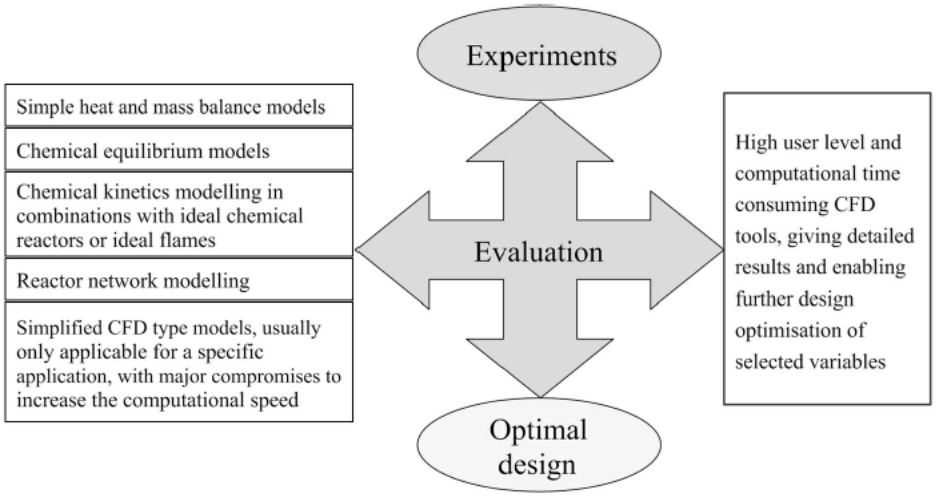

Figure 1.14. Modeling tools[235]

Modeling improves understanding of the fundamental processes involved in biomass combustion, and may significantly reduce the 'trial and error' development time needed, if experiments only are used for design optimization. By combining modeling with experiments, an improved design is possible with respect to the reduction of emissions from both incomplete and complete combustion. Parametric studies can be carried out that reveal the relative influence of different combustion process variables on emission levels and energy efficiency. This enables us to make the correct decisions with respect to the optimal design and operational principles of the biomass combustion application.

The CFD modeling tools have a high user level and the amount of computational time needed is high, when combining flow calculations and chemical kinetics, even with the most advanced computers. Hence, in reality, simplifications have to be made that reduce the reliability of the modeling results. Also, the fact that biomass is a solid fuel, which introduce additional complications with regard to devolatilization behavior and solids combustion, compared to gas combustion. At present, research is being carried out in many countries to improve understanding of the fundamental processes involved in biomass combustion and in the development of models that can effectively be included in CFD tools. A number of parameters are required as inputs to existing CFD particle combustion models, such as devolatilization yields and rates, composition of volatiles, amount of char formed and char burning rates.

There are other modeling tools also, which can be combined with experiments, such as simple heat and mass balance models, chemical equilibrium models, chemical kinetics modeling in combination with ideal chemical reactors, reactor network modeling, and simplified CFD-type models.[235] Further information and references on CFD modeling of biomass combustion are given in Chapter 5 (Section 5.1).

1.7 SCOPE OF THE PRESENT WORK

It is evident from the literature review presented here that extensive work on modeling of multiphase reactors has been carried out previously. But, the focus to analyze multistep, complex multiphase reactions has been inadequate. Therefore, investigations on more case studies of practical relevance with special emphasis on reaction engineering aspects will be immensely valuable for process optimization as well as for designing of multiphase

reactors for industrial scale operations with high level of confidence. Further, the results would allow the development of diagnostic tools to evaluate the significance of various parameters such as mass transfer, mixing, heat transfer, hydrodynamics and reaction parameters in the overall performance of the reactors and to propose scale up guidelines. Therefore, the following specific problems were chosen for the present work, divided in two parts:

PART-I:

- √ Kinetics and modeling of semi-batch slurry reactor for reductive alkylation of phenylenediamines with methyl ethyl ketone: Influence of substrates isomeric structures
- √ Modeling of bubble column slurry reactor (BCSR) for reductive alkylation of *p*-phenylenediamine
- √ Comparative modeling of fixed bed and slurry reactors for reductive alkylation of *p*-phenylenediamine

PART-II:

- √ CFD modeling of pulverized biomass combustion in an entrained flow reactor

NOMENCLATURE

A^*	saturation solubility of gas A, kmol/m^3
B_{li}	concentration of component B at t=0, kmol/m^3
D_e	effective diffusivity, m^2/s
$k_L a_B$	gas-liquid mass transfer coefficient, s^{-1}
$k_s a_p$	liquid-solid mass transfer coefficient, s^{-1}
k_i	reaction rate constants (m^3/kg)(m^3/kmol.s)
R	radius of catalyst pellet, m
w	catalyst weight, kg/m^3
t_B	batch time required to achieve conversion of B, s
X_B	conversion of B
ρ_l	density of particle, kg/m^3
ν	stoichiometric coefficient

REFERENCES

1. Ranade, V. V. Computational Flow Modeling for Chemical Reactor Engineering, Academic Press, London, **2002**.
2. Weissermel, K.; Arpe, H-J. Industrial organic chemistry, 2nd edition; VCH Press: Weinheim, **1993**.
3. Duducovic, M. P.; Larachi, F.; Mills, P.L. Multiphase Catalytic Reactors: A perspective on current knowledge and future trends. *Catalysis Reviews*, **2002**, *44 (1)*, 123.
4. (a) Shah, Y. T. Gas-Liquid-Solid Reactor Design, McGraw Hill, New York. 1979. (b) Shah, Y. T. Design Parameters for Mechanically Agitated Reactors. *Adv. Chem. Eng.*, **1991**, *17*, 1. (c) Ramachandran, P. A.; Chaudhari, R. V. *Three Phase Catalytic Reactors*. Gordon & Breach: New York, **1983**. (d) Doraiswamy, L. K.; Sharma, M. M. Heterogeneous Reactions, Wiley, New York. **1984**, *vol-2*. (e) Gianetto, A.; Silveston, P.L. eds., Multiphase chemical reactors, Hemisphere, Washington, DC. **1986**. (f) Mills, P. L.; Ramachandran, P. A.; Chaudhari, R. V. Multiphase chemical reactors for fine chemicals and pharmaceuticals. *Rev.Chem. Eng*., **1992**, *8*, 1. (g) Donati, G.; Paludetto, R. Scale up of multiphase reactors. *Catalysis Today*, **1997**, *34*, 483. (h) Thoenes, D. Current problems in modeling of chemical reactors. *Chem. Eng. Sci.*, **1980**, *35*, 1840.
5. Doraiswamy, L.K.; Gokarn, A.N. Less known behavior of gas-solid reactions: The expanding core model in catalytic and non-catalytic systems. *Chem. Eng. Technol.*, **1988**, *11*, 438.
6. Bonnemann, H.; Brijoux, W.; Tilling, A. S.; Siepen, K. Application of heterogeneous colloid catalysts for the preparation of fine chemicals. *Top. Catal.*, **1998**, *4*(3,4), 217.
7. Kukula, P.; Cerveny, L. The kinetics of methyl sorbate hydrogenation. *Appl. Catal., A*, **1999**, *177*(1), 79.
8. Mori, T.; Matsuo, N. Preparation of trans-3-(1-propynyl)-2,2-dimethylcyclopropanecarboxylate compounds. EP 955287, **1999**.
9. Broecker, F.-J.; Arnold, L.; Grafen, P. Palladium catalysts, their preparation, and their use as hydrogenation catalysts. EP 412415, **1991** by BASF.
10. (a) Zajacek, J. G.; Shum, W. P. Hydroformylation process and rhodium-dimethyl (alkyl) phosphine catalysts for the manufacture of 1,4-butanediol from allyl alcohol and synthesis gas. WO 00/63143, **2000** by Arco Chemical Technology. (b) Chen, S. C.; Chu, C. C.; Lin, F. S.; Chou, J. Y.; Huang, C. C. Modified Raney nickel catalyst and a process for preparing diols by using the same. US 5888923, **1999,** by Dairen Chemical Corporation, Taiwan.
11. (a) Blaser, H.-U,; Studer, M. Critical issues for using enantioselective catalysis for fine chemicals production. *Chirality*, **1999**, *11*(5/6), 459. (b) Chen, B.; Dingerdissen, U.; Krauter, J. G. E.; Lansink Rotgerink, H. G. J.; Moebus, K.; Ostgard, D. J.; Panster, P.; Riermeier, T. H.; Seebald, S.; Tacke, T.; Trauthwein, H. New developments in hydrogenation catalysis particularly in synthesis of fine and intermediate chemicals. *Applied Catalysis A: General*, **2005**, *280*(1), 17.
12. Ashina, Y.; Fujita, T.; Fukatsu, M.; Yagi, J. Dimethylamine. EP 130407 A1, **1985** by Nitto Chemical Industry Co., Ltd., Japan.
13. Studer, M.; Baumeister, P. Process for the catalytic hydrogenation of aromatic nitro compounds. WO 9636597, **1996** by Ciba Geigy AG.
14. Auer, E.; Freund, A.; Gross, M.; Hartung, R. Multimetallic catalyst and method for production of substituted aromatic amines. US 6316381, **1998** by Degussa AG.
15. Mitsui, O.; Fukuoka, Y. Process for producing cycloolefins. US 4678861, **1987** by Asahi Chemical Industry Co., Ltd., Japan
16. Ross, S. K.; Meehan, N. J.; Poliakoff, M.; C., Daniel N. Supercritical hydrogenation of substrates. WO 2002081414, **2002** by Thomas Swan & Co. Ltd., UK.
17. Chen, B.; Dingerdissen, U.; Krauter, J. G. E.; Lansink Rotgerink, H. G. J.; Moebus, K.; Ostgard, D. J.; Panster, P.; Riermeier, T. H.; Seebald, S.; Tacke, T.; Trauthwein, H. New developments in hydrogenation catalysis particularly in synthesis of fine and intermediate chemicals. *App. Cat. A: Gen.*, **2005**, *280*(1), 17.
18. (a) Mills, P. L.; Ramachandran, P. A.; Chaudhari R. V. Multiphase reaction engineering for fine chemicals and pharmaceuticals. *Rev. Chem. Eng.*, **1992**, *8*, 1. (b) Carpenter K. J. Chemical reaction engineering aspects of fine chemicals manufacture, *Chem. Eng. Sc.*, **2001**, *56*, 305.
19. (a) Rajashekharam, M. V.; Nikalje, D. D.; Jaganathan, R.; Chaudhari, R. V. Hydrogenation of 2,4-dinitrotoluene using a Pd/Al2O3 catalyst in a slurry reactor: a molecular level approach to kinetic modeling and nonisothermal effects. *Ind. Eng. Chem. Res.*, **1997**, *36*(3), 592. (b) Benaissa, M.; Le Roux,

G. C.; Joulia, X.; Chaudhari, R. V.; Delmas, H. Kinetic modeling of the hydrogenation of 1,5,9-cyclododecatriene on Pd/Al2O3 catalyst including isomerization. *Ind. Eng. Chem. Res.*, **1996**, *35*(7), 2091. (c) Lylykangas, M. S.; Rautanen, P. A.; Krause, A. O. I. Hydrogenation and Deactivation Kinetics in the Liquid-Phase Hydrogenation of Isooctenes on Pt/Al2O3. *Ind. Eng. Chem. Res.*, **2004**, *43*(7), 1641. (d) Chaudhari, R. V.; Jaganathan, R.; Kolhe, D. S.; Emig, G.; Hofmann, H. Kinetic modeling of a complex consecutive reaction in a slurry reactor: hydrogenation of phenyl acetylene. *Chem. Eng. Sci.*, **1986**, *41*(12), 3073.

20. Kuipers, J.A.M.; Van Swaaij, W.P.M. Computational fluid dynamics applied to chemical reaction engineering. *Rev. Chem. Eng.*, **1997**, *3*, 1.
21. Deemter Van, J. J. Third symposium on chemical reaction engineering. Pergamon press. Elmstord New York, **1965**, p-215.
22. Conen, W.E. *J. Am. Oil Chemists Soc.*, **1976**, *53*, 382.
23. Applevard, C.J.; Gartshore F.C. Manufacture of butynediol at IC cudwigs hafen. BIOS Report 367, item 22, **1946**.
24. Rosenwald, R. H.; Springs, W.; James, R. Reductive alkylation process. US 2779789, **1957**.
25. Goodyear tyre and rubber company, USA. Catalytic reductive alkylation process. US 1116967, **1968**.
26. Fujimoto, K. *Ind. Eng. Prod. Res. Dev.*, **1976**, *15*, 259.
27. Komiyama, H.; Smith, J. M. Sulfur dioxide oxidation in slurries of activated carbon: Part-1: Kinetics. *A.I. Ch. E. J.*, **1975**, *21(4)*, 664.
28. Pitman, C.U.; Smith, L.R.; Hanes, R.M. *J. Am. Chem. Soc.*, **1972**, *27*, 867.
29. Kale S.S.; Chaudhari, R.V. Paper presented on 4th National Symposium on Catalysis. IIT Bombay, **1978**.
30. Shah Y. T., Gas-Liquid-Solid reactor design, McGraw-Hill, New York, **1979**
31. Chaudhari, R. V.; Ramachandran, P. A. Three phase slurry reactors. *A.I.Ch.E. J.*, **1980**, *26 (2)*, 177.
32. Chaudhari, R. V.; Shah, Y. T.; Foster, N.R. Novel gas-liquid-solid reactors. *Catal. Rev. Sci. Eng.*, **1986**, *28(4)*, 431.
33. Mills, P. L.; Chaudhari, R. V. Multiphase catalytic reactor engineering and design for pharmaceuticals and fine chemicals. *Catalysis Today*, **1997**, *37*, 367.
34. Goto, S.; Smith, J.M. Performance of slurry and trickle bed reactors: Application to sulfur dioxide removal. *A.I.Ch.E. J.*, **1978**, *24*, 286,
35. Goto, S.; Watabe, S.; Matsubara, M. The role mass transfer in trickle bed reactors. *Can. J. Che. Eng.*, **1976**, *54*, 551.
36. Ramachandran, P.A.; Smith, J.M. Mixing cell method for the design of trickle bed reactors. *Chem. Eng. J.*, **1979**, *17*, 91.
37. Kenney, C. N.; Sedriks, W. Effectiveness factors in a three-phase slurry reactor: the reduction of crotonaldehyde over a palladium catalyst. *Chem. Eng. Sci.*, **1972**, 27, 2029.
38. Kawakami, K.; Kusunoki K. Selectivity in consecutive hydrogenation of chlorobenzene in liquid phase. *Kagaku Kogaku Ronbunshu*, **1975**, *1*, 559.
39. Kawakami, K.; Kusunoki K. The effects of Intraparticle diffusion on the yield of the liquid phase hydrogenation of phenylacetylene in a stirred basket reactor. *J. Chem. Eng. Japan*, **1976**, *9 (6)*, 469.
40. Kut, O. M.; Gut, G.; Buehlmann, T.; Lussy, A. Mass transfer with chemical reaction in multiphase systems. Ed. Alper E., (NATO series), Martinus Nijhoff Publishers, The Hauge, **1983**, *2*, 228.
41. Chaudhari, R. V.; Parande, M. G.; Ramachandran, P. A.; Brahme, P. H.; Vadgaonkar, H. G.; Jaganathan R. Hydrogenation of butynediol to cis-butenediol catalyzed by Pd-Zn-CaCO3, Reaction kinetics and modeling of a batch slurry reactor. *A.I.Ch.E. J.*, **1985**, *31*, 1891.
42. Chaudhari, R. V.; Jaganathan, R.; Kohle, D. S.; Emig G.; Hofmann H. Kinetic modeling of a complex consecutive reaction in a slurry reactor: Hydrogenation of phenyl acetylene. *Chem. Eng. Sci.*, **1986**, 41, 3073.
43. Chaudhari, R. V.; Jaganathan, R.; Kohle, D. S.; Emig, G.; Hofmann H. Kinetic modeling of hydrogenation of butynediol using a 0.2%Pd/C catalyst in a slurry reactor. *Appl. Catal.*, **1987**, *29*, 141.
44. Santacesaria, E.; Di Serio, M.; Velotti, R.; Leone, U. Kinetics, mass transfer and palladium catalyst deactivation in the hydrogenation step of the hydrogen peroxide synthesis via anthraquinone. *Ind. Eng. Chem. Res.*, **1995**, *33*, 2349.
45. Holm, D. R.; Hill, Jr. C. G.; Connor, A. H. Kinetics of liquid phase hydrogenations of furan amines. *Ind. Eng. Chem. Res.*, **1995**, *34*, 2349.

46. Toppinen, S.; Rantakyla, T. K.; Salmi, T.; Aittamaa J. Kinetics of the liquid phase hydrogenation of benzene and some mono substituted alkylbenzenes over a nickel catalyst. *Ind. Eng. Chem. Res.*, **1996**, *35*, 1824.
47. Benaissa, M.; Le Roux, G. C.; Joulia, X.; Chaudhari, R. V.; Delmas H. Kinetic modeling of the hydrogenation of the hydrogenation of 1,5,9-Cyclododecatriene on Pd/Al2O3 catalyst including isomerization. *Ind. Eng. Chem. Res.*, **1996**, *35*, 2091
48. Bergault, I.; Fouilloux, P.; Joly-Vuillemin, C.; Delmas H. Kinetics and Intraparticle Diffusion Modeling of a complex Multistep Reaction: Hydrogenation of Acetophenone over a Rhodium Catalyst. *J. Cat*., **1998**, *175*, 328.
49. Rajasekharam, M.V.; Chaudhari, R.V. Hydrogenation of 2,4-dinitrotoloune using a supported Ni catalyst: Reaction kinetics and semibatch slurry reactor modeling. *Ind. Eng. Chem. Res.*, **1999**, *38*, 906.
50. Jaganathan, R.; Ghugikar, V. G.; Gholap, R. V.; Chaudhari, R. V.; Mills, P. L. Catalytic hydrogenation of *p*-nitrocumene in a slurry reactor. *Ind. Eng. Chem. Res.*, **1999**, *38*(12), 4634.
51. Rajashekharam, M. V.; Nikalje, D. D.; Jaganathan, R.; Chaudhari, R. V. Hydrogenation of 2,4-dinitrotoluene using a Pd/Al2O3 catalyst in a slurry reactor: a molecular level approach to kinetic modeling and nonisothermal effects. *Ind. Eng. Chem. Res.*, **1997**, *36*(3), 592.
52. Lylykangas, M. S.; Rautanen, P. A.; Krause, A. O. I. Hydrogenation and Deactivation Kinetics in the Liquid-Phase Hydrogenation of Isooctenes on Pt/Al2O3. *Ind. Eng. Chem. Res.*, **2004**, *43*(7), 1641.
53. Neri, G.; Bonaccorsi, L.; Mercadante, L.; Galvagno, S. Kinetic analysis of cinnamaldehyde hydrogenation over alumina-supported ruthenium catalysts. *Ind. Eng. Chem. Res.*, **1997**, *36*(9), 3554.
54. Toppinen, S.; Rantakylae, T.-K.; Salmi, T.; Aittamaa, J. Kinetics of the liquid-phase hydrogenation of benzene and some monosubstituted alkylbenzenes over a nickel catalyst. *Ind. Eng. Chem. Res.*, **1996**, *35*(6), 1824.
55. Zhang, Z.; Jackson, J. E.; Miller, D. J. Kinetics of aqueous-phase hydrogenation of lactic acid to propylene glycol. *Ind. Eng. Chem. Res.*, **2002**, *41*(4), 691.
56. Lehtonen, J.; Salmi, T.; Vaori, A.; Tirronen, E. On the principles of modeling of homogeneous-heterogeneous reactions it the production of fine chemicals. A case study: Reductive alkylation of aromatic amines. *Org. Pros. Res. Dev.*, **1998**, *2(2)*, 78.
57. Roy, D.; Jaganathan, R.; Chaudhari, R. V.; Kinetic modeling of Aniline with Acetone using 3% Pd/Al2O3 catalyst in a batch slurry reactor. *Ind. Eng. Chem. Res.*, **2005**, *44*, 5388.
58. Gerstenberg, H. Bubble column reactors. *Chemie Ingenieur Technik*, **1979**, *51*, 208.
59. Steiner, R. Operation characteristics of special bubble column reactors. *Chem. Eng. Process.*, **1987**, *21*, 1.
60. Jakobsen, H.A.; Lindborg, H.; Dorao, C.A. Modeling of bubble column reactors: Progress and limitations. *Ind. Eng. Chem.Res.*, **2005**, *44*, 5107.
61. Kantarci, N.; Borak, F.; Ulgen, K.O. Bubble column reactors. *Process Biochemistry*, **2005**, *40*, 2263.
62. Joshi, J.B. Computational flow modeling and design of bubble column reactors. *Chem. Eng. Sci.*, **2001**, *56*, 5893.
63. Schluter, S. Modellierung and Simulation von Blasensaulenreaktoren, *Doctoral Thesis*, Univ. Dortmund, **1992**.
64. Wachi, S.; Morikawa, H. Chlorination of ethylene in a boiling bubble column reactor, *J. Chem. Eng. Jpn.*,**1987**, *20*, 238.
65. Levenspiel, O. *Chemical Reaction Engineering*, Wiley, New York, 2nd edn. **1972**.
66. Ueyama, K.; Miyauchi, T. Properties of recirculating turbulent two phase flow in gas bubble columns. *A.I.Ch.E. J.*, **1979**, *25*, 258.
67. Wachi, S.; Morikawa, H.; Ueyama, K. Gas holdup and axial dispersion in gas-liquid cocurrent bubble columns, *J. Chem. Eng. Jpn.* **1987**, *20*, 309.
68. Whalley, P.B.; Davidson, J.F. Liquid circulation in bubble columns. *Inst. Chem. Eng. Symp.* **1974**, *38*, 1.
69. Joshi, J.B.; Sharma, M.M. A circulation cell model for bubble columns. *Trans. Inst.* Chem. *Eng.*, **1979,** *57*, 244.
70. Joshi, J.B. Axial mixing in multiphase contactors-a unified correlation. *Trans. Inst.* Chem. *Eng.*, **1980**, *58*, 155.
71. Zehner, P. Impuls-, StoB- und Warmetransport in BlasensHulen -Teil 1: Stromungsmodell der Blasensiiule und Fliissigkeitsgeschwindigkeiten, *Verfahrenstechnik*, **1982**, *16*, 347.
72. Zehner, P. Impuls-, Stotf**, a**nd Wlrmetransport in Blasen- saulen-Teil 2: Axiale Durchmischtmg and WPrmeiibergang, *Verfahrenstechnik*, **1982**, *16*, 514.

73. Joseph, S.; Shah, Y.T. A two bubble class model for churn turbulent bubble column slurry reactor. *ACS Symp.*, **1983**, *Ser. No. 237*, 151.
74. Joseph, S.; Shah, Y.T.; Smith, D.N.; Ruether, J.A. Two-bubble class model for churn turbulent bubble column reactor. *Ind. Eng. Chem., Process Des. Dev.* **1985**, *24*, 1096.
75. Popovic, M.; Deckwer, W.D. Berechnung axialdurchmischter Rohrreaktoren als Riihrkesselkaskade mit Rticklauf. *Chem.-Ing.-Tech.*,**1973**, *45*, 984.
76. Popovic, M. Eindimensionale Zellenmodelle fiir Gas-Fhissigphase-Reaktoren mit axialer Durchmischung, *Doctoral Thesis*,Tech. Univ. Berlin, **1975**.
77. Mecklenburgh, J.C.; Hartland, S. Design of reactors with backmixing: Parts I- III. *Chem. Eng. Sci.*, **1968**, *23*, 57.
78. Roemer, M.H.; Durbin, L.D. Transient response and moments analysis of backflow cell model for flow systems with longitudinal mixing. *Ind. Eng. Chem., Fundam.*, **1967**, *6*, 120.
79. Wasowski, T.; BlaB, E. Neue Aspekte zum EinfluB des Blasenwakesauf die Hydrodynamik und den Stoffaustausch in der Blasensaule. *Chem.-Zng.-Tech.*, **1989,** *61*, 519.
80. Torvik, R.; Svendsen, H.F. Modeling of slurry reactors: A fundamental approach. *Chem. Eng. Sci.*,**1990**, *45*, 2325.
81. Gasche, H.E. Modellierung von BlasensPulen, *Doctoral Thesis*,Univ. Erlangen, **1989**.
82. Chianese, A.; Annesini, M.C.; De Santis, R.; Marelli, L. A model of a pilot bubble column reactor for benzene alkylation by ethylene. Chem. *Eng. J.*, **1981**, *22*, 151.
83. Deckwer, W.D.; Serpemen, Y.; Ralek, M.; Schmidt, B. Modeling the Fischer-Tropsch Synthesis in the slurry phase. *Ind. Eng.* Chem. *Process Des. Dev.*, **1982**, *21*, 231.
84. Turner, J. R.; Mills, P.L. Comparison of axial dispersion and mixing cell models for design and simulation of Fischer-Tropsch slurry bubble column reactors. *Chem. Eng. Sci.*, **1990**, *45*, 2317.
85. Brown, D.M. Modeling of methanol synthesis in the liquid phase. *ACS Symp.*, **1983**, *Ser. No. 87*, 699.
86. Ozturk, S.S.; Shah, Y.T.; Deckwer, W.D. Comparison of gas and liquid phase methanol synthesis processes. *Chem. Eng.J.*, **1988**, *37*, 177.
87. Kuo, J. C. W. et.al. Slurry Fischer-Tropsch/Mobil-two stage process of converting syngas to high octane gasoline. *Final Rep. US Dep. Energy. Contract No. DOEPC-30022-10.* Mobil Res. Dev. Corp., NJ. **1983.**
88. Kralik, M.; Ilavsky, J. A mathematical dynamic model of the continuous bubble column slurry reactor. *Chem. Eng.Process.*, **1990**, *28*, 127.
89. Satterfield, C. N. Trickle-bed reactors. *A.I.Ch.E. J.*, **1975**, *21(2)*, 209.
90. Shah Y. T., Gas-Liquid-Solid reactor design, McGraw-Hill, New York, **1979**
91. Al-Dahhan, M. H.; Larachi, F.; Dudukovic, M. P.; Laurent A. High-pressure trickle-bed reactors: A review. *Ind. Eng. Chem. Res.*, **1997**, 36, 3292.
92. Saroha, A. K.; Nigam K. D. P. Trickle bed reactors. *Rev. Chem. Eng.*, **1996**, *12(3-4)*, 207.
93. Enright, J. T.; Chuang, T. T. Deuterium exchange between hydrogen and water in a trickle bed reactor, *Can. J. Chem. Eng.*, **1978**, *56*, 246.
94. Seirafi, H. A.; Smith J. M. Mass transfer and adsorption in liquid full and trickle beds. *A.I.Ch.E. J.*, **1980**, *26*, 711.
95. Meyers, R. A. Handbook of petroleum refining processes, 2nd ed., McGraw-Hill, New York, **1996**
96. Hofmann, H. P. Multiphase catalytic packed bed reactors. *Catal. Rev. Sci. Eng.*, **1978**, *17(1)*, 71.
97. Herskowitz, M.; Smith J. M. Trickle bed reactors: A review. *A.I.Ch.E. J.*, **1983**, *29*, 1.
98. Gianetto, A.; Specchia V. Trickle-bed reactors: State of art and perspectives. *Chem. Eng. Sci.*, **1992**, 47, 3197.
99. Lamine, A. S.; Gerth, L.; Le Gall, H.; Wild, G. Heat transfer in a packed bed reactor with cocurrent downflow of a gas and a liquid. *Chem. Eng. Sci.*, **1996**, *51(15)*, 3813.
100. Julcour-Lebigue, C.; Augier, F.; Maffre, H.; Wilhelm, A.;Delmas, H. Measurement and modeling of wetting efficiency in trickle bed reactors : Liquid viscosity and bed packing effects. *Ind. Eng. Chem. Res.*, **2009**, *48(14)*, 6811.
101. Al-Dahhan, M. H.; Dudukovic M. P. Catalyst wetting Efficiency In trickle-bed Reactors at high pressure. *Chem. Eng. Sci.*, **1995**, *50 (15)*, 2377.
102 Goto, S.; Smith, J.M. Trickle bed reactor performance Part II: reaction studies. *A.I.Ch.E. J.*, **1975**, *21*, 706.
103. Rajashekharam, M. V.; Jaganathan, R.; Chaudhari, R. V. A trickle-bed reactor model for hydrogenation of 2,4 dinitrotoluene: Experimental verification. *Chem. Eng. Sci.*, **1998**, *53(4)*, 787.

104. Khadilkar, M. R.; Jiang, Y.; Al-Dahhan, M.; Dudukovic, M. P. Chou, S. K.; Ahmed, G.; Kahney, R. Investigations of a complex reaction network: I Experiments in a high-pressure trickle bed reactor. *A.I.Ch.E. J.*, **1998**, *44 (4)*, 912.
105. Huang, T.; Kang B. Naphthalene hydrogenation over Pt/Al_2O_3 catalyst in a trickle bed reactor. *Ind. Eng. Chem. Res.*, **1995**, *34*, 2349.
106. Bergault, I.; Rajashekharam, M. V.; Chaudhari, R. V.; Schweich, D.; Delmas, H. Modeling of comparison of acetophenone hydrogenation in trickle-bed and slurry airlift reactors. *Chem. Eng. Sci.*, **1997**, *52 (21/22)*, 4033.
107. Collins, G. M., Hess, R. K.; Hook, B. D.; Ackgerman, A. Paper 31p *A.I.Ch.E. Annual Meeting*, San Fransisco, CA, **1984**.
108. Kheshgi, H. S.; Reyes, S. C.; Hu, R.; Ho, T. C. Phase Transition and Steady State Multiplicity in a Trickle-bed Reactor. *Chem. Eng. Sci.*,**1992**, *47*, 1771.
109. Mills, P. L.; Beaudry, E.G.; Duducovic, M. P. Comparison and Prediction of reactor Performance for Packed Beds with Two Phase Row: Down-flow. Up-flow and Countercurrent Row .*Inst. Chem. Eng. Symp. Ser.*, **1984**, *87*, 527.
110. Hekmat, D.; Vortmeyer, D. Modeling of Biodegradation Processes in Trickle Bed Bioreactors. *Chem. Eng. Sci.*, **1994**, *49*, 25.
111. Chu, C. F.; Ng, K. M. Liquid Dispersion in Trickle Bed Reactors with Gas-LiquidCocurrent Downflow. Paper lOp, *A.I.Ch.E. Annual Meeting, Miami Beach, FL*,**1986**.
112. El-Hisnawi, A.A. Tracer and reaction studies in trickle-bed reactors. D.Sc. Dissertation, Washington University, St. Louis, MS, **1981**.
113. Khadilkar, M. R.; Wu, Y. X.; Al-Dahhan, M. H.; Dudukovic, M. P. Comparison of trickle bed and upflow reactor performance at high pressure: Model prediction and experimental observations. *Chem. Eng. Sci.*, **1996**, *51 (10)*, 2139.
114. Sims, B. W.; Gaskey, S. W.; Luss, D. Effect of flow regime and liquid velocity on conversion in a trickle bed reactor. *Ind. Eng. Chem. Res.*, **1994**, *30*, 2530.
115. Vergel, C.; Euzen, J. P.; Trambouze, P.; Wauquier, J. P. Two-phase flow catalytic reactors, influence of hydrodynamics on selectivity. *Chem. Eng. Sci.*, **1995**, 50, 3303.
116. Valerius, G.; Zhu, X.; Hofmann, H.; Arntz, D.; Haas, T. Modeling of a trickle-bed reactor II. The hydrogenation of 3-hydroxypropanal to 1,3-propanediol. *Chem. Eng. Proc.*, **1996**, *35*, 11.
117. Korsten, H.; Hoffmann, U. Three phase reactor model for hydrotreating in pilot plant trickle-bed reactors. *A.I.Ch.E. J.*, **1996**, *42(5)*, 1350.
118. Khadilkar, M. R.; Wu, Y. X.; Al-Dahhan, M. H.; Dudukovic, M. P. Comparison of trickle bed and upflow reactor performance at high pressure: Model prediction and experimental observations. *Chem. Eng. Sci.*, **1996**, *51(10)*, 2139.
119. Stuber, F.; Benaissa, M.; Delmas, H. Partial hydrogenation of 1, 5, 9-cyclododecatriene in three phase catalytic reactors. *Catalysis Today*, **1995**, *24*, 95.
120. Ravindra, P. V.; Rao, D. P.; Rao, M. S. A model for the oxidation of sulfur dioxide in a trickle bed reactor. *Ind. Eng. Chem. Res.*, **1997**, *36*, 5125.
121. Iliuta, I.; Iliuta, M. C. Comparison of two-phase upflow and downflow fixed bed reactors performance: Catalytic SO_2 oxidation. *Chem. Eng. Technol.*, **1997**, 20, 455.
122. Pintar, A.; Bercic, G.; Levec J. Catalytic liquid-phase oxidation of aqueous phenol solutions in a trickle bed reactor. *Chem. Eng. Sci.*, **1997**, *52*, 4143.
123. Castellari, A. T.; Cechini, J. O.; Gabarian, L. J.; Haure, P. M. Gas-phase reaction in a trickle-bed reactor operated al low liquid flow rates. *A.I.Ch.E. J.*, **1997**, *43(7)*, 1813.
124. Devetta, L.; Canu, P.; Bertucco, A.; Steiner, K. Modeling of a trickle-bed reactor for a catalytic hydrogenation in supercritical CO_2. *Chem. Eng. Sci.*, **1997**, *52(21/22)*, 4163.
125. Jiang, Y.; Khadilkar, M. R.; Al-Dahhan, M. H.; Dudukovic, M. P.; Chou, S. K.; Ahmed, G.; Kahney, R. Investigations of a complex reaction network: II Kinetics, mechanism and parameter estimation. *A.I.Ch.E. J.*, **1998**, *44(4)*, 921.
126. Tukac, V.; Hanika, J. Catalytic wet oxidation of substituted phenols in the trickle bed reactor. *Chem. Eng. Technol.*, **1998**, *21*, 262.
127. Herrmann, U.; Emig, G. Liquid phase hydrogenation of maleic anhydride to 1-4, butanediol in a packed bubble column reactor. *Ind. Eng. Chem. Res.*, **1998**, *37*, 759.

128. Chaudhari, R.V.; Jaganathan, R.; Mathew, S.P.; Julcour, C.; Delmas, H. Hydrogenation of 1,5,9 Cyclododecatriene in fixed bed reactors: down-Vs-upflow modes. *A.I.Ch.E. Journal*, **2002**, *48*, 110.
129. Dietz, A.; Julcour, C.; Delmas, W.H. Selective hydrogenation in trickle bed reactor: Experimental and modeling including partial wetting. *Catalysis Today*, **2003**, *79-80*, 293.
130. Avraam, D.G.; Vasalos, I.A. Hdpro: a mathematical model of trickle bed reactors for the catalytic hydroprocessing of oil feedstocks. *Catalysis Today*, **2003**, *79-80*, 275.
131. Guo, J.; Muthanna, J.G. A sequential approach to modeling catalytic reactions in packed bed reactors. *Chem.Eng. Sci.*, **2004**, *59*, 2023.
132. Guo, J.; Al-Dahaan, M. Modeling catalytic trickle bed and upflow packed bed reactors for wet air oxidation of phenol with phase change. *Ind. Eng. Chem.. Res.*, **2005**, *44*, 6634.
133. Suwanprasop, S.; Eftaxias, A.; Stuber, F.; Polaert, I.; Julcour, C.; Delmas, H. Scaleup and modeling of fixed bed reactors for catalytic phenol oxidation over adsorptive active carbon. *Ind. Eng. Chem.. Res.*, **2005**, *44*, 9513.
134. Guo, J.; Jiang, Y.; Al-Dahaan, M.H. Modeling of trickle bed reactors with exothermic reactions using cell network approach. *Chem. Eng. Sci.*, **2008**, *63*, 751.
135. Roininen, J.; Alopaeus, V.; Toppinen, S.; Aitamma, J. Modeling and simulation of industrial trickle bed reactor for benzene hydrogenation: -Model validation against plant data. *Ind. Eng. Chem.. Res.*, **2009**, *48*, 1866.
136. Wu, Q.; Hu, X.; Yue, P.; Feng, J.; Chen, X.; Zhang, H.; Qiao, S. Modeling of a pilot scale trickle bed reactor for the catalytic oxidation of phenol. *Separation and Purification Technology*, **2009**, *67*, 158.
137. Al-Dahhan, M. H.; Dudukovic, M. P. Catalyst Bed Dilution for improving catalyst wetting in laboratory trickle bed reactors. *A.I.Ch.E. J.*, **1996**, *42(9)*, 2595.
138. Yang,. J.; Li, J. Simulation of Hydrodewaxing Reactor by Stochastic Method. *J. Chem. Eng. Chin. Univ.*, **1992**, *6*, 264.
139. Harold, M. P.; Watson, P. C. Bimolecular Exothermic Reaction with Vaporization in the Half-wetted Slab Catalyst. *Chem. Eng. Sci.*, **1998**, *48*, 981.
140. Brad Sims, W.; Gaskey, S. W.; Luss, D. Effect of Flow Regime and Liquid Velocity on Conversion in a Trickle Bed Reactor. *Ind. Eng. Chem. Res.*, **1994**, *22*, 2530.
141. Tsamatsoulis, D.; Papayannakos, N. Simulation of Non-ideal Flow in a Trickle Bed Reactor by a Cross-flow Model. *Chem. Eng. Sci.*, **1995**, *50*, 3685.
142. Jaganathan, R.; Gholap, R. V.; Brahme, P. H.; Chaudhari, R.V. Performance of a continuous bubble column slurry reactor for hydrogenation of butynediol.Proceedings of ICREC 2, NCL, India II 141,**1987**.
143. Barhme, P. H.; Chaudhari, R. V.; Ramachandran, P. A. Modeling of hydrogenation of glucose in a continuous slurry reactor. *Ind. Eng. Chem. Proc. Des. Dev.*, **1984**, *23*, 57.
144. Funk, G. A.; Harold, M. P.; Ng, K. M. Novel Model for Reaction in Trickle Beds with flow Maldistribution. *Ind. Eng. Chem. Res.*, **1990**, *29*, 738.
145. Froment, G.F.; Depauw, G.A.; Vanrysselberghe, V. Kinetic modeling and reactor simulation in hydrodesulfurization of oil fractions. Ind. Eng. Chem. Res., **1994**, *33*, 2975.
146. Berger, R.J.; Perez-Ramirez, J.; Kapteijn, F.; Moulijn, J.A. Catalyst performance testing: bed dilution revisited. *Chem. Eng. Sci.*, **2002**, *57*, 4921.
147. Iliuta, I.; Thyrion, F.C.; Muntean, O. Residence time distribution of the liquid in gas–liquid cocurrent upflow fixed-bed reactors. *Chem. Eng. Sci.*, **1996**, 51, 4579.
148. Hochman, J.M.; Effron, E. Two-phase cocurrent downflow in packed-beds. *Ind. Eng. Chem. Fundam.*, **1969**, *8*, 63.
149. Deans, H.A.; Lapidus, L. A computational model for predicting and correlating the behavior of fixed-bed reactors: 1. Derivation of model for nonreactive systems. *A.I.Ch.E. J.*, **1960**, *6*, 656.
150. Jaffe, S.B. Hot spot simulation in commercial hydrogenation processes. *Ind. Eng. Chem. Proc. Des. Dev.*, **1976**, *15*, 410.
151. Schnitzlein, K.; Hofmann, H. An alternative model for catalytic fixed bed reactors. *Chem. Eng. Sci.*, **1987**, *42*, 2569.
152. Kufner, R.; Hofmann, H. Implementation of radial porosity and velocity distribution in a reactor model for heterogeneous catalytic gas phase reactions (TORUS-Model). *Chem. Eng. Sci.*, **1990**, *45*, 2141.
153. Beaudry, E. G.; Duducovic, M. P.; Mills, P. L. Trickle Bed Reactors: Liquid Diffusional Effects in a Gas Limited Reaction. *A.l.Ch.E. J.*,**1987**, *33*, 1435.

154. Lemcoff, N. 0.; Cukierman, A.L.; Martinez, O.M. Effectiveness Factor of Partially Wetted Catalyst Particles: Evaluation and Application to the Modeling of Trickle Bed Reactors. *Catal. Rev. Sci. Eng.* , **1988**, *30*,393.
155. Herskowitz, M. Hydrogenation of benzaldehyde to benzyl alcohol in a slurry and fixed-bed reactor. *Stud. Surf. Sci. Catal.*, **1991**, *59 (Heterog. Catal. Fine Chem. 2)*, 105.
156. Iliuta, I.; Larachi, F. Wet air oxidation solid catalysis analysis of fixed and sparged three-phase reactors. *Chem. Eng. Proc.*, **2001**, *40*, 175.
157. Dassori, C. G. Three Phase Reactor Modeling with significant back mixing in the liquid phase using modified cell model (MCM). *Chem. Eng. Sci.*, **1998**, *22*, S679.
158. Goto S., Chatani T. and Matouq M. H., Hydration of 2-methyl-2-butene in gas-liquid cocurrent upflow and downflow reactors, Can. J. Chem. Eng., 71, 821, 1993
159. Wu, Y.; Khadilkar, M. R.; Al-Dahhan, M. H.; Dudukovic, M. P. Comparison of upflow and downflow two-phase flow packed bed reactors with and without fines: Experimental observations. *Ind. Eng. Chem. Res.* **1996**, *35*, 397.
160. Ragaini, V.; Tine, C. Upflow reactor for the selective hydrogenation of pyrolysis gasoline: Comparative study with respect to down flow. *Appl. Catal.*, **1984**, *10*, 43.
161. Mochizuki, S.; Matsui T. Selective hydrogenation and mass transfer in a fixed bed catalytic reactor with gas-liquid concurrent upflow. *A.I.Ch.E. J.*, **1976**, *22(5)*, 904.
162. Van Gelder, K. B.; Damhof, J. K.; Krouenga, P. J.; Westertrep, K. R. Three phase packed bed reactor with an evaporating solvent I: Experimental: The hydrogenation of 2,4,6 - trinitrotoluene in methanol. *Chem. Eng. Sci.*, **1990**, *45*, 3159.
163. Van Gelder, K. B.; Borman, P. C.; Weenink, R. E.; Westertrep, K. R. Three phase packed bed reactor with an evaporating solvent II: Modeling the reactor. *Chem. Eng. Sci..*, **1990**, *45*, 3171.
164. Hofmann, H. P. Multiphase catalytic packed bed reactors. *Catal. Rev. Sci. Eng.*, **1978**, *17(1)*, 71.
165. Julcour, C.; Stuber, F.; Le Lann, J. M.; Wilhelm, A. M.; Delmas, H. Dynamics of a three-phase upflow fixed-bed catalytic reactor. *Chem. Eng. Sci.*, **1999**, *54*, 2391.
166. Visser, J. B. M.; Stankiewicz, A.; van Dierendonck, L. L.; Manna, L.; Sicardi, S.; Baldi, G. Dynamic operation of a three-phase upflow reactor for the hydrogenation of phenyl acetylene. *Catalysis Today*, **1994**, *20*, 485.
167. Goto, S.; Mabuchi, K. Oxidation of ethanol in gas-liquid cocurrent upflow and downflow reactors. *Can. J. Chem. Eng.*, **1984**, *62*, 865.
168. Goto, S.; Chatani, T.; Matouq, M. H. Hydration of 2-methyl-2-butene in gas-liquid cocurrent upflow and downflow reactors. *Can. J. Chem. Eng.*, **1993**, *71*, 821.
169. De Wind et al. Upflow versus downflow testing of hydrotreating catalysts. *Applied Catalysis*, **1988**, *43*, 239.
170. Larachi, F.; Laurent, A.; Wild, G.; Midoux, N. Some experimental liquid saturation results in fixed bed reactors operated under elevated pressure in cocurrent upflow and downflow of the gas and the liquid. *Ind. Eng. Chem. Res.*, **1991**, *30*, 2404.
171. Yang, X. L.; Wild, G.; Euzen, J. P. A comparison of hydrodynamics between packed-bed reactors with cocurrent upflow and downflow of gas and liquid. *Chem. Eng. Sci.*, **1992**, *47*, 1323.
172. Vergel, H. ; Les reacteurs a lit fixe avec ecoulement de gaz et de liquide. Comparaison sur le plan theorique et experimental de la performance du reacteur dans differents sens d'ecoulement. These de Doctorat de l'INP Lorraine, **1993**.
173. Mills, P. L.; Beaudry, E. G.; Dudukovic, M. P. Comparison and prediction of reactor performance for packed beds with two-phase flow : downflow, upflow and countercurrent flow. *I. Chem. E. Symp. Ser.*, **1984**, *87*, 527.
174. Julcour, C.; Jaganathan, R.; Chaudhari, R. V.; Wilhelm, A. M.; Delmas, H. Selective Hydrogenation of 1,5,9-cyclododecatrien in up flow and down flow fixed bed reactors, experimental observations and modeling. *Chem. Eng. Sci.*, **2001**, *56*, 557.
175. Pohl, J. H.; Sarofim, A. F. *16th Symposium (Int.) on Combustion*, The Combustion Institute, Pittsburgh, PA, **1977**, p-491.
176. Solomon, P. R.; Hamblen, D. G. Finding order in coal pyrolysis kinetics. *Prog. EnergyCombust. Sci.*, **1984**, *9*, 323.
177. Solomon, P. R.; Semo, M. A.; Carangelo, R. M.; Markham, J. R. Very rapid coal pyrolysis. *Fuel*, **1986**, *65*, 182.

178. Serio, M. A.; Hamblen, D. G.; Markham, J. R.; Solomon, P. R. Kinetics of volatile product evolution in coal pyrolysis: Experiment and theory. *Energy Fuels*, **1987**, *1*, 138.
179. Wanzl, W.; Kabler, P.; Van Heek, K. H.; Jontgen, H. *ACS Div. Fuel Chem. Prepr*, **1987**, *32(3)*, 125.
180. Solomon, P. R.; Hamblen, D. G. *Chemistry of Coal Conversion*, R.H. Schlosberg (Ed.), Plenum Press, NY, **1985**, Chapter 5, p.121.
181. Solomon, P. R.; Hamblen, D. G.; Carangelo, R. M.; Krause, J. L. *19th Symposium (Int.) on Combstion*, The Combustion Institute, Pittsburgh, PA, **1983**, p-1139.
182. Malonev, D. J.; Jenions, R. G.; *20th Symposium (Int.) on Combustion*, The Combustion Institute, Pittsburgh, PA, **1985**, p-1435.
183. Tasi, C. Y.; Scatonl, A. W. *20th Symposium (Int.) on Combustion*, The Combustion Institute, Pittsburgh, PA, **1985**, p-1455.
184. Kobayashi, H.; Howard, J. B.; Sarofim, A. F. *16th Symposium (Int.) on Combustion*, The Combustion Institute, Pittsburgh, PA (1977); and Kobayashi, H., Ph.D. Thesis, M.I.T. Dept of Mechanical Eng., Cambridge, MA, **1976**, p-411.
185. Fletcher, T. H. Time-resolved particle temperature measurements and mass loss measurements of a bituminous coal during devolatilization. *Combust. Flame*, **1989**, *78*, 223.
186. Fletcher, T. H. Time resolved temperature measurements of individual coal particles during devolatilization. *Combust. Sci. Technol.*, **1989**, *63*, 89.
187. Barbara toole O Neil. *Dry Scrubbing Technologies for Flue Gas Desulfurization*. Kluwer Academic Publishers, USA, **1998**.
188. Ballester, J.; Jimenez, S. Kinetic parameters for the oxidation of pulverized coal as measured from drop tube tests, *Combust. Flame*, **2005**, *142*, 210.
189. (a) Vamvuka, D.; Woodburn, E.T.; Senior, P.R. Modeling of an entrained flow coal gasifier. I. Development of the model and general predictions. *Fuel*, **1995**, *74*, 1452. (b) Vamvuka, D.; Woodburn, E.T.; Senior, P.R. Modeling of an entrained flow coal gasifier. II. Effect of operating conditions on reactor performance. *Fuel*, **1995**, *74*, 1461.
190. (a) Brown, B.W.; Smoot, L.D. Measurement and prediction of entrained flow gasification processes. *A.I.Ch.E. J.*, **1988**, *34*, 435. (b) Watanabe, H.; Otaka, M. Numerical simulation of coal gasification in entrained flow coal gasifier. *Fuel*, **2006**, *85*, 1935.
191. (a) Watanabe, H.; Otaka, M. Numerical simulation of coal gasification in entrained flow coal gasifier. *Fuel*, **2006**, *85*, 1935. (b) Vicente, W.; Ochoa, S.; Aguillon, J.; Barrios, E. An Eulerian model for the simulation of an entrained flow coal gasifier. *Appl. Therm. Eng.*, **2003**, *23*, 1993.
192. (a) Texier-Boullet, F. A simple, convenient and mild synthesis of imines on an alumina surface without solvent. *Synthesis*, **1985**, *6-7*, 679. (b) Ross, L. J.; Levy, S. D. Reductive alkylation of substituted anilines. US 4261926, **1981** by American Cyanamid Co., USA.
193. Gilbert, S., Brizzolara, A.; Landesman, H.; Szmuszkovicz, J.; Terrell, R. The enamine alkylation and acylation of carbonyl compounds. *J. Amer. Chem. Soc.*, **1965**, *85*, 207.
194. Taguchi, K.; Westheimer, F. H. Catalysis by molecular sieves in the preparation of ketimines and enamines. *J. Org. Chem.*, **1971**, *36*(11), 1570.
195. (a) Kaneko, M., Tanaka, S. Method of manufacturing alkylaniline compounds. European Patent 760360, **1997** by Konica Corporation, Japan (b) Nishimura, T., Takeda, F., Wada, M., kanemura, Y. Preparation of N-alkyl-Substituted aromatic amines. JP 2000095739, **2000,** by Mitsui Chemicals Inc., Japan.
196. Greenfield, H.; Malz, R. E. Jr. *Catalysis of organic reactions*, Ed. Kosak, J. R. Marcel Dekker, New York. **1984**, 309.
197. Bonds, A. P.; Greenfield, H. The reductive alkylation of aromatic amines with formaldehyde. *Catalysis of organic reactions*, Ed. Pascoe, W. E. Marcel Dekker, New York.**1991**, *47*, 65.
198. de Angelis, A.; Ingallina, P.; Perego, C. Solid acid catalysts for industrial condensations of ketones and aldehydes with aromatics. *Ind. & Eng. Chem. Res.*, **2004**, *43*(5), 1169.
199. Archer, S.; Lewis, T. R.; Unser, M. J.; Hoppe, J. O.; Lape, H. 1 -Ethyl-4-(3-tropanyl) -tetrahydro-1 H-1,4-benzodiazepine. *J. Amr. Chem. Soc.*, **1957**, *79*, 5783.
200. Emerson, W. S. *Organic reactions*, **1948**, *4*, 174.
201. (a) Stieber, J.; Reynolds, M. Impurity formation during the reductive alkylation of aniline with methyl isoamyl ketone. *Catalysis of organic reactions*, Ed. Pascoe, W. E. Marcel Dekker, New York.**1991**, *47*, 87. (b) Greenfield, H. Side reactions in reductive alkylation of aromatic amines with aldehydes and with ketones. *Catalysis of organic reactions*, **1995**, *53*, 265.

202. (a) Klyuev M. V.; Bulatov A. V.; Kushch L. A; Khidekel M. L. Method of preparing n-alkylaromatic amines. SU Patent 802264, **1981**, By Institute of chemical physics, USSR. (b) Harada T.; Arita H. Preparation of N-alkylaminodiarylamine. JP 55139343, **1980** by Mitsui Petrochemical Ind. (c) Yoshigaki S.; Ando S.; Otsuki T.; Kawasaki T. Production Of N-Alkayl-N'-Phenyl-P-Phenylenediamines as stabilizers for rubbers. JP 63051362, **1988** by Ouchi Shinko Chemical Industrial Co. Ltd., Japan.
203. (a) Fache, F.; Jacquot, L.; Lemaire, M. Extension of the Eschweiler-Clarke procedure to the N-alkylation of amides. *Tetrahedron Lett.*, **1994**, *35*(20), 3313. (b) Fache, F.; Bethmont, V.; Jacquot, L.; Valot, F.; Milenkovic, A.; Lemaire, M. Reductive O- and N-alkylations. Alternative catalytic methods to nucleophilic substitution. *Stud. Surf. Sci. Catal.*, **1997**, *108* (Heterogeneous Catalysis and Fine Chemicals IV), 115.
204. Rusek M. Effect of promoters on Pt/SiO2 catalysts for the N-alkylation of sterically hindered anilines in the vapor phase. *Het. Cat. and fine chem. II*, Elsevier Science Publishers B. V., Amsterdam. **1991**, 359.
205. Su, B., Barthomeuf, D. Effect of reaction temperature on the alkylation of aniline by methanol over almost neutral zeolites LiY and NaY. *Studies in surface science and catalysis* (Catalysis by microporous materials): Elsevier Science. **1995**, *94*, 598.
206. Kaneko, M., Tanaka, S. Method of manufacturing alkylaniline compounds. EP 760360, **1997**, by Konica Corporation, Tokyo, Japan.
207. Nishimura, T., Takeda, F., Wada, M., kanemura, Y. Preparation of N-alkyl-Substituted aromatic amines. JP 2000095739, **2000**, by Mitsui Chemicals Inc.
208. Lehtonen, J. Salmi, T., Vuori, A., Tirronen, E. On the principles of modeling of homogeneous-heterogeneous reactions in the production of fine chemicals. A case study: Reductive alkylation of aromatic amines. *Org. Process Res. Dev.*, **1998**, *2(2)*, 78.
209. Salmi, T., Lehtonen, J., Kaplin, J., Vuori, A., Tirronen, E., Haario, H. A homogeneous-heterogeneously catalyzed reaction system in a loop reactor. *Catal. Today*, **1999**, *48(1-4)*, 139.
210. Wilson, Jr. Modified nickel catalyst systems and their use in reductive alkylation reactions. US 4043942, **1977**, by Goodyear Tire and Rubber Co., Ohio.
211. Ross, L. J.; Levy, S. D. Reductive alkylation of substituted anilines. US 4261926, **1981**, by American Cyanamid Company, Stanford.
212. Watanabe, T. Preparation of di-(substituted amino) diphenylamines as antioxidants and antiozonants for polymers. JP 10168038, **1998**, by Yanai Kagaku Kogyo K. K., Japan.
213. Malz, R. E. Jr.; Jancis, E. H.; Reynolds, M. P.; O'Leary, S. T. Reductive alkylation of acetophenone with aniline. *Chem. Ind. (Dekker)*, **1995**, *62* (Catalysis of organic reactions), 263.
214. Hiskey R. G.; Northrop R. C. Azomethine chemistry. I. Formation of optically active a-amino acids by asymmetric induction. *J. Amr. Chem. Soc.*, **1961**, *83*, 4798.
215. Merten, H. L.; Baclawski, L. M. Process for producing N, N'-disubstituted paraphenylene diamine mixtures by sequential reductive alkylation. US 4900868, **1990**, by Monsanto Company.
216. Vogel, C.; Aebi, R. Herbicidal and plant growth inhibiting agent. US 4324580, **1982**, by Ciba-Geigy Corporation, Newyork.
217. Malz, R.E.; Greenfield, H. Tertiary amine preparation by reductive alkylation of aliphatic secondary amines with ketones. *Stud. Surf. Sci. Catal.*, **1991**, *59*, 351.
218. Riehen, R.B.; Binningen, P.F.; Therwil, P.R. Process for the preparation of 2-Alkyl-6-Methyl-N (1'-Methoxy-2'-Propyl)-Aniline and a process for the preparation of their chloracetanilides. US 5430188, **1995**.
219. Barman, S.; Pradhan, N.C. Kinetics of reductive isopropylation of benzene with acetone over nano-copper chromite loaded H-Mordenite. *Ind. Eng. Chem. Res.*, **2006**, *45*, 3481.
220. Rylander, P. N. Catalytic hydrogenation over platinum metals. Academic Press, New York. 277, **1967**.
221. Malone, R. J.; Merten, H. L. A comparative mass transfer study in the reductive N-alkylation of aromatic nitro compounds. *Catalysis of organic reactions*, Ed. Pascoe, W. E. Marcel Dekker, New York. **1991**, *47*, 79.
222. Sami, M.; Annamalai, K.; Wooldridge, M. Co-firing of coal and biomass fuel blends. *Progress Energy Combust. Sci.*, **2001**, *27*, 171.
223. Hein, KRG; Bemtgen, J.M. EU clean coal technology, co-combustion of coal and biomass. *Fuel Process Technol.*, **1998**, *54*,*159*.
224. Spliethoff, H; Hein, KRG. Effect of co-combustion of biomass on emissions in pulverized fuel furnaces. *Fuel Process Technol.*, **1998**, *54*, 189.

225. Nussbaumer, T. Combustion and co-combustion of biomass: Fundamentals, Technologies, and primary measures for emission reduction. *Energy Fuels*, **2003**, *17*, 1510.
226. Demirbas, A. Combustion characteristics of different biomass fuels. *Progress Energy Combus. Sci.* **2004**, *30*, 219.
227. Dogru, M.; Howarth, C.R..; Akay, G.; Keskinler, B.; Malik, A.A. Gasification of hazelnut shells in a downdraft gasifier. *Energy*, **2002**, *27*, 415.
228. Hughes E. Biomass co-firing: economics, policy and opportunities. *Biomass Bioenergy*, **2000**, *19*, 457.
229. Fallot, A.; Girard, P. Spatial assessment of biomass potentials for energy scenarios. *Proceedings of the 14th European Biomass Conference & Exhibition*, Paris, France, ETA-Renewable Energies, Italy, **2005,** p-104.
230. William, A.; Pourkashanian, M.; Jones, J.M. Combustion of pulverized coal and biomass. *Prog. Eng. Combust. Sci.*, **2001**, *27*, 587.
231. Demirbas, A. Potential applications of renewable energy sources, biomass combustion problems in boiler power systems and combustion related environmental issues. *Progress Energy Combs. Sci.*, **2005**, *31*, 171.
232. Demirbas, A. Combustion characteristics of different biomass fuels. *Progress Energy Combus. Sci.* **2004**, *30*, 219.
233. Bushnell, D.J.; Haluzok, C.; Dadkhah-Nikoo, A. Biomass fuel characterization testing and evaluating the combustion characteristics of selected biomass fuels. Corvallis, OR: Bonneville Power Administration, **1989**.
234. Hughes, E.E.; Tillman, D.A. Biomass cofiring: status and prospects 1996. *Fuel Process Technol.*, **1998**, *54*, 127.
235. Van Loo, S.; Koppejan, J. The handbbok of biomass combustión and co-firing. Earthscan, UK and USA, **2008**.

CHAPTER 2

PART-A

Kinetic Modeling of Reductive Alkylation of *p*-Phenylenediamine with Methyl Ethyl Ketone using Pt/Al_2O_3 Catalyst in a Slurry Reactor

2(A).1 INTRODUCTION

Reductive alkylation of amines is commercially practiced in a variety of industrial processes for the manufacture of higher alkylated (secondary and tertiary) amine derivatives, which find applications as intermediates in fine chemicals and specialty products.[1,2] An important example of this class of reaction is the reductive alkylation of *p*-phenylenediamine (PPDA) with methyl ethyl ketone (MEK) to *N, N'*-di-secondary-alkyl-*p*-phenylenediamine (Di-amine), which is used as an inhibitor, a sweetening agent, an antioxidant in rubber and petroleum industries [2,3, 4]and also as an intermediate in dyestuff industries.[1,5,6] The reductive alkylation reaction goes through a condensation reaction between an amine compound and a carbonyl compound or an alcohol to form an imine (*Schiff Base*) intermediate,[7] which undergoes hydrogenation in the presence of a metallic catalyst to form *N*-alkylated product. The general schematic of the reductive alkylation reaction is shown in Figure 2.1.

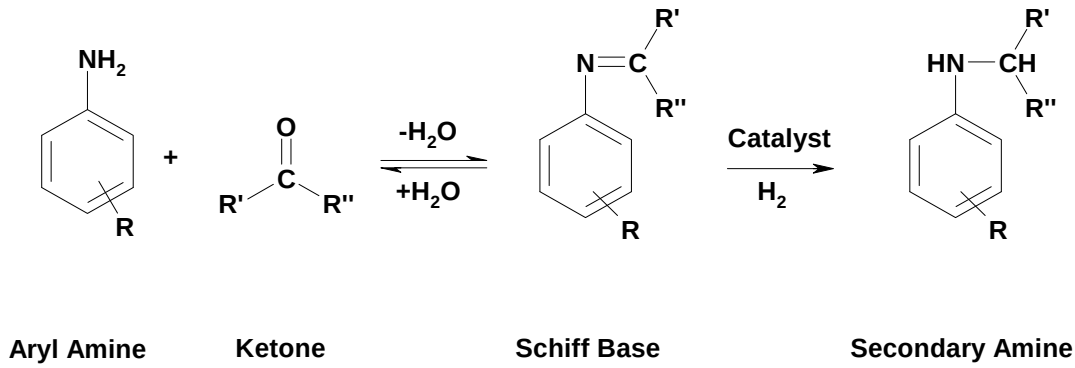

Figure 2.1. General reaction scheme for reductive alkylation reaction

Reductive alkylation of nitro or amine compounds has been investigated using a wide variety of catalysts and alkylating agents, mainly ketones and aldehydes. While aldehydes[1, 8, 9, 10, 11] give the *N, N*-dialkylated products, *N*-monoalkylated compounds are the major products with ketones due to their relatively higher molecular size and lower activity.[10,12,13,14,15] Greenfield[10] has studied the reductive alkylation of aromatic amines with aldehydes and ketones using different transition metal catalysts, and compared those catalysts with respect to activity and selectivity towards desired products. Among the transition metals, palladium has the lowest efficiency for the two major side reactions, viz., the ring hydrogenation and hydrogenation of the carbonyl compounds to the corresponding

alcohols. It was also pointed out that platinum is more effective than palladium for higher molecular weight ketones and amines as substrates. Different promoters like organic/inorganic acids [16] (trichloroacetic acid), alkali metal salts (e.g. sodium acetate) and modifiers (sulfur dichloride)[17] were also studied to forward the equilibrium condensation reaction ultimately to increase the overall rate of reaction and to improve the yield and selectivity of the desired *N*-alkylated product.

Most of the previous work on reductive alkylation has been focused on improving the catalytic activity and selectivity to *N*-alkylated compounds. However, the reaction system has not been well studied from reaction engineering viewpoint. Though, there is an obvious advantage in conducting the condensation and hydrogenation reactions in a single step and effectively drive the equilibrium reaction step to complete conversion, understanding of the reaction kinetics of all steps involved is of significant importance to optimize the overall rate of reductive alkylation. There are only a few kinetic modeling reports in the literature, which deal with combinations of homogeneous-heterogeneous, non-catalytic-catalytic reactions. Lehtonen *et. al.*[1] followed by Salmi *et. al.*[18] have developed a semibatch slurry reactor model and loop reactor model for reductive alkylation of aromatic amines with short chain aldehydes (carbon chain length less than three) using Pt/C catalyst. A systematic analysis of mass transfer effects and a detailed kinetic study of reductive alkylation of aromatic monoamines (aniline) have been reported earlier,[19] in which, the impact of homogeneous and heterogeneously catalyzed reactions on the overall reaction kinetics was addressed. The reaction network becomes highly complex with the increasing number of amine functionalities. In this context, a detailed reaction scheme of reductive alkylation of phenylenediamines (PDAs) with methyl ethyl ketone is shown in Figure 2.2. A summary of the previous work on reductive alkylation of di-amines is presented in Table 2.1. While, numerous reports on catalyst performance evaluation appeared in the previous literature, no attempts have been made to study the kinetics and mechanism of reductive alkylation of di-amines (or its precursors) using ketones as alkylating agents. Therefore, a systematic kinetic study on reductive alkylation of di-amines with ketone has been selected as the objective of this work.

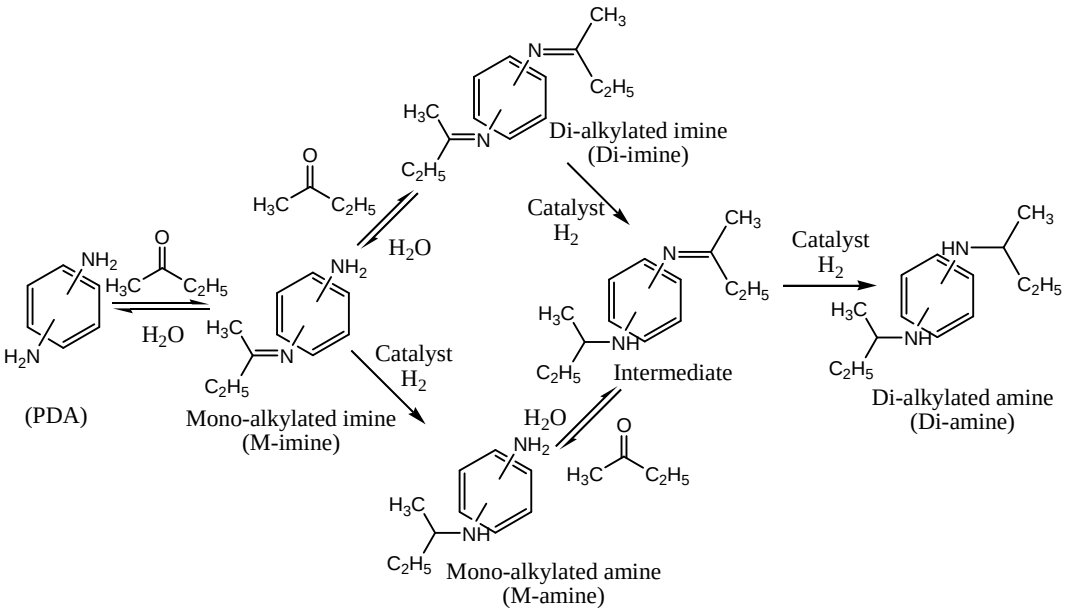

Figure 2.2. Detailed reaction scheme for reductive alkylation of phenylenedimines with methyl ethyl ketone

This chapter is divided in two parts, in which Part-A describes a detailed study of intrinsic kinetics of reductive alkylation of PPDA with MEK using 3% Pt/Al_2O_3 catalyst in a slurry reactor. In Part-B, the effect of relative positions of amine groups in phenylenediamine isomers (PDAs) on their activities and selectivities in the reductive alkylation reaction has been discussed to understand the substrate structure activity correlation. This reaction system involves combination of parallel and consecutive reactions comprising multiple non-catalytic equilibrium (homogeneous) and catalytic hydrogenation (heterogeneous) reaction steps in the overall reaction scheme, where the selective synthesis of Di-amine is an important issue. The effect of substrate concentration, catalyst loading, agitation speed and partial pressure of hydrogen on concentration-time and hydrogen consumption–time profiles was studied at different temperatures. Rate equations have been proposed based on the elementary steps involving catalytic and noncatalytic reactions, which lay stress on different types of interactions occurring between the reactants and the active catalyst sites, and the rate parameters were evaluated. The kinetic parameters of the individual steps were evaluated and compared to understand the differences in the activity and selectivity patterns for OPDA, MPDA and PPDA substrates.

Table 2.1. A Summary of Literature on Reductive Alkylation of Di-amines

Substrates	Catalyst	Reaction conditions	Remarks	Ref.
PPDA and 2-octanone	63% Nickel on kiselguhr	Temp.: 438 K, P_{H2}: 5.2-6.9 MPa	Yield of *N*, *N'*- di-2-octyl-PPDA increased by addition of sulfur modifier	20
PPDA and 2-octanone	63%Nickel on kieselguhr; sulfur dichloride, Thiodipropionic acid	Temp: 438 K P_{H2}: 5.18 - 6.89 MPa Time: 4 hrs.	Yield increased from 57.2 to 88.6 by using sulfur containing modifier and it increased from 88.6 to 92.3% by the addition of small amount of an org/inorg. acid	17
p-nitroaniline Methyl ethyl ketone	Mixture of CrO_3, CuO and BaO	Temp.: 433 K P_{H2} : 6 MPa	*N*, *N'*- di-sec-butyl-PPDA was the major product	21
p-nitroaniline and acetone	Pt/Al_2O_3	Temp.: 373 K P_{H2} : 6.21 MPa Time: 4 –5.2 hrs.	Solvent effect studied and 2-methoxyethanol was found to be the best solvent	3
N-phenyl- PPDA, Methyl isobutyl ketone	5% Pt-sulfide/C	Temp.: 453 K P_{H2}: 4.1 MPa. Time: 0.75 hrs.	The comparison of the sulfides of different metals suitable for reductive alkylation studied.	22
p-nitroaniline, Ethyl amyl ketone	2% Pt/Al_2O_3 and sulfided Pt catalyst	Temp. : 408.70K P_{H2}: 8.3 MPa	Sulfided catalysts showed better selectivity over the non-sulfided one.	23
p-nitroaniline, Methyl ethyl ketone	0.3% Pt/Al_2O_3 also contains 0.3% of fluorine	Temp.: 421 K P_{H2}: 8 moles per mole of ketone LHSV: 0.5 and 6.8 MPa total pressure	Continuous reactor studies have been reported. As ratio of hydrogen to ketone increases and as temperature decreases the formation of side products decreases	24
p-nitroaniline, Methyl ethyl ketone	0.3% Pt/Al_2O_3 pretreated with hydrogen	Temp.: 433 K P_{H2}: 10.3 MPa	*N*, *N'*- di-sec-butyl-PPDA was the major product	25
p-nitroaniline, Acetone, 37% Formaldehyde	Decaborane ($B_{10}H_{14}$)	MeOH Temp.: 300 K Time: 0.5 + 10 hrs.	Reductive alkylation and reductive methylation of aromatic amines with formaldehyde gave higher yield of N-alkylated products	26
4-nitrodiphenylamine, Methyl isoamyl ketone, Methyl isobutyl ketone	1% Pt/C Acidic carbon co-catalyst	Temp.: 423K P_{H2}: 2.8-3.5 Mpa. Time: 3.5 hrs.	Production of mixture of p-phenylenediamine by using two different ketones one after another had been studied	27

2(A).2 EXPERIMENTAL SECTION

2(A).2.1 Materials

p-Phenylenediamine from Loba Chemie, India, methyl ethyl ketone from E-Merck, India, were procured as ultra pure reagents and used without any further purification. The 3% Pt/Al_2O_3 catalyst was purchased from Arora Matthey Ltd., India. The catalyst was spherical with an average diameter of 3×10^{-3} m. For kinetic studies in a slurry reactor, the catalyst was powdered and sieved to obtain very fine particles in a size range of 1×10^{-3} m to 1×10^{-7} m. The specifications of the powdered catalyst are as follows: Pt content: 3% (w/w); support: γ-Al_2O_3; average particle size: 1×10^{-5} m; particle density: 1.26×10^{3} kg/m^3; surface area: 1.68×10^{5} m^2/kg. Hydrogen and nitrogen gases with >99% purity were supplied by Inox Air Products Ltd., India and were used as received.

2(A).2.2 Reactor Set-up

All the reductive alkylation batch reactions were carried out in a 3×10^{-4} m^3 capacity high pressure stirred autoclave supplied by Parr Instrument Company, Moline, USA. The autoclave vessel having an internal diameter of 6.4×10^{-2} m and an impeller diameter of 4×10^{-2} m was equipped with heating arrangement, overhead stirrer, thermo well, internal cooling loop, pressure gauge as well as transducer, gas inlet, gas outlet, sampling valve and a rupture disc. The liquid sample line and the thermocouple well were well immersed in the reaction mixture. The temperature in the liquid phase and the speed of agitation were controlled by means of a Parr 4842 controller. The pressure transducer connected to the Parr controller was used to digitally monitor the pressure inside the reactor. Water circulation through the internal cooling loop equipped with automatic cutoff arrangement controlled the temperature inside the reactor with an accuracy of ±1 °C. While taking a liquid sample, a chilled water condenser was fitted on the sample valve exit line to avoid flashing of the sample. A schematic of the slurry reactor set-up is shown in Figure 2.3.

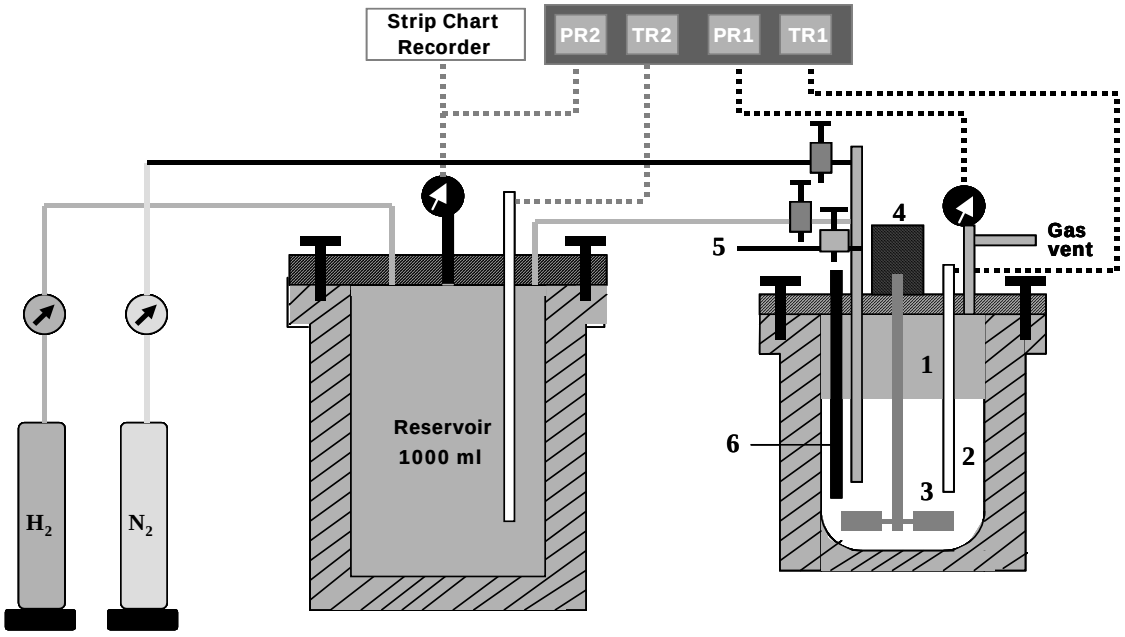

1: Reactor; 2: Thermo well; 3: stirrer shaft with impeller; 4: magnetic stirrer; 5: sampling valve; 6: internal cooling tube; TR1: Reactor temperature indicator; PR1: Reactor pressure indicator; TR2: Reservoir temperature indicator; PR2: Reservoir pressure indicator; N_2: Nitrogen cylinder H_2: Hydrogen cylinder

Figure 2.3. Schematic of a slurry reactor set-up

2(A).2.3 Experimental Procedure

2(A).2.3.1 Homogeneous Reaction

In a typical homogeneous reaction experiment, predefined amount of PPDA and MEK were charged into the reactor bomb and the vessel was closed. Total volume of the liquid phase was always kept to 1×10^{-4} m^3. Then the reactor bomb was heated to a desired temperature and samples were withdrawn at regular intervals of time for analysis by gas chromatography. In each experiment, concentration-time data were obtained to study the equilibrium reaction. After attaining equilibrium, the reaction was further continued for one hour and then the reactor was allowed to cool down to room temperature.

2(A).2.3.2 Catalytic Hydrogenation Reaction

In a typical hydrogenation experiment, predefined amount of PPDA and MEK were charged into the reactor keeping the total volume of the liquid phase at 1×10^{-4} m^3. A known amount of powdered 3% Pt/Al_2O_3 catalyst was then charged into the reactor bomb

carefully and the vessel closed. The reactor was flushed 2-3 times with nitrogen and then with hydrogen at room temperature. The reactor bomb was then heated to a desired temperature under low agitation speed (4 Hz). The agitation was increased to 20 Hz after attaining the temperature and the reaction continued for a predetermined time to attain equilibrium of the homogeneous reaction. A liquid sample was collected at this point as the initial sample and this was considered to be the zero time for the hydrogenation reaction. Hydrogen gas from an intermediate reservoir was then introduced into the reactor through the gas inlet to the desired pressure under low agitation speed and hydrogenation reaction was started by putting the agitation to a set value (20 Hz). A constant pressure regulator situated between the reservoir and the reactor maintained the constant pressure inside the reactor and the absorption due to reaction was monitored from the pressure drop in the reservoir (the entire system was in semi batch mode). Samples were withdrawn at regular intervals after sufficient flushing of the sample line and analyzed by gas chromatography. In each experiment, concentration-time and H_2 consumption-time data were recorded. The reaction was allowed to proceed for a prescribed time after which the reactor was allowed to cool down to room temperature. The range of operating conditions studied in this work is given in Table 2.2.

Table 2.2. Range of Experimental Conditions

Catalyst loading	0.2-2 kg/m^3
p-phenylenediamine concentration	0.5-1.5 kmol/m^3
Hydrogen partial pressure	2.07-6.21 MPa
Agitation speed	13.33-20 Hz
Temperature	373-413 K
Volume of liquid	1 x 10^{-4} m^3
Reaction time	3 h

2(A).2.4 Analysis

The liquid samples were analyzed by gas chromatography (GC model HP 6890) using a HP-5 Capillary column (5% phenyl methyl siloxane as the stationary phase, 30 m × 320 μm × 0.25 μm). The conditions of GC analysis were as follows: Injector temperature, 523

K; Column temperature ramp, 373 K hold for 1 min, @ of 8 K min^{-1} up to 413 K, hold for 3 min, @ of 8 K min^{-1} up to 429 K, hold for 2 min, @ of 10 K min^{-1} up to 513 K, hold for 2 min; FID temperature, 523 K. Helium was used as the carrier gas. A few samples were characterized using GC-MS (Shimadzu QP 2000A) using the same analytical method stated above for the identification of products.

2(A).3 RESULTS AND DISCUSSION

2(A).3.1 Preliminary Experiments

2(A).3.1.1 Identification of Products

Preliminary experiments for reductive alkylation of PPDA with MEK were carried out to assess the reproducibility of the experimental data and to identify the key products in the reaction. For this purpose Pt/Al_2O_3 catalyst was used based on the literature survey. MEK was used as one of the reactants in excess that also served the role of a solvent. In preliminary equilibrium experiments, it was observed that a small fraction of PPDA precipitates out from the liquid samples withdrawn from the reactor due to the low solubility of PPDA in MEK leading to analytical errors. To overcome such a problem, a known volume of liquid sample was diluted with five times volume of methanol to ensure that PPDA is completely soluble in the sample used for GC analysis. An appropriate volume correction factor for this injected sample was introduced in the material balance calculations and the mass balance problem was resolved. Few samples were analyzed by GC-MS to identify the products in the overall reaction. In another set of preliminary hydrogenation experiments using PPDA and MEK in presence of Pt/Al_2O_3 catalyst, the mono- and di-alkylated products viz. mono- and di-amines in high concentration and two imine products viz. mono-alkylated imine (M-imine) and di-alkylated imine (Di-imine) were identified. Also, one intermediate product formation (Figure 2.4) was also observed in the reaction. The product Intermediate can be formed by the alkylation reaction with the mono-alkylated amine or by the hydrogenation reaction with the di-alkylated imine. Based on this study, a possible reaction scheme (in Figure 2.4) is proposed for the reductive alkylation of PPDA with MEK.

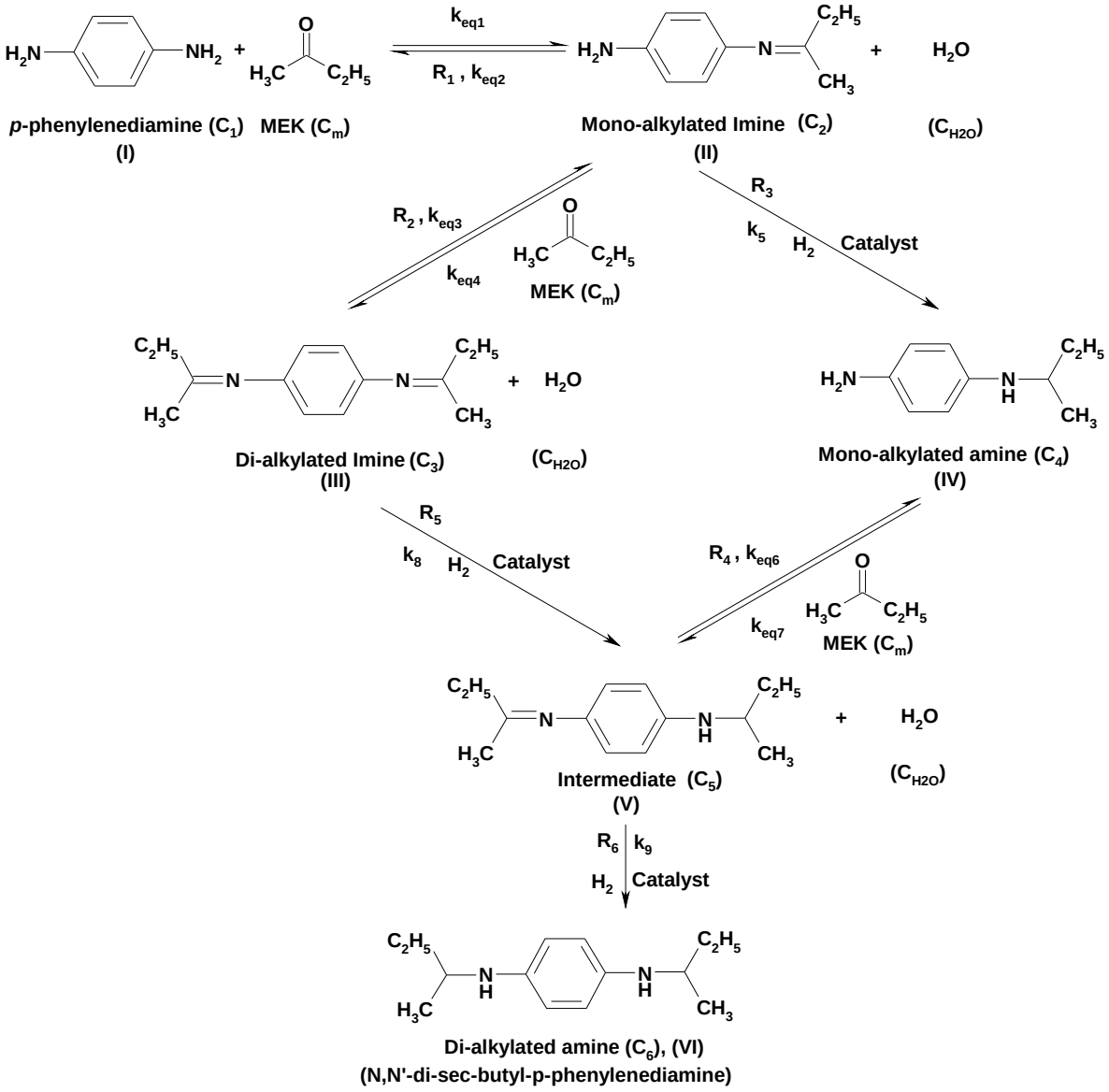

Figure 2.4. Detailed reaction scheme for reductive alkylation of PPDA with MEK in presence of 3% Pt/Al_2O_3 catalyst

2(A).3.1.2 Equilibrium Reaction Studies

The equilibrium reaction (non-catalytic) in homogeneous phase was studied to assess the approximate time required to attain equilibrium among PPDA (I), M-imine (II) and Di-imine (III). A typical concentration-time profile of the homogeneous reaction is shown in Figure 2.5. Both Mono- and Di-imines were formed simultaneously as the reaction progressed and all three components (PPDA, M-imine, Di-imine) co-existed at equilibrium. It was observed that no undissolved PPDA remained (with the PPDA used in our

experimental conditions) when the equilibrium was reached. Therefore, all the hydrogenation reactions were started after the reaction reached equilibrium to ensure complete dissolution of PPDA in MEK and the homogeneity of the reaction mixture.

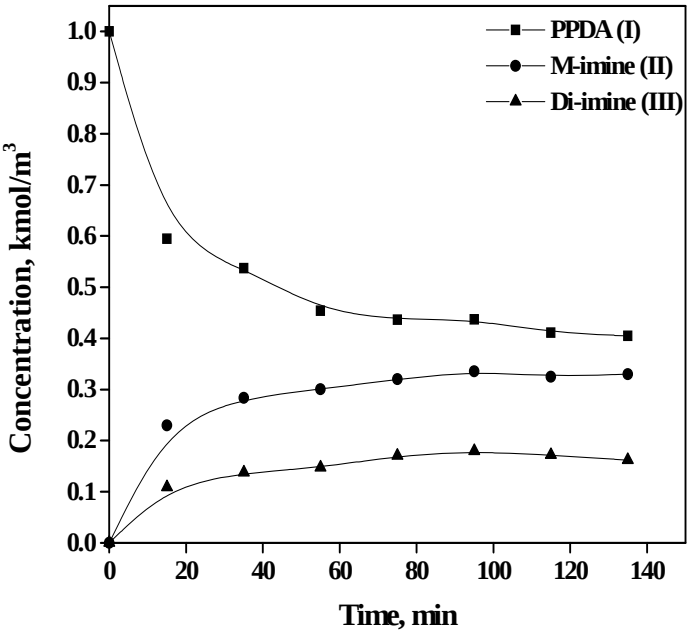

Figure 2.5. Typical concentration-time profile for homogeneous reaction of PPDA with MEK

Reaction Conditions: PPDA: 1.0 kmol/m^3; Temperature: 373 K; Agitation: 16.67 Hz; reaction volume: 1 × 10^{-4} m^3; MEK is the solvent and one of the reactants.

2(A).3.1.3 Hydrogenation Reaction and Catalyst Screening Studies

To select a suitable catalyst for selective synthesis of Di-amine by reductive alkylation of PPDA with MEK, we screened Pd, Pt, Ru and Rh catalysts supported on alumina. The catalyst screening results were compared in terms of conversion of PPDA and products selectivity. The results are presented in Table 2.3. The terms conversion and selectivity were defined as follows.

$$Conversion\,(\%) = \frac{Amount\ of\ PPDA\ consumed\ (kmol)}{Total\ amount\ of\ PPDA\ initially\ taken\ (kmol)} \times 100 \qquad 2.1$$

$$Selectivity\,(\%) = \frac{Amount\ of\ the\ particular\ product\ formed\,(kmol)}{Total\ amount\ of\ PPDA\ converted\,(kmol)} \times 100 \qquad 2.2$$

It was observed that Pd/Al_2O_3 and Ru/Al_2O_3 gave lower conversion of PPDA and lower selectivity to the amine products as compared to Pt/Al_2O_3 and Rh/Al_2O_3 under identical conditions. Though Rh/Al_2O_3 gave comparable conversion of PPDA, the total selectivity to amine products (92.1%) was higher for Pt/Al_2O_3 catalyst than Rh/Al_2O_3 catalyst (80.4%). Therefore, Pt/Al_2O_3 was the best choice to achieve high activity and selectivity to *N, N'*-dialkylated product. Also from Table 2.1, it is evident that Pt is the most commonly used catalyst for synthesis of *N, N'*-di-secondary-butyl-*p*-Phenylenediamine (Di-amine, VI) by reductive alkylation of PPDA (or *p*-nitroaniline) and MEK. A detailed comparison of the catalysts used in this work was not possible because of the absence of specific data about the commercial process for PPDA. However, in this study, a selectivity to *N, N'*-di-secondary-butyl-*p*-Phenylenediamine (Di-amine, VI) of >95% was achieved for nearly complete conversion of PPDA (as shown in Figure 2.6), which is comparable to the reported data in the patented literature (Yield: 42-95%, 0.3% Pt/Al_2O_3, 433 K, *p*-nitroaniline: MEK = 1:8).[25]

Table 2.3. Catalyst Screening Studies

Catalyst	Conversion of PPDA (%)	Products Selectivity (%)			
		M-amine (IV)	Intermediate (V)	Di-amine (VI)	Others (Schiff bases) (II & III)
3% Pt/Al_2O_3	87.96	39.94	23.68	28.47	7.91
3% Pd/Al_2O_3	65.23	2.66	63.42	5.63	28.29
3% Ru/Al_2O_3	40.64	0	37.52	0	62.48
3% Rh/Al_2O_3	80.4	24.85	4.69	50.88	19.58

Reaction Conditions: PPDA: 1.0 kmol/m^3; Catalyst: 1 kg/m^3; P_{H2}: 5.17 MPa; Temperature: 373 K; Agitation: 16.67 Hz; reaction volume: 1×10^{-4} m^3; MEK is the solvent and one of the reactants.

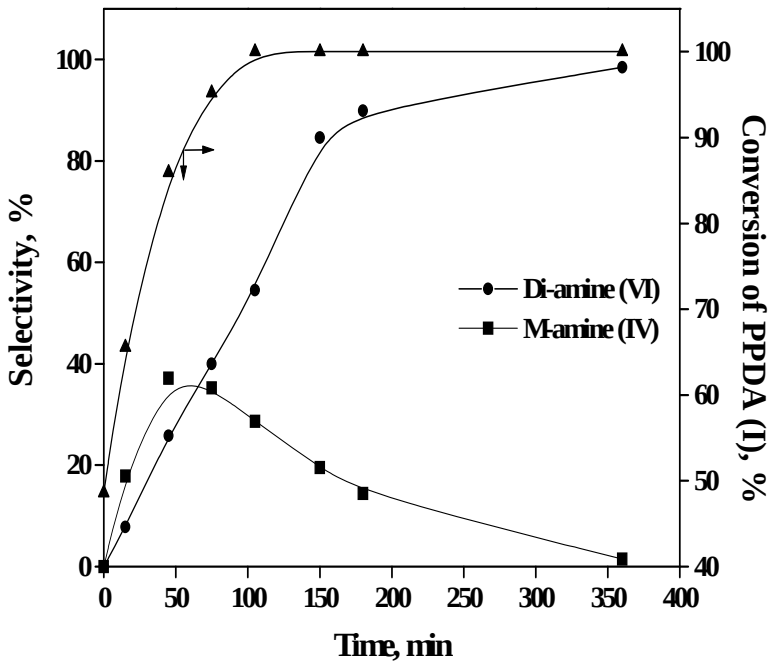

Figure 2.6. Selectivity versus conversion graph of complete conversion reaction
Reaction Conditions: PPDA: 0.5 kmol/m^3; Catalyst (3% Pt/Al_2O_3): 1 kg/m^3; P_{H2}: 5.17 MPa; Temperature: 413 K; Agitation: 16.67 Hz; reaction volume: 1×10^{-4} m^3; MEK is the solvent and one of the reactants.

In order to investigate the intrinsic kinetics of reductive alkylation of PPDA with MEK using Pt/Al_2O_3 catalyst, a few preliminary experiments were carried out to check the material balance of liquid and gas phase components in the overall reaction. For all the reactions, MEK was used as one of the reactants in excess that also served the role of a solvent. From equilibrium reaction studies (section 2(A).3.1.2), it was found that, the reaction took approximately 75 min. to reach the equilibrium among PPDA, M-imine and Di-imine. Hence, all the hydrogenation reactions were started after the reaction reaches equilibrium. A typical concentration-time profile observed is shown in Figure 2.7, which indicates that Mono-imine (II), Di-imine (III), Mono-amine (IV), Intermediate (V) and Di-amine (VI) were the major products. The formation of possible dimerization products of the aromatic compound and hydrogenated product of MEK to 2-butanol were observed to be negligible (<0.5%) for all cases. The effect of catalyst on the equilibrium reaction was studied separately, and it was observed that the catalyst had no effect on the condensation reaction. Also, in the previous report on the reductive alkylation of aniline with acetone, it was observed that the condensation reaction was not affected either by the catalyst (Alumina supported palladium) or by hydrogen.[19] In all the reactions, material balance of

liquid phase components and hydrogen consumed agreed with the products formed to the extent of >95% and consistent with the reaction scheme shown in Figure 2.4.

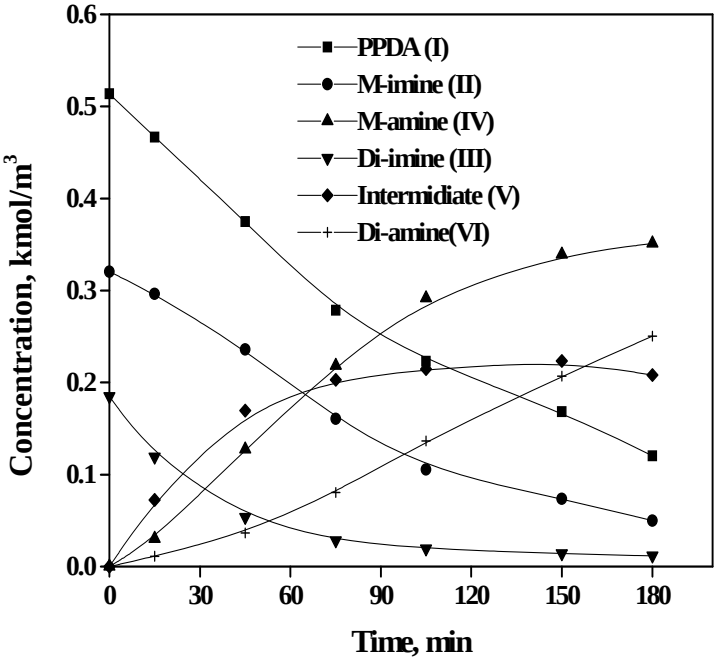

Figure 2.7. Typical concentration-time profile of reductive alkylation of PPDA with MEK. Reaction Conditions: PPDA: 1.0 kmol/m^3; Catalyst (3% Pt/Al_2O_3): 1 kg/m^3; P_{H2}: 5.17 MPa; Temperature: 373 K; Agitation: 16.67 Hz; reaction volume: 1×10^{-4} m^3; MEK is the solvent and one of the reactants.

2(A).3.1.4 Catalyst Stability and Recycle Studies

It is important to ensure the consistent activity of the Pt/Al_2O_3 catalyst through out a reaction. This is because, if the catalyst deactivates during a reaction, reactor performance will be a function of catalyst deactivation rate and may give falsified kinetic parameters. Therefore, the Pt/Al_2O_3 catalyst was recycled several times for reductive alkylation of PPDA with MEK to check its activity. For recycle studies, to avoid loss of catalyst, the experiments were conducted with the pellets by using a basket in the slurry reactor. The results of catalyst recycle studies are shown in the Figure 2.8, which indicates the consistency of catalyst activity even after five recycles. The initial rates of hydrogenation were also calculated for each recycle and it was observed that those values were identical. Therefore, it was concluded that the 3% Pt/Al_2O_3 catalyst showed no deactivation during the batch experiments.

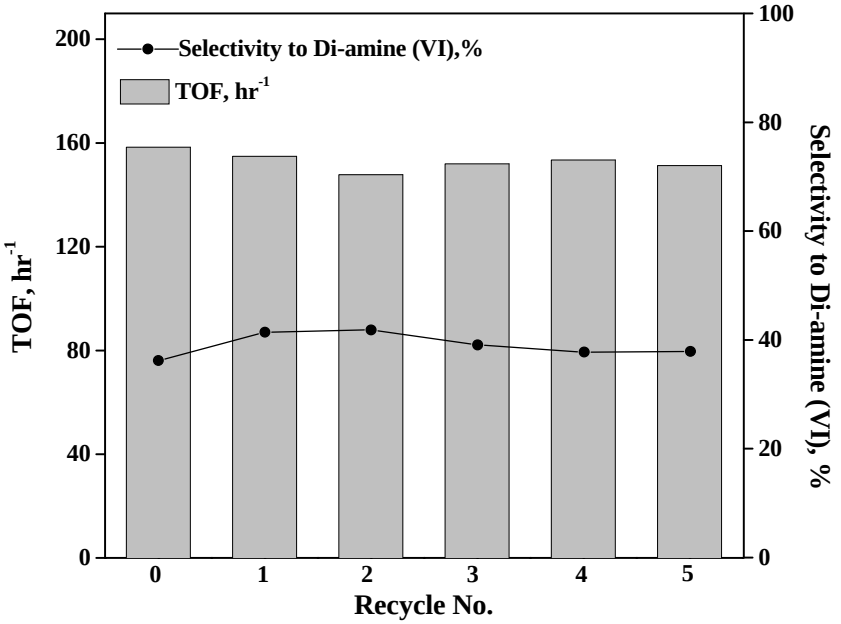

Figure 2.8. Recycle experiments for reductive alkylation of PPDA with MEK using 3% Pt/Al_2O_3 catalyst

Reaction Conditions: PPDA: 1.0 kmol/m^3; Catalyst (3% Pt/Al_2O_3 pellets): 4 kg/m^3; P_{H2}: 5.17 MPa; Temperature: 373 K; Agitation: 16.67 Hz; reaction volume: 1×10^{-4} m^3; MEK is the solvent and one of the reactants.

Few experiments were conducted for the complete conversion of PPDA to Di-amine using 3% Pt/Al_2O_3 catalyst. The reaction was continued till hydrogen absorption stopped and the selectivity for mono- and di-amine were found to be 1.5% and 98.5 % respectively. The results on variation of selectivity and conversion of PPDA with time are discussed in Section 2(A).3.1.3, Figure 2.6, which clearly indicate that the reaction continues even after the complete conversion of PPDA for the conversion of M-amine to Di-amine, with high selectivity to Di-amine. The material balance of reactants consumed and products formed agreed to > 98% as per the stoichiometry. This result showed that Pt/Al_2O_3 is a good choice of catalyst for selective synthesis of Di-amine. In a few cases, the reaction mixture was processed further to remove unreacted MEK and recover Di-amine by vacuum distillation. Almost 99 % of the unreacted MEK was recovered at 313 K and 100 mmHg of vacuum with 99.5% purity as shown by GC and from the residue containing M-amine and Di-amine, the later was recovered at 373 K and 100 mmHg of vacuum with 92.5 % isolated yield. The purity of the separated Di-amine was found to be 99% by GC.

2(A).3.2 Solubility Data

2(A).3.2.1 Experimental Procedure for Solubility Measurement

The solubility of H_2 in PPDA/MEK mixtures was determined experimentally at 373, 393 and 413 K, using a method described elsewhere.[28] In a typical experiment, a known volume (100 ml) of PPDA in MEK solution was introduced into the autoclave and the contents were heated to the desired temperature after flushing with nitrogen. After the thermal equilibrium was attained, the void space in the reactor was pressurized with H_2 to a desired level and the gas inlet valve was closed to disconnect the gas supply. The contents were then stirred for about ten minutes to equilibrate the liquid phase with the solute gas. The change in pressure in the autoclave was recorded on-line as a function of time till it remained constant, indicating the saturation of the liquid phase with hydrogen.

2(A).3.2.2 Quantitative Analysis of Solubility Data

For the quantitative analysis of mass transfer effects and interpretation of kinetic data for reductive alkylation of PPDA and MEK, the concentration of dissolved hydrogen in MEK (solubility) with various concentrations of PPDA is required. The solubility of hydrogen in PPDA-MEK mixtures with different compositions were determined experimentally using the procedure described in section 2(A).3.2.1. The solubility of hydrogen in a liquid (A^*) can be expressed by Henry's law as follows:

$$A^* = H_e P_{H_2} \qquad 2.3$$

where, H_e is the Henry's constant, kmol/m^3/atm and P_{H2} is the partial pressure of hydrogen, atm. The values of Henry's constants at different temperatures and for various mixtures of PPDA and MEK as determined experimentally are given in Table 2.4.

Table 2.4. Henry's Constant for Various Compositions of PPDA in MEK

Sr. No.	Temp., K	H_e values for PPDA in MEK mixtures × 10^3, kmol/m^3/atm		
		5% PPDA	10% PPDA	15% PPDA
1	373	3.473	3.978	3.933
2	393	3.288	4.231	4.640
3	413	3.875	4.345	5.191

2(A).3.3 Analysis of Initial Rate Data

The initial rates of hydrogenation were calculated from the H_2 consumption-time profiles observed in a semi batch slurry reactor for a wide range of conditions (Table 2.2). The H_2 consumption-time data were fitted by a second order polynomial of the form

$$Y = a + b\,t + c\,t^2 \qquad 2.4$$

where, Y is the hydrogen consumed in kmol/m^3; t is reaction time in sec.; a, b and c are constants. The rate of reaction at any time t can be calculated as

$$R_A = \frac{dY}{dt} = b + 2\,c\,t \qquad 2.5$$

where, R_A is the overall rate of hydrogenation, kmol/m^3/sec. When time t approaches to zero, Equation 2.5 can be written as

$$\left(R_A\right)_{t\to o} = R_{H_2} = b \qquad 2.6$$

where, R_{H_2} is the initial rate of hydrogenation, kmol/m^3/sec

This initial rate data were used to evaluate the effect of different parameters like, agitation speed, PPDA concentration, partial pressure of hydrogen and catalyst concentration as shown in Figures 2.9 and 2.10, respectively. The rate of reaction was found to be unaffected by change in the agitation speed from 13.34 to 20 Hz (Figure 2.9-A), indicating the absence of gas-liquid and liquid-solid mass transfer resistances. In addition, the significance of various mass-transfer resistances was also evaluated using the criteria suggested by Ramachandran and Chaudhari[29] (See Section 2(A).3.4). The initial rate of hydrogenation increased marginally on variation of PPDA concentration at lower temperature but showed negligible effect at higher temperatures (Figure 2.9-B). The initial rate of hydrogenation was found to increase linearly with hydrogen partial pressure up to 5.17 MPa, but showed no variation on further increase in partial pressure (Figure 2.10-A). The initial rates increased linearly with catalyst loading at higher temperatures but showed negligible effect at lower temperature (Figure 2.10-B). The unusual effect of catalyst loading at lower temperatures is due to the non-catalytic imine formation step (Figure 2.4) as rate limiting. These initial rate data were used for the analysis of mass transfer effects as given in the following section.

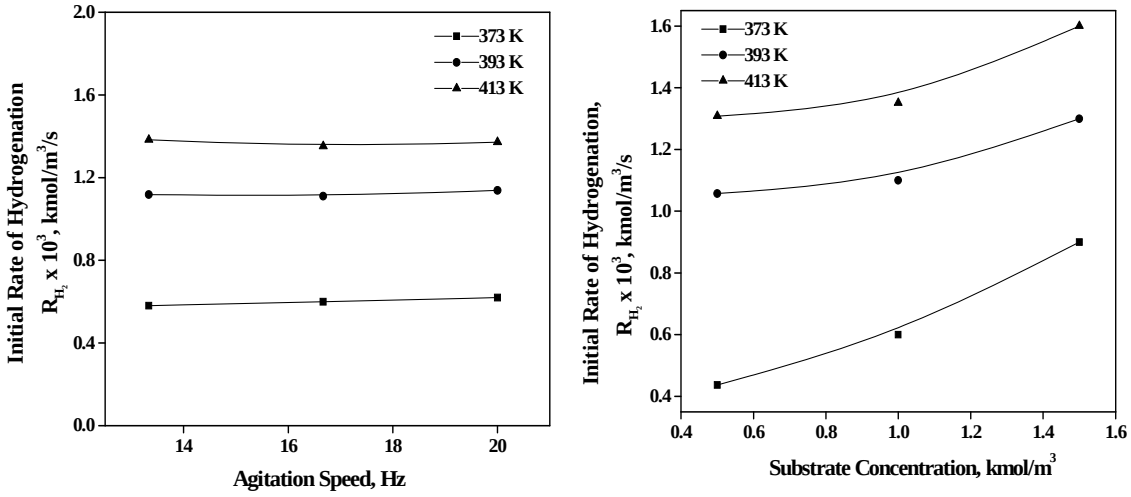

(A) (B)

Figure 2.9. (A) Effect of agitation speed and **(B)** Effect of PPDA concentration on initial rate of hydrogenation for reductive alkylation of PPDA with MEK in presence of 3% Pt/Al_2O_3 catalyst

Reaction Conditions: Catalyst (3% Pt/Al_2O_3): 1 kg/m^3; P_{H2}: 5.17 MPa; reaction volume: 1 × 10^{-4} m^3; MEK is the solvent and one of the reactants. For **(A)** PPDA: 1.0 kmol/m^3; **(B)** Agitation speed: 16.66 Hz

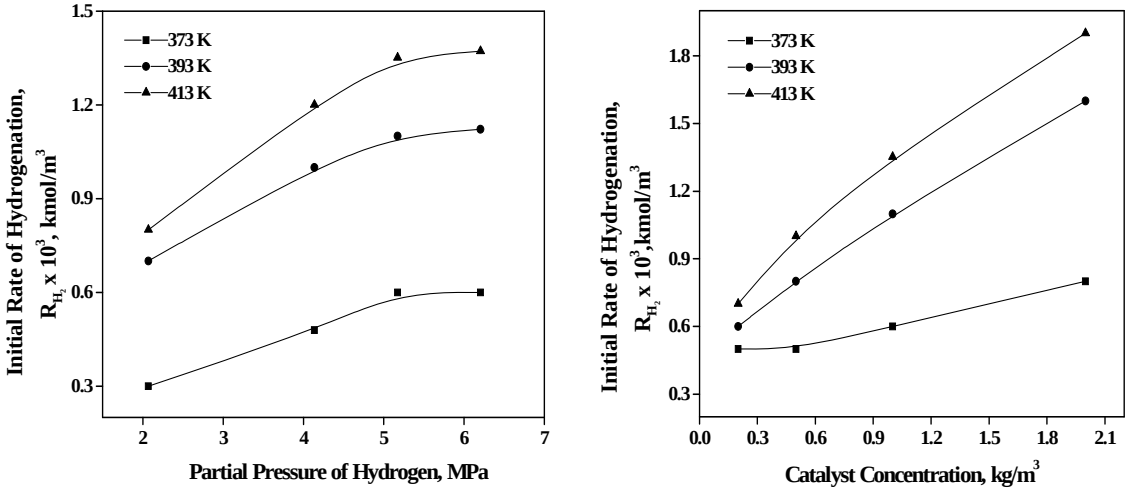

(A) (B)

Figure 2.10. (A) Effect of partial pressure of hydrogen and **(B)** Effect of catalyst loading on initial rate of hydrogenation for reductive alkylation of PPDA with MEK in presence of 3% Pt/Al_2O_3 catalyst

Reaction Conditions: PPDA: 1.0 kmol/m^3; Agitation: 16.67 Hz; reaction volume: 1 × 10^{-4} m^3; MEK is the solvent and one of the reactants. For **(A)** Catalyst (3% Pt/Al_2O_3): 1 kg/m^3; **(B)** P_{H2}: 5.17 MPa

2(A).3.4 Analysis of Mass Transfer Effects

For the purpose of kinetic study, it is important to ensure that the rate data obtained are in kinetically controlled regime. Therefore, initial rate data were used to analyze the significance of various mass transfer resistances using the criteria discussed by Ramachandran and Chaudhari.[29]

1. Gas-liquid mass transfer resistance can be negligible if,

$$\alpha_1 = \frac{R_{H_2}}{k_L a_B A^*} < 0.1 \qquad 2.7$$

where, $k_L a_B$ is the gas-liquid mass-transfer coefficient.

2. Liquid-solid mass transfer resistance can be negligible if,

$$\alpha_2 = \frac{R_{H_2}}{k_s a_p A^*} < 0.1 \qquad 2.8$$

where, k_s is the liquid-solid mass transfer coefficient and a_p is the external surface area of the catalyst per unit volume.

3. Pore diffusion resistance can be considered as negligible if,

$$\phi_{\exp} = \frac{d_p}{6}\left[\frac{(m+1)}{2D_e}\frac{\rho_p R_{H_2}}{wA^*}\right]^{1/2} < 0.2 \qquad 2.9$$

where, D_e is the effective diffusivity.

For using the criteria given by equations 2.7-2.9, a knowledge of the gas-liquid mass transfer coefficient, $k_L a_B$, the liquid-solid mass transfer coefficient, $k_s a_p$, effective diffusivity, D_e, overall rate of hydrogenation, R_{H_2} and the specific data for the catalyst used such as particle diameter, d_p, particle density, ρ_p are required. $k_L a_B$ was calculated according to the correlation proposed by Gholap *et. al.*[30]

$$k_L a_B = 1.48\times10^{-3}\times(N)^{2.18}\times(V_g/V_l)^{1.88}\times(d_I/d_t)^{2.16}\times(h_1/h_2)^{1.16} \qquad 2.10$$

The specifications of the slurry reactor used in this study and typical value of $k_L a_B$ are presented in Table 2.5.

Table 2.5. Specifications of Reactor and k_La_B Calculations

N	Agitation speed, 16.67 Hz	d_t	Tank diameter, 0.064 m
V_g	Volume of gas in the reactor, 2.2×10^{-4} m^3		Height of the tank, 0.1 m
			Height of impeller from the head, 0.09 m
		h_1	Height of the first impeller from the bottom = 0.1 – 0.09 = 0.01 m
V_l	Volume of liquid in the reactor, 1×10^{-4} m^3	h_2	Height of the liquid, 0.033 m
d_I	Impeller diameter, 0.04 m	$\boldsymbol{k_La_B}$ = 0.27 s^{-1}	

k_s was calculated by the correlation proposed by Sano *et al.*[31]

$$\frac{k_s d_p}{D_M F_c} = 2 + 0.4\left[\frac{e\left(d_p\right)^4 \rho_l^3}{\mu_l^3}\right]^{0.25}\left[\frac{\mu_l}{\rho_l D_M}\right]^{0.333} \qquad 2.11$$

where, e, the energy supplied to the liquid was calculated according to Calderbank *et. al.*[32], and F_c, is the shape factor, was assumed to be unity for spherical particles.

$$e = \frac{N_p N^3 d_i^{\,5} \Psi}{\rho_l V_l} \qquad 2.12$$

where, N_p is the power number assumed to be 6.3 for flat blade turbine[29] and ψ, the correction factor for gas bubbles was obtained from the correlation:

$$\Psi = 1 - 1.26\left[\frac{Q_g}{N d_I^{\,3}}\right] \text{ when } \left[\frac{Q_g}{N d_I^{\,3}}\right] < 3.5\times10^{-2} \qquad 2.13$$

$$\Psi = 0.62 - 1.85\left[\frac{Q_g}{N d_I^{\,3}}\right] \text{ when } \left[\frac{Q_g}{N d_I^{\,3}}\right] > 3.5\times10^{-2} \qquad 2.14$$

where, Q_g is volumetric flow rate of gas (m^3/s) and can be calculated as

$$Q_g = r_{\max} \times V_l \times V_M \qquad 2.15$$

where, V_M is molar gas volume (m^3/kmol) and can be calculated as

$$V_M = V/n = RT/P_{H_2} \qquad 2.16$$

Molecular diffusivity, D_M was calculated from the correlation proposed by Wilke and Chang[33]

$$D_M = \frac{7.4\times10^{-8}\, T\left(\chi M_w\right)^{1/2}}{\mu_l\, v_M^{\,0.6}} \qquad 2.17$$

where, χ, M_w, μ_l and v_M are the association factor of the solvent, molecular weight of solvent, viscosity of the liquid and molar volume of hydrogen respectively.

External surface area of the catalyst per unit volume, a_p was calculated using the following correlation:

$$a_p = \frac{6w}{\rho_p\, d_p} \qquad 2.18$$

where, ρ_p and d_p are the particle density and particle diameter respectively.

To calculate ϕ_{exp}, effective diffusivity (D_e) was calculated using the following correlation:

$$D_e = D_M \varepsilon/\tau \qquad 2.19$$

where, ε and τ are the porosity and tortuosity of the catalyst, which were considered to be 0.5 and 3 respectively.

The values of different parameters required to calculate α_1, α_2 and ϕ_{exp} are given in Table 2.6.

Table 2.6. Values of Different Parameters Used in Evaluating the Role of External and Internal Mass Transfer Resistances at Different Temperatures

Temperature, (K)	$K_L a_B$ **(s^{-1})**	$k_s \times 10^3$ **(m/s)**	a_p **(m^2/m^3)**	$D_M \times 10^8$**, (m^2/s)**	$D_e \times 10^9$**, (m^2/s)**
373	0.27	3.146	600	1.35	2.25
393	0.27	3.29	600	1.42	2.37
413	0.27	3.46	600	1.49	2.49

The saturation solubility of hydrogen, A^* at a particular temperature, composition and partial pressure of hydrogen was calculated from the data given in Table 2.4. Initial rate of hydrogenation, R_{H2} for a reaction was obtained from the procedure described in Section

2(A).3.3. The highest calculated values of parameters α_1, α_2 and ϕ_{exp} were 2.57×10^{-3}, 2.11×10^{-4}, and 2.21×10^{-2} respectively indicating the absence of mass transfer limitations in the range of conditions used for kinetic study.

The initial rate data are useful for evaluation of mass transfer effects, however, these are not directly useful for kinetic analysis since the hydrogenation step in the reaction sequence comes after two homogeneous non-catalytic reversible reactions, which could be rate limiting. Hence, for such a complex reaction system comprising of multiple homogeneous and heterogeneous reaction steps, integral concentration-time data should be considered in interpretation of the intrinsic kinetics.

2(A).3.5 Kinetic Modeling

For kinetic analysis, the concentration-time profiles obtained at different initial sets of conditions with variation in PPDA concentration, H_2 pressure and catalyst loading over a temperature range of 373 to 413K was used. The reaction scheme considered is shown in Figure 2.4. Several forms of rate equations were considered to represent the different reaction steps involved. For the non-catalytic homogeneous (liquid phase) condensation reactions (R_1, R_2 and R_4), the following forms of rate equations were considered:

$$R_1 = k_{eq1m} C_1 C_m - k_{eq2} C_2 C_{H_2O} \qquad 2.20$$

$$R_2 = k_{eq3m} C_2 C_m - k_{eq4} C_3 C_{H_2O} \qquad 2.21$$

$$R_4 = k_{eq6m} C_4 C_m - k_{eq7} C_5 C_{H_2O} \qquad 2.22$$

where, k_{eq1m}, k_{eq3m}, k_{eq6m} and k_{eq2}, $k_{eq4,}$ k_{eq7} were the forward and backward reaction rate constants respectively for the steps R_1, R_2 and R_4 mentioned in Figure 2.4. For all the kinetic experiments, MEK was used in large excess with respect to PPDA and change in its concentration during the course of reaction was negligible. Therefore, all the forward reaction steps were considered to be as pseudo first order reactions. The concentration of water at any time was expressed as

$$C_{H_2O} = C_2 + 2C_3 + C_4 + 2C_5 + 2C_6 \qquad 2.23$$

Hence, Equations 2.20, 2.21 and 2.22 could be written as

$$R_1 = k_{eq1} C_1 - k_{eq2} C_2 \left(C_2 + 2C_3 + C_4 + 2C_5 + 2C_6\right) \qquad 2.24$$

$$R_2 = k_{eq3}C_2 - k_{eq4}C_3\left(C_2 + 2C_3 + C_4 + 2C_5 + 2C_6\right) \quad 2.25$$

$$R_4 = k_{eq6}C_4 - k_{eq7}C_5\left(C_2 + 2C_3 + C_4 + 2C_5 + 2C_6\right) \quad 2.26$$

where, $k_{eq1} = k_{eq1m}C_m$, $k_{eq3} = k_{eq3m}C_m$, $k_{eq6} = k_{eq6m}C_m$

For catalytic hydrogenation steps (R_3, R_5 and R_6), rate equations based on different mechanisms were considered (see Table 2.7-A and Table 2.7-B). The interaction of hydrogen with platinum metal is believed to give a α-hydride (Pt (H_2)) or β-hydride (Pt (H)) species.[34] Therefore, rate equations based on Langmuir-Hinshelwood (L-H) models were proposed based on the possible interactions of H_2 and liquid phase components on Pt metal surface. Several basic assumptions made to derive the rate equations were as follows:

(i) The rate of surface reaction is rate limiting for the hydrogenation steps

(ii) Adsorption and desorption rates were much higher than the rate of surface reactions

(iii) Di-amine desorbed very fast from the catalyst surface

The basis of selecting rate models 1 to 8 (Table 2.7-A and Table 2.7-B) is given below:

Model 1: Reaction of adsorbed α-hydride (Pt (H_2)) species with the adsorbed liquid phase components.

Model 2: Reaction of adsorbed α-hydride (Pt (H_2)) species with the adsorbed liquid phase components (A case of competitive adsorption)

Model 3: Reaction of adsorbed β-hydride (Pt (H)) species with the adsorbed liquid phase components

Model 4: Reaction of adsorbed β-hydride (Pt (H)) species with the adsorbed liquid phase components (A case of competitive adsorption)

Model 5: Reaction of dissolved hydrogen gas with adsorbed liquid phase components

Model 6: Reaction of dissolved hydrogen gas with adsorbed liquid phase components (A case of competitive adsorption)

Model 7: Reaction of adsorbed α-hydride (Pt (H_2)) species with liquid phase components

Model 8: Reaction of adsorbed β-hydride (Pt (H)) species with liquid phase components

Table 2.7-A. Comparison of Various Models for Reductive Alkylation of PPDA with MEK in presence of 3% Pt/Al_2O_3 Catalyst for Model-1 to Model-4

Rate Parameters	**Model-1** $R_j = \frac{wk_j A^* c_j}{\left(1 + K_{H_2} A^* + \sum_{\substack{k=11,12,13 \\ l=2,3,5}} k_k c_l\right)}$			**Model-2** $R_j = \frac{wk_j A^* c_j}{\left(1 + K_{H_2} A^* + \sum_{\substack{k=11,12,13 \\ l=2,3,5}} k_k c_l\right)^2}$		
	373K	**393K**	**413K**	**373K**	**393K**	**413K**
$k_{eq1} \times 10^3$	0.1278	0.1943	0.2560	0.1238	0.1634	0.2890
$k_{eq2} \times 10^4$	0.2655	0.5118	0.01655	0.1848	0.03768	0.6175
$k_{eq3} \times 10^4$	0.8303	2.434	3.185	1.050	1.936	3.609
$k_{eq4} \times 10^4$	0.4652	1.662	0.2019	0.05506	0.00804	0.1172
$k_5 \times 10^2$	0.1728	0.3085	0.5975	0.2243	0.8416	1.693
$k_{eq6} \times 10^4$	0.5902	0.4422	0.6245	0.4676	0.4335	0.7626
$k_{eq7} \times 10^5$	0.8247	0.1148	0.1739	0.9797	0.1118	0.9353
$k_8 \times 10^2$	0.3864	0.9381	1.484	0.5781	3.185	3.961
$k_9 \times 10^3$	0.9107	1.897	2.110	1.249	4.530	5.497
K_{H2}	1.2049	2.6485	3.3270	0.8918	2.4545	2.9725
K_{11}	1.2024	2.7059	3.4793	0.9408	2.4038	3.1798
K_{12}	1.3763	2.9795	3.8757	1.0691	2.6604	2.8938
K_{13}	1.3870	3.3362	2.9630	0.7215	2.7977	2.5409
% RR	±8.02	±23.38	±2.78	±9.79	±36.12	±0.107
$\phi_{min.} \times 10^4$	2.03	14.6	9.49	1.15	14.2	1.14
Rate Parameters	**Model-3** $R_j = \frac{wk_j \sqrt{A^*} c_j}{\left(1 + K_{H_2} \sqrt{A^*} + \sum_{\substack{k=11,12,13 \\ l=2,3,5}} k_k c_l\right)}$			**Model-4** $R_j = \frac{wk_j \sqrt{A^*} c_j}{\left(1 + K_{H_2} \sqrt{A^*} + \sum_{\substack{k=11,12,13 \\ l=2,3,5}} k_k c_l\right)^2}$		
	373K	**393K**	**413K**	**373K**	**393K**	**413K**
$k_{eq1} \times 10^3$	0.1270	0.1479	0.2697	0.1299	0.1901	0.2553
$k_{eq2} \times 10^4$	0.1471	0.04365	0.3084	0.1493	0.2284	0.2019
$k_{eq3} \times 10^4$	1.566	2.051	3.364	1.606	2.179	2.852
$k_{eq4} \times 10^4$	0.4422	0.5205	1.380	0.2882	0.02996	1.296
$k_5 \times 10^2$	0.0841	0.1932	0.3722	0.1466	0.5207	1.758
$k_{eq6} \times 10^4$	0.0299	0.3592	0.8131	0.005032	0.1993	1.125
$k_{eq7} \times 10^5$	0.0250	0.0506	0.5316	0.01195	0.03620	0.6058
$k_8 \times 10^2$	0.2653	0.5628	0.8763	0.5748	1.791	3.403
$k_9 \times 10^3$	0.5504	1.333	1.342	0.9987	3.567	5.241
K_{H2}	1.151	2.4377	3.171	1.036	2.189	3.1869
K_{11}	1.2629	3.0177	3.4725	1.0782	2.4467	3.5357
K_{12}	1.5156	3.9924	3.9125	1.1485	2.7521	3.9691
K_{13}	1.5230	3.2857	3.0302	1.0557	2.4662	3.1738
% RR	±14.25	±62.09	±7.14	±11.49	±41.61	±16.56
$\phi_{min.} \times 10^4$	1.27	12.2	5.01	1.63	12.1	10.5

Table 2.7-B. Comparison of Various Models for Reductive Alkylation of PPDA with MEK in presence of 3% Pt/Al_2O_3 Catalyst for Model-5 to Model-8

Rate Parameters	**Model-5** $R_j = \frac{wk_j A^* c_j}{\left(1+\sum_{\substack{k=11,12,13 \\ l=2,3,5}} k_k c_l\right)}$			**Model-6** $R_j = \frac{wk_j A^* c_j}{\left(1+\sum_{\substack{k=11,12,13 \\ l=2,3,5}} k_k c_l\right)^2}$		
	373K	**393K**	**413K**	**373K**	**393K**	**413K**
$k_{eq1} \times 10^3$	0.1371	0.1865	0.2545	0.1258	0.1809	0.2590
$k_{eq2} \times 10^4$	0.3909	0.2664	0.05340	0.1824	0.00083	0.13
$k_{eq3} \times 10^4$	1.526	2.501	3.030	1.352	2.262	3.127
$k_{eq4} \times 10^4$	0.9154	0.2534	0.0805	0.5893	0.0005	0.4382
$k_5 \times 10^2$	0.1192	0.2113	0.4530	0.0809	0.1112	0.1976
$k_{eq6} \times 10^4$	0.0366	0.2251	0.6474	0.0598	0.3358	0.7740
$k_{eq7} \times 10^5$	0.0451	0.0104	0.0345	0.0466	0.0139	0.4488
$k_8 \times 10^2$	0.4757	0.8147	1.163	0.2803	0.4582	0.5402
$k_9 \times 10^3$	0.7093	1.299	1.530	0.4784	0.7335	0.7491
K_{H2}	-	-	-	-	-	-
K_{11}	1.1947	2.608	3.407	0.01	0.05	0.1
K_{12}	1.3869	3.115	3.7346	0.0529	0.1472	0.1964
K_{13}	1.4149	2.000	3.000	0.0634	0.1913	0.2703
% RR	±7.53	±26.51	±19.36	±9.84	±22.48	±10.43
$\phi_{min.} \times 10^4$	1.52	13.1	5.79	1.71	15.1	3.72
Rate Parameters	**Model-7** $R_j = \frac{wk_j A^* c_j}{\left(1+K_{H_2} A^*\right)}$			**Model-8** $R_j = \frac{wk_j \sqrt{A^*} c_j}{\left(1+K_{H_2} \sqrt{A^*}\right)}$		
	373K	**393K**	**413K**	**373K**	**393K**	**413K**
$k_{eq1} \times 10^3$	0.1330	0.1742	0.2535	0.1248	0.2091	0.2440
$k_{eq2} \times 10^4$	0.3682	0.0175	0.0695	0.03508	0.2562	0.8807
$k_{eq3} \times 10^4$	1.553	2.177	3.447	1.214	2.910	2.982
$k_{eq4} \times 10^4$	0.6980	0.0463	0.6875	0.0692	0.3732	0.3981
$k_5 \times 10^2$	0.0971	0.1436	0.2008	0.0639	0.1091	0.1481
$k_{eq6} \times 10^4$	0.0345	0.2937	0.5567	0.2539	0.2018	0.6497
$k_{eq7} \times 10^5$	0.0078	0.01	0.4223	0.072	0.2397	1.267
$k_8 \times 10^2$	0.3963	0.3998	0.5101	0.2035	0.3980	0.3923
$k_9 \times 10^3$	0.6447	0.9731	0.8889	0.4110	0.5147	0.6609
K_{H2}	1.3054	1.4413	1.0053	1.605	1.111	1.6395
K_{11}	-	-	-	-	-	-
K_{12}	-	-	-	-	-	-
K_{13}	-	-	-	-	-	-
% RR	±10.54	±27.70	±11.77	±12.03	±9.83	±12.87
$\phi_{min.} \times 10^4$	2.09	13.3	3.47	1.48	10.2	3.76

For a typical case of Model 8, the change in the concentration of reactants and products can be represented by the following mass balance equations for constant pressure of hydrogen under isothermal conditions:

$$\frac{dC_1}{dt} = -R_1 = -\left[k_{eq1}C_1 - k_{eq2}C_2C_{H_2O}\right] \tag{2.27}$$

$$\frac{dC_2}{dt} = R_1 - R_2 - R_3 = \left[k_{eq1}C_1 - k_{eq2}C_2C_{H_2O}\right] - \left[k_{eq3}C_2 - k_{eq4}C_3C_{H_2O}\right] - \frac{wk_5\sqrt{A^*}C_2}{\left(1+K_{H2}\sqrt{A^*}\right)} \tag{2.28}$$

$$\frac{dC_3}{dt} = R_2 - R_5 = \left[k_{eq3}C_2 - k_{eq4}C_3C_{H_2O}\right] - \frac{wk_8\sqrt{A^*}C_3}{\left(1+K_{H2}\sqrt{A^*}\right)} \tag{2.29}$$

$$\frac{dC_4}{dt} = R_3 - R_4 = \frac{wk_5\sqrt{A^*}C_2}{\left(1+K_{H2}\sqrt{A^*}\right)} - \left[k_{eq6}C_4 - k_{eq7}C_5C_{H_2O}\right] \tag{2.30}$$

$$\frac{dC_5}{dt} = R_4 + R_5 - R_6 = \left[k_{eq6}C_4 - k_{eq7}C_5C_{H_2O}\right] + \frac{wk_8\sqrt{A^*}C_3}{\left(1+K_{H2}\sqrt{A^*}\right)} - \frac{wk_9\sqrt{A^*}C_5}{\left(1+K_{H2}\sqrt{A^*}\right)} \tag{2.31}$$

$$\frac{dC_6}{dt} = R_6 = \frac{wk_9\sqrt{A^*}C_5}{\left(1+K_{H2}\sqrt{A^*}\right)} \tag{2.32}$$

Initial conditions:

$$\text{At } t = 0,\ C_1 = C_{eq1},\ C_2 = C_{eq2},\ C_3 = C_{eq3} \ \&\ C_4,\ C_5,\ C_6 = 0 \tag{2.33}$$

where, C_1 to C_6 were the concentrations of PPDA, M-imine, Di-imine, M-amine, Intermediate and Di-amine respectively in kmol/m^3 (as given in Figure 2.4) and C_{eq1}, C_{eq2} and C_{eq3} were the equilibrium concentrations of PPDA, M-imine and Di-imine respectively at that particular reaction temperature. Also k_5, k_8, k_9 were the hydrogenation rate constants for the steps shown in Figure 2.4 and K_{H2} was the adsorption constant for hydrogen.

The overall rate of hydrogenation can be represented as

$$R_{H_2} = R_3 + R_5 + R_6 \tag{2.34}$$

Above-mentioned equations (Equation 2.27-2.34) were solved using an optimization routine based on Marquardt's algorithm[35] combined with fourth order Runge-Kutta method. A non-linear least square regression analysis was used for each rate equation to get the best fit for the particular set of parameters. The optimization method involved an objective function of mean square, the value of which was calculated based on the following formula, which was minimized during the optimization

$$\phi_{\min} = \sum_{i=1}^{6}\sum_{i=1}^{n}\left(Y_{i_{\exp t}} - Y_{i_{\mathrm{mod}}}\right)^2 \qquad 2.35$$

where, $Y_{i_{\exp t}}$ and $Y_{i_{\mathrm{mod}}}$ represented experimental and predicted concentrations of i^{th} species and n represented the number of samples. The mean average of relative residuals (% RR) was calculated based on the following expression:

$$\%RR = \sum_{i=1}^{6}\sum_{i=1}^{n}\frac{\left(Y_{i_{\exp t}} - Y_{i_{\mathrm{mod}}}\right)}{Y_{i_{\exp t}}} \times 100 \qquad 2.36$$

Following criterions were used for the model discrimination:

(i) The estimated parameters must have physico-chemical significance: i.e. the reaction rate constants and the adsorption equilibrium constants should be positive

(ii) The objective function of optimization should be a minimum

(iii) The relative residuals should be distributed with a zero mean and these residuals should have no trend effects as a function of the independent variables.

From the Table 2.7-A and Table 2.7-B, it is evident that none of the models had negative rate or adsorption constants. Also, all the models in Table 2.7-A and Table 2.7-B had similar values of ϕ_{min}. Based on above-mentioned criteria of % RR, Models 2, 3 and 4 were rejected as they had very high values of % RR (±36, ±62 and ±41 respectively). Among the other models (Model 1, 5, 6, 7 and 8), for Model 8 the relative residual values were the lowest at all the temperatures. Two representative graphs of %RR vs. partial pressure of hydrogen for Model 1, 2, 3, 5, 7 and Model 8 are shown in Figures 2.11 and 2.12 respectively. It is seen from Figure 2.11 that the %RR values were not distributed with a zero mean. On the other hand, Model 8 (Figure 2.12) showed a random distribution of relative residual values with a zero mean without any particular trend with change in pressure.

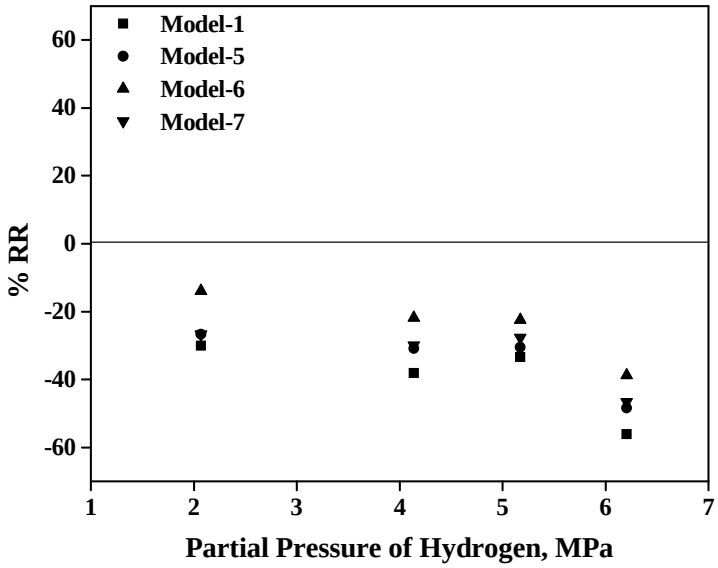

Figure 2.11. % RR versus partial pressure of hydrogen for different models
Reaction Conditions: PPDA: 1.0 kmol/m^3; Catalyst (3% Pt/Al_2O_3): 1 kg/m^3; Temperature: 393 K; Agitation: 16.67 Hz; reaction volume: 1×10^{-4} m^3; MEK is the solvent and one of the reactants.

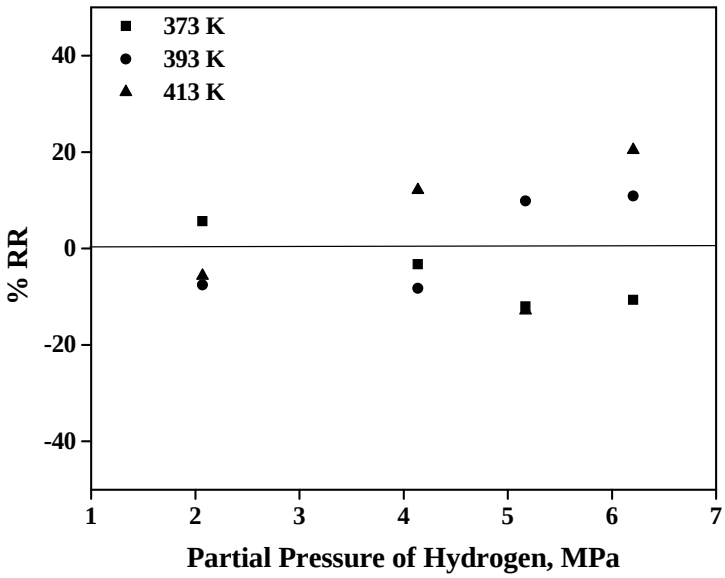

Figure 2.12. % RR versus partial pressure of hydrogen for Model-8 at different temperatures
Reaction Conditions: PPDA: 1.0 kmol/m^3; Catalyst (3% Pt/Al_2O_3): 1 kg/m^3; Agitation: 16.67 Hz; reaction volume: 1×10^{-4} m^3; MEK is the solvent and one of the reactants.

All these models were also verified by comparing all the concentration-time profiles obtained at different initial sets of operating conditions and it was observed that only Model 8 gave satisfactory predictions compared to other models. Therefore, Model 8 was considered to be the best model to predict the experimental results in the range of operating conditions given in Table 2.2. The experimental and predicted concentration-time profiles and hydrogen consumption-time data for this model at various temperatures are shown in Figures 2.13-2.15. The representative concentration-time profiles showed that agreement between model prediction and experimental data were very good.

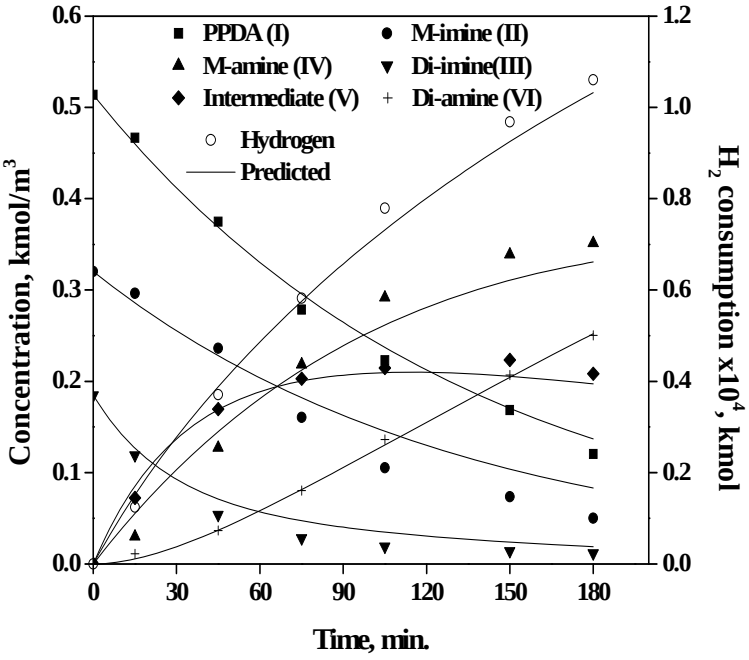

Figure 2.13. Concentration-time profile at 373 K
Reaction Conditions: PPDA: 1.0 kmol/m^3; Catalyst (3% Pt/Al_2O_3): 1 kg/m^3; P_{H2}: 5.17 MPa; Agitation: 16.67 Hz; reaction volume: 1×10^{-4} m^3; MEK is the solvent and one of the reactants.

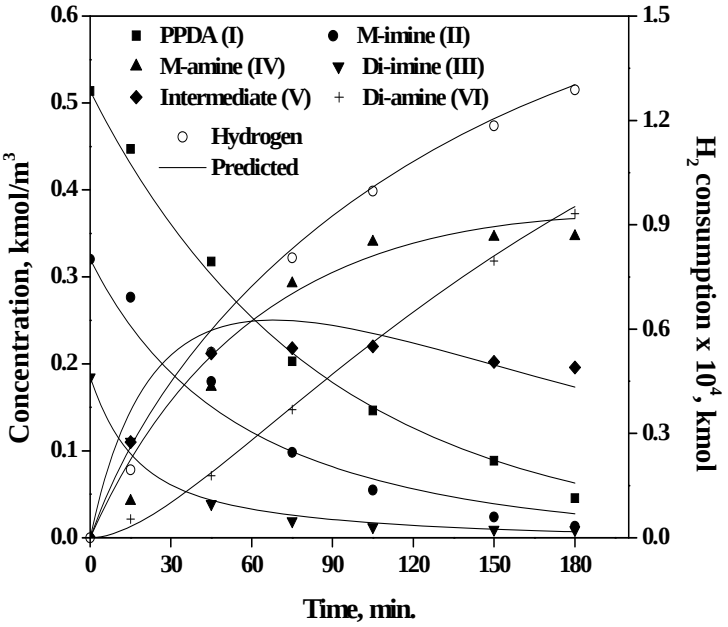

Figure 2.14. Concentration-time profile at 393 K
Reaction Conditions: PPDA: 1.0 kmol/m^3; Catalyst (3% Pt/Al_2O_3): 1 kg/m^3; P_{H2}: 5.17 MPa; Agitation: 16.67 Hz; reaction volume: 1×10^{-4} m^3; MEK is the solvent and one of the reactants.

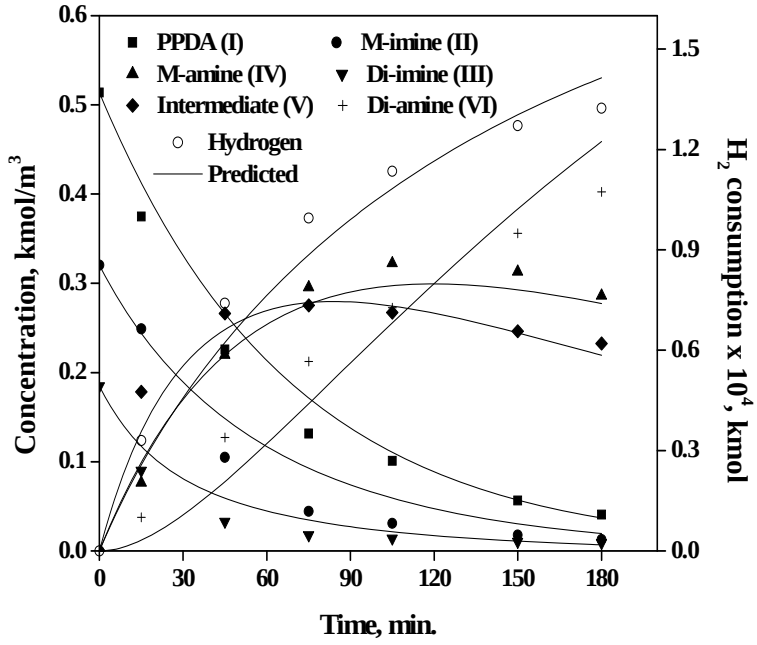

Figure 2.15. Concentration-time profile at 413 K
Reaction Conditions: PPDA: 1.0 kmol/m^3; Catalyst (3% Pt/Al_2O_3): 1 kg/m^3; P_{H2}: 5.17 MPa; Agitation: 16.67 Hz; reaction volume: 1×10^{-4} m^3; MEK is the solvent and one of the reactants.

The temperature dependency of the rate constants is shown in Figure 2.16, from which the activation energies of the individual reactions were calculated as 21.65, 103.51, 29.21, 56.86, 26.97, 29.29, 91.49, 21.37, 15.18 kJ/mol for steps R_1 to R_6 respectively. The enthalpy of adsorption was calculated from the following equation:

$$K_i = K_{io} \exp\left(\frac{-\Delta H_i}{RT}\right) \qquad 2.37$$

The calculated enthalpy of adsorption value for K_{H2} was 10.82 kJ/mol which falls in the range (9-28 kJ/mol) observed earlier for liquid phase hydrogenation reactions catalyzed by supported Pt metal catalysts.[36]

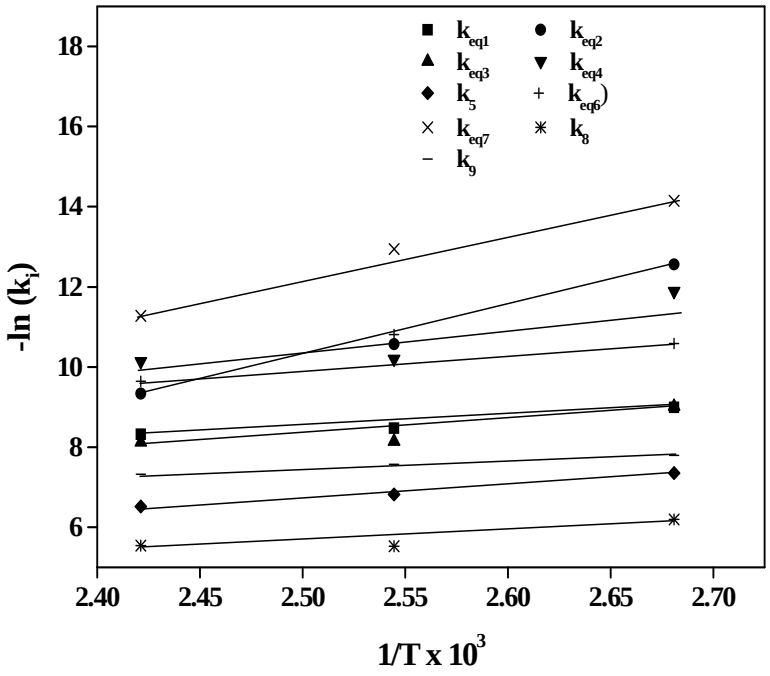

Figure 2.16. Temperature dependency of rate constants

2(A).4 CONCLUSIONS

Platinum on alumina was found to be the best catalyst for selective synthesis of *N, N'*-di-sec-butyl-*p*-Phenylenediamine (Di-amine, VI) by reductive alkylation of *p*-phenylenediamine (PPDA,) and methyl ethyl ketone (MEK). Kinetic modeling of reductive alkylation of PPDA with MEK using 3% Pt/Al_2O_3 catalyst was studied in a temperature range of 373-413 K in a slurry reactor. The external and intraparticle diffusion resistances were found to be negligible in the range of operating conditions studied. A semi batch slurry reactor model was developed to simulate the experimental concentration-time data and evaluate suitability of different rate equations. Rate equations were proposed for both homogeneous (non-catalytic) and heterogeneous (catalytic) reactions and intrinsic kinetic parameters were evaluated. Rate models considering dissociative adsorption of hydrogen followed by reaction with liquid phase components as the rate-limiting step for catalytic reaction steps were found to represent the experimental data satisfactorily.

CHAPTER 2

PART-B

Kinetic Modeling of Reductive Alkylations of Phenylenediamines: Influence of Substrates Isomeric Structure

2 (B).1 INTRODUCTION

Reductive alkylation of nitro or amine compounds to secondary or tertiary amines is an important class of multiphase reaction, which involves homogeneous non-catalytic condensation as well as heterogeneous catalytic reactions. The alkylated products have applications as intermediates in agrochemicals and dyestuffs[5], as anti-oxidants in rubber and petroleum industries, [12,37] and is particularly attractive as a single step process for these specialty products. Because of homogeneous-heterogeneous combination, this is an important class of reaction from academic point of view also.

In Part-A of this chapter, the complexity in the reaction network, product distribution and kinetic modeling for reductive alkylation of *p*-phenylenediamine (PPDA) with MEK in presence of 3% Pt/Al_2O_3 catalyst was studied. In Part-B, the effect of positions of amine groups in phenylenediamine (PDAs) isomers on their relative activities and selectivities in the reductive alkylation reaction using the same catalyst (3% Pt/Al_2O_3) has been studied. Experimental concentration-time data for reductive alkylation of *ortho*-phenylenediamine (OPDA) and *meta*-phenylenediamine (MPDA) with MEK in a semibatch slurry reactor at different sets of initial conditions were obtained to develop suitable semi batch slurry reactor models under isothermal conditions. The kinetic parameters of the individual steps were evaluated following the methodology used for PPDA and compared to understand the differences in the activity and selectivity patterns for OPDA, MPDA and PPDA substrates. A general reaction scheme for the reductive alkylation of PDAs with MEK is shown in Figure 2.17. The systematic study on reductive alkylation of PDAs to understand the substrate structure-activity relationship has not been addressed in previous reports.

2(B).2 EXPERIMENTAL SECTION

OPDA and MPDA were purchased from Loba Chemie, Mumbai, India and used as it is. The other chemicals, catalyst, reactor set up and experimental procedure were same as discussed in section 2(A).2. It should be noted here that experimental concentration-time data for PPDA as substrate were taken from the Part-A of this chapter wherever required for comparison with OPDA and MPDA. The ranges of experimental conditions used for reductive alkylation of PDAs are given in Table 2.8.

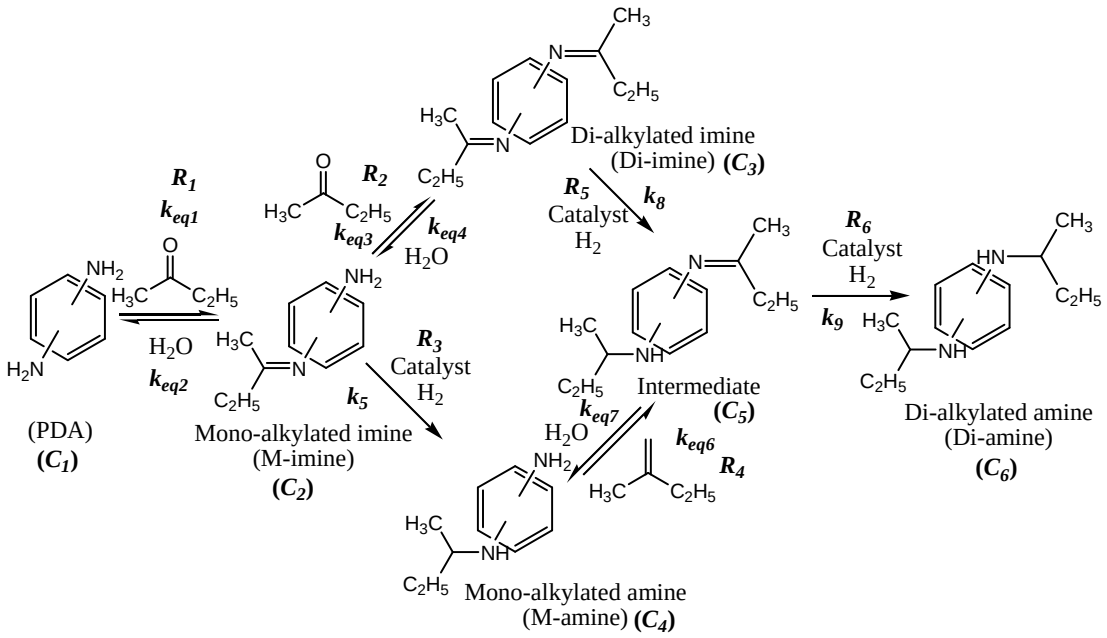

Figure 2.17. General reaction scheme for reductive alkylation of phenylenediamines with methyl ethyl ketone in presence of 3% Pt/Al_2O_3 catalyst

Table 2.8. Range of Operating Conditions for Kinetic Studies of PDAs

Parameter	**PPDA** (Table 2.2)	**OPDA**	**MPDA**
PDA concentration, kmol/m^3	0.5-1.5	0.5-1.5	0.5-1.5
Catalyst loading, kg/m^3	0.2-2	0.5-2	50-75
Hydrogen partial pressure, MPa	2.07-6.21	2.07-6.21	2.07-6.21
Temperature, K	373-413	373-413	413-453
Agitation speed, Hz	13.33-20	13.33-20	13.33-20
Volume of reaction, m^3	1 x 10^{-4}	1 x 10^{-4}	1 x 10^{-4}
Reaction time, h	3	3	6.5

2(B).3 RESULTS AND DISCUSSION

2(B).3.1 Experimental Results

In order to understand the substrate structure and reductive alkylation activity correlation, the influence of relative positions of the amine groups in PDAs on equilibrium and hydrogenation reactions was studied separately.

2(B).3.1.1 Equilibrium Reaction Studies

The equilibrium condensation reactions of OPDA and MPDA with MEK were studied separately and the concentration-time profiles for all the PDAs are shown in Figure 2.18. It was observed that though all the PDAs reached equilibrium at the same time, there was a significant difference in the overall activity and product distribution. The conversion of PDAs at the equilibrium follows an order: OPDA > PPDA > MPDA. Condensation of PPDA with MEK produced both M-imine and Di-imine in appreciable concentrations, whereas for OPDA and MPDA, M-imine remained as the major product.

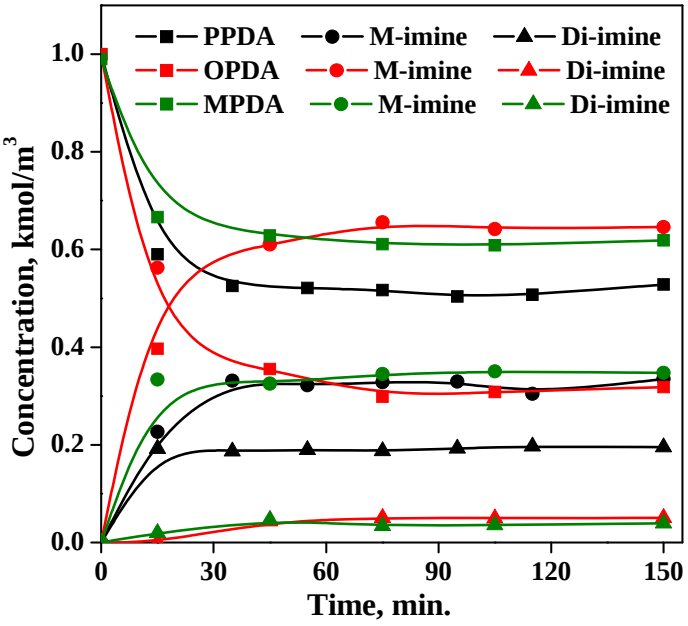

Figure 2.18. Equilibrium concentration-time profiles for PDAs at 413 K.
Reaction Conditions: Substrate: 1.0 kmol/m^3; Agitation: 16.67 Hz; reaction volume: 1×10^{-4} m^3; MEK is the solvent and one of the reactants.

The equilibrium conversion order of PDAs can be explained by considering the activity of PDA reactants and stability of the imine products. As the amines (-NH_2) are ortho- and para- directing groups due to resonance effect,[38] it is expected that the activity (conversion) of OPDA and PPDA will be higher than MPDA. However, to explain the higher equilibrium conversion of OPDA than that of PPDA, stability of the imine products should be considered. The M-imine formed from OPDA has a possibility of intramolecular hydrogen bonding by a five membered ring as shown in Figure 2.19,[39,40] which makes the M-imine stable. On the other hand, there is no possibility of intramolecular hydrogen bonding in the M-imine formed from PPDA. Therefore, higher stability of the M-imine derived from OPDA drags the equilibrium to the imine side more than that of PPDA. Again, the stability of the M-imine derived from OPDA due to intramolecular hydrogen bonding and the possible steric hindrance if the Di-imine forms lead to very poor selectivity of Di-imine from OPDA. On the other hand, the imine functionality in MPDA does not support the other amine group by resonance effect (as it is possible with OPDA and PPDA) and the intrinsic rate of formation of M-imine is very poor for MPDA at the experimental conditions. Therefore, it is expected that Di-imine formation will be significantly lower for MPDA.

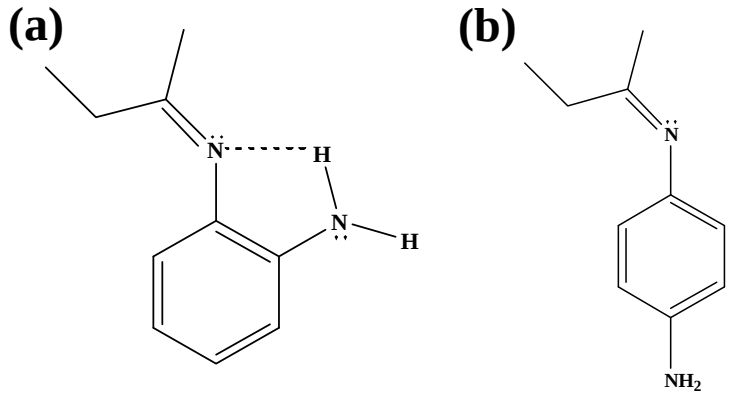

Figure 2.19. (a) Possible intramolecular hydrogen bonding in the M-imine derived from OPDA; (b) intramolecular hydrogen bonding is not possible for M-imine derived from PPDA

2(B).3.1.2 Catalytic Hydrogenation Reaction Studies

The hydrogenation reactions of different PDAs were carried out separately at identical reaction conditions and the typical concentration-time profiles are shown in Figure 2.20. It is evident from these data that for OPDA and MPDA, di-imine formation is negligible even

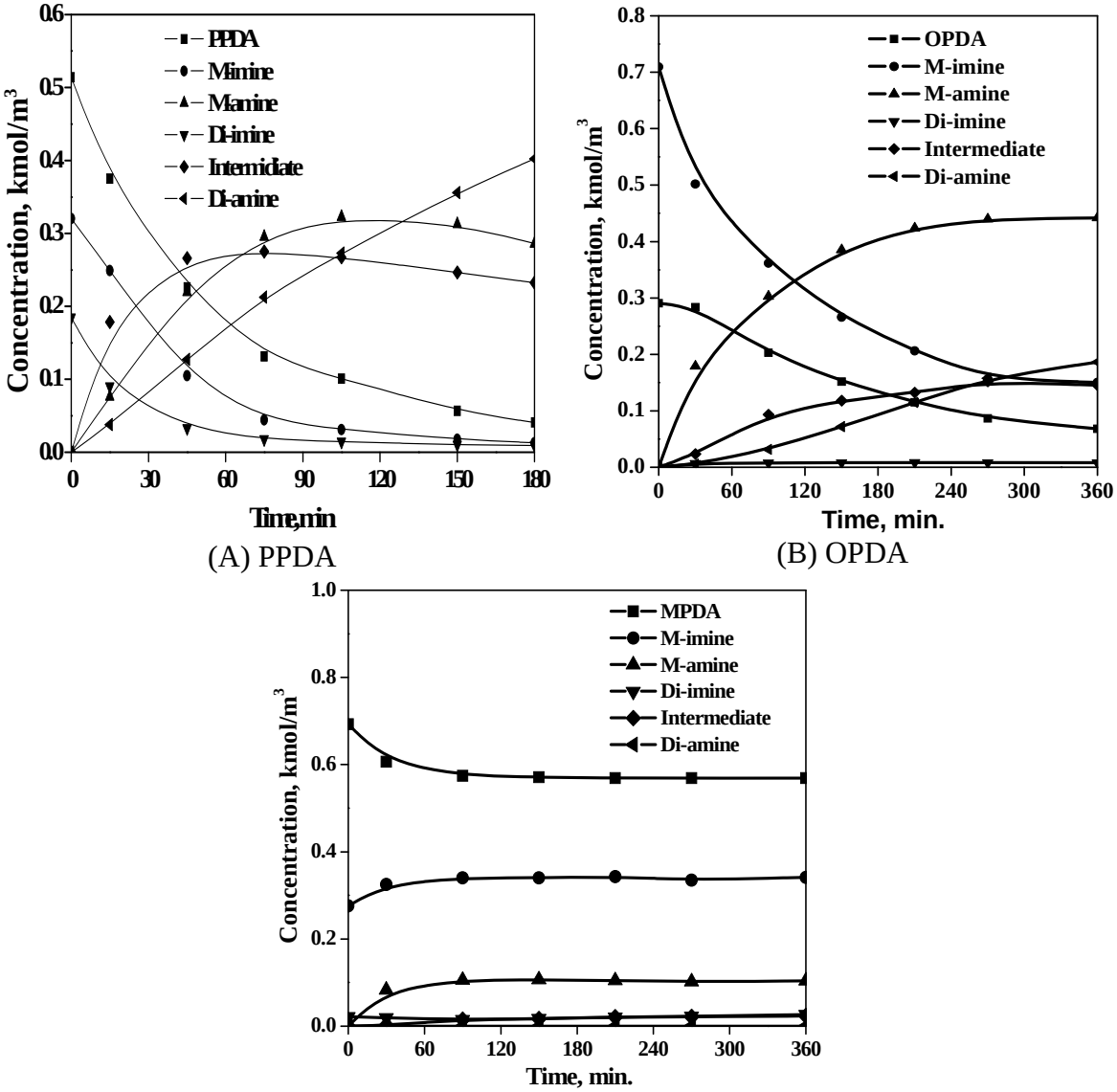

(A) PPDA (B) OPDA

(C) MPDA

Figure 2.20. Typical concentration-time profiles for reductive alkylation PDAs with MEK (A) PPDA (B) OPDA (C) MPDA.

Reaction Conditions: Substrate: 1.0 kmol/m^3; Catalyst (3% Pt/Al_2O_3): 1 kg/m^3; P_{H2}: 5.17 MPa; Temperature: 413 K; Agitation: 16.67 Hz; reaction volume: 1×10^{-4} m^3; Time: 3 h for PPDA and 6 h for OPDA and MPDA; MEK is the solvent and one of the reactants.

under hydrogenation conditions. The selectivity profiles for the final desired products, Di-amines, are shown in Figure 2.21, which showed that it is strongly dependent upon the relative positions of the amine groups in the aromatic ring. The overall rate of hydrogenation also followed the order PPDA > OPDA > MPDA (see Figure 2.22). The overall rate of hydrogenation was very low for MPDA and M-amine was the major product. The selectivity profiles to M-amines as a function of time is shown in Figure 2.23, which showed that M-amine is an intermediate in the overall reaction network for PPDA. Contrary to this, for OPDA and MPDA, the reaction almost stopped after M-amine formation. For MPDA, di-amine formation was improved only with very high catalyst loading (50 times with respect to Fig. 2.20-2.23) and lower substrate concentration conditions as shown in Figure 2.24.

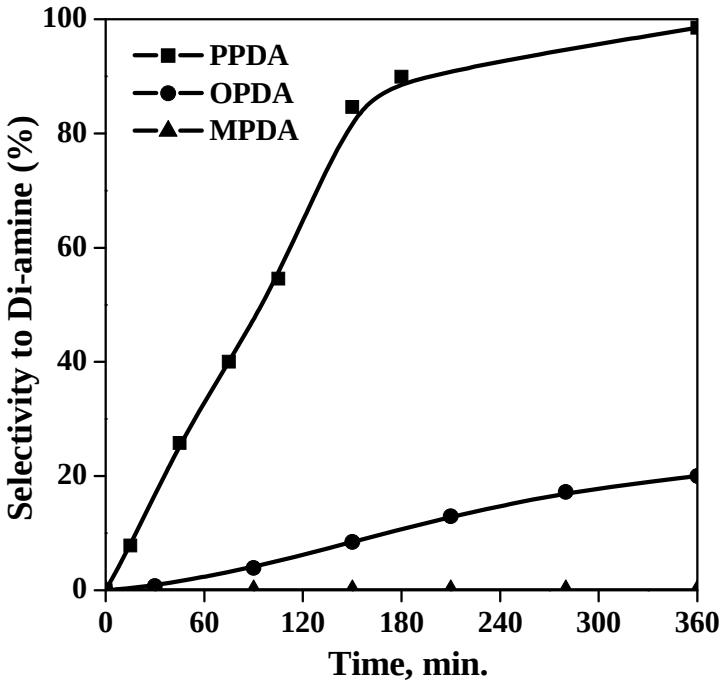

Figure 2.21. Typical selectivity-time profiles for reductive alkylation of PDAs.
Reaction Conditions: Substrate: 1.0 kmol/m^3; Catalyst (3% Pt/Al_2O_3): 1 kg/m^3; P_{H2}: 5.17 MPa; Temperature: 413 K; Agitation: 16.67 Hz; reaction volume: 1×10^{-4} m^3; Time: 3 h for PPDA and 6 h for OPDA and MPDA at the identical conditions. MEK is the solvent and one of the reactants.

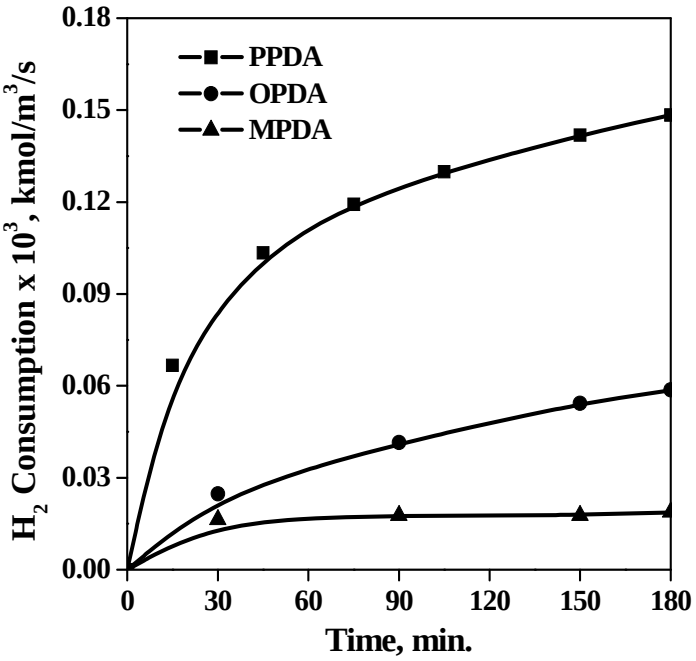

Figure 2.22. Typical H_2 consumption-time profile for reductive alkylation of PDAs with MEK.

Reaction Conditions: Substrate: 1.0 kmol/m^3; Catalyst (3% Pt/Al_2O_3): 1 kg/m^3; P_{H2}: 5.17 MPa; Temperature: 413 K; Agitation: 16.67 Hz; reaction volume: 1×10^{-4} m^3; Time: 3 h for PPDA and 6 h for OPDA and MPDA at the identical conditions. MEK is the solvent and one of the reactants.

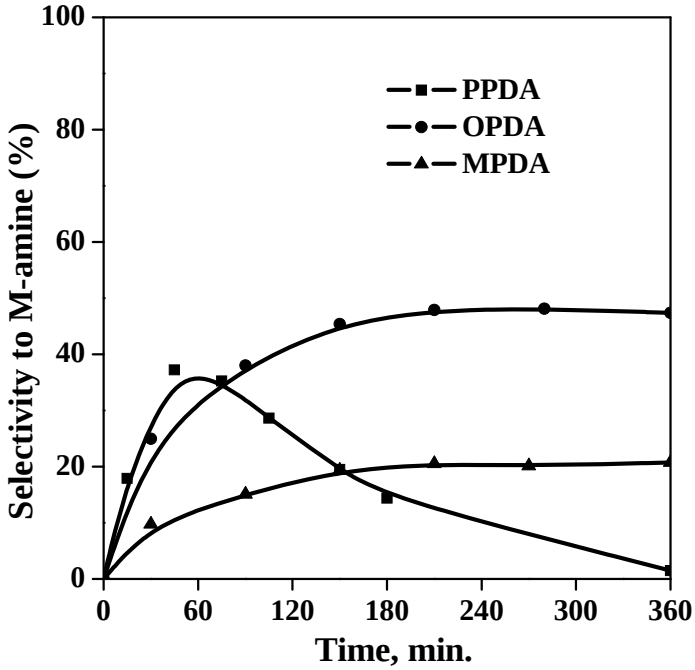

Figure. 2.23. Selectivity to M-amine Vs time profiles for reductive alkylation of PDAs.

Reaction Conditions: Substrate: 1.0 kmol/m^3; Catalyst (3% Pt/Al_2O_3): 1 kg/m^3; P_{H2}: 5.17 MPa; Temperature: 413 K; Agitation: 16.67 Hz; reaction volume: 1×10^{-4} m^3; Time: 3 h for PPDA and 6 h for OPDA and MPDA at the identical conditions. MEK is the solvent and one of the reactants.

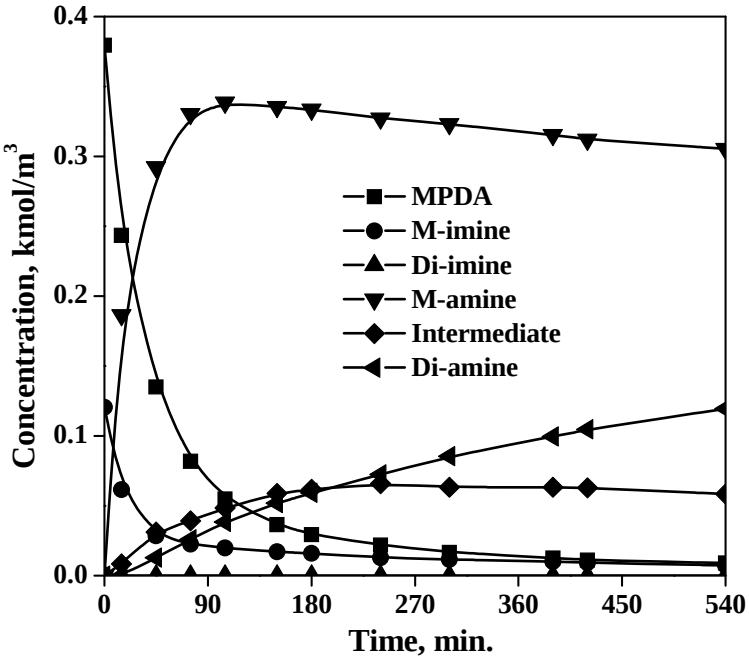

Figure 2.24. Typical concentration-time profiles for reductive alkylation of MPDA with MEK.
Reaction Conditions: Substrate: 0.5 kmol/m^3; Catalyst (3% Pt/Al_2O_3): 50 kg/m^3; P_{H2}: 5.17 MPa; Temperature: 413 K; Agitation: 16.67 Hz; reaction volume: 1×10^{-4} m^3; MEK is the solvent and one of the reactants.

2(B).3.2 Kinetic Modeling

In order to understand the differences in reductive alkylation activity and selectivity of the PDAs, kinetics of reductive alkylation of PDAs with MEK in presence of 3% Pt/Al_2O_3 catalyst were studied. A few preliminary experiments were carried out to identify products, establish mass balance and stability of catalyst during batch reactions. Typical concentration-time profiles for OPDA and MPDA are shown in Figure 2.20. In all the reactions, the material balance of liquid phase components and hydrogen consumed agreed with the products formed to the extent of > 95%. As the overall rate of hydrogenation followed the order PPDA > OPDA > MPDA, it is expected that the mass transfer effects will be negligible for OPDA and MPDA and hence a detailed analysis of the mass transfer effects was not considered for OPDA and MPDA substrates. As shown in Figures 2.18 and 2.20, the formation of di-imine is not significant for OPDA and MPDA throughout the course of the reaction and hence the formation of di-imine from M-imine was not considered for the kinetic modeling of these two substrates. To generalize the notations of

kinetic parameters for all the PDAs, the kinetic parameters are shown in Figure 2.17, where R_2, R_5, k_{eq3}, k_{eq4}, k_8 are applicable only for PPDA. The solubility data for H_2 in liquid medium for OPDA and MPDA were assumed to be the same as that of PPDA substrate, as discussed in Section 2(A).3.2. As discussed earlier, due to the very slow rate of reaction for MPDA, the kinetic study was performed at higher catalyst concentrations and higher temperatures with respect to other PDAs (see Table 2.8).

Several forms of rate equations were considered to represent the different reaction steps involved in reductive alkylation of OPDA and MPDA. For the homogeneous condensation reactions R_1 and R_4, the following rate equations were considered,

$$R_1 = k_{eq1m} C_1 C_m - k_{eq2} C_2 C_{H_2O} \quad 2.38$$

$$R_4 = k_{eq6m} C_4 C_m - k_{eq7} C_5 C_{H_2O} \quad 2.39$$

where, C_m is the concentration of MEK, k_{eq1m}, k_{eq6m} and k_{eq2}, k_{eq7} were the forward and backward reaction rate constants respectively for the steps R_1 and R_4 mentioned in Figure 2.17. For all the kinetic experiments, MEK was used in huge excess with respect to the substrates (OPDA and MPDA) and its change in concentration during the course of reaction was negligible. Therefore, all the forward reaction steps were considered to be pseudo first order reactions. The concentration of water at any time was expressed as

$$C_{H_2O} = C_2 + C_4 + 2C_5 + 2C_6 \quad 2.40$$

Hence, equations 2.36 and 2.37 could be written as

$$R_1 = k_{eq1} C_1 - k_{eq2} C_2 \left(C_2 + C_4 + 2C_5 + 2C_6 \right) \quad 2.41$$

$$R_4 = k_{eq6} C_4 - k_{eq7} C_5 \left(C_2 + C_4 + 2C_5 + 2C_6 \right) \quad 2.42$$

where, $k_{eq1} = k_{eq1m} C_m$, $k_{eq6} = k_{eq6m} C_m$

For catalytic hydrogenation steps (R_3, R_5 and R_6), all the eight rate models as described for PPDA (see Section 2(A).3.5) were considered. Typical semi-batch slurry reactor mass balance equations for reductive alkylation of OPDA and MPDA with MEK considering reaction of adsorbed β-hydride [Pt (H)] species with liquid phase components for the hydrogenation steps are shown below:

$$\frac{dC_1}{dt} = -R_1 = -\left[k_{eq1} C_1 - k_{eq2} C_2 \left(C_2 + C_4 + 2C_5 + 2C_6 \right) \right] \quad 2.43$$

$$\frac{dC_2}{dt} = R_1 - R_3 = \left[k_{eq1}C_1 - k_{eq2}C_2\left(C_2 + C_4 + 2C_5 + 2C_6\right)\right] - \frac{wk_5\sqrt{A^*}C_2}{\left(1 + K_{H_2}\sqrt{A^*}\right)} \quad 2.44$$

$$\frac{dC_4}{dt} = R_3 - R_4 = \frac{wk_5\sqrt{A^*}C_2}{\left(1 + K_{H2}\sqrt{A^*}\right)} - \left[k_{eq6}C_4 - k_{eq7}C_5\left(C_2 + C_4 + 2C_5 + 2C_6\right)\right] \quad 2.45$$

$$\frac{dC_5}{dt} = R_4 - R_6 = \left[k_{eq6}C_4 - k_{eq7}C_5\left(C_2 + C_4 + 2C_5 + 2C_6\right)\right] - \frac{wk_9\sqrt{A^*}C_5}{\left(1 + K_{H_2}\sqrt{A^*}\right)} \quad 2.46$$

$$\frac{dC_6}{dt} = R_6 = \frac{wk_9\sqrt{A^*}C_5}{\left(1 + K_{H2}\sqrt{A^*}\right)} \quad 2.47$$

Initial conditions:

At t = 0, $C_1 = C_{eq1}$, $C_2 = C_{eq2}$ & $C_4, C_5, C_6 = 0$

where, C_1 to C_6 were the concentrations of the species mentioned in Figure 2.17 and C_{eq1}, and C_{eq2} were the equilibrium concentrations of PDA and M-imine respectively at that particular reaction temperature. K_{H2} was the adsorption constant for hydrogen.

Total rate of hydrogenation can be represented as:

$$R_{H_2} = R_3 + R_5 + R_6 \quad 2.48$$

Equations 2.43-2.48 were solved using fourth order Runge-Kutta method combined with an optimization program based on Marquardt's algorithm.[35] A non-linear least square regression analysis was used for each rate equations to get the best fit for the particular set of parameters. An objective function (ϕ_{min}) and mean average relative residuals (%RR), which were defined in Section 2(A).3.5, were considered as mathematical criteria to select a suitable model after optimization. Among several forms of rate equations considered for the hydrogenation steps, the rate equation which was suitable for PPDA also represented OPDA and MPDA for the range of operating conditions used (see Table 2.8). The experimental and predicted concentration-time profiles for OPDA and MPDA at different conditions are shown in Figures 2.25 and 2.26. It is evident from Figures 2.25 and 2.26 that the model predicts the experimental results quite well and the nature of interaction of the imine species with the catalyst surface during the hydrogenation reactions are similar for all

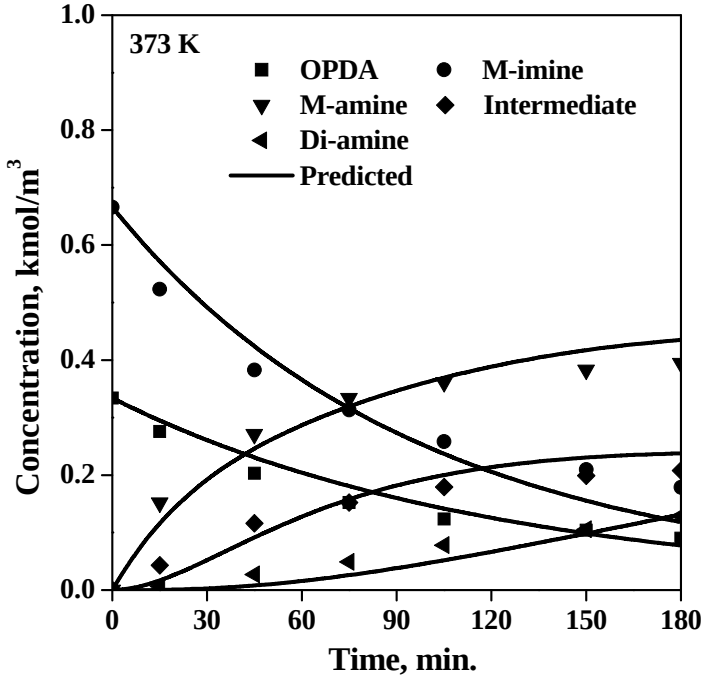

(A) 373K

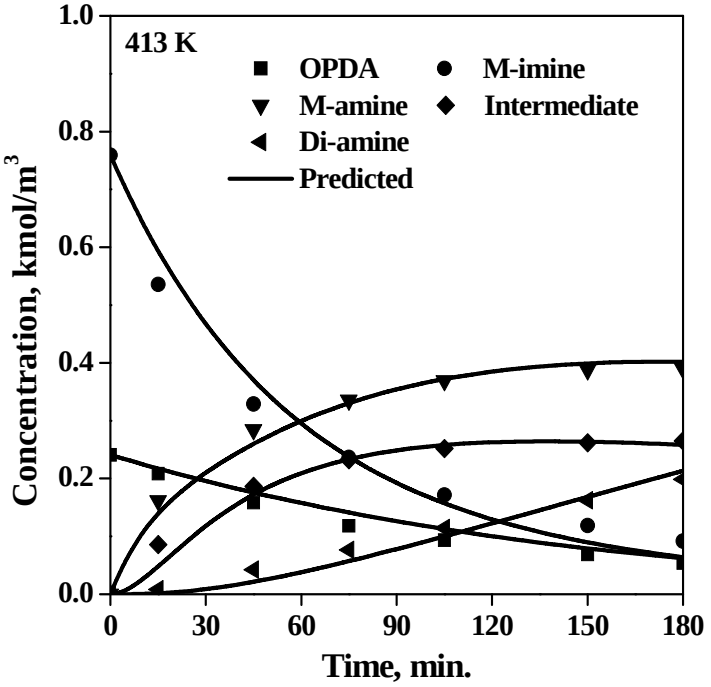

(B) 413K

Figure 2.25. Concentration-time profiles for reductive alkylation of OPDA at 373 K and 413 K.

Reaction Conditions: Substrate: 1.0 kmol/m^3; Catalyst (3% Pt/Al_2O_3): 1 kg/m^3; P_{H2}: 5.17 MPa; Agitation: 16.67 Hz; reaction volume: 1×10^{-4} m^3; Time: 3 h; MEK is the solvent and one of the reactants.

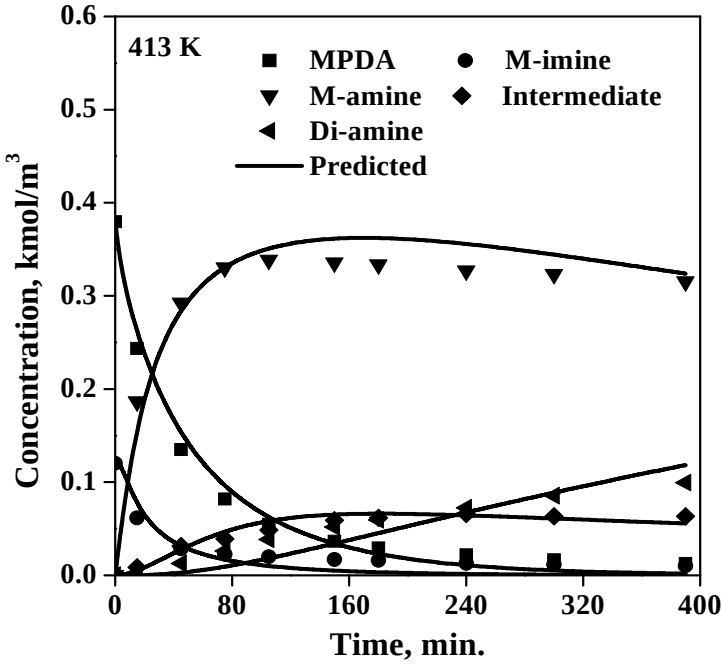

(B) 413K

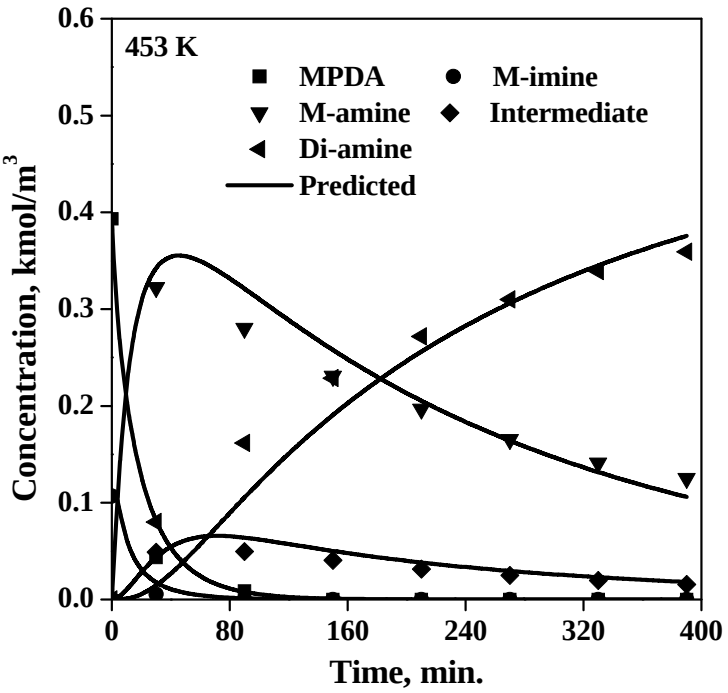

(B) 453K

Figure 2.26. Concentration-time profiles for reductive alkylation of MPDA at 413 K and 453K

Reaction Conditions: Substrate: 0.5 kmol/m^3; Catalyst (3% Pt/Al_2O_3): 50 kg/m^3; P_{H2}: 5.17 MPa; Agitation: 16.67 Hz; reaction volume: 1×10^{-4} m^3; Time = 6.5 hrs. MEK is the solvent and one of the reactants.

the PDAs. The optimized kinetic parameters for PPDA, OPDA and MPDA at different temperatures are presented in Table 2.9.

The optimized kinetic parameters presented in Table 2.9 explained the trends observed in reductive alkylation of PDAs. The rate constant for hydrogenation of M-imine to M-amine (k_5) followed the trend PPDA > OPDA > MPDA. More interestingly, the values of k_{eq6} and k_{eq7} clearly indicated that the formation of intermediate from M-amine is not so favorable for OPDA and very difficult for MPDA. This also explains why Di-imine was not formed in appreciable amounts in the equilibrium studies for OPDA and MPDA. Steric hindrance of bulky groups in the *ortho-* position and the possible intramolecular hydrogen bonding may be the reasons for lower activity toward Di-imine or intermediate products for OPDA with respect to PPDA. On the other hand, the intrinsically lower activity of MPDA as discussed in section 2(B).3.1.1 may be attributed to poor Di-imine and intermediate selectivity with MPDA. However, energy calculations by molecular modeling of the species formed during reductive alkylation of PDAs could be a useful approach to further understand the reductive alkylation activity and selectivity trends for different substrates.

Table 2.9. Comparison of Kinetic Parameters for Reductive Alkylation of PDAs with MEK in Presence of 3% Pt/Al_2O_3 Catalyst

	Temp K	k_{eq_1} **× 10³**	k_{eq_2} **× 10⁴**	k_{eq_3} **× 10⁴**	k_{eq_4} **× 10⁴**	k_5 **× 10²**	k_{eq_6} **× 10⁴**	k_{eq_7} **× 10⁵**	k_8 **× 10²**	k_9 **× 10³**	K_{H_2}	**% RR**	**Ø min** $\times 10^4$
PPDA (Table 2.7-B)	373	0.1248	0.0351	1.214	0.0692	0.0639	0.2539	0.072	0.2035	0.4110	1.605	±12.03	1.48
	393	0.2091	0.2562	2.910	0.3732	0.1091	0.2018	0.2397	0.3980	0.5147	1.111	±9.83	10.2
	413	0.2440	0.8807	2.981	0.3981	0.1481	0.6497	1.267	0.3923	0.6609	1.6395	±12.87	3.76
OPDA	373	0.1464	0.0638	--	--	0.0558	3.347	40.66	--	0.1847	0.15	±15.14	7.47
	393	0.1489	0.1953	--	--	0.0688	6.754	77.19	--	0.1902	0.3905	±12.63	5.5
	413	0.1644	0.2105	--	--	0.0877	8.589	89.46	--	0.27	0.804	±6.67	4.51
MPDA	413	0.984	91.3	--	--	0.0088	0.72	51.0	--	0.0048	0.3	±26.46	1.89
	433	1.742	105.0	--	--	0.017	0.98	59.81	--	0.014	0.8	±32.29	5.35
	453	1.942	118.0	--	--	0.032	1.55	62.0	--	0.031	1.80	±14.77	3.69

2(B).4 CONCLUSIONS

The effect of positions of amine groups in phenylenediamine isomers on their relative activities and selectivities in the reductive alkylation reaction using 3% Pt/Al_2O_3 catalyst was studied. It was observed that the activity and selectivity to Di-amine product followed the order: PPDA > OPDA > MPDA. To understand the isomeric structure-activity relationship, the equilibrium and hydrogenation steps involved in reductive alkylation reaction were studied separately. It was observed that Di-imine formation is not favorable in the equilibrium condition for OPDA and MPDA. However, it is formed in appreciable amounts with PPDA. To explain the observed structure-activity relationship, kinetic modeling for reductive alkylation of PDAs and the optimized kinetic parameters were presented. The kinetic parameters (k_5) showed that formation of M-amine from M-imine followed the order PPDA > OPDA > MPDA and insertion of the second alkylating group on the second amine functionality (to form intermediate) was not so feasible for OPDA and very difficult for MPDA. Therefore, formation of Di-amine also followed the order PPDA > OPDA > MPDA.

NOMENCLATURE

a_B	=	gas-liquid interfacial area per unit volume of reactor, m^2/m^3
a_p	=	liquid-solid interfacial area, m^{-1}
$_A^*$	=	saturation solubility of H_2 in liquid phase, $kmol/m^3$
C_1 *to* C_6	=	concentrations of species involved in overall reaction sequence, $kmol/m^3$
C_m	=	concentration of methyl ethyl ketone
C_{eq1}, C_{eq2} and C_{eq3}	=	equilibrium concentration of PPDA, M-imine and Di-imine respectively, $kmol/m^3$
D_e	=	effective diffusivity, m^2/s
d_I	=	impeller diameter, m
D_M	=	molecular diffusivity, m^2/s
d_p	=	particle diameter, m
d_t	=	tank diameter, m
e	=	energy supplied (by agitator or gas bubbling) to the liquid per unit mass, cm^2/s^3
F_c	=	shape factor of the catalyst
H_e	=	henry's law constant, $kmol/m^3/atm$
h_1	=	height of the first impeller from the bottom, m
h_2	=	height of the liquid, m
k_L	=	liquid film mass-transfer coefficient, m/s
$k_L a_B$	=	gas-liquid mass-transfer coefficient, s^{-1}
k_s	=	liquid-solid mass-transfer coefficient, m/s
K_{H2}	=	adsorption equilibrium constant for hydrogen, $(kmol/m^3)^{-0.5}$
k_5, k_8 *and* k_9	=	reaction rate constants, $(kg/m^3)^{-1}(kmol/m^3)^{-0.5}\ s^{-1}$

$k_{eq1}, k_{eq3}, k_{eq6}$ = forward reaction rate constants, s^{-1}

$k_{eq2}, k_{eq4}, k_{eq7}$ = backward reaction rate constants, $(kmol/m^3)^{-1}\ s^{-1}$

m = order of reaction w.r.t. hydrogen

M_W = molecular weight of solvent, g/gmol

n = moles of gas at constant pressure, kmol

N = agitation speed, Hz

N_p = power number

P_{H2} = partial pressure of hydrogen, MPa

Q_g = volumetric flow rate of gas, m^3/s

R = universal gas constant, N m/mol K

R_{H_2} = overall rate of hydrogenation, $kmol/m^3/s$

R_1 *to* R_6 = reaction rates for individual reaction steps, $(kmol/m^3/s)$

r_{max} = maximum rate of hydrogenation, $kmol/m^3/s$

T = temperature, K

t = time, s

V_g = volume of the gas in the reactor, m^3

V_l = volume of the liquid in the reactor, m^3

w = catalyst loading, kg/m^3

Greek letters

α_1 = parameter defined by eq. 2.5

α_2 = parameter defined by eq. 2.6

Φ_{exp} = parameter defined by eq. 2.7

Φ_{min} = parameter defined by eq. 2.33

ρ_l = density of liquid, kg/m^3

μ_l = viscosity of liquid, poise

χ = association factor

v_M = molar volume of solvent, cm^3/mol

ρ_p = density of particle, kg/m^3

ε = porosity of the catalyst particle

τ = tortuosity

ψ = correction factor for gas bubbles

REFERENCES

1. Lehtonen, J.; Salmi, T.; Vaori, A.; Tirronen, E. On the principles of modeling of homogeneous-heterogeneous reactions it the production of fine chemicals. A case study: Reductive alkylation of aromatic amines. *Org. Pros. Res. Dev.,* **1998**, *2(2)*, 78.
2. Hayes, K. S. Industrial processes for manufacturing amines. *App. Cat. -A General,* **2001**, *221*, 187.
3. Symon, T. Preparation of N, N'-di-alkyl-phenylenediamines. *US 4140718*, **1979**.
4. Kirby, A. F.; Willingboro, N. J. Reductive alkylation process for production of N-alkylated amines. *US 3522309*, **1970**.
5. Mylorie, V. L. Reductive alkylation process to prepare tertiary aminoaryl cyan dye-transfer intermediates. *US 5861535*, **1999**.
6. Zhou, X.; Wu, Z.; Lin, L.; Wang, G.; Li, J. Selective synthesis of N-monoalkyl aryl-amines from nitro aromatic compounds by reductive alkylation. *Dyes and Pig.* , **1998**, *36(4)*, 365.
7. Ege, S. *Organic chemistry, Structure and Reactivity*, 3rd ed.; D. C. Heath and Co.; Lexington, KY, **1994**, p535.
8. Kaneko, M.; Tanaka, S. Method of manufacturing alkyl-aniline compounds. *EP 760360*, **1997**.
9. Nishimura, T.; Takeda, F.; Wada, M.; Kanemura, Y.; Preparation of N-alkyl-substituted aromatic amines. *JP 2000095739*, **2000**.
10. Greenfield, H. Side Reactions in reductive alkylation of aromatic amines with aldehydes and ketones. *Chem Ind. (Dekker)*, **1994**, *53* (catalysis of organic reactions), 265.
11. Bonds, A. P.; Greenfield, H. The reductive alkylation of aromatic amines with formaldehyde. *Chem. Ind. (Dekker),* (catalysis of organic reactions), 65.
12. Watanabe, T. Preparation of di- (substituted amino) diphenylamines as antioxidants and antiozonants for polymers. *JP 10168038*, **1998**.
13. Malz, R. E., Jr.; Greenfield, H. Tertiary Amine preparation by reductive alkylation of aliphatic secondary amines with ketones. *Heterogeneous catalysis and fine chemicals II*, Elsevier science publishers B.V., Amsterdam, **1991**, 351.
14. Mylorie, V. L.; Valente, L.; Fiorella, L.; Osypian, M. A. Reductive alkylation optimized by techniques of experimental design. *Chem. Ind. (Dekker),* **1996**, *68* (Catalysis of organic reactions), 301.
15. Malz, R. E., Jr.; Jancis, E. H.; Renolds, M. P.; O'leary, S. T. Reductive alkylation of acetophenone with aniline. *Chem. Ind. (Dekker)*, **1995**, *62* (Catalysis of organic reactions), 263.

16. Ross, L. J.; Levy, S. D. Reductive alkylation of substituted anilines. *US 4190601*, **1980**.
17. Wilson, F. H., Jr. Modified nickel catalyst systems and their use in reductive alkylation reactions. *US 4043942*, **1977**.
18. Salmi, T.; Lehtonen, J.; Kaplin, J.; Vuori, A.; Tirronen, E.; Haarrio, H. A homogeneoys-heterogeneously catalysed reaction system in a loop reactor. *Cat. Today*, **1999**, *48*, 139.
19. Roy, D.; Jaganathan, R.; Chaudhari, R. V.; Kinetic modeling of Aniline with Acetone using 3% Pd/Al_2O_3 catalyst in a batch slurry reactor. *Ind. Eng. Chem. Res.*, **2005**, *44*, 5388.
20. Goodyear tyre and rubber company, USA. Catalytic reductive alkylation process. *US 1116967*, **1968**.
21. Universal oil products company, USA. Improvements in or relating to reductive alkylation process. *US 774345*, **1957**.
22. United states rubber company, USA. Reductive alkylation process. *US 1064958*, **1967**.
23. Edward, J. B. Reductive alkylation of amines. *US 3209030*, **1965**.
24. Universal oil products company, USA. Improvements in or relating to reductive alkylation process. *US 797224*, **1958**.
25. Rosenwald, R. H. Reductive alkylation process. *US 2779789*, **1957**.
26. Yeon, J. J.; Jong, W. B.; Eun, S. P.; Yu, M. C.; Cheol, M. Y. An efficient conversion of nitroaromatics and aromatic amines to tertiary amines in one-pot way. *Tetrahedron*, **2003**,*59*,1031.
27. Merten, H. L.; Baclawski, L. M. Process for producing N, N'-disubstituted p-phenylenediamine mixtures by sequential reductive alkylation. *US 4900868*, **1990**.
28. Seayad, A. M.; Seayad, J.; Mills, P. L.; Chaudhari, R.V. Kinetic modeling of carbonylation of 1-(4-Isobutylphenyl) ethanol using a homogeneous $PdCl_2(PPh_3)_2$/TsOH/LiCl catalyst system. *Ind. Eng. Chem. Res.,* **2003**, *42,* 2496.
29. Ramachandran, P. A.; Chaudhari, R. V. *Three Phase Catalytic Reactors*. Gordon & Breach: New York, **1983**.
30. Gholap, R. V.; Chaudhari, R. V.; Hofmann, H. Gas-liquid mass transfer in 'dead end' autoclave reactors. *Can. J. Chem. Eng.*, **1987**, *65(5)*, 744.
31. Sano, Y.; Yamaguchi, N.; Adachi, T. Mass transfer coefficients for suspended particles in agitated vessels and bubble columns. *J. Chem. Eng. Jpn.*, **1974**, *1*, 255.
32. Calderbank, P. H. Physical rate processes in industrial fermentation Part I. The interfacial area in gas-liquid contacting with mechanical agitation. *Trans. Inst. Chem. Eng.*, **1958**, 36, 443.
33. Wilke, C. R.; Chang, P. Correlation of diffusion coefficients in dilute solutions. *AIChE J.*, **1955**, *1*, 264.
34. (a) Paal, Z., Menon, P. G. Hydrogen effects in metal catalysts. *Catal. Rev. Sci. Eng.*, **1983**, *25*, 229. (b) Dyall, K. G. Relativistic effects on the bonding and properties of the hydrides of platinum. *J. Chem. Phys.*, **1993**, *98(12)*, 9678. (c) Fast, J. D. *Gases in metals*. Philips Technical Library, Eindhoven, **1976**.
35. Marquardt, D.W. An algorithm for least squares estimation of nonlinear parameters. *Journal of the Society of Industrial and Applied Mathematics (SIAM)*, **1963**, *11*:431.
36. (a) Rode, C. V.; Chaudhari, R. V. Hydrogenation of *m*-Nitrochlorobenzene to *m*-nitrochloroaniline: Reaction kinetics and modeling of a non-isothermal slurry reactor. *Ind. Eng. Chem. Res.* **1994***, 33*, 1645. (b) Rode, C. V.; Vaidya, M. J.; Jaganathan R.; Chaudhari, R. V. Hydrogenation of nitrobenzene to *p*-aminophenol in a four phase reactor: Reaction kinetics and mass transfer effects. *Chem. Eng. Sci.*, **2001**, *56,* 1299 (c) Vaidya, M. J.; Kulkarni, S. M.; Chaudhari, R. V. Synthesis of *p*-aminophenol by catalytic hydrogenation of *p*-nitrophenol. *Org. Proc. Res. & Dev.*, **2003**, *7* 202.
37. Deblase, F.J.; Fox, B.E.; Migdal, C.A. Aromatic diamine-hindered phenol mixtures as antioxidants for biodiesel fuels. US 2007289203, **2007,** A1.
38. Solomons, T.W.G. Organic chemistry. Sixth Edition. John Wiley & Sons, Inc., **1996**, 655.
39. Sadekov, I.D.; Minkin, V.I.; Lutskii, A.E. The intramolecular hydrogen bond and the reactivity of organic compounds. Russian Chemical Reviews, **1970**, *39 (3)*, 179-195.
40. Yu, W-S.; Cheng, C.C.; Cheng, Y.-M.; Wu, P.-C.; Song, Y.-H.; Chi, Y.; Chou, P.-T., (2003). Excited-state intramolecular proton transfer in five-membered hydrogen-bonding systems: 2-pyridyl pyrazoles. J. Am. Chem. Soc. **2003**, *125*, 10800-10801.

CHAPTER 3

Modeling of Bubble Column Slurry Reactor for Reductive Alkylation of *p*-Phenylenediamine

3.1 INTRODUCTION

Bubble column slurry reactors (BCSR), which involve contacting of gaseous and liquid reactants in the presence of suspended solid catalyst particles are extensively used in several industrial chemical and petroleum refining processes due to their better heat and mass transfer efficiencies. Fine catalyst particles can be used in these reactors, which eliminate intraparticle diffusional resistance, leading to more effective use of the catalyst. The design and scale up of these reactors is of considerable interest, since a number of fundamental and practical issues can be defined that introduce uncertainties in the prediction of reactor performance. Important developments in the reaction engineering analysis of BCSRs were reviewed in earlier work by Shah[1], Ramachandran and Chaudhari[2], and Deckwer[3]. More recent reviews have been provided by Saxena[4], Duducovic[5], Krishna[6], Jakobsen *et. al.*[7], and in the monograph of Schumpe and Nigam[8]. Some examples of the commercial applications of BCSRs include Fischer-Tropsch-synthesis,[9,10,11,12] hydrogenation of adiponitrile,[13] hydrogenation of oils,[14] and several unsaturated compounds. In these studies, either a semi-batch or continuous mode is used, or in some cases, a continuous flow with recycle operation is employed.

The overall performance of these reactors depends on the specific reaction kinetics, mass transfer effects, hydrodynamics, solid catalyst distribution and thermal energy management. In addition, the mixing pattern of gas and liquid phases is also important in deciding the overall efficiency of such reactors. While the analysis of multiphase catalytic reactors has been well developed from a theoretical perspective for simple reactions, the information on the analysis of reactor performance for industrially useful processes in BCSRs is very limited. In previous work on the modeling of BCSRs, detailed consideration has been given to hydrodynamic modeling, particularly CFD modeling,[11, 12,15] evaluation of mixing,[16] and mass-transfer parameters.[17,18] Although, reactor performance models have been proposed for several reactions, such as the Fischer-Tropsch synthesis,[10,11,12] hydrogenation of glucose,[19] and the hydrogenation of butynediol,[20] in most of these cases, only single reactions with simplified kinetics have been considered. Thakar *et. al.*[21] have modeled the hydrogenation of maleic acid to tetrahydrofuran (THF) in BCSR, taking into account the distribution pattern of the product THF in the gas and liquid phases. Industrial BCSRs typically involve complex multistep catalytic reactions with complexities such as

nonlinear kinetics, catalyst deactivation, exothermic reactions and non-uniform distribution of catalyst particles. One such application is the reductive alkylation of amine compounds for the manufacture of higher alkylated (secondary and tertiary) amine derivatives, which find applications as intermediates in fine chemicals and speciality products.[22] The reductive alkylation reaction proceeds through a condensation reaction between an amine compound or its precursor and a carbonyl compound or alcohol to form an imine – a Schiff Base,[23] which is hydrogenated in the presence of a metallic catalyst to *N*-alkylated products. Reductive alkylation of nitro or amine compounds has been investigated using a wide range of alkylating agents and catalysts.[24]

Most of the previous work on reductive alkylation was focused on catalysis aspects with the aim of improving catalytic activity and selectivity to *N*-alkylated compounds. However, the reaction system has not been studied much from reaction engineering viewpoint. There are only a few reports in the literature, which deal with combinations of homogeneous-heterogeneous, non-catalytic-catalytic reactions. Lehtonen *et. al.*[22], followed by Salmi *et. al.*,[25] developed semibatch slurry reactor and loop reactor models for reductive alkylation of aromatic amines with short chain aldehydes (carbon chain length less than three) using Pt/C catalyst. Roy *et. al.*[26] have studied a detailed kinetics for the reductive alkylation of aromatic monoamines (aniline), in which the impact of homogeneous and heterogeneously catalyzed reactions on the overall reaction kinetics was addressed.

Considering the wider applicability of bubble column slurry reactors, investigations on more case studies of practical relevance like reductive alkylation reactions will further establish the confidence in the use of predictive models for understanding BCSR performances. In this context, this work was undertaken in which the modeling of BCSR for reductive alkylation of *p*-phenylenediamine (PPDA) with methyl ethyl ketone (MEK), wherein two amine functionalities are available for the alkylation reaction, was undertaken as an objective of this work. A schematic of the reaction network considered in this work is shown in Figure 3.1.

The mixing cell model[2] has been developed for BCSR using the kinetics presented in Chapter-2. The model incorporates the gas-liquid, liquid-solid mass transfer, heat effects and complex multistep reaction kinetics. The changes in gas and liquid velocities influence the hydrodynamics of slurry bubble column reactors and therefore alter degree of back

mixing in liquid phase.[15] Therefore, liquid phase back-mixing was accounted for in this study by including a backflow (obtained using CFD) among mixing cells. The effect of gas and liquid velocities, catalyst loading, inlet substrate concentration and temperature on the conversion, selectivity and temperature rise is discussed. The comparison of the current approach with the traditional mixing cell model is also discussed. The details of BCSR model are discussed in the following sections.

3.2 BCSR MODEL

A detailed analysis of a BCSR model has been presented using a mixing cell approach. A mixing cell approach proposed earlier by Ramachandran and Smith[27], Brahme *et. al.*[19] and Jaganathan *et. al.*[20] has been extended in this work by including a liquid-backflow stream from all but the bottom most mixing cell. This model incorporated the complexities of reaction kinetics coupled with mass transfer and the thermal effects.

3.2.1 Intrinsic Kinetics

The intrinsic kinetics for the reductive alkylation of PPDA with MEK to *N, N'*-di-sec-butyl-*p*-Phenylenediamine using 3% Pt/Al_2O_3 as catalyst has been presented in Chapter-2, Part-A, for a semi-batch slurry reactor. Based on this work, the reaction network is described as shown in Figure 3.1. The following types of rate equations for non-catalytic (R_1, R_2 and R_4) steps has been found to adequately describe the individual homogeneous reaction steps,

$$R_1 = k_{eq1} B_l - k_{eq2} D_l C_{H_2O} \quad 3.1$$

$$R_2 = k_{eq3} D_l - k_{eq4} F_l C_{H_2O} \quad 3.2$$

$$R_4 = k_{eq6} G_l - k_{eq7} H_l C_{H_2O} \quad 3.3$$

where, $k_{eq1} = k_{eq1m} C_m$, $k_{eq3} = k_{eq3m} C_m$, $k_{eq6} = k_{eq6m} C_m$

$$C_{H_2O} = \left(D_l + 2F_l + G_l + 2H_l + 2P_l\right)$$

where, k_{eq1}, k_{eq3}, k_{eq6} and k_{eq2}, k_{eq4}, k_{eq7} were the forward and backward reaction rate constants respectively for the steps R_1, R_2 and R_4 mentioned in Figure 3.1 and C_m represents the concentration of methyl ethyl ketone. For all the kinetic experiments, MEK was used in

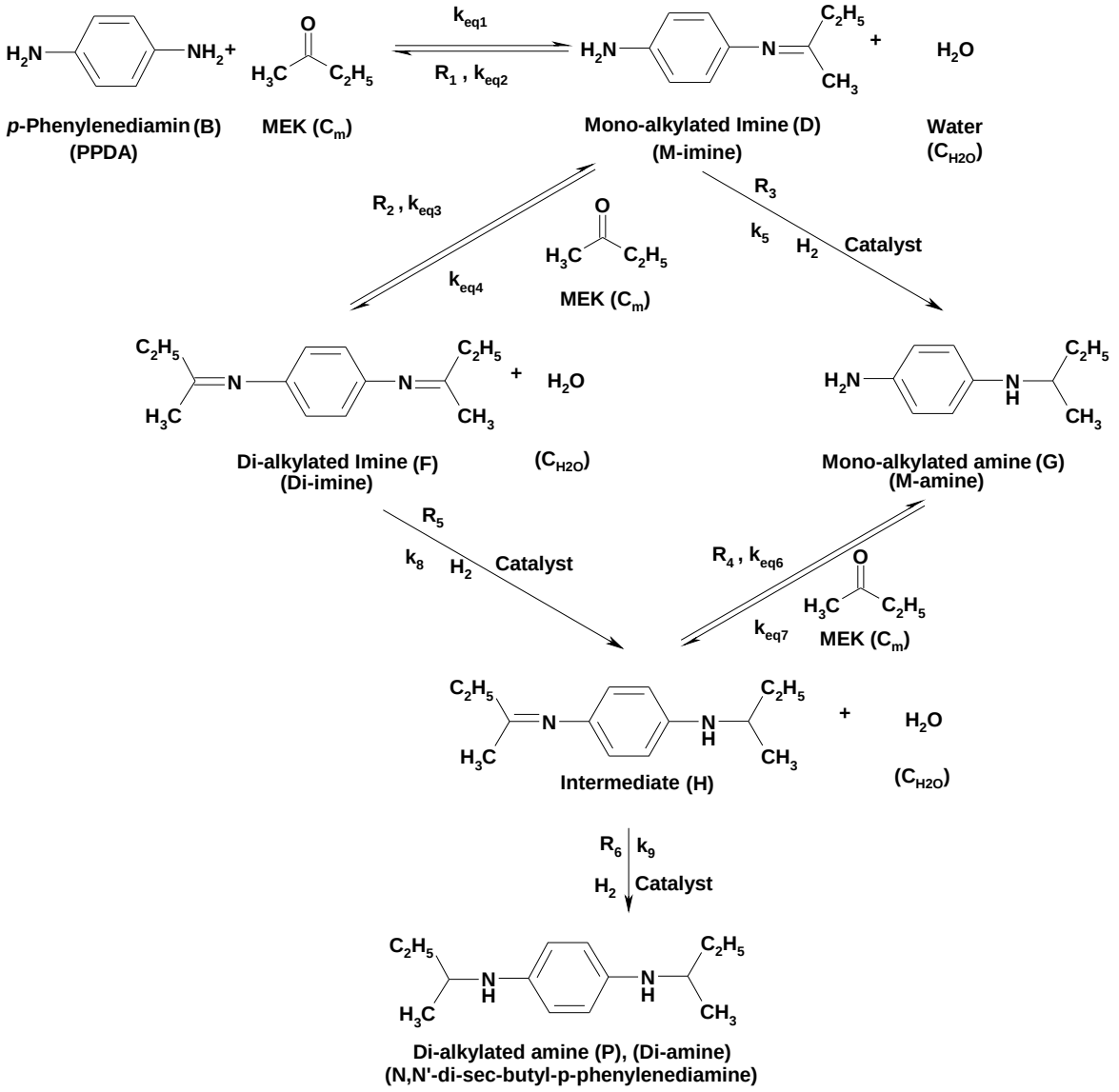

Figure 3.1. Detailed reaction scheme of reductive alkylation of PPDA with MEK in presence of 3% Pt/Al_2O_3 catalyst

large excess with respect to PPDA and its change in concentration during the course of reaction was negligible. Therefore, all the forward reaction steps were considered to be as pseudo first order reactions.

The following types of Langmuir-Hinshelwood rate equations have been found to adequately describe the individual catalytic reaction steps (R_3, R_5 and R_6) involved,

$$R_3 = \frac{wk_5 D_l \sqrt{A_s}}{\left(1 + K_A \sqrt{A_s}\right)} \quad 3.4$$

$$R_5 = \frac{wk_8 F_l \sqrt{A_s}}{\left(1 + K_A \sqrt{A_s}\right)} \quad 3.5$$

$$R_6 = \frac{wk_9 H_l \sqrt{A_s}}{\left(1 + K_A \sqrt{A_s}\right)} \quad 3.6$$

The overall rate of hydrogenation using equations 3.4-3.6 can be given as

$$R_A = R_3 + R_5 + R_6$$

$$\therefore R_A = \frac{w\left(k_5 D_l + k_8 F_l + k_9 H_l\right)\sqrt{A_s}}{\left(1 + K_A \sqrt{A_s}\right)} \quad 3.7$$

In equations 3.4-3.6, A_s represents the concentration of dissolved hydrogen on the catalyst surface. Definitions for the remaining variables in rate equations appear in the Notation Section. The intrinsic kinetic parameters are given in Table 3.1.

Table 3.1. Kinetic Rate Equation Parameters

Temp. K	$k_{eq1} \times 10^3$	$k_{eq2} \times 10^4$	$k_{eq3} \times 10^4$	$k_{eq4} \times 10^4$	$k_5 \times 10^2$	$k_{eq6} \times 10^4$	$k_{eq7} \times 10^5$	$k_8 \times 10^2$	$K_9 \times 10^3$	K_A
373	0.1248	0.0351	1.214	0.0692	0.0639	0.2539	0.072	0.2035	0.4110	1.605
393	0.2091	0.2562	2.910	0.3732	0.1091	0.2018	0.2397	0.3980	0.5147	1.111
413	0.2440	0.8807	2.982	0.3981	0.1481	0.6497	1.267	0.3923	0.6609	1.6395

3.2.2 Mixing Cell Model (MCM)

The schematic of mixing cell model used in this work is shown in Figure 3.2. The assumptions are given below.

a) The BCSR was visualized as reactor consisting of N cells of stirred tanks in series where the liquid is completely backmixed and gas is in plug flow in each cell. Thus, for $N \rightarrow \infty$, plug flow will prevail, while for N =1, the reactor performance will be equal to backmixed slurry reactor. Intermediate values will describe the liquid phase flow patterns between these two extremes.

b) The catalyst particles were assumed to be dispersed uniformly throughout the reactor. This assumption has been verified using the approach of Kato *et. al.*[28]

c) The liquid phase components are non-volatile since the bubble point of mixture was much larger than the operating temperature.

d) Gas-liquid and liquid-solid mass transfer resistances were incorporated for hydrogen. Since, the gas feed generally consists of pure hydrogen and the liquid phase components are non-volatile, mass transfer resistance in gas phase was assumed to be negligible. Also since pure hydrogen is generally used, mixing in the gas phase was considered to be unimportant.

e) The solubility of hydrogen (A) in the liquid phase follows Henry's law

f) The intraparticle diffusion resistance was assumed to be negligible since very fine catalyst particles (30 microns) were considered for all calculations. To verify this assumption, the criterion given by Bischoff[29] was followed.

g) The interference of small catalyst particles (30 microns) with the gas absorption near the gas-liquid interface was assumed to be insignificant.[30]

h) Interphase and intraparticle heat transfer resistances were assumed to be negligible, but the overall heat transfer from the bulk liquid phase to the reactor wall was considered to incorporate the non-isothermal effects. To verify the first assumption, the criterion proposed by Mears[31] was used.

The extent of backflow among mixing cells was estimated using the CFD model. The detailed procedure of CFD model is discussed in later sections.

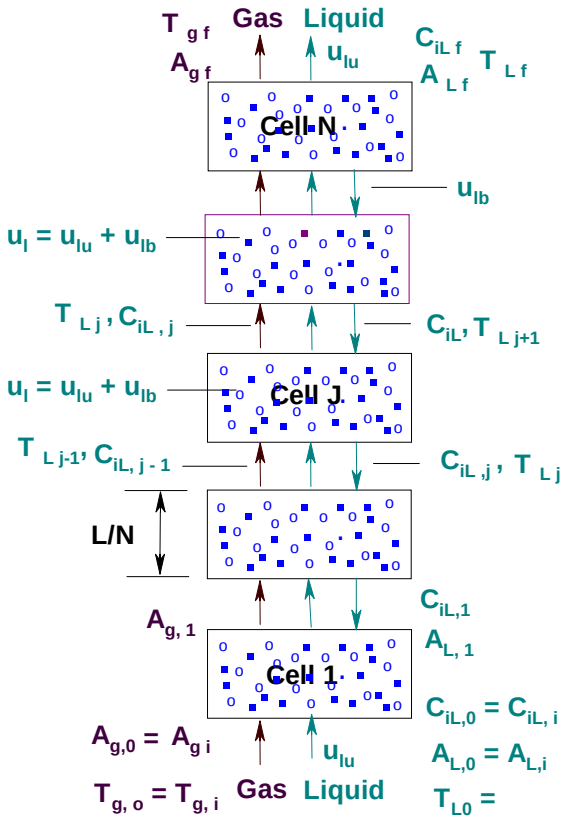

Figure 3.2. Schematic representation of bubble column slurry reactor model

3.2.3 Model Equations

The mass and energy balance equations for various species in a BCSR are summarized below. The detailed derivations are given in Appendix-A. Here, the variables a_j, b_j, d_j, f_j, g_j, h_j and p_j represent the dimensionless concentrations of the gas and liquid phase species, leaving the j^{th} cell while those entering the j^{th} cell, from previous cell were represented by a_{j-1}, b_{j-1}, d_{j-1}, f_{j-1}, g_{j-1}, h_{j-1}, and p_{j-1}, and those coming down from the next cell were represented by a_{j+1}, b_{j+1}, d_{j+1}, f_{j+1}, g_{j+1}, h_{j+1}, and p_{j+1}. An analogous approach was used for the cell temperatures. The backflow stream (Figure 3.2) for the liquid velocity can be represented as:

$$u_{lb} = \phi\, u_{lu} \qquad 3.8$$

where, ϕ is a constant obtained from the CFD simulations using time-averaged values for the axial slurry velocity. The detailed procedure for the estimation of ϕ is discussed in later

section (Section 3.2.5). The value of ϕ will obviously change with superficial gas and liquid velocities. Here, u_{lb} and u_{lu} represent the back flow liquid velocity and the net liquid velocity respectively. It should be noted here that the net flow rate is the same throughout the reactor, but because of the liquid backflow rate (u_{lb}), the flow rate in the middle cells increases to $u_{lu} + u_{lb}$. Therefore, the mass balance of reactants and products is different for the first, middle and N^{th} top cell. The mass balance for various species exiting the j^{th} cell is given below in dimensionless form. The dimensionless parameters used in these equations are defined in Table 3.2.

For species A (Hydrogen).

The mass balance of hydrogen in the gas phase is same for all the cells and can be represented as:

$$-\frac{da_{g_j}}{dz} = \alpha_A \left[a_{g_j} - a_{l_j}\right] \tag{3.9}$$

The mass balance of hydrogen in the liquid phase can be written as

First cell:

$$\int_0^{1/N} \alpha_A \beta_A \left[a_{g_j} - a_{l_j}\right] dz = (1+\phi)a_{l_j} - \left(a_{l_{j-1}} + \phi a_{l_{j+1}}\right) + \frac{\alpha_{s,A}}{N}\left[a_{l_j} - a_{s_j}\right] \tag{3.10}$$

Middle cells:

$$\int_0^{1/N} \alpha_A \beta_A \left[a_{g_j} - a_{l_j}\right] dz = (1+2\phi)a_{l_j} - \left((1+\phi)a_{l_{j-1}} + \phi a_{l_{j+1}}\right) + \frac{\alpha_{s,A}}{N}\left[a_{l_j} - a_{s_j}\right] \tag{3.11}$$

N^{th} (Top) cell:

$$\int_0^{1/N} \alpha_A \beta_A \left[a_{g_j} - a_{l_j}\right] dz \quad = \quad (1+\phi) a_{l_j} - (1+\phi) a_{l_{j-1}} + \frac{\alpha_{s,A}}{N}\left[a_{l_j} - a_{s_j}\right] \tag{3.12}$$

where mass balance of hydrogen on catalyst surface can be calculated as

$$\alpha_{l_s}\left(a_{l_j} - a_{s_j}\right) = \alpha_{R_5} q_B \left[\frac{\left(d_{l_j} + k_{85} f_{l_j} + k_{95} h_{l_j}\right)\sqrt{a_{s_j}}}{1 + k_a \sqrt{a_{s_j}}}\right] \tag{3.13}$$

The mass balance for various liquid phase species can be represented as

For species B (PPDA).

$$b_{l_j}\Big]_{j=1-N} = \frac{\varphi_x + \frac{\alpha_{R2}}{N} d_{l_j} c_{H_2O}}{\psi + \frac{\alpha_{R1}}{N}} \tag{3.14}$$

For species D (M-imine).

$$d_{l_j}\Big]_{j=1-N} = \frac{\varphi_x + \left(\frac{\alpha_{R1}}{N}\right) b_{l_j} + \left(\frac{\alpha_{R4}}{N}\right) f_{l_j} c_{H_2O}}{\psi + \left(\frac{\alpha_{R2}}{N}\right) c_{H_2O} + \frac{\alpha_{R3}}{N} + \frac{\alpha_{R5}}{N q_B}\left(\frac{\sqrt{a_{s_j}}}{1 + k_a \sqrt{a_{s_j}}}\right)} \tag{3.15}$$

For species F (Di-imine).

$$f_{l_j}\Big]_{j=1-N} = \frac{\varphi_x + \left(\frac{\alpha_{R3}}{N}\right) d_{l_j}}{\psi + \frac{\alpha_{R4}}{N} c_{H_2O} + \frac{\alpha_{R8}}{N q_B}\left(\frac{\sqrt{a_{s_j}}}{1 + k_a \sqrt{a_{s_j}}}\right)} \tag{3.16}$$

For species G (M-amine).

$$g_{l\,j}\Big]_{j=1-N} = \frac{\varphi_x + \dfrac{\alpha_{R5} d_{l\,j}}{N q_B}\left(\dfrac{\sqrt{a_{s\,j}}}{1+k_a\sqrt{a_{s\,j}}}\right) + \dfrac{\alpha_{R_7}}{N} h_{l\,j}\, c_{H_2O}}{\psi + \dfrac{\alpha_{R6}}{N}} \qquad 3.17$$

For species H (Intermediate).

$$h_{l\,j}\Big]_{j=1-N} = \frac{\varphi_x + \left(\dfrac{\alpha_{R6}}{N}\right) g_{l\,j} + \dfrac{\alpha_{R8} f_{l\,j}}{N q_B}\left(\dfrac{\sqrt{a_{s\,j}}}{1+k_a\sqrt{a_{s\,j}}}\right)}{\psi + \dfrac{\alpha_{R7}}{N} c_{H_2O} + \dfrac{\alpha_{R9}}{N q_B}\left(\dfrac{\sqrt{a_{s\,j}}}{1+k_a\sqrt{a_{s\,j}}}\right)} \qquad 3.18$$

For species P (Di-amine).

$$p_{l\,j}\Big]_{j=1-N} = \frac{\varphi_x + \dfrac{\alpha_{R9} h_{l\,j}}{N q_B}\left(\dfrac{\sqrt{a_{s\,j}}}{1+k_a\sqrt{a_{s\,j}}}\right)}{\psi} \qquad 3.19$$

where, φ_x is the parameter defined in equations 3.14-3.19 can be represented according to the j^{th} cell as

when $j = 1$, $\varphi_x = \left(x_{l\,j-1} + \phi x_{lj+1}\right)$

when $1 < j < N$, $\varphi_x = \left((1+\phi)x_{l\,j-1} + \phi\, x_{lj+1}\right)$

when $j = N$, $\varphi_x = (1+\phi)x_{l\,j-1}$

where, x represents the concentration of liquid phase species *b*, *d*, *f*, *g*, *h* and *p* in equations 3.14-3.19, respectively.

The factor ψ defined in equations 3.14-3.19 can be represented according to the j^{th} cell as,

when j = *1* and *N*, $\psi = 1 + \phi$

when $1 < j < N$, $\psi = 1 + 2\phi$

The term c_{H_2O} in equations 3.14-3.19 is the dimensionless concentration of water and can be represented as

$$c_{H_2O} = d_{lj} + 2f_{lj} + g_{lj} + 2h_{lj} + 2p_{lj}$$

In deriving energy balance equation for the non-isothermal BCSR model, the temperature dependence of various key parameters such as reaction rate constants, reaction equilibrium constant and saturation solubility are accounted for. The solubility of hydrogen in PPDA with MEK was experimentally determined (Chapter-2, Section-2(A).3.2), so the Henry's constant of solubility H_e could be expressed by the following correlation in terms of solution temperature

$$H_e(T) = 1.2\times10^{-3} \times e\,\mathrm{xp}(2.7\times10^{-3}\times T) \qquad \text{for 5\% PPDA} \qquad 3.20$$

$$H_e(T) = 1.8\times10^{-3} \times e\,\mathrm{xp}(2.2\times10^{-3}\times T) \qquad \text{for 10\% PPDA} \qquad 3.21$$

$$H_e(T) = 3\times10^{-4} \times e\,\mathrm{xp}(6.9\times10^{-3}\times T) \qquad \text{for 15\% PPDA} \qquad 3.22$$

The change in rate and equilibrium constants with temperature can be expressed as

$$k_i(T_o) = k_i(T_i)\exp\left[\frac{E_i}{R_g}\left(\frac{1}{T_i} - \frac{1}{T_o}\right)\right] \qquad 3.23$$

$$K_i(T_o) = K_i(T_i)\exp\left[\frac{E_{AD}}{R_g}\left(\frac{1}{T_i} - \frac{1}{T_o}\right)\right] \qquad 3.24$$

The heat evolved during the reaction was assumed to be carried away by the heat transfer to the reactor wall, which is characterized by the bed-to-wall heat transfer coefficient, U_w. Under such conditions where interphase and intraparticle heat transfer resistances were assumed to be negligible, the energy balance in the reactor in dimensionless form can be expressed as

First cell:

$$\theta = \frac{\alpha_{R5}}{N q_B}\beta_1\left[\frac{\left(d_{lj}+k_{85}f_{lj}+k_{95}h_{lj}\right)\sqrt{a_{sj}}}{1+k_a\sqrt{a_{sj}}}\right]+\frac{\beta_2}{N}\left[\alpha_{R1}b_{lj}-\alpha_{R2}d_{lj}\,c_{H_2O}\right]$$
$$+\frac{\beta_3}{N}\left[\alpha_{R3}d_{lj}-\alpha_{R4}f_{lj}\,c_{H_2O}\right]+\frac{\beta_4}{N}\left[\alpha_{R6}g_{lj}-\alpha_{R7}h_{lj}\,c_{H_2O}\right]-\frac{\beta_5}{N}\left(\theta_j-\theta_w\right)+\beta_6\theta_{j+1}+\beta_7\theta_{j-1} \quad 3.25$$

Middle cells:

$$\theta = \frac{\alpha_{R5}}{N q_B}\beta_8\left[\frac{\left(d_{lj}+k_{85}f_{lj}+k_{95}h_{lj}\right)\sqrt{a_{sj}}}{1+k_a\sqrt{a_{sj}}}\right]+\frac{\beta_9}{N}\left[\alpha_{R1}b_{lj}-\alpha_{R2}d_{lj}\,c_{H_2O}\right]$$
$$+\frac{\beta_{10}}{N}\left[\alpha_{R3}d_{lj}-\alpha_{R4}f_{lj}\,c_{H_2O}\right]+\frac{\beta_{11}}{N}\left[\alpha_{R6}g_{lj}-\alpha_{R7}h_{lj}\;c_{H_2O}\right]-\frac{\beta_{12}}{N}\left(\theta_j-\theta_w\right)+\beta_{13}\theta_{j-1}+\beta_{14}\theta_{j+1} \quad 3.26$$

N^{th} (Top) cell:

$$\theta = \frac{\alpha_{R5}}{N q_B}\beta_1\left[\frac{\left(d_{lj}+k_{85}f_{lj}+k_{95}h_{lj}\right)\sqrt{a_{sj}}}{1+k_a\sqrt{a_{sj}}}\right]+\frac{\beta_2}{N}\left[\alpha_{R1}b_{lj}-\alpha_{R2}d_{lj}\,c_{H_2O}\right]$$
$$+\frac{\beta_3}{N}\left[\alpha_{R3}d_{lj}-\alpha_{R4}f_{lj}\,c_{H_2O}\right]+\frac{\beta_4}{N}\left[\alpha_{R6}g_{lj}-\alpha_{R7}h_{lj}\,c_{H_2O}\right]-\frac{\beta_5}{N}\left(\theta_j-\theta_w\right)+\theta_{j-1} \quad 3.27$$

3.2.4 Method of Solution

The solution of the preceding set of non-linear algebraic equations 3.9-3.19 allow the prediction of the concentrations of all species and the temperature at the exit of each cell as well as the N^{th} cell (exit of the reactor) for any given set of inlet parameters. Mass balance of hydrogen can be calculated by integrating equation 3.9 to give

$$\frac{a_{gj}-a_{lj}}{a_{g_{j-1}}-a_{l_j}} = \exp\left(-\alpha_A\, z\right) \quad 3.28$$

By substituting $z = 1/N$, the dimensionless concentration of A in the stream leaving the cell j is

$$a_{g_j} = a_{g_{j-1}}\exp\left(-\frac{\alpha_A}{N}\right)+a_{l_j}\chi \quad 3.29$$

Substituting equation 3.28 in equation 3.10, 3.11 and 3.12 and solving the resulting integral equation gives the following expression for the dimensionless concentration of *A* in the liquid stream leaving cell *j*

First cell:

$$a_{l\,j} = \frac{\left(a_{l\,j-1} + \phi a_{l\,j+1}\right) + \beta_A \chi a_{g\,j-1} + \left(\frac{\alpha_{ls}}{N}\right) a_{s\,j}}{1 + \phi + \frac{\alpha_{ls}}{N} + \beta_A \chi} \qquad 3.30$$

Middle cells:

$$a_{l\,j} = \frac{\left((1+\phi) a_{l\,j-1} + \phi a_{l\,j+1}\right) + \beta_A \chi a_{g\,j-1} + \left(\frac{\alpha_{ls}}{N}\right) a_{s\,j}}{1 + 2\phi + \frac{\alpha_{ls}}{N} + \beta_A \chi} \qquad 3.31$$

N^{th} (Top) cell:

$$a_{l\,j} = \frac{\left((1+\phi) a_{l\,j-1}\right) + \beta_A \chi a_{g\,j-1} + \left(\frac{\alpha_{ls}}{N}\right) a_{s\,j}}{1 + \phi + \frac{\alpha_{ls}}{N} + \beta_A \chi} \qquad 3.32$$

where, χ is the parameter defined in equations 3.29-3.32 and can be represented as

$$\chi = 1 - \exp\left(-\frac{\alpha_A}{N}\right)$$

Once a_{lj} is known, the concentration of *A* on the catalyst surface, A_s, can be obtained from equation 3.13. Equations 3.9 to 3.19 were combined with equations 3.25-3.27 and solved simultaneously using the FSOLVE, non linear equation solver (MATLAB 7, 2004)[32] to predict the concentrations of the individual species and the temperature at the exit of each cell.

The initial conditions for the first cell are as follows:

$$z = 0,\ b_l = 1;\ a_l = d_l = f_l = g_l = h_l = p_l = 0;\ \theta = 1; \qquad 3.33$$

For any given set of inlet conditions, the concentrations of reactant/product species and temperature were calculated at the exit of each cell and also the exit of the reactor. The

dimensionless parameters used in the above equations are presented in Table 3.2. The hydrodynamic and mass transfer parameters required for the calculations of the dimensionless parameters were calculated from literature correlations presented in Table 3.3.

At any given length of the reactor, the fractional conversion of PPDA was calculated as

$$X_B = 1 - b_{lj} \tag{3.34}$$

The global rate of hydrogenation taking into account all the hydrogenation reaction steps involved in the overall reaction sequence (Figure 3.1) was calculated as

$$R_{H2} = \tau' \left(g_{lj} + h_{lj} + 2p_{lj} \right) B_{li} \tag{3.35}$$

In equation 3.35, τ' is the mean residence time of the liquid in the reactor ($\tau' = u_{lu} / L$), u_{lu} is the liquid velocity, L is the length of the reactor, g_{lj}, h_{lj}, and p_{lj} are the concentrations of M-amine, Intermediate and Di-amine respectively, at the exit of the reactor.

The selectivity to M-imine, Di-imine, M-amine, Intermediate and Di-amine was evaluated using the following relationships:

$$S_{m-i\min e} = \frac{d_{lj}}{1 - b_{lj}} \times 100 \tag{3.36}$$

$$S_{di-i\min e} = \frac{f_{lj}}{1 - b_{lj}} \times 100 \tag{3.37}$$

$$S_{m-a\min e} = \frac{g_{lj}}{1 - b_{lj}} \times 100 \tag{3.38}$$

$$S_{\text{int}ermediate} = \frac{h_{lj}}{1 - b_{lj}} \times 100 \tag{3.39}$$

$$S_{di-a\min e} = \frac{p_{lj}}{1 - b_{lj}} \times 100 \tag{3.40}$$

Table 3.2. Dimensionless Parameters Used in the Model

Mass transfer parameters	
Gas-liquid mass transfer	$\alpha_A = L k_L a_B / u_g H_A \qquad \beta_A = u_g H_A / u_l$
Liquid-solid mass transfer	$\alpha_{l_s} = L k_s a_p / u_l$
Heat transfer parameters	$\beta_x\big\|_{x=1-4} = \dfrac{\left(-\Delta H_x\big\|_{x=1-4}\right) B_{li}}{T_i \rho_l C_{pl} \alpha_1}$; $\beta_5 = \dfrac{4U_w L}{D_T u_l \rho_l C_{pl} \alpha_1}$; $\beta_6 = \phi / \alpha_1$ $\beta_7 = \left(1 + \dfrac{u_g \rho_g C_{pg}}{u_{lu} \rho_l C_{pl}}\right) \Big/ \alpha_1$; $\beta_x\big\|_{x=8-11} = \dfrac{\left(-\Delta H_x\big\|_{x=1-4}\right) B_{li}}{T_i \rho_l C_{pl} \alpha_2}$ $\beta_{12} = \dfrac{4U_w L}{D_T u_{lu} \rho_l C_{pl} \alpha_2}$; $\beta_{13} = \alpha_1 / \alpha_2$; $\beta_{14} = \phi / \alpha_2$ $\alpha_1 = \left[1 + \phi + \dfrac{u_g \rho_g C_{pg}}{u_{lu} \rho_l C_{pl}}\right]$; $\alpha_2 = \left[1 + 2\phi + \dfrac{u_g \rho_g C_{pg}}{u_{lu} \rho_l C_{pl}}\right]$
Reaction rate and equilibrium constants	$k_{85} = \dfrac{k_8}{k_5}$; $k_{95} = \dfrac{k_9}{k_5}$; $k_a = K_A \sqrt{A_{sj}}$ $\alpha_{R_1} = \dfrac{L k_{eq_1}}{u_{lu}}$; $\alpha_{R_2} = \dfrac{L k_{eq_2} B_{li_1}}{u_{lu}}$; $\alpha_{R_3} = \dfrac{L k_{eq3}}{u_{lu}}$; $\alpha_{R_4} = \dfrac{L k_{eq4} B_{li_1}}{u_{lu}}$; $\alpha_{R_5} = \dfrac{L w k_5 \sqrt{B_{li_1}}}{u_{lu}}$; $\alpha_{R_6} = \dfrac{L k_{eq6}}{u_{lu}}$; $\alpha_{R_7} = \dfrac{L k_{eq7} B_{li_1}}{u_{lu}}$; $\alpha_{R_8} = \dfrac{L w k_8 \sqrt{B_{li_1}}}{u_{lu}}$; $\alpha_{R_9} = \dfrac{L w k_9 \sqrt{B_{li_1}}}{u_{lu}}$

Table 3.3. Correlations Used for Hydrodynamic, Mass and Heat Transfer Parameters

Parameter	Correlation	Reference
Gas-liquid mass-transfer coefficient	$k_l a_B = 0.6 D_m^{0.5} \left(\frac{\mu_L}{\rho_L}\right)^{-0.12} \left(\frac{S_T}{\rho_L}\right)^{-0.62} d_T^{0.17} g^{0.93} \varepsilon_g^{1.1}$	33
Gas hold up	$\varepsilon_g = \frac{u_g \left(S_{TW} / S_T / \rho_l\right)^{1/3}}{30 + 2u_g}$	34
Liquid-solid mass transfer coefficient	$\frac{k_s d_p}{D_m} = 2 + 0.212 \left[\frac{d_p^3 \left(\rho_p - \rho_L\right)}{\mu_L D_m} g\right]^{1/3} \left[\frac{d_p u \rho_L}{\mu_L}\right]^{0.112}$	35
Heat transfer coefficient	$S_t = 0.1\left(R_e F_r P_r^2\right)^{-0.25} = U_w / \rho_{s_l} C_{p,sl} u_g$	36
Diffusivity coefficient	$D_m = 7.4 \times 10^{-8} \frac{\left(\phi M_B\right)^{1/2} T}{\mu_B V_A^{0.6}}$	37

3.2.5 Estimation of Backflow with CFD Model (ϕ)

The extent of back-mixing in bubble column reactors depends mainly on column dimensions and superficial gas velocity (provided that liquid superficial velocity is rather small). When gas is sparged at the bottom of bubble column reactor, bubbles move upwards from the central region of the column creating a radial gradient of gas hold-up. Such a radial gradient sets up a liquid circulation within the column causing severe backmixing. CFD models can provide quantitative relationship between internal liquid circulation and design and operating parameters of bubble columns.[38,39,40,15] Hence, in this work a CFD model developed in Rampure *et. al.*[15] was considered to simulate the hydrodynamics of bubble column reactor for simulating the current study.

The catalyst particle size and loading is fairly small for the considered case (30 microns and 0.025-10% w/w respectively). Therefore, the hydrodynamics of bubble column slurry reactor was modeled as a two phase flow by considering gas as a dispersed phase and slurry as a pseudo-homogeneous continuous phase. The gas-liquid flow in bubble column was simulated using the Eulerian-Eulerian approach. In this approach both mass and momentum balances were solved for each phase.[38] The standard k-ε mixture turbulence model was used in the present work. Influence of gas hold-up on effective drag coefficient was

accounted. Appropriate properties of gas and liquid (slurry) phase (corresponding to 4 MPa operating pressure and average operating temperature) were used in the simulations [Gas: density of 2.48 kg/m^3 and viscosity of 1×10^{-5} kg/m-s; Slurry: density of 845.68 kg/m^3 and viscosity of 0.0618 kg/m-s]. A sieve-plate sparger was assumed to distribute the gas uniformly throughout the sparger region and was modelled as inlet. The bubble velocity was set as gas inlet and volume fraction at inlet was set in such a way that it ensures desired net gas flow rate. The top surface of the column was modeled as velocity inlet, applying same boundary condition as that for sparger. The overall gas hold-up in the column was still a free variable. Simulations were carried out till the unsteady flow was established with acceptable mass balance for all fluid phases. The time averaging was started after discarding the initial transients. Mass transfer and reactions were not considered in the CFD model since the focus was on quantifying the extent of backmixing. The details of model equations and solution strategies were discussed by Rampure *et. al.*[15] The geometry of the considered reactor was modeled using GAMBIT v2.0. The geometry was discretized using 80,000 computational cells. The commercial CFD code FLUENT 6.3 (of Ansys-Fluent Inc. USA)[41] was used to carry out simulations.

The CFD simulations were carried out for superficial gas velocities ranging from 0.02-0.10 m/s. For the range of gas velocities studied, the homogeneous flow regime prevails up to 0.05 m/s. Transition regime occurs at the superficial gas velocities near to 0.05-0.06 m/s and thus extends to churn turbulent regime at gas velocity of 0.1 m/s.[42] Since the maximum liquid velocity considered for the reactor simulations was only 0.001 m/s, actual value of liquid superficial velocity will not influence internal liquid circulation within the column. Therefore, all the CFD simulations were carried out with setting liquid superficial velocity to zero. Unsteady simulations were carried out until the quasi steady-state was reached. Time averaging of hydrodynamic parameters was carried out after achieving such quasi-steady state. After time averaging, the extent of back flow between mixing cells was estimated as follows: According to the number of cells used in the mixing cell model, corresponding cross-sectional planes were formed at different axial locations that mimic number of cells. For example for three mixing cell model, the column was compartmented into three equal parts by forming two virtual planes. The simulated time-averaged values for the axial slurry velocity at these planes were used to estimate the up-flow and down-

flow values of slurry velocity. The average values of up-flow and down-flow were used to calculate the down-flow values of slurry velocity (u_{lb}) for the estimation of ϕ in equation 3.8. Use of radial baffles has been proposed for reducing liquid phase back mixing in bubble columns.[43] In this work, therefore, a case with radial baffles located at height equal to column diameter (to realize aspect ratio each mixing cell as unity) was simulated. The considered radial baffles had an opening of 0.7 times column diameter. The results of CFD simulations and estimated internal circulations are discussed in the following sections.

3.3 RESULTS AND DISCUSSION

In order to understand the effect of various operating parameters on the performance of BCSR, simulations were performed for the range of operating conditions as presented in Table 3.4. For any given set of operating and inlet parameters, the corresponding mass transfer and hydrodynamic parameters were calculated using the correlations discussed earlier (Table 3.3). The effect of individual parameters on the conversion of PPDA, selectivity of the products, global rate of hydrogenation and temperature rise were calculated. The results are discussed in the following section.

3.3.1 Reactor Performance Without Backflow (ϕ=0)

The liquid phase mixing is an important factor in the performance of a BCSR. This was studied by evaluating the reactor performance for different number of cells (N) in the mixing cell model for the same total reactor volume. The results showing the conversion of PPDA as a function of liquid velocity for different number of cells N are presented in Figure 3.3. The conversion of PPDA was found to increase with increase in the number of cells but decreases with increasing liquid velocity. The higher conversion for N = 10 is consistent with plug flow conditions. Similar trends with respect to variation in number of cells, N, were observed for global rate of hydrogenation and temperature rise (at the exit of the reactor), when the inlet PPDA concentration, catalyst loading and H_2 pressure were varied.

Table 3.4. Range of Operating Conditions for BCSR Investigated

Design parameters/ Operating conditions	Values
Catalyst	3% Pt/Al_2O_3
Catalyst loading, w	0.2 - 84.6 kg/m^3 (0.025%-10% w/w)
Temperature	373-413 K
Initial concentration of PPDA, B_{li}	0.5 - 1.5 kmol/m^3, (5%-15% w/w)
H_2 pressure, P	2 - 6.2 MPa
Solvent	Methyl Ethyl Ketone
Liquid velocity, u_{lu}	2×10^{-4}-10×10^{-4} m/s
Gas velocity, u_g	2×10^{-2}-10×10^{-2} m/s
Reactor diameter, d_T	0.25 m
Total reactor length, L	4 m
Particle diameter, d_p	30 microns
Density of catalyst, ρ_p	1260 kg/m^3

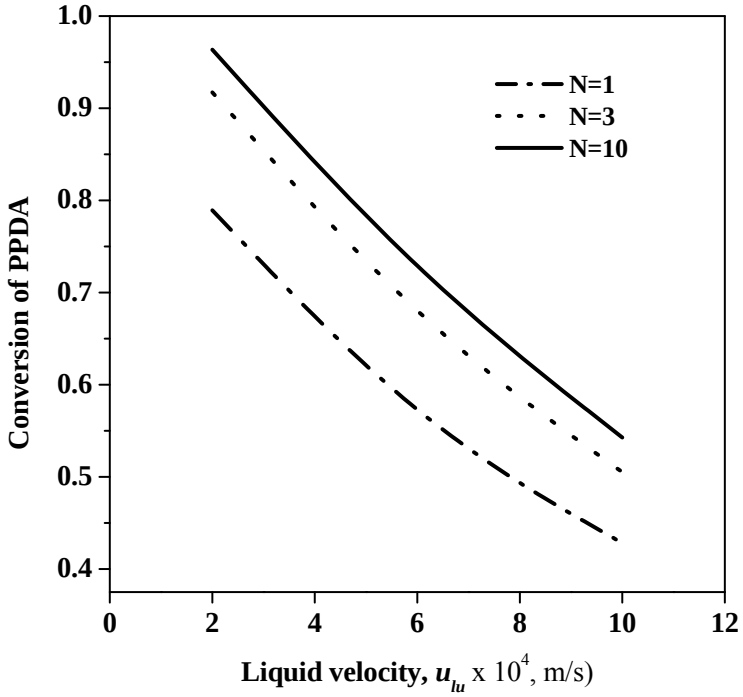

Figure 3.3. Effect of number of cells (N) on the conversion of PPDA
Reaction conditions: w = 84.6 kg/m^3, B_{li} = 1 kmol/m^3, $u_g = 5 \times 10^{-2}$ m/s, T = 393 K, P = 4 Mpa

In predicting the reactor performance, the correlation proposed by Yoshida and Akita[33] was used for calculating the gas liquid mass transfer coefficient. It was found that there was no significant change in the reactor performance when the mass transfer coefficient was varied in ± ten fold. It may be noted here the gas-liquid mass transfer coefficients predicted by literature correlations[44,45,46,47] varied only ±60% to that predicted by Yoshida and Akita[33].

The effect of liquid velocity on temperature rise for different inlet temperatures is shown in Figure 3.4. The temperature rise was calculated for different reaction conditions and found to increase with the increase in inlet temperature. The maximum temperature rise was observed for the highest substrate concentration (not more than 10 °C). The temperature rise was found to be insignificant, might be due to the equilibrium steps involved in the overall reaction scheme and better heat transfer efficiency of BCSR.

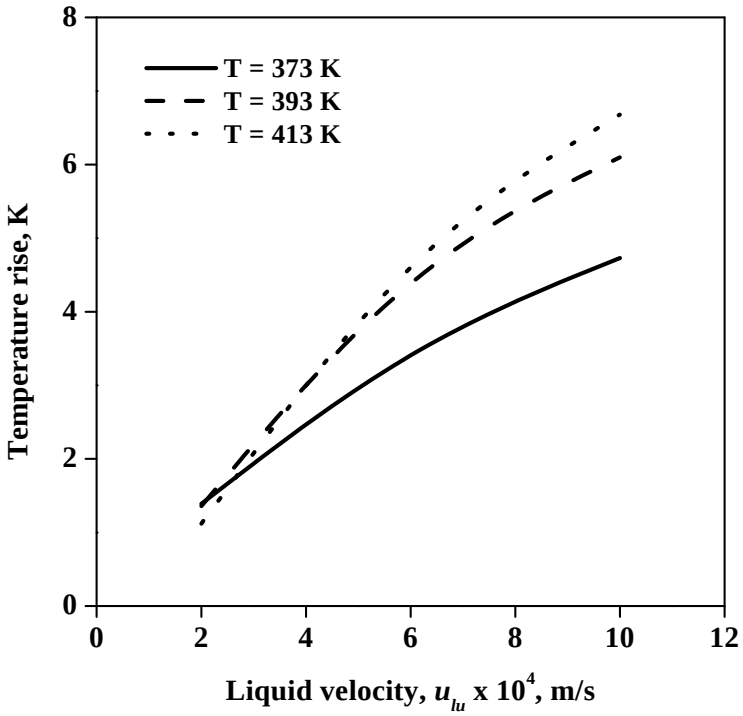

Figure 3.4. Temperature rise as a function of liquid velocity: Effect of inlet temperature
Reaction conditions: w = 84.6 kg/m^3, B_{li} = 1 kmol/m^3, $u_g = 5 \times 10^{-2}$ m/s, P = 4 Mpa, N = 10

The effects of catalyst loading and inlet PPDA concentration on the selectivity to products are shown in Figures 3.5 and 3.6 respectively, for different inlet liquid velocities. It was observed that the selectivity to M-amine and Di-amine increases with increase in the catalyst loading (Figure 3.5). It is clear from Figures 3.5-A and 3.5-B that selectivity to M-amine increases steeply within a catalyst range of 0.2-2 kg/m^3, which indicates that the reaction is in kinetic regime. The reaction slowly moves to mass transfer regime beyond this catalyst loading. It should be noted here that the selectivity towards the products were independent at higher catalyst loading (more than 84 kg/m^3). At lower liquid velocities and catalyst loading, a high selectivity (up to 50%) can be achieved. The selectivity to M-amine decreased with increase in inlet PPDA concentration whereas selectivity to Intermediate increased and Di-amine remained constant. With increase in PPDA concentration, M-amine concentration increases which then transforms to Intermediate by the equilibrium reaction (Figure 3.1). As the kinetic modeling data presented in Table 3.1 clearly indicates the slow hydrogenation rate for the Intermediate to Di-amine, in a continuous flow reactor the results presented in Figure 3.6 were expected.

The product concentration profiles at the reactor exit as a function of N, for minimum and maximum liquid velocity are presented in Figures 3.7-A and 3.7-B respectively. The concentrations of all species are constant after N=10, indicating plug flow conditions. As the liquid velocity increased to its maximum value, the concentration of M-amine and Di-amine decreases while the concentration of M-imine, Di-imine and Intermediate increases. To understand the effect of back mixing in the liquid phase, the mixing cell model was extended by including a backflow term. The results obtained are discussed in the following section.

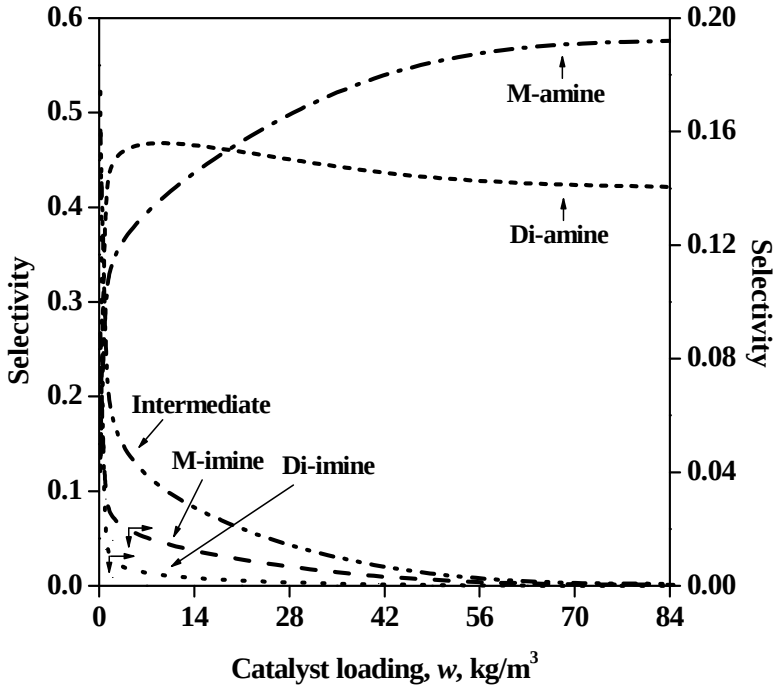

(A) $u_{lu} = 2 \times 10^{-4}$ m/s

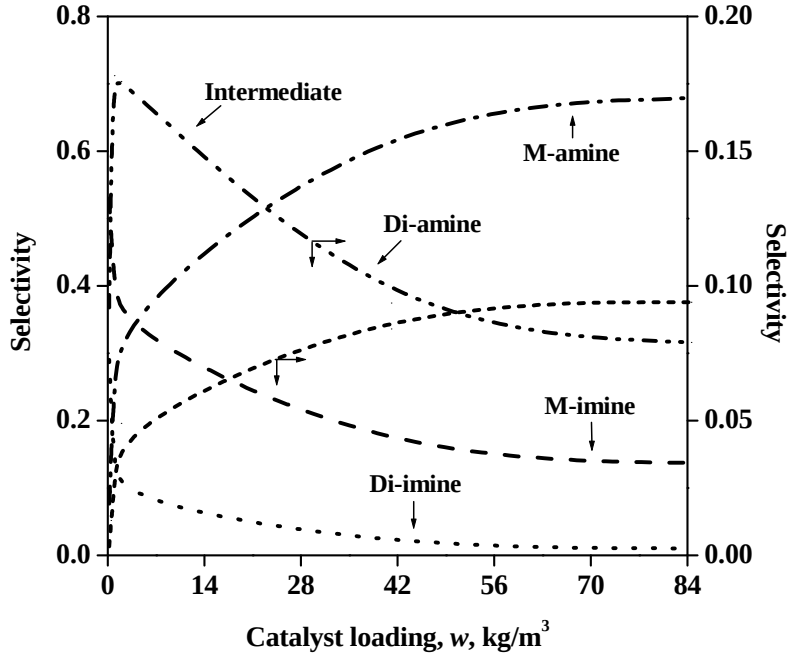

(B) $u_{lu} = 10 \times 10^{-4}$ m/s

Figure 3.5. Selectivity as a function of catalyst loading: Effect of liquid velocity
Reaction conditions: $B_{li} = 1$ kmol/m^3, $u_g = 5 \times 10^{-2}$ m/s, $T = 393$ K, $P = 4$ Mpa, $N = 10$

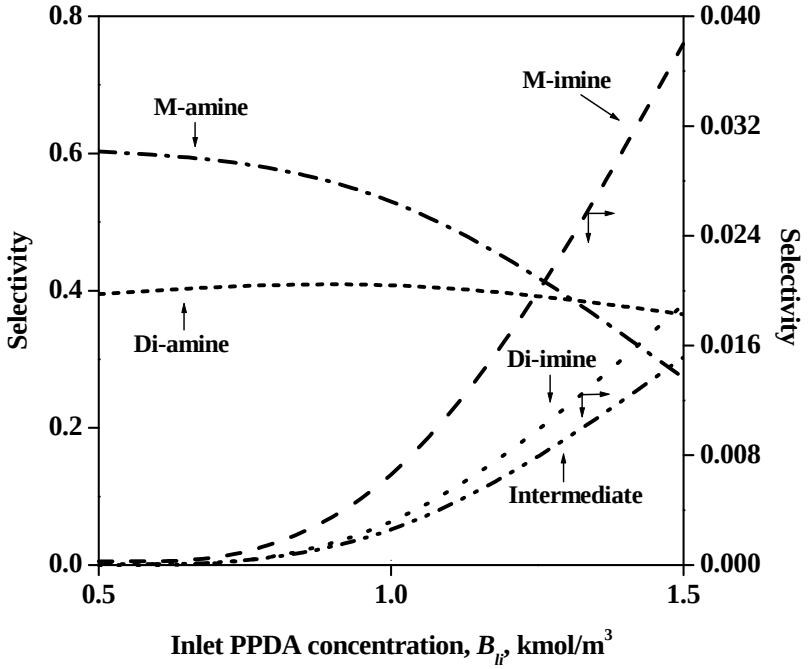

(A) $u_{lu} = 2 \times 10^{-4}$ m/s

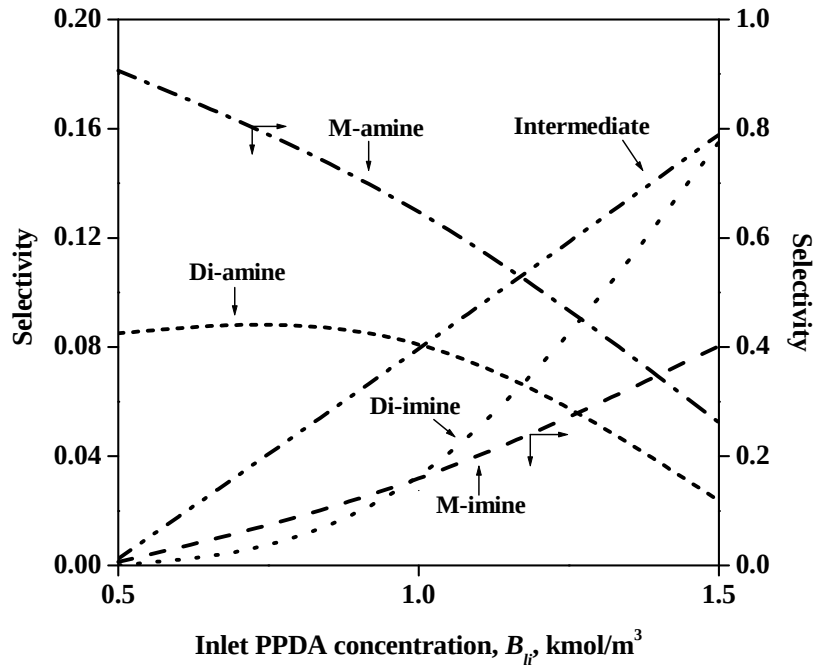

(B) $u_{lu} = 10 \times 10^{-4}$ m/s

Figure 3.6. Selectivity as a function of inlet PPDA concentration: Effect of liquid velocity

Reaction conditions: $w = 84.6$ kg/m^3, $u_g = 5 \times 10^{-2}$ m/s, $T = 393$ K, $P = 4$ Mpa, $N = 10$

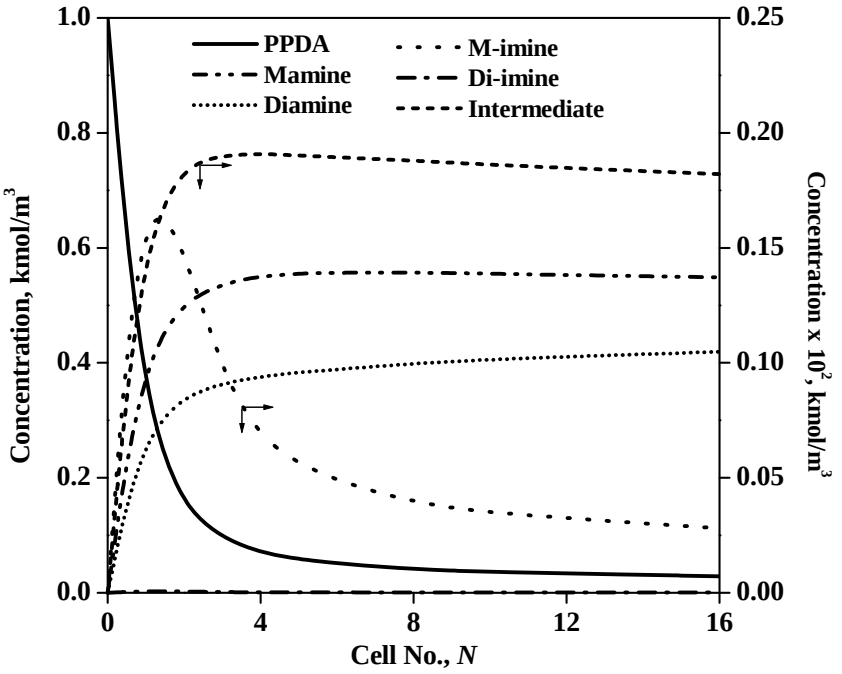

(A) $u_{lu} = 2 \times 10^{-4}$ m/s

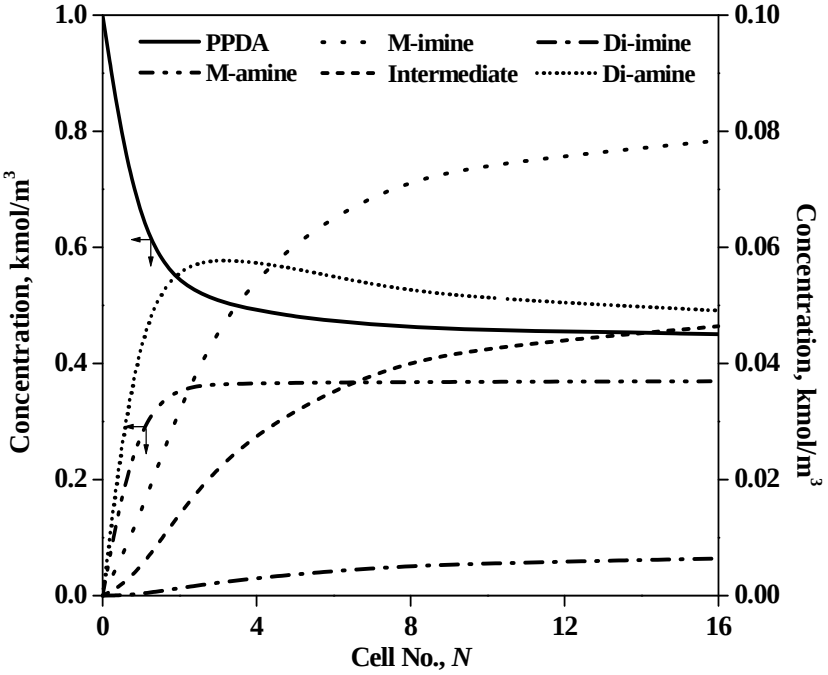

(B) $u_{lu} = 10 \times 10^{-4}$ m/s

Figure 3.7. Effect of number of cells (N) on the species concentration profile for different liquid velocities

Reaction conditions: $w = 84.6$ kg/m^3, $B_{li} = 1$ kmol/m^3, $u_g = 5 \times 10^{-2}$ m/s, $T = 393$ K, $P = 4$ Mpa

3.3.2 Reactor Performance With Backflow ($\phi > 0$)

The liquid phase back mixing was accounted for by including a backflow stream from all but the bottom most mixing cell. The changes in gas and liquid velocities influence the hydrodynamics of slurry bubble column reactor and therefore, alter the back mixing in the liquid phase. The hydrodynamics of the considered column was simulated using the CFD model described earlier. The predicted results are shown in Figure 3.8-A and 3.8-B, which shows that the effective backflow increased with superficial gas velocity. The estimated backflow values were used to calculate parameter ϕ and the values are listed in Table 3.5.

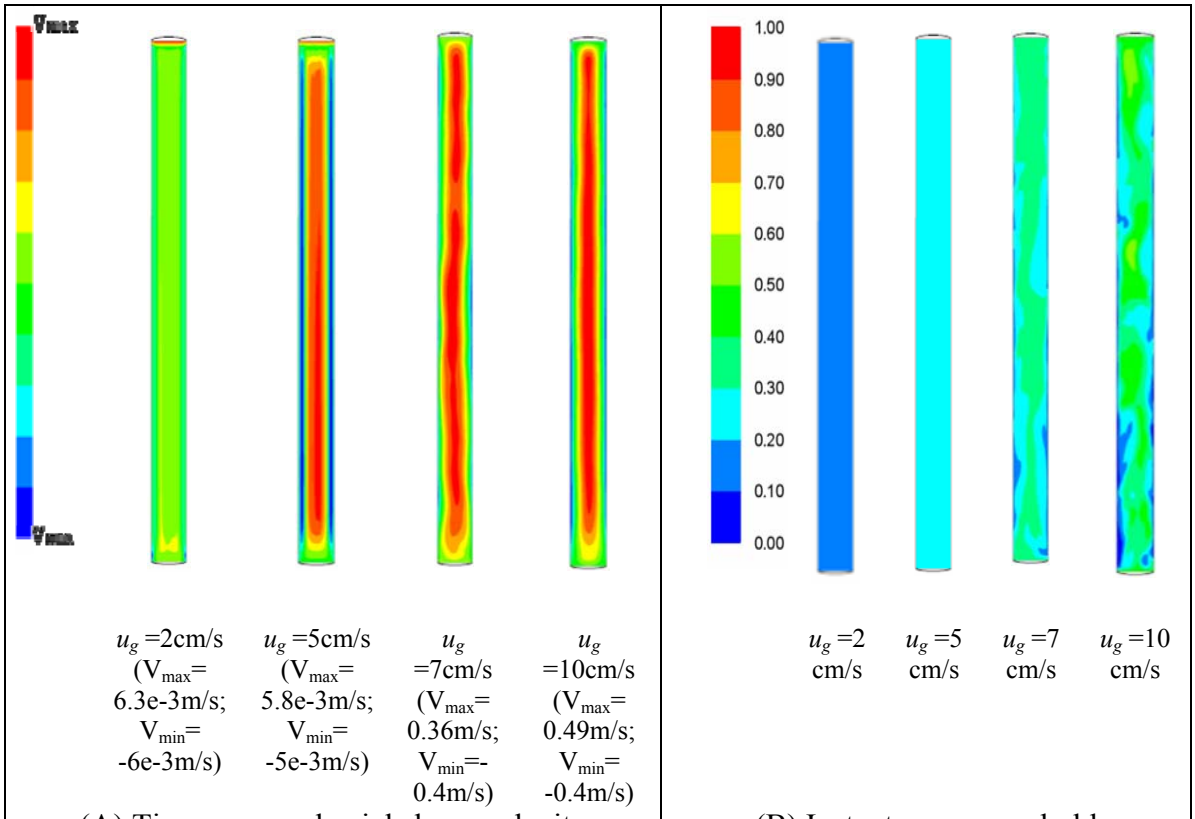

(A) Time averaged axial slurry velocity (B) Instantaneous gas holdup

Figure 3.8. CFD simulations for the estimation of the backflow in bubble column

The liquid phase back mixing was studied by evaluating the reactor performance along the length of the reactor in the mixing cell model for the same total reactor volume. The result showing the conversion of PPDA as a function of number of cells (i.e. along the length of the reactor) for different ϕ values is presented in Figure 3.9. It is evident that

backflow significantly affects the reactor performance. Also, at maximum ϕ values, studied in the range of gas velocities, conversion of PPDA did not change along the length of the reactor and the reactor behaved like a completely back mixed. Similar trends were observed for the selectivity of Mono- and Di-amine as shown in Figure 3.10.

Table 3.5. Values of ϕ at Different Gas Velocities From CFD Simulation

u_g x 10^2 (m/s)	u_{lb} (m/s)	ϕ (Min.)	ϕ (Max.)
2	5.39×10^{-4}	0.54	2.69
5	9.56×10^{-4}	0.96	4.78
7	5.71×10^{-2}	57.07	285.33
10	7.22×10^{-2}	72.18	360.90
10 (With 15 Baffles)	1.89×10^{-2}	18.97	94.86

Figure 3.11 shows the temperature rise along the reactor length for different ϕ values. It is important to note that with the extent of back-mixing, the pattern of temperature rise profile changes slowly. In the absence of backflow ($\phi = 0$), the temperature profile passes through maxima. As ϕ value increases, the pattern of the temperature profile changes slowly and become a straight line at maximum ϕ value.

The comparison of selectivity profile of Mono- and Di-amine as a function of liquid velocity considering with and without backflow are presented in Figure 3.12. It was observed that the selectivity to M-amine increases and Di-amine decreases with the backflow. Also, it can be seen from Figure 3.12 that with increase in liquid velocity at fixed gas velocity, the results (selectivity of both M-amine and Di-amine) with backflow case approaches to the results without backflow case. This is because of the decrease in backflow (ϕ) in the range of 4.78-0.96 with increase in liquid velocity (2-10 $\times$ 10^{-4} m/s) at fixed gas velocity.

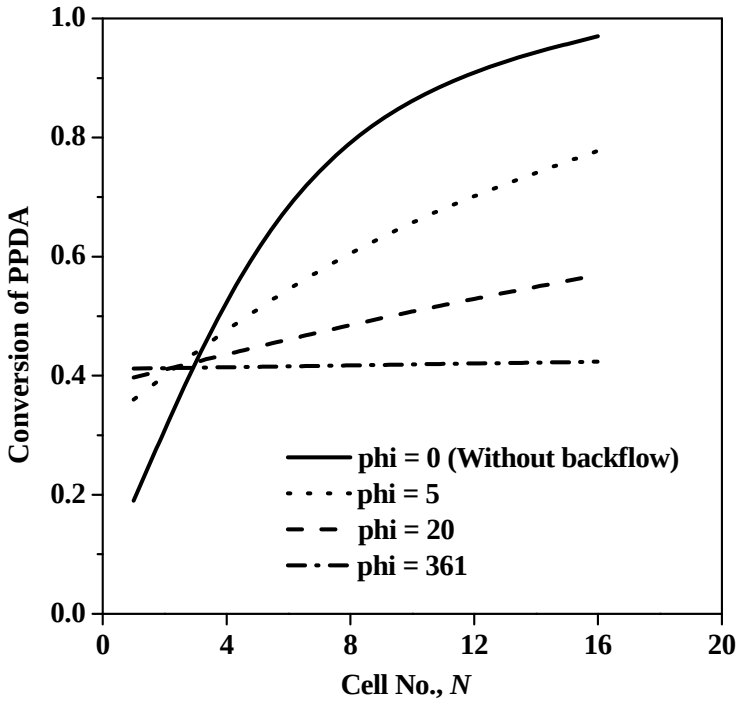

Figure 3.9. Conversion of PPDA as a function of number of cells: Effect of backflow stream

Reaction conditions: w = 84.6 kg/m^3, B_{li} = 1 kmol/m^3, $u_{lu} = 2 \times 10^{-4}$ m/s, $u_g = 5 \times 10^{-2}$ m/s, T = 393 K, P = 4 Mpa, N=16

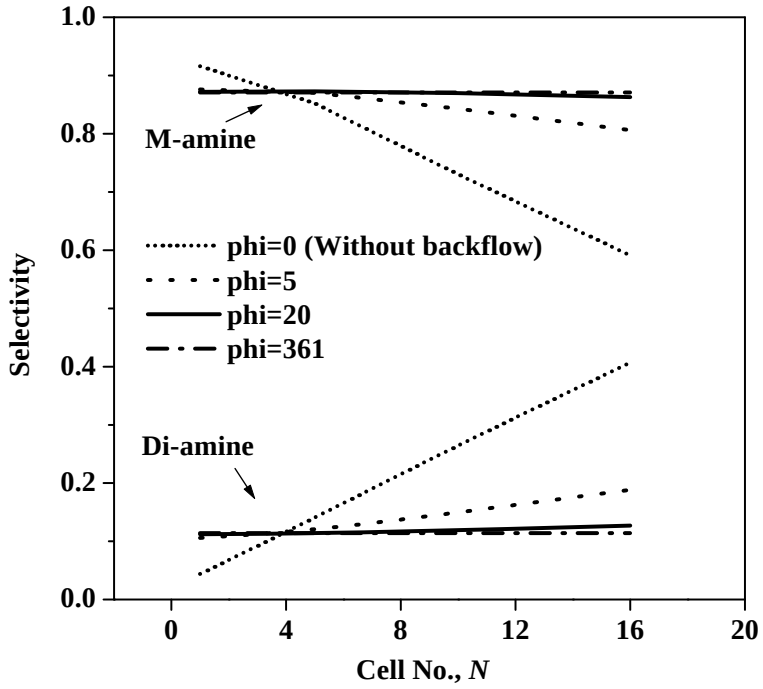

Figure 3.10. Selectivity as a function of number of cells: Effect of backflow stream

Reaction conditions: w = 84.6 kg/m^3, B_{li} = 1 kmol/m^3, $u_{lu} = 2 \times 10^{-4}$ m/s, $u_g = 5 \times 10^{-2}$ m/s, T = 393 K, P = 4 Mpa, N=16

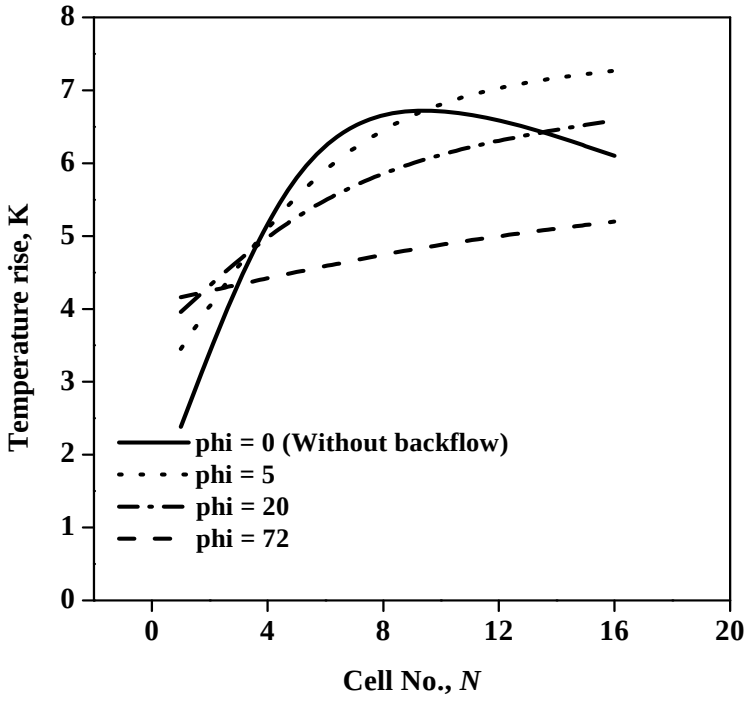

Figure 3.11. Temperature rise as a function of number of cells: Effect of backflow stream
Reaction conditions: w = 84.6 kg/m^3, B_{li} = 1 kmol/m^3, u_{lu} = 10 × 10^{-4} m/s, T = 393 K, P = 4 Mpa, N=16

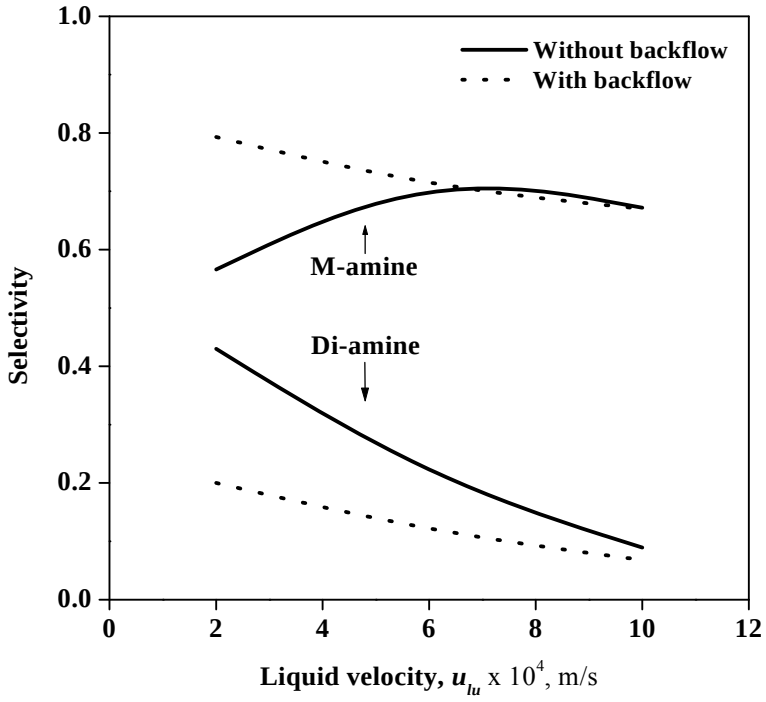

Figure 3.12. Selectivity as a function of inlet liquid velocity: Effect of backflow stream
Reaction conditions: w = 84.6 kg/m^3, B_{li} = 1 kmol/m^3, u_g = 5 × 10^{-2} m/s, T = 393 K, P = 4 Mpa, N=16

The comparison of temperature profile as a function of gas velocity with and without considering backflow is presented in Figure 3.13. At higher gas velocity, the temperature rise is less for the case with backflow as compared to that without backflow. As the gas velocity increases, the backflow in the reactor increases steeply (see Table 3.5) and hence, temperature rise was less compared to that without backflow model.

Influence of degree of backmixing (which increases with gas velocity) on the predicted selectivity of products is shown in Figure 3.14. It can be seen that degree of backmixing has significant influence on conversion while its influence on the selectivity was less significant. It is therefore useful to evaluate possible ways to control and manipulate degree of backmixing.

As mentioned earlier, the use of radial baffles for reducing backmixing in bubble columns as proposed by Khare *et. al.*[43] was evaluated using the CFD model. The case of superficial gas velocity of 0.1 m/s, which has a maximum degree of backmixing among the considered cases, was considered for evaluating influence of radial baffles. The flow generated in the bubble columns with 15 internal horizontal radial baffles with opening of $0.7d_T$ (d_T = Diameter of Reactor) was simulated using the CFD model. The predicted results are shown in Figures 3.15-A and 3.15-B. Presence of radial baffles significantly reduced the extent of backflow [by almost 70%, (see Figure 3.15-C)]. The backflow predicted in presence of radial baffles was then used to simulate the considered reductive alkylation reaction. The predicted influence of radial baffles on selectivity and conversion is shown in Figure 3.16. It can be seen that the presence of baffles showed 20% increase in conversion without affecting selectivity. The radial baffles can therefore be considered to be useful for controlling and manipulating degree of backmixing in bubble column slurry reactors.

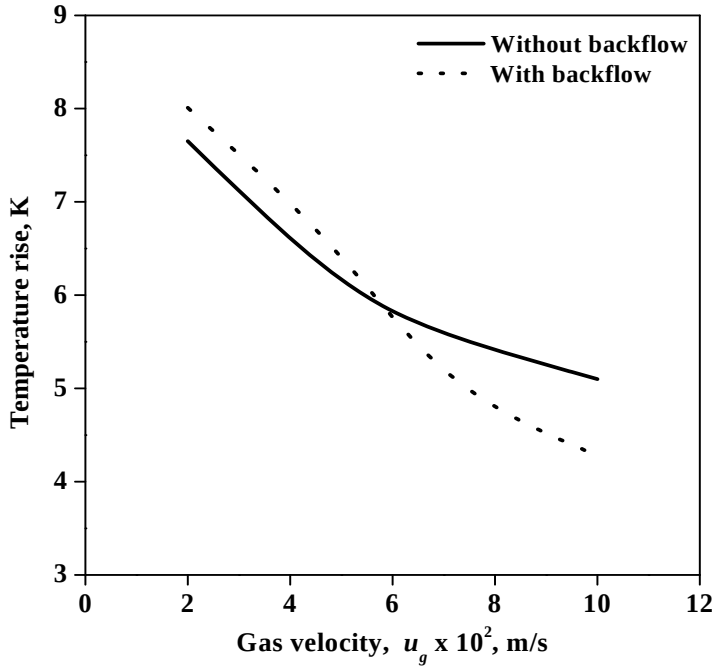

Figure 3.13. Temperature rise as a function of number of cells: Effect of backflow stream
Reaction conditions: w = 84.6 kg/m^3, B_{li} = 1 kmol/m^3, u_{lu} = 10 × 10^{-4} m/s, T = 393 K, P = 4 Mpa, N=16

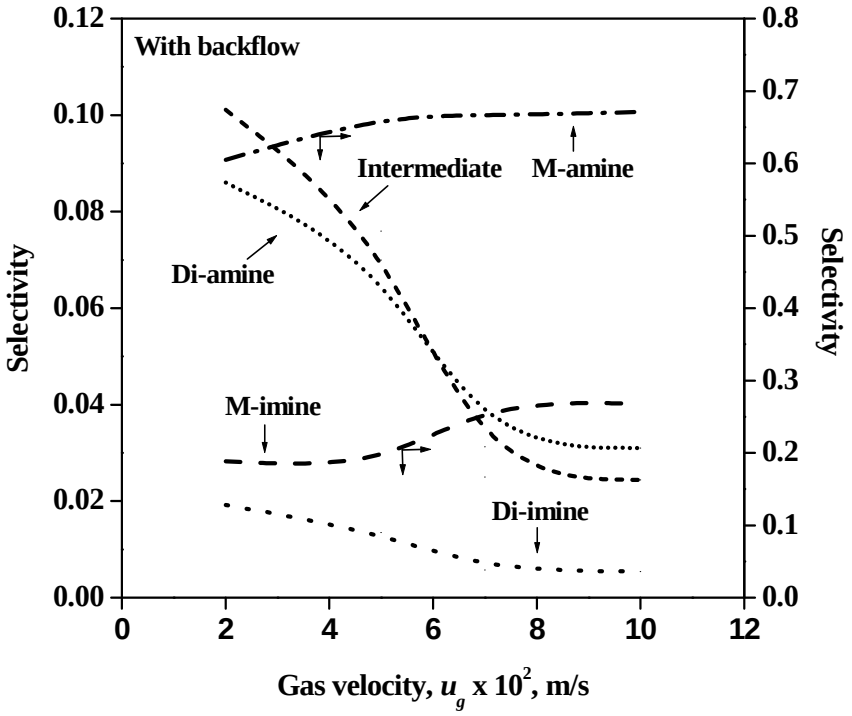

Figure 3.14. Selectivity as a function of gas velocity: Effect of backflow stream
Reaction conditions: w = 84.6 kg/m^3, B_{li} = 1 kmol/m^3, u_{lu} = 10 × 10^{-4} m/s, T = 393 K, P = 4 Mpa, N=16

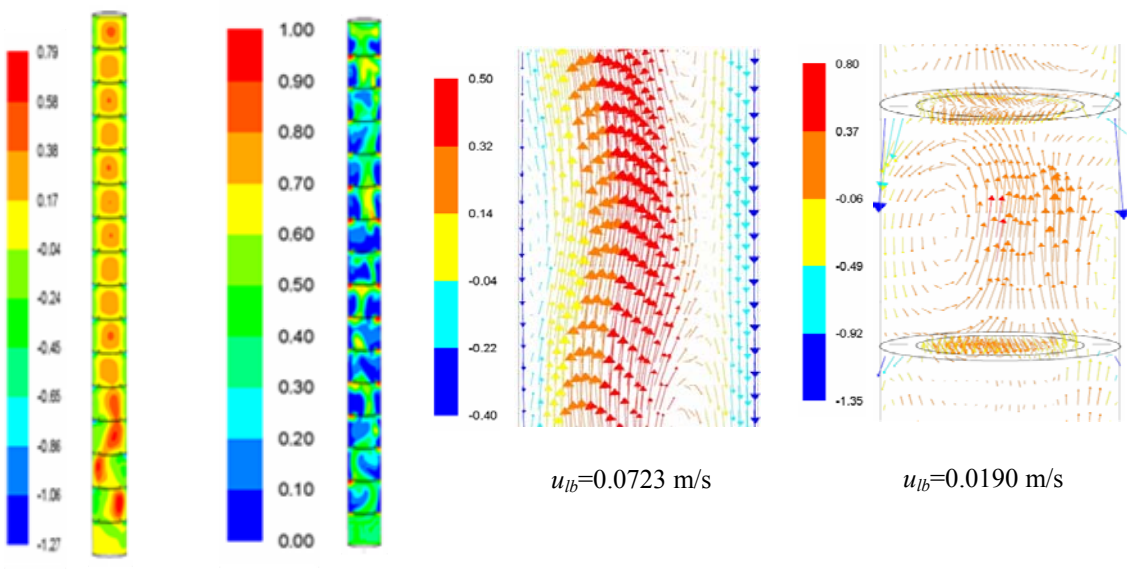

(A) Time averaged axial liquid velocity

(B) Instantaneous gas holdup

(C) Time averaged axial liquid velocity without and with radial baffle

Figure 3.15. CFD simulations for slurry bubble column reactor with baffle for u_g=0.1m/s

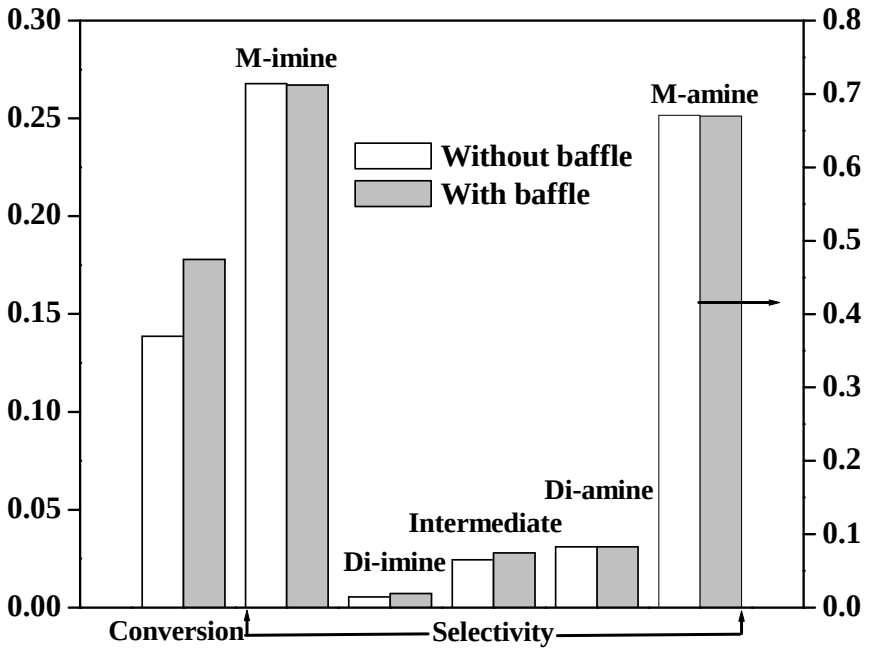

Figure 3.16. Effect of baffles on conversion of PPDA and selectivity to products
Reaction conditions: w = 84.6 kg/m^3, B_{li} = 1 kmol/m^3, u_{lu} = 10 × 10^{-4} m/s, u_g = 10 × 10^{-2} m/s, T = 393 K, P = 4 Mpa, N=16

3.4 CONCLUSIONS

A mixing cell model for a BCSR was developed for the reductive alkylation of *p*-phenylenediamine incorporating the complex intrinsic reaction kinetics, mass transfer and thermal effects. The degree of backmixing was accounted for by considering a backflow stream from all but the bottom most mixing cell. The backflow stream was quantified using a CFD model. The combination of mixing cell model coupled with CFD model for estimating degree of backmixing for a range of design and operating parameters was found to be useful for predicting reactor performance over a wide range of operating parameters. The use of radial baffles can be considered to be useful for controlling and manipulating the degree of backmixing in BCSRs. The bubble column slurry reactor model proposed here could be useful to provide guidelines for designing and improving the overall performance of bubble column reactors.

APPENDIX-A

The mixing cell model has been extended in this work by including liquid backflow stream from all but the bottom most mixing cell. Therefore, the net flow rate is same throughout the reactor, but because of the liquid backflow rate (u_{lb}), the flow rate in the middle cells increases to $u_{lu} + u_{lb}$. Therefore, the mass balance of reactants and products is different for the first, middle and N^{th} top cell (Figure 3.2). Hence, the mass and energy balance equations were developed for first cell, middle cells and N^{th} top cell separately for the gas and liquid species involved in the overall reaction. In this section, the detailed derivations of bubble column slurry reactor model equations (section 3.2.3) are presented in the following sections. The dimensionless parameters used in the model are given in Table 3.2 and are not repeated in this section. The definitions of all parameters are given in notation section.

A.1 Mass Balance of Hydrogen in Gas Phase

The mass balance for hydrogen in gas phase can be written as

$$-u_g \frac{dA_{g_j}}{dx} = k_L a_B \left[\frac{A_{g_j}}{H_A} - A_{l_j} \right] \qquad \text{A.1}$$

The above equation can be expressed in dimensionless form using the following variables

$$a_{g_j} = \frac{A_{g_j}}{A_{gi}}; \quad a_{l_j} = \frac{A_{l_j}}{A^*}; \quad A^* = \frac{A_{gi}}{H_A} \quad \therefore a_{l_j} = \frac{A_{l_j}}{\left(A_{gi}/H_A\right)}; \; z = \frac{x}{L}$$

Hence, equation A.1 can be written as

$$\therefore -\frac{da_{g_j}}{dz} = \alpha_A \left(a_{g_j} - a_{l_j} \right)$$

Integrating the above equation,

$$\therefore -\int_{a_{g_{j-1}}}^{a_{g_j}} \frac{da_{g_j}}{\left(a_{g_j} - a_{l_j}\right)} = \alpha_A \int_0^z dz$$

$$\therefore \left[\frac{a_{g_j} - a_{l_j}}{a_{g_{j-1}} - a_{l_j}} \right] = \exp(-\alpha_A z) \qquad \text{A.2}$$

$$\therefore a_{g\,j} - a_{l\,j} = a_{g\,j-1}\exp(-\alpha_A z) - a_{l\,j}\exp(-\alpha_A z)$$

where, z = dimensionless axial distance, $1/N$

$$\therefore a_{g\,j} = a_{g\,j-1}\exp\left(\frac{\alpha_A}{N}\right) - \left[1 - \exp\left(\frac{\alpha_A}{N}\right)\right] a_{l\,j} \qquad \text{A.3}$$

A.2 Mass Balance of Hydrogen in Liquid Phase

Middle cells:

The mass balance for hydrogen in liquid phase for the middle cells (Figure 3.2) can be written as

$$\begin{aligned}&\int_0^{L/N} k_L a_B \left[\frac{A_{g\,j}}{H_A} - A_{l\,j}\right] dx = \left(u_{lu} + u_{lb}\right) A_{l\,j} + u_{lb} A_{l\,j} \\ &-\left[\left(u_{lu} + u_{lb}\right) A_{l\,j-1} + u_{lb} A_{l\,j+1}\right] + k_s a_p \left(\frac{L}{N}\right)\left(A_{l\,j} - A_{s\,j}\right)\end{aligned} \qquad \text{A.4}$$

The equation A.4 can be expressed in dimensionless form as

$$\therefore \int_0^{1/N} \frac{L k_L a_B}{u_{l\,u}}\left(a_{g\,j} - a_{l\,j}\right) dz = \left(1 + 2\phi\right) a_{l\,j} - \left[\left(1 + \phi\right) a_{l\,j} - 1 + \phi\, a_{l\,j+1}\right] + \frac{\alpha_{l\,s}}{N}\left(a_{l\,j} - a_{s\,j}\right)$$

$$\therefore \int_0^{1/N} \alpha_A \beta_A \left(a_{g\,j} - a_{l\,j}\right) dz = \left(1 + 2\phi\right) a_{l\,j} - \left[\left(1 + \phi\right) a_{l\,j} - 1 + \phi\, a_{l\,j+1}\right] + \frac{\alpha_{l\,s}}{N}\left(a_{l\,j} - a_{s\,j}\right) \qquad \text{A.5}$$

By substituting equation A.2 in equation A.5

$$\therefore \int_0^{1/N} \alpha_A \beta_A \left(a_{g\,j-1} - a_{l\,j}\right) e^{-\alpha_A z} dz = \left(1 + 2\phi\right) a_{l\,j} - \left[\left(1 + \phi\right) a_{l\,j} - 1 + \phi\, a_{l\,j+1}\right] + \frac{\alpha_{l\,s}}{N}\left(a_{l\,j} - a_{s\,j}\right)$$

On integrating the above equation w. r. t. z,

$$\therefore \beta_A\left(a_{g\,j-1}-a_{l\,j}\right)\left(1-e^{-\alpha_A/N}\right)=(1+2\phi)a_{l\,j}-\left[(1+\phi)a_{l\,j}-1+\phi\, a_{l\,j+1}\right]+\frac{\alpha_{l\,s}}{N}\left(a_{l\,j}-a_{s\,j}\right)$$

$$\therefore a_{l\,j}=\frac{\left((1+\phi)\,a_{l\,j-1}+\phi a_{l\,j+1}\right)+\beta_A\left[1-\exp\left(-\frac{\alpha_A}{N}\right)\right]a_{g\,j-1}+\left(\frac{\alpha_{ls}}{N}\right)a_{s\,j}}{1+2\phi+\frac{\alpha_{ls}}{N}+\beta_A\left[1-\exp\left(-\frac{\alpha_A}{N}\right)\right]} \qquad \text{A.6}$$

Similarly for the first and top cell concentration of hydrogen in liquid phase can be written as

First cell:

$$\int_0^{L/N} k_L a_B\left[\frac{A_{g\,j}}{H_A}-A_{l\,j}\right]dx=\left(u_{lu}+u_{lb}\right)A_{l\,j}-u_{lu}\,A_{l\,j-1}-u_{lb}\,A_{l\,j+1}+k_s a_p\left(\frac{L}{N}\right)\left(A_{l\,j}-A_{S\,j}\right) \qquad \text{A.7}$$

Final dimensionless form

$$a_{l\,j}=\frac{\left(a_{l\,j-1}+\phi a_{l\,j+1}\right)+\beta_A\left[1-\exp\left(-\frac{\alpha_A}{N}\right)\right]a_{g\,j-1}+\left(\frac{\alpha_{l\,s}}{N}\right)a_{s\,j}}{1+\phi+\frac{\alpha_{l\,s}}{N}+\beta_A\left[1-\exp\left(-\frac{\alpha_A}{N}\right)\right]} \qquad \text{A.8}$$

***N^th* Top cell:**

$$\int_0^{L/N} k_L a_B\left[\frac{A_{g\,j}}{H_A}-A_{l\,j}\right]dx=u_{lu}\,A_{l\,j}+u_{lb}\,A_{l\,j}-\left(u_{lu}+u_{lb}\right)A_{l\,j-1}+k_s a_p\left(\frac{L}{N}\right)\left(A_{l\,j}-A_{S\,j}\right) \qquad \text{A.9}$$

Final dimensionless form

$$a_{l\,j} = \frac{\left((1+\phi)a_{l\,j-1}\right) + \beta_A\left[1-\exp\left(-\frac{\alpha_A}{N}\right)\right]a_{g\,j-1} + \left(\frac{\alpha_{l\,s}}{N}\right)a_{s\,j}}{1+\phi+\frac{\alpha_{l\,s}}{N}+\beta_A\left[1-\exp\left(-\frac{\alpha_A}{N}\right)\right]} \qquad \text{A.10}$$

A.3 Concentration of Hydrogen on Catalyst Surface

The concentration of hydrogen on catalyst surface can be calculated as

$$k_s a_p\left(\frac{L}{N}\right)\left(A_{l\,j} - A_{s_j}\right) = \frac{L}{N}\left[\frac{k_5 D_{l\,j} + k_8 F_{l\,j} + k_9 H_{l\,j}}{1+K_A\sqrt{A_{s_j}}}\right] \qquad \text{A.11}$$

In dimensionless form

$$\alpha_{l\,s}\left(a_{l\,j} - a_{s\,j}\right) = \alpha_{R_5} q_B\left[\frac{\left(d_{l\,j} + k_{85} f_{l\,j} + k_{95} h_{l\,j}\right)\sqrt{a_{s\,j}}}{1+k_a\sqrt{a_{s\,j}}}\right] \qquad \text{A.12}$$

A.4 Mass balance of PPDA in Liquid Phase

Middle cells:

The mass balance of PPDA in liquid phase can be written as

$$\left[\left(u_{lu}+u_{l\,b}\right)B_{lj-1} + u_{lb}B_{l\,j+1}\right] - \left(\left(u_{lu}+u_{l\,b}\right)B_{l\,j} + u_{lb}B_{lj}\right) = \left(\frac{L}{N}\right)R_1 \qquad \text{A.13}$$

$$\therefore \left(1+\phi\right)B_{l\,j-1} + \phi B_{l\,j+1} - B_{lj}\left(1+2\phi\right) =$$
$$\left(\frac{L}{u_{lu}N}\right)\left[k_{eqi}B_{l\,j} - k_{eq2}D_{l\,j}\left(D_{l\,j} + 2F_{lj} + G_{l\,j} + 2H_{l\,j} + 2P_{l\,j}\right)\right]$$

The above equation has been made dimensionless on the basis of initial substrate concentration B_{li} as

$$\left(1+\phi\right)b_{l\,j-1} + \phi b_{l\,j+1} - b_{lj}\left(1+2\phi\right) = \frac{\alpha_{R1}}{N}b_{l\,j} - \frac{\alpha_{R2}}{N}d_{l\,j}\left[d_{l\,j} + 2f_{l\,j} + g_{l\,j} + 2h_{l\,j} + 2p_{l\,j}\right]$$

Final dimensionless form

$$b_{l\,j} = \frac{\left((1+\phi)b_{l\,j-1} + \phi b_{lj+1}\right) + \frac{\alpha_{R2}}{N} d_{l\,j}\left[d_{l\,j} + 2f_{l\,j} + g_{l\,j} + 2h_{l\,j} + 2p_{l\,j}\right]}{1 + 2\phi + \frac{\alpha_{R1}}{N}} \qquad \text{A.14}$$

First cell:

$$\left[u_{l\,u} B_{lj-1} + u_{lb} B_{l\,j+1} - \left(u_{lu} + u_{l\,b}\right) B_{l\,j}\right] = \left(\frac{L}{N}\right) R_1 \qquad \text{A.15}$$

Final dimensionless form

$$b_{l\,j} = \frac{\left(b_{l\,j-1} + \phi b_{lj+1}\right) + \frac{\alpha_{R2}}{N} d_{l\,j}\left[d_{l\,j} + 2f_{l\,j} + g_{l\,j} + 2h_{l\,j} + 2p_{l\,j}\right]}{1 + \phi + \frac{\alpha_{R1}}{N}} \qquad \text{A.16}$$

Top cell:

$$\left[\left(u_{lu} + u_{l\,b}\right) B_{lj-1} - u_{lb} B_{l\,j}\right] = \left(\frac{L}{N}\right) R_1 \qquad \text{A.17}$$

Final dimensionless form

$$b_{l\,j} = \frac{\left((1+\phi)b_{l\,j-1}\right) + \frac{\alpha_{R2}}{N} d_{l\,j}\left[d_{l\,j} + 2f_{l\,j} + g_{l\,j} + 2h_{l\,j} + 2p_{l\,j}\right]}{\phi + \frac{\alpha_{R1}}{N}} \qquad \text{A.18}$$

Similarly, the mass balance of M-imine, Di-imine, M-amine, Intermediate and Di-amine can be derived. The final dimensionless forms are given in section 3.2.3.

A.5 Non-isothermal Model

Middle cells:

The non-isothermal model for the middle cells can be written as

$$\left(u_g\rho_g C_{pg}+u_{lu}\rho_l C_{pl}+2u_{lb}\rho_l C_{pl}\right)T_j-\left(u_g\rho_g C_{pg}+u_{lu}\rho_l C_{pl}+u_{lb}\rho_l C_{pl}\right)T_{j-1}+u_{lb}\rho_l C_{pl}T_{j+1}=$$

$$\frac{(-\Delta H_1)L}{N}[R_A]+\frac{(-\Delta H_2)L}{N}[R_1]+\frac{(-\Delta H_3)L}{N}[R_2]+\frac{(-\Delta H_4)L}{N}[R_4]-U_w A_w(T_j-T_w)$$

A.19

Final dimensionless form

$$\theta=\frac{\eta_c\alpha_{R5}}{Nq_B}\beta_8\left[\frac{\left(d_{lj}+k_{85}f_{lj}+k_{95}h_{lj}\right)\sqrt{a_{sj}}}{1+k_a\sqrt{a_{sj}}}\right]+\frac{\beta_9}{N}\left[\alpha_{R1}b_{lj}-\alpha_{R2}d_{lj}\left(d_{lj}+2f_{lj}+g_{lj}+2h_{lj}+2p_{lj}\right)\right]$$
$$+\frac{\beta_{10}}{N}\left[\alpha_{R3}d_{lj}-\alpha_{R4}f_{lj}\left(d_{lj}+2f_{lj}+g_{lj}+2h_{lj}+2p_{lj}\right)\right]$$
$$+\frac{\beta_{11}}{N}\left[\alpha_{R6}g_{lj}-\alpha_{R7}h_{lj}\left(d_{lj}+2f_{lj}+g_{lj}+2h_{lj}+2p_{lj}\right)\right]-\frac{\beta_{12}}{N}\left(\theta_j-\theta_w\right)$$
$$+\beta_{13}\theta_{j-1}+\beta_{14}\theta_{j+1}$$

A.20

Similarly for the first and top cell, the non-isothermal model can be derived. The final dimensionless forms of non-isothermal models for first and N^{th} top cell are given in section 3.2.3.

NOMENCLATURE

a_B = gas-liquid interfacial area, m^2/m^3

a_l = dimensionless concentration of hydrogen in the liquid phase, $(A_l.H_A/A_{go})$

a_p = external surface area of the pellet, $[6w/\rho_p d_p]$, m^{-1}

A^* = saturation solubility of hydrogen, $kmol/m^3$

A_l = concentration of hydrogen in the liquid phase, $kmol/m^3$

A_s = concentration of hydrogen on the catalyst surface, $kmol/m^3$

b_l = dimensionless concentration of PPDA in the liquid phase, (B_l/B_{li1})

B_l = concentration of PPDA in the liquid phase, $kmol/m^3$

B_{li} = initial concentration of PPDA in the liquid phase, $kmol/m^3$

C_m = concentration of MEK, $kmol/m^3$

C_{H2O} = concentration of water, $kmol/m^3$

c_{H2O} = dimensionless concentration of water

C_{pl} = heat capacity of liquid, kJ/kg/K

C_{pg} = heat capacity of gas, kJ/kg/K

d_l = dimensionless concentration of M-imine in liquid phase, (D_l/B_{li})

D_l = concentration of M-imine in the liquid phase, $kmol/m^3$

D_e = effective diffusivity, m^2/s

D_m = molecular diffusivity, m^2/s

d_p = particle diameter, m

d_T = reactor diameter, m

E_i = activation energy for hydrogenation step *i*, kJ/mol

f_l = dimensionless concentration of di-imine in liquid phase, (F_l / B_{li})

F_l = concentration of di-imine in liquid phase, kmol/m^3

F_r = froude number, ($u_g^2 / (g \times d_p)$)

g_l = dimensionless concentration of M-amine in liquid phase, (G_l / B_{li})

G_l = concentration of M-amine in liquid phase, kmol/m^3

g = acceleration due to gravity, m/s^2

h_l = dimensionless concentration of intermediate in liquid phase, (H_l / B_{li})

H_l = concentration of intermediate in liquid phase, kmol/m^3

H_e = henry's constant of solubility for H_2, kmol/m^3/atm

H_A = solubility coefficient of hydrogen, (A_g/A_l)

k_5, k_8 *and* k_9 = reaction rate constants, (m^3/kg)(m^3/kmol)$^{0.5}$$s^{-1}$

k_{85} = dimensionless rate constant, (k_8/k_5)

k_{95} = dimensionless rate constant, (k_9/k_5)

k_a = dimensionless adsorption equilibrium constant, ($K_A A_S^{0.5}$)

$k_l a_B$ = gas-liquid mass transfer coefficient, s^{-1}

k_s = liquid-solid mass transfer coefficient, s^{-1}

K_A = adsorption equilibrium constant, m^3/kmol

L = length of reactor, m

N = number of cells

p_l = dimensionless concentration of Di-amine (P_l/B_{li})

P_l = concentration of Di-amine in liquid phase, kmol/m^3

P_r = prandtl number, ($C_{pl}\, \mu_{ls}/\lambda$)

q_B = stoichiometric ratio ($B_{li}/A_{go}/H_A$)

R_1 to R_6 = reaction rates for individual reaction steps (Figure 3.1), kmol/m^3/s

R = radius of catalyst particle, m

R_e = reynold's number, ($d_p u_g \rho_{sl}/\mu_{ls}$)

R_A = overall rate of hydrogenation, kmol/m^3/s

R_{H2} = global rate of hydrogenation, kmol/m^3/s

R_g = universal gas constant, kJ/kmol/K

S_{TW} = surface tension of water, dyne/cm

S_T = surface tension of liquid, dyne/cm

T_i = inlet temperature, K

T_o = outlet temperature, K

T_w = wall temperature, K

U_w = bed-to-wall heat transfer coefficient, kJ/m^2/K/s

u_g = gas velocity, m/s

u_{lu} = net liquid velocity, m/s

u_{lb} = back liquid velocity, m/s

u_{tp} = terminal settling velocity of particle, m/s

V_R = reactor volume, m^3

W = catalyst loading, kg/m^3

z = dimensionless reactor length

Greek letters

α_A = dimensionless gas-liquid mass transfer coefficient

α_{ls} = dimensionless liquid-solid mass transfer coefficient

$\alpha_{R1}, \alpha_{R3}, \alpha_{R6}$ = dimensionless forward reaction rate constants

$\alpha_{R2}, \alpha_{R4}, \alpha_{R7}$	=	dimensionless backward reaction rate constants
$\alpha_{R5}, \alpha_{R8}, \alpha_{R9}$	=	dimensionless reaction rate constant
β_1-β_4, & β_8-β_{11}	=	dimensionless thermicity parameters
β_5 & β_{12}	=	dimensionless heat transfer parameters
$\beta_6, \beta_7 - \beta_{13}, \beta_{14}$	=	dimensionless parameters defined by eqs. 3.25 and 3.26
β_A	=	dimensionless parameter defined by equation 3.9, ($u_g H_A/u_l$)
ΔH_1	=	heat of reaction for catalytic hydrogenation steps, kJ/kmol
ΔH_2, ΔH_3, ΔH_4	=	heat of reaction for equilibrium reaction steps R_1, R_2 and R_4 respectively, kJ/kmol
ε_g	=	gas hold up
θ_j	=	dimensionless exit temperature, (T_o/T_i)
θ_w	=	dimensionless wall temperature, (T_w/T_i)
θ_{j-1}	=	dimensionless inlet temperature, (T_{j-1}/T_i)
λ_{eff}	=	effective thermal conductivity, kJ/s.m.°C
ρ_l	=	density of the liquid, kg/m^3
ρ_{sl}	=	density of the slurry, kg/m^3
ρ_g	=	density of gas, kg/m^3
ρ_p	=	density of catalyst particle, kg/m^3
μ_l	=	viscosity of the liquid, kg/m/s
μ_{sl}	=	viscosity of the slurry, kg/m/s
μ_g	=	viscosity of the gas, kg/m/s
ϕ	=	parameter defined by equation 3.8

REFERENCES

1. Shah, Y. T. Gas- Liquid- Solid Reactor Design, McGraw-Hill, New York, **1979**.
2. Ramachandran, P. A., & Chaudhari, R. V. Three Phase Catalytic Reactors, Gorden & Breach, New York, **1983**.
3. Deckwer, W. D. Bubble Column Reactors, Wiley, New York, **1992**.
4. Saxena, S. C. Bubble column reactors and Fischer-Tropsch synthesis. *Catalysis Reviews: Science and Engineering*, **1995**, *37*, 227-309.
5. Duducovic, M.P. Trends in Catalytic Reaction Engineering. *Catalysis Today*, **1999**, *48*, 5.
6. Krishna, R. A Scale up strategy for a commercial scale bubble column slurry reactor for Fischer-Tropsch synthesis. *Oil and Gas Science and Technology*, **2000**, *55*, 359.
7. Jakobsen, H.A.; Lindborg, H.; Dorao, C.A. Modeling of bubble column reactors: Progress and limitations. *Ind. Eng. Chem. Res.*, **2005**, *44*, 5107.
8. Schumpe, A. and K. D. P. Nigam. Mass transfer in three-phase sparged reactors. *Topics in Chemical Engineering*, **1996**, *8*, 169, 679.
9. Bukur, Dragomir. B. Some comments on models for Fischer-Tropsch Reaction in Slurry Bubble Column Reactors. *Chem. Eng. Sci.*, **1983**, *38*, 440.
10. Mills, P.L.; Turner, J. R.; Ramchandran, P.A.; Duducovic M.P. The Fischer-Trospch synthesis in slurry bubble column reactors: Analysis of reactor performance using the axial dispersion model. *Topics in Chemical Engineering*, **1996**, *8* (Three Phase Sparged Reactors), 339-386, 679-739.
11. Krishna, R. and Maretto, C. Scale up of a bubble column slurry reactor for Fischer-Tropsch synthesis. Studies in Surface Science and Catalysis (Natural Gas Conversion V), **1998**, *119*, 197.
12. Krishna, R.; van Baten, J.M.; Urseanu, M. I.; Ellenberger, J. Design and scale up of a bubble column slurry reactor for Fischer-Tropsch synthesis. *Chem. Eng. Sci.*, **2001**, *56*, 537.
13. Mathieu, C.; Dietrich, E.; Delmas, H.; Jenck, J. Hydrogenation of adiponitrile catalyzed by raney nickel: Use of intrinsic kinetics to measure gas-liquid mass transfer in a gas induced stirred slurry reactor. *Chem. Eng. Sci.*, **1992**, *47*, 2289-2294.
14. Bern, L.; Hell, M.; Schoon, N.H. Kinetics of the hydrogenation of rapeseed oil. Rate Equations of Chemical Reactions. *Journal of the American Oil Chemists' Society*, **1975**, *52*, 391.
15. Rampure, M.; Kulkarni, A.A.; Ranade, V.V. Hydrodynamics of Bubble Column Reactors at High Gas Velocity: Experiments and CFD simulations. *Ind. Eng. Chem. Res.*, **2007**, *46(25)*, 8431.
16. Govindrao, V. M. H.; Chidambaram, M. On the steady state Performance of Cocurrent Bubble Column Slurry Reactors. *Chemical Engineering Journal*, **1983**, *27*, 29.
17. Kawakami, K.; Aio, T.; Kusunoki, K. Selectivity of butadiene hydrogenation in a bubble column slurry reactor. Kagaku Kogaku Ronbunshu, (Japanese), **1981**, *7* ,105.
18. Dassori, C. G. Three Phase Reactor Modeling with Significant Back Mixing in the Liquid Phase Using Modified Cell Model (MCM). *Computers & Chemical Engineering*, **1998***, 22* (Supplement 1), S679.
19. Brahme, P. H.; Chaudhari, R. V.; Ramachandran, P. A. Modeling of hydrogenation of glucose in a continuous slurry reactor. *Ind. Eng. Chem. Process Des. Dev.*, **1984**, *23*, 857.
20. Jaganathan, R.; Gholap, R. V.; Brahme, P. H.; Chaudhari, R. V. Performance of a continuous bubble column slurry reactor for hydrogenation of butynediol. *Proc.* of ISCRE 2, Vol. II, NCL, India, **1987**, 141.
21. Thakar, N. N.; Jaganathan, R.; Chaudhari, R.V.; Mills P.L. Modeling of hydrogenation of maleic acid in a bubble column slurry reactor. *A.I.Ch.E. Journal*, **2003**, *49*, 3199.
22. Lehtonen, J.; Salmi, T.; Vaori, A.; Tirronen, E. On the principles of modeling of homogeneous-heterogeneous reactions it the production of fine chemicals. A case study: Reductive alkylation of aromatic amines. *Org. Process Res. Dev.*, **1998**, *2*, 78.
23. Ege, S. Organic chemistry, Structure and Reactivity, 3rd ed. (D. C. Heath and Co.; Lexington, KY), **1994**, p-535.
24. Greenfield, H. Side Reactions in reductive alkylation of aromatic amines with aldehydes and ketones. Chemical Industry (Dekker), (catalysis of organic reactions), **1994**, *53*, 265.
25. Salmi, T.; Lehtonen, J.; Kaplin, J.; Vuori, A.; Tirronen, E.; Haarrio, H. A homogeneous-heterogeneously catalyzed reaction system in a loop reactor. *Catalysis Today*, **1999**, *48*, 139.
26. Roy, D.; Jaganathan, R.; Chaudhari, R. V. Kinetic modeling of aniline with acetone using 3% Pd/Al2O3 catalyst in a batch slurry reactor. *Ind. Eng. Chem. Res.*, **2005**, *44*, 5388.

27. Ramachandran, P. A., & Smith, J. M. Mixing-cell model for design of trickle-bed reactors. *Chem. Eng. Sci.*, **1979**, *17*, 91.
28. Kato, Y.; Nishiwaki, A.; Fakuda, T.; Tanaka S. The behavior of suspended solid particles and liquid in bubble columns. *Journal of Chemical Engineering of Japan*, **1972**, *5*, 112.
29. Bischoff, K. B. Effectiveness factors for general reaction rate forms. *A.I.Ch.E. Journal*, **1965**, *11*, 351.
30. Vinke, H.; Hamersma, P. J.; Fortuin, J.M.H. Particle-to-bubble adhesion in gas /liquid/ solid slurries. *A.I.Ch.E. Journal*, **1991**, *37*,1801.
31. Mears, D.E. Tests for transport limitations in experimental catalytic reactors. *Ind. Eng. Chem. Process Des. and Dev.*, **1971**, *10*, 541.
32. MATLAB 7, Release 14, The MathWorks, Inc., **2004**.
33. Yoshida, F.; Akita, K. Performance of gas bubble columns. volumetric liquid phase mass transfer coefficient and gas hold up. *A.I.Ch.E. Journal*, **1965**, *11*, 9.
34. Mashelkar, R.A. Bubble Columns. British Chemical Engineering, **1970**, *15*, 1297.
35. Sano, Y.; Yagamuchi, N.; Adachi T. Mass transfer coefficients for suspended particles in agitated vessels and bubble columns. *Journal of Chemical Engineering Japan*, **1974**, *1*, 255.
36. Deckwer, W. D. On the Mechanism of Heat Transfer in Bubble Column reactors. *Chem. Eng. Sci.*, **1980**, *35*, 1341.
37. Wilke, C. R.; Chang P. Correlation of diffusion coefficients in dilute solutions. *A. I.Ch.E. Journal*, **1955**, *1*, 264.
38. Ranade, V. V. Computational Flow Modeling for Chemical Reactor Engineering, Academic Press, London, **2002**.
39. Ekambara, K.; Joshi, J. B. CFD simulations of residence time distribution and mixing in bubble column reactors. *Canadian J. Chem. Eng.*, **2003**, *81*, 669.
40. Buwa, V. V.; Ranade, V. V.. Mixing in bubble columns reactors: Role of unsteady flow structures. *Canadian J. Chem. Eng.*, **2003**, *81*, 402.
41. Ansys Fluent 6.3, Fluent Inc., 10 Cavendish Court, Lebanon, NH03766, U.S.A
42. Thorat, B. N.; Joshi, J. B. Regime transition in bubble columns: Experimental and predictions. *Experimental Thermal and Fluid Science*, **2004**, *28*, 423-430.
43. Khare, A. S.; Dharwadkar, S.V.; Joshi, J.B.; Sharma, M. M. Liquid- and solid-Phase mixing in sectionalized bubble column slurry reactor. *Ind. Eng. Chem. Res.*, **1990**, *29*, 1503.
44. Behkish, A.; Zhuowu, M.; Inga, J.R.; Morsi, B.I. Mass transfer characteristics in a large- scale slurry bubble column reactor with organic mixtures. *Chem. Eng. Sci.*, **2002**, *57*, 3307.
45. Jordan, U.; Schumpe, A. The gas density effect on mass transfer in bubble columns with organic liquids. *Chem. Eng. Sci.*, **2001**, *56*, 6267.
46. Hikita, H.; Asai, S.; Tanigawa, K.; Segawa, K.; Kitao, M. The volumetric liquid phase mass transfer coefficient in bubble columns. *Chemical Engineering Journal*, **1981**, *22*, 61.
47. Koide, K., Takazawa, A., Komura, M., Matsunaga, H., Gas hold up and volumetric liquid phase mass transfer coefficient in solid suspended bubble columns. *Journal of Chemical Engineering of Japan*, **1984**, *17*, 459.

CHAPTER-4

Modeling of Fixed Bed and Slurry Reactors for Reductive Alkylation of *p*-Phenylenediamine: A Comparative Study

4.1 INTRODUCTION

Three phase catalytic reactors are used in a large number of chemical processes such as hydrogenation, oxidation and alkylation.[1] They can be classified in two main types: fixed bed reactors (FBR) wherein gas and liquid phase reactants flow through a bed of large catalyst particles, and slurry reactors wherein small particles of catalyst are suspended in the gas-liquid mixture. For any catalytic reaction, it is often possible to use either a slurry or a fixed bed reactor. The selection of appropriate multiphase reactor is important since it greatly impacts the total capital cost and manufacturing costs for any industrial chemical process.[2] The important factors to consider in the selection of reactors for any chemical process are to achieve highest possible conversion of reactant and selectivity to desired product with minimum byproducts and the feasibility of scale-up to commercial scales. It is also important to identify the most effective mode of operation for the selected reactor. Possible approaches for selecting the most suitable reactor configuration[3] are discussed in the following.

The different approaches for the selection of a reactor type are being discussed in the literature such as heuristic-numeric consulting scheme,[4] stochastic optimization technique[5,6] etc. [7,8] Krishna and Sie[9] proposed an effective approach for selecting reactors based on three levels: catalyst design, injection and dispersion strategy, and choice of hydrodynamic flow regime. Such analysis can guide the development of the catalyst with desirable properties and the development of right size and shape to fit into the best reactor type. Moreover, the approach requires the quantitative models for the flow pattern, phase contacting and transport in various multiphase reactors.[2] Mathematical modeling of reactors to simulate their performance is crucial for the selection of best reactor type for a given chemistry and catalyst. The modeling facilitates examination and comparison of the distinguishing features of the reactors for successful scale-up. Development of efficient and reliable models for multiphase reactors is still a difficult task because it involves many aspects including hydrodynamics, gas-liquid and liquid-solid mass transfer, heat transfer, pore diffusion and reaction kinetics.[10,11,12,13,14] Model assessment has mostly been reported for a single reaction or reactions with simplified kinetic laws under isothermal conditions.[15,16,17,18] The selection among multiphase reactors for industrially important case studies based on detailed analysis and modeling has hardly ever been published.[19,20]

The relevant literature survey on modeling of three phase catalytic reactors has been presented in Chapter-1 (Section 1.3).

In this chapter, a detailed theoretical analysis of fixed bed (downflow and upflow) and slurry reactors (CSTR and BCSR) has been presented with reductive alkylation of *p*-phenylenediamine with methyl ethyl ketone using 3%Pt/Al_2O_3 catalyst as an example of complex multistep reaction. The complete reaction scheme was elucidated and the intrinsic kinetics of the reaction has been discussed in Chapter 2, Part-A. There is no detailed analysis and comparison of different types of multiphase reactors for this particular reaction system. A schematic of the reaction considered in this work is shown in Figure 4.1 in Section 4.2.1. It should be noted here that the BCSR model is already described in Chapter-3, which when used for number of cells $N = 1$ reduces to the CSTR model (see Section 4.3.2). The detailed modeling of fixed bed reactor with downflow and upflow mode is described in this chapter. First, the fixed bed reactor models were used to evaluate the performance characteristics of the reactors and a comparison of the salient features of the reactor configuration for the considered reaction system is discussed. Finally, the performance of various reactors (FBR, BCSR, and CSTR) was carried out to evaluate comparative reactor performances based on the selectivity and productivity towards the desired product Di-amine. The different multiphase reactor models presented here will be useful for developing insight into the effects of various operating parameters on the overall reactor performance.

4.2 FIXED BED REACTOR (FBR) MODEL

In this work, the effect of axial dispersion on the FBR performance has been investigated by establishing both 'axial dispersion' and 'plug flow' models. For predicting the fixed bed reactor performance with downflow i.e. trickle bed reactor (TBR) mode, the approach of Rajashekharam *et. al.*[21] has been followed and further extended to account for the axial dispersion. The axial dispersion is accounted for in the reactor model via the axial dispersion coefficient D_{EL} for the reactants as well as for the products. For the upflow reactor, the TBR model has been modified suitably. Thus, the model explicitly describes the following issues in the reactor:

i) Axial mixing in dynamic liquid phase

ii) External and intraparticle mass transfer for a gas phase reactant (hydrogen)

iii) Partial wetting of catalyst particles (for trickle bed mode)

iv) Role of stagnant liquid pockets (for trickle bed mode)

v) The reactant and products concentration variation across the reactor in dynamic and stagnant liquid portions of liquid texture (for trickle bed mode)

vi) Heat generation by catalytic and noncatalytic reaction steps (for plug flow model)

For the purpose of developing FBR model for the reductive alkylation of PPDA, the intrinsic kinetics reported in Chapter-2 (Part-A) has been used. The proposed rate equations for the different reaction steps (Figure 4.1) are explained in the following section. A detailed description of FBR model equations is given in the subsequent sections.

4.2.1 Intrinsic Kinetics

The intrinsic kinetics for the reductive alkylation of PPDA with MEK to *N, N'*-di-sec-butyl-*p*-Phenylenediamine using 3% Pt/Al_2O_3 as catalyst has been presented in Chapter-2 for a batch slurry reactor. Based on this work, the reaction network is described as shown in Figure 4.1.

The following types of rate equations for non-catalytic (R_1, R_2 and R_4) steps have been found to adequately describe the individual homogeneous reaction steps involved,

$$R_1 = k_{eq1} B_l - k_{eq2} D_l C_{H_2O} \quad 4.1$$

$$R_2 = k_{eq3} D_l - k_{eq4} F_l C_{H_2O} \quad 4.2$$

$$R_4 = k_{eq6} G_l - k_{eq7} H_l C_{H_2O} \quad 4.3$$

where, $k_{eq1} = k_{eq1m} C_m$, $k_{eq3} = k_{eq3m} C_m$, $k_{eq6} = k_{eq6m} C_m$

$$C_{H_2O} = \left(D_l + 2F_l + G_l + 2H_l + 2P_l\right)$$

where, k_{eq1}, k_{eq3}, k_{eq6} and k_{eq2}, k_{eq4}, k_{eq7} are the forward and backward reaction rate constants respectively for the steps R_1, R_2 and R_4 as shown in Figure 4.1 and C_m represents the concentration of methyl ethyl ketone. For most practical situations, MEK is used in large excess with respect to PPDA and its change in concentration during the course of a reaction is negligible. Therefore, all the forward reaction steps were considered to be pseudo first order reactions.

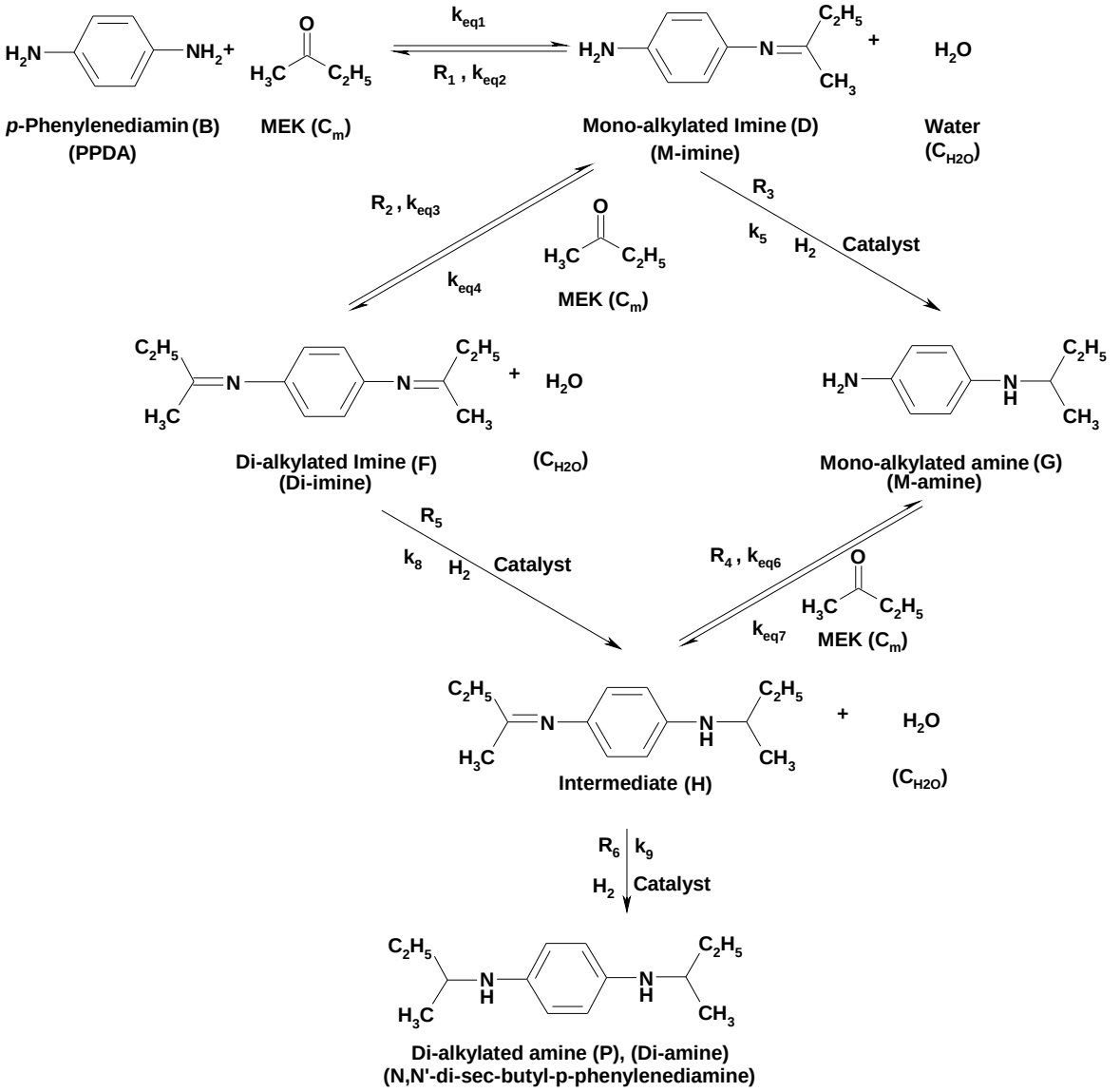

Figure 4.1. Detailed reaction scheme of reductive alkylation of PPDA with MEK in presence of 3% Pt/Al_2O_3 catalyst

The following types of Langmuir-Hinshelwood rate equations have been found to adequately describe the individual catalytic reaction steps (R_3, R_5 and R_6), (Section 2(A).3.5)

$$R_3 = \frac{\eta_c w k_5 D_l \sqrt{A_s}}{\left(1 + K_A \sqrt{A_s}\right)} \qquad 4.4$$

$$R_5 = \frac{\eta_c w k_8 F_l \sqrt{A_s}}{\left(1 + K_A \sqrt{A_s}\right)} \qquad 4.5$$

$$R_6 = \frac{\eta_c w k_9 H_l \sqrt{A_s}}{\left(1 + K_A \sqrt{A_s}\right)} \qquad 4.6$$

In equations 4.4-4.6, A_s represents the concentration of hydrogen on the catalyst surface. Definitions for the remaining variables are given in the Notation Section. The kinetic parameters are presented in Table 4.1 based on the experimental study discussed in Chapter 2.

Table 4.1. Kinetic Rate Equation Parameters

Temp. K	k_{eq1} $\times 10^3$	k_{eq2} $\times 10^4$	k_{eq3} $\times 10^4$	k_{eq4} $\times 10^4$	k_5 $\times 10^2$	k_{eq6} $\times 10^4$	k_{eq7} $\times 10^5$	k_8 $\times 10^2$	K_9 $\times 10^3$	K_A
373	0.1248	0.0351	1.214	0.0692	0.0639	0.2539	0.072	0.2035	0.4110	1.605
393	0.2091	0.2562	2.910	0.3732	0.1091	0.2018	0.2397	0.3980	0.5147	1.111
413	0.2440	0.8807	2.982	0.3981	0.1481	0.6497	1.267	0.3923	0.6609	1.6395

4.2.2 Trickle Bed Reactor (TBR) Model

4.2.2.1 Assumptions of the model

For the purpose of developing a trickle bed reactor (TBR) model applicable to reductive alkylation of PPDA with MEK, the approach of Tan and Smith[22] and Chaudhari and Ramachandran[23] was used to evaluate an approximate solution of the catalytic effectiveness factor under conditions of partial wetting and in the presence of significant stagnant liquid pockets in between the catalyst particles. The spherical catalyst particle was assumed to be divided into three zones as shown in Figure 4.2: (1) a dry zone, (2) a wetted zone covered by the flowing dynamic liquid and (3) a wetted zone covered by the stagnant liquid.[21] It was also assumed that

(a) gas and liquid are in plug flow

(b) dissolved organics are nonvolatile and the reaction takes place only in liquid phase

(c) liquid phase reactants are in excess when compared to the gaseous reactant

(d) the solubility of hydrogen in the liquid phase follows Henry's law

(e) the gas-liquid, liquid-solid and intraparticle mass transfer resistances for H_2 are considered, whereas the liquid-solid and intraparticle mass transfer resistances for the liquid-phase components are assumed to be negligible

(f) since, the gas feed generally consists of pure hydrogen and the liquid phase components are non-volatile, mass transfer resistance in gas phase was assumed to be negligible; also since pure hydrogen is generally used, mixing in the gas phase was considered to be unimportant

(g) the interphase and intraparticle heat transfer resistances are negligible, but bed-to-wall heat transfer has been considered to incorporate the non-isothermal effects

(h) the catalyst is wetted completely internally due to capillary forces

(i) the overall catalytic effectiveness factor can be expressed as a sum of the weighted average of the effectiveness factor in the dynamic covered, stagnant liquid covered and complete gas covered zones, respectively, i.e.,

$$\eta_c = f_d \eta_{c_d} + f_s \eta_{c_s} + (1 - f_d - f_s)\eta_{c_g} \qquad 4.7$$

where, η_c is the overall catalytic effectiveness factor, f_d and f_s are the fractions of the catalyst particle covered by the dynamic and stagnant zones and η_{cd}, η_{cs} and η_{cg} are the catalytic effectiveness factors in the dynamic, stagnant and dry zones, respectively.

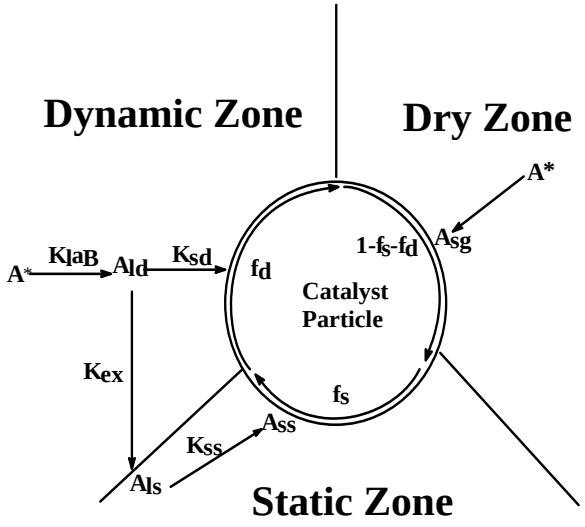

Figure 4.2. Spherical catalyst particle shown as divided in three zones

4.2.2.2 Estimation of Overall Catalytic Effectiveness Factor

The catalytic effectiveness factor equations applicable to reductive alkylation of PPDA can be developed following the well-known approaches.[1,24] Under the conditions of significant intraparticle gradients for the gas-phase reactant (H_2) and when the liquid-phase

reactant is in excess, the following equations can be used. The overall rate of hydrogenation can be expressed as (combining equations 4.4-4.6)

$$R_A = \frac{\eta_c w\left(k_5 D_l + k_8 F_l + k_9 H_l\right)\sqrt{A^*}}{\left(1 + K_A\sqrt{A^*}\right)} \qquad 4.8$$

where, η_c is the overall catalytic effectiveness factor and for spherical catalyst particle expressed as

$$\eta_c = \frac{1}{\phi}\left(\coth 3\phi - \frac{1}{3\phi}\right) \qquad 4.9$$

where, ϕ is the Thiele parameter and can be derived by Bischoff approximation[24] method as

$$\phi = \frac{R}{3}\rho_p \Omega(A_s)\left\{\int_0^{A_s} 2D_e \rho_p \Omega(A) dA\right\}^{-1/2}$$

$$\phi = \frac{R}{3}\frac{\rho_p\left(k_5 D_l + k_8 F_l + k_9 H_l\right)\sqrt{A_s}}{\left(1 + K_A\sqrt{A_s}\right)}\left\{\int_0^{A_s} \frac{2D_e\rho_p\left(k_5 D_l + k_8 F_l + k_9 H_l\right)\sqrt{A}}{\left(1 + K_A\sqrt{A}\right)} dA\right\}^{-1/2} \qquad 4.10$$

or in terms of dimensionless form as

$$\phi = \phi_o\left[\frac{\left(d_l + k_{85} f_l + k_{95} h_l\right)^{0.5}\sqrt{a_s}}{1 + k_a\sqrt{a_s}}\right] \times \left[\left(1 + k_a\sqrt{a_s}\right)^2 - 4\left(1 + k_a\sqrt{a_s}\right) + 2\ln\left(1 + k_a\sqrt{a_s}\right) + 3\right]^{-0.5} \qquad 4.11$$

with

$$\phi_o = \frac{R}{3}\left[\frac{\rho_p k_5 B_{li} A^* K_A^{\ 3}}{2D_e}\right]^{0.5} \qquad 4.12$$

The magnitude of the Thiele modulus determines the contribution of intraparticle diffusion to the overall reaction. Hence, for dynamic, stagnant and dry zones, the Thiele parameter

(ϕ) was calculated based on the catalyst surface concentration of hydrogen in respective zones as

$$\phi_x = \phi_o \left[\frac{\left(d_l + k_{85} f_l + k_{95} h_l\right)^{0.5} \sqrt{a_{sx}}}{1 + k_a \sqrt{a_{sx}}} \right] \times \left[\left(1 + k_a \sqrt{a_{sx}}\right)^2 - 4\left(1 + k_a \sqrt{a_{sx}}\right) + 2\ln\left(1 + k_a \sqrt{a_{sx}}\right) + 3 \right]^{-0.5} \quad 4.13$$

Hence, the catalytic effectiveness factor in respective zones can be calculated as

$$\eta_{cx} = \frac{1}{\phi_x}\left(\coth 3\phi_x - \frac{1}{3\phi_x} \right) \quad 4.14$$

where the subscript *x* denotes the dynamic (d), stagnant (s) and dry (g) zones in the reactor respectively.

With this, the overall catalytic effectiveness factor can be calculated from equation 4.7. The dimensionless parameters used in expressing ϕ are listed in Table 4.2 in the next section.

4.2.2.3 Axial Dispersion Model

The axial dispersion model (ADM) at steady state for the different species involved in the reaction (Figure 4.1) is described as follows. The axial dispersion model can be reduced to the plug flow model by considering negligible axial dispersion. The detailed derivations are given in Appendix-B. For the purpose of normalizing the governing equations, the model parameters were grouped into the various dimensionless parameters as defined in Table 4.2.

The mass balance of hydrogen (A) in dynamic liquid phase is given as

$$D_{EL} \frac{d^2 A_{ld}}{dx^2} - u_l \frac{dA_{ld}}{dx} + k_L a_B \left(A^* - A_{ld} \right) = f_d k_{sd} a_p \left(A_{ld} - A_{s_d} \right) + K_{ex} \varepsilon_{ls} \left(A_{ld} - A_{l_s} \right) \quad 4.15$$

At steady-state conditions, the sum of convection term and the gas-liquid mass transfer term are in equilibrium with the liquid-solid mass transfer term in the dynamic zone and the volumetric mass exchanged between the dynamic and stagnant zones. In a previous study by Hochmann and Effron[25], it was shown that the exchange rates between the dynamic and stagnant zones can be explained by the volumetric mass exchange coefficient, K_{ex}, and with the help of a cross flow model. Thus in the dynamic zone, we also have

$$\frac{f_d L k_{sd} a_p}{u_l}\left(A_{ld} - A_{sd}\right) = \frac{f_d \eta_c L w\left(k_5 D_l + k_8 F_l + k_9 H_l\right)\sqrt{A_{s_d}}}{u_l\left(1 + K_A\sqrt{A_{s_d}}\right)} \qquad 4.16$$

In the stagnant zone we have

$$K_{ex}\varepsilon_{ls}\left(A_{l_d} - A_{l_s}\right) = f_s k_{s_s} a_p\left(A_{l_s} - A_{s_s}\right) = \frac{f_s \eta_c w\left(k_5 D_l + k_8 F_l + k_9 H_l\right)\sqrt{A_{s_s}}}{\left(1 + K_A\sqrt{A_{s_s}}\right)} \qquad 4.17$$

The liquid entering the stagnant zone from the dynamic zone, characterized by the volumetric mass exchange coefficient, K_{ex}, containing the dissolved gaseous species A, at steady state, is in equilibrium with liquid-solid mass transfer term in the stagnant zone and the reaction in the catalyst particles in the stagnant zones (including pore diffusion effects).

The mass balance for species A in the dry zone is

$$\left(1 - f_d - f_s\right) k_{g_s} a_p\left(A^* - A_{s_g}\right) = \frac{\left(1 - f_d - f_s\right)\eta_c\, w\left(k_5 D_l + k_8 F_l + k_9 H_l\right)\sqrt{A_{s_g}}}{\left(1 + K_A\sqrt{A_{s_g}}\right)} \qquad 4.18$$

Equations 4.15-4.18 can be simplified and expressed in terms of dimensionless parameters. The unknown catalyst surface concentrations of H_2 can be suitably expressed in terms of known parameters. The final mass balance equations in dimensionless form for species A are given as

$$\frac{1}{P_e}\frac{d^2a_{ld}}{dz^2}-\frac{da_{ld}}{dz}+\alpha_{gl}\left(1-a_{ld}\right)=f_d\alpha_{lsd}\left(a_{ld}-a_{sd}\right)+\frac{L\,K_{ex}\varepsilon_{ls}}{u_l}\left(a_{ld}-a_{ls}\right) \tag{4.19}$$

with

$$\alpha_{ls_d}\left(a_{l_d}-a_{s_d}\right)=\eta_c\alpha_{R5}q_B\left[\frac{\left(d_l+k_{85}f_l+k_{95}h_l\right)\sqrt{a_{s_d}}}{1+k_a\sqrt{a_{s_d}}}\right] \tag{4.20}$$

$$\alpha_{s_s}\left(a_{l_s}-a_{s_s}\right)=\eta_c\alpha_{R5}q_B\left[\frac{\left(d_l+k_{85}f_l+k_{95}h_l\right)\sqrt{a_{s_s}}}{1+k_a\sqrt{a_{s_s}}}\right] \tag{4.21}$$

$$\alpha_{g_s}\left(1-a_{s_g}\right)=\eta_c\alpha_{R5}q_B\left[\frac{\left(d_l+k_{85}f_l+k_{95}h_l\right)\sqrt{a_{s_g}}}{1+k_a\sqrt{a_{s_g}}}\right] \tag{4.22}$$

Similarly, the mass balances of liquid phase reactants/products in dimensionless form can be given as

$$\frac{1}{P_e}\frac{d^2b_{ld}}{dz^2}-\frac{db_{ld}}{dz}-\varepsilon_l\left[\alpha_{R1}b_l-\alpha_{R2}d_lc_{H_2O}\right]=0 \tag{4.23}$$

$$\frac{1}{P_e}\frac{d^2d_{ld}}{dz^2}-\frac{dd_{ld}}{dz}+\left\{\varepsilon_l\left[\alpha_{R1}b_l-\alpha_{R2}d_lc_{H_2O}\right]-\varepsilon_l\left[\alpha_{R3}d_l-\alpha_{R4}f_lc_{H_2O}\right]-\frac{\eta_c\alpha_{R5}d_l\chi}{q_B}\right\}=0 \tag{4.24}$$

$$\frac{1}{P_e}\frac{d^2f_{ld}}{dz^2}-\frac{df_{ld}}{dz}-\left\{\varepsilon_l\left[\alpha_{R3}d_l-\alpha_{R4}f_lc_{H_2O}\right]-\frac{\eta_c\alpha_{R8}f_l\chi}{q_B}\right\}=0 \tag{4.25}$$

$$\frac{1}{P_e}\frac{d^2 g_{ld}}{dz^2} - \frac{dg_{ld}}{dz} - \left\{ \frac{\eta_c \alpha_{R5} d_l \chi}{q_B} - \varepsilon_l \left[\alpha_{R6} g_l - \alpha_{R7} h_l c_{H_2O} \right] \right\} = 0 \qquad 4.26$$

$$\frac{1}{P_e}\frac{d^2 h_{ld}}{dz^2} - \frac{dh_{ld}}{dz} - \left\{ \varepsilon_l \left[\alpha_{R6} g_l - \alpha_{R7} h_l c_{H_2O} \right] - \frac{\eta_c \left(\alpha_{R8} f_l - \alpha_{R9} h_l \right) \chi}{q_B} \right\} = 0 \qquad 4.27$$

$$\frac{1}{P_e}\frac{d^2 p_{ld}}{dz^2} - \frac{dp_{ld}}{dz} - \left\{ \frac{\eta_c \alpha_{R9} h_l \chi}{q_B} \right\} = 0 \qquad 4.28$$

where,

$$\chi = \frac{f_d \sqrt{a_{s_d}}}{1 + k_a \sqrt{a_{s_d}}} + \frac{f_s \sqrt{a_{s_s}}}{1 + k_a \sqrt{a_{s_s}}} + \frac{(1 - f_d - f_s) \sqrt{a_{s_g}}}{1 + k_a \sqrt{a_{s_g}}} \qquad 4.29$$

and

$$c_{H_2O} = d_l + 2 f_l + g_l + 2 h_l + 2 p_l \qquad 4.30$$

Lastly, in deriving non-isothermal trickle bed reactor model, the dependencies of various parameters like reaction rate constants, equilibrium constants, effective diffusivity and saturation solubility on temperature are accounted for. The change in rate and equilibrium constants with respect to temperature can be represented as:

$$k_i(T) = k_i(T_o) \exp\left[\frac{E_i}{R T_i} \left(1 - \frac{1}{\theta} \right) \right]$$

$$K_i(T) = K_i(T_o) \exp\left[\frac{-\Delta H_i}{R T_i} \left(1 - \frac{1}{\theta} \right) \right] \qquad 4.31$$

where $\theta = T / T_i$ and T_i is the inlet operating temperature. The effective diffusivity was calculated as

$$D_e(T) = D_m \frac{\varepsilon}{\tau} \qquad 4.32$$

where, D_m is the molecular diffusivity and is evaluated from the correlation of Wilke and Chang[26], and ε and τ represent the porosity and the tortuosity factors. The dependence of saturation solubility on temperature is given as

$$\left(A^*\right)_T = \left[P - \left(P_v\right)_T\right]\left[\left(H_e\right)_T\right] \qquad 4.33$$

where, P_v is the change in vapor pressure of the solvent (MEK) due to temperature rise, given as:

$$P_V = Exp\left[72.698 - \left(\frac{6143.6}{T}\right) - 7.5779 \times \ln(T) + \left(5.6476 \times 10^{-06} \times T^2\right)\right] \qquad 4.34$$

H_e is the Henry's law constant (Chapter-2, Section-2(A).3.2), expressed as

$$(H_e)_T = 1.2 \times 10^{-3} \times \exp\,(2.7 \times 10^{-3} \times T) \quad \text{for 5\% PPDA} \qquad 4.35$$

$$(H_e)_T = 1.8 \times 10^{-3} \times \exp\,(2.2 \times 10^{-3} \times T) \quad \text{for 10\% PPDA} \qquad 4.36$$

$$(H_e)_T = 3 \times 10^{-4} \times \exp\,(6.9 \times 10^{-3} \times T) \quad \text{for 15\% PPDA} \qquad 4.37$$

The above equations 4.35-4.37 are applicable when methyl ethyl ketone and a particular PPDA composition are considered. Owing to the exothermicity of the reaction, an increase in the bed temperature is expected and as a consequence might lead to enhanced rates. The heat generated within the reactor is mainly carried away by the flowing liquid and also due to transfer of heat from the catalyst particle to the reactor wall, which is characterized by the bed to wall heat transfer coefficient, U_w. Under such conditions, where the interphase and intraparticle heat transfer resistances are assumed to be negligible, the heat balance of the reactor can be given as[1]

$$\left(u_l\rho_l C_{pl}+u_g\rho_g C_{pg}\right)\frac{dT}{dx}=\left\{\begin{array}{l}\left(-\Delta H_1\right)R_A+(-\Delta H_2)R_1+(-\Delta H_3)R_2\\+(-\Delta H_4)R_4-\dfrac{4U_w\left(T_b-T_w\right)}{d_T}\end{array}\right\}$$

$$\therefore\left(u_l\rho_l C_{pl}+u_g\rho_g C_{pg}\right)\frac{dT}{dx}=\left\{\begin{array}{l}\dfrac{\left(-\Delta H_1\right)\eta_c w\left(k_5 D_l+k_8 F_l+k_9 H_l\right)\sqrt{A_s}}{\left(1+K_A\sqrt{A_s}\right)}\\+(-\Delta H_2)\left[k_{eq1}B_l-k_{eq2}D_l C_{H_2O}\right]\\+(-\Delta H_3)\left[k_{eq3}D_l-k_{eq4}F_l C_{H_2O}\right]\\+(-\Delta H_4)\left[k_{eq6}G_l-k_{eq7}H_l C_{H_2O}\right]-\dfrac{4U_w\left(T_b-T_w\right)}{d_T}\end{array}\right\} \qquad 4.38$$

The above equation in dimensionless form can be written as

$$\frac{d\theta}{dz}=\left\{\begin{array}{l}\dfrac{\beta_1\eta_c\alpha_{R5}\left(d_l+k_{85}f_l+k_{95}h_l\right)\chi}{q_B}+\beta_2\left[\alpha_{R1}b_l-\alpha_{R2}d_l c_{H_2O}\right]\\+\beta_3\left[\alpha_{R3}d_l-\alpha_{R4}f_l c_{H_2O}\right]+\beta_4\left[\alpha_{R6}g_l-\alpha_{R7}h_l c_{H_2O}\right]-\beta_5\left(\theta_b-\theta_w\right)\end{array}\right\} \qquad 4.39$$

where, β_1 to β_4 are thermicity parameters. Equation 4.39 can be used to predict the maximum temperature rise along the length of the reactor. The dimensionless parameters used in the above equations are presented in Table 4.2. The hydrodynamic and mass transfer parameters required for the calculations of the dimensionless parameters were calculated from literature correlations and are presented in Table 4.3.

Table 4.2. Dimensionless Parameters Used in the Model

Mass transfer parameters	
Gas-liquid mass transfer	$\alpha_{gl} = L k_L a_B / u_l$
Liquid-solid mass transfer	$\alpha_{lsd} = L k_{sd} a_p / u_l$
Gas-solid mass transfer	$\alpha_{gs} = L k_{gs} a_p / u_l$
Exchange parameter for stagnant zone	$\alpha_{s_s} = L k_{ss} a_p / u_l$
Axial mixing parameter Peclet Number	$P_e = u_l L / D_{EL}$
Heat transfer parameters Thermicity parameters	$\beta_x\big\|_{x=1-4} = \dfrac{\left(-\Delta H_x\big\|_{x=1-4}\right) B_{li}}{T_0 \rho_l C_{pl}\left[1+\left(u_g \rho_g C_{pg} / u_l \rho_l C_{pl}\right)\right]}$
Bed-to-wall heat transfer	$\beta_5 = \dfrac{4 U_w L}{D_T u_l \rho_l C_{pl}\left[1+\left(u_g \rho_g C_{pg} / u_l \rho_l C_{pl}\right)\right]}$
	$\beta_x\big\|_{x=6-9} = \dfrac{\left(-\Delta H_x\big\|_{x=1-4}\right) B_{li}}{T_0 \rho_l C_{pl}\left\{1+\left(\dfrac{u_g \rho_g C_{pg}}{u_l \rho_l C_{pl}}\right)+\left(\dfrac{L}{u_l \tau}\right)\left[\left(1-\varepsilon_g-\dfrac{w}{\rho_p}\right)+\dfrac{\varepsilon_g \rho_g C_{pg}}{\rho_l C_{pl}}+\dfrac{w C_{ps}}{\rho_l C_{pl}}\right]\right\}}$
	$\beta_{10} = \dfrac{4 U_w L}{D_T u_l \rho_l C_{pl}\left\{1+\left(\dfrac{u_g \rho_g C_{pg}}{u_l \rho_l C_{pl}}\right)+\left(\dfrac{L}{u_l \tau}\right)\left[\left(1-\varepsilon_g-\dfrac{w}{\rho_p}\right)+\dfrac{\varepsilon_g \rho_g C_{pg}}{\rho_l C_{pl}}+\dfrac{w C_{ps}}{\rho_l C_{pl}}\right]\right\}}$
Reaction rate and equilibrium constants	$k_{85} = \dfrac{k_8}{k_5}; \quad k_{95} = \dfrac{k_9}{k_5}; \quad k_a = K_A \sqrt{A^*}$
	$\alpha_{R_1} = \dfrac{L k_{eq_1}}{u_{lu}}; \quad \alpha_{R2} = \dfrac{L k_{eq_2} B_{li_1}}{u_{lu}}; \quad \alpha_{R3} = \dfrac{L k_{eq3}}{u_{lu}};$
	$\alpha_{R4} = \dfrac{L k_{eq4} B_{li_1}}{u_{lu}}; \alpha_{R_5} = \dfrac{L w k_5 \sqrt{B_{li_1}}}{u_{lu}}; \quad \alpha_{R_6} = \dfrac{L k_{eq6}}{u_{lu}};$
	$\alpha_{R7} = \dfrac{L k_{eq7} B_{li_1}}{u_{lu}}; \quad \alpha_{R_8} = \dfrac{L w k_8 \sqrt{B_{li_1}}}{u_{lu}}; \alpha_{R_9} = \dfrac{L w k_9 \sqrt{B_{li_1}}}{u_{lu}}$

Table 4.3. Correlations Used for Downflow Modeling

Parameter	Correlation	Reference
Gas-liquid mass-transfer coefficient	$k_L a_B = \frac{6 \times D_m \times \rho_l \times u_l}{\mu_l^{0.4} \times S_{cl}^{0.5}}$	27
Liquid-solid mass transfer coefficient	$\frac{K_s d_p}{D_m}\frac{a_w}{a_p} = 0.815 R_{eL}^{0.822}\left(\frac{\mu_l}{\rho_l D_m}\right)^{0.333}$	28
Gas-solid mass transfer coefficient	$\frac{k_g D}{L} = 0.023 \mathrm{R}_{e_L}^{0.83} S_c^{0.33}$	29
Volumetric mass exchange coefficient	$K_{ex} = 0.01 \mathrm{R}_{e_L}^{0.6}$	25
Total liquid hold up	$\frac{\varepsilon_l}{\in_B} = 0.185 a_t^{1/3} \chi^{0.22}$	30
Bed-to-wall heat transfer coefficient	$\frac{U_w d_p}{\lambda_L} = 0.057\left(\frac{\mathrm{R}_{e_L}}{\in_L}\right)^{0.09}\left(\frac{Cpl\,\mu_l}{\lambda_L}\right)^{1/3}$	31
Wetting efficiency	$f_w = 1.104 \mathrm{R}_{e_L}^{1/3}\left[\frac{1+[(\Delta P/Z)/\rho_L g]}{G_{a_L}}\right]^{1/9}$	32
Diffusivity coefficient	$D_m = 7.4 \times 10^{-8} \frac{(\phi M_w)^{1/2} T}{\mu_l \upsilon_m^{0.6}}$	26
Axial dispersion coefficient	$\frac{u_l d_p}{D_{EL}} = \left(\frac{\mathrm{R}_{eL}}{\varepsilon_{ld}}\right)^{0.7}\left(G_{aL}\right)^{-0.32}$	33

4.2.2.4 Estimation of Hydrodynamic Parameters

As indicated earlier, the model is applicable for conditions of complete wetting of the catalyst particles ($f_d = 1, f_s = 0$), partial wetting of the catalyst particles ($f_d < 1, f_s = 0$) and when there are significant stagnant liquid pockets ($f_d < 1, f_s < f_d$). In order to evaluate the wetted fractions in the two zones (dynamic and static) separately, as a first approximation we have assumed that the ratio of the wetted fractions in the dynamic and static zones is proportional to their respective liquid hold ups, i.e.

$$\left(\frac{f_d}{f_s}\right)=\left(\frac{\varepsilon_{ld}}{\varepsilon_{ls}}\right) \qquad 4.40$$

On the other hand, the sum of the two wetted fractions ($f_d + f_s = f_w$) is equal to the total wetted fraction f_w. Also, the total liquid hold up ε_l is equal to sum of the stagnant liquid hold up, ε_{ls} and the dynamic liquid hold up, ε_{ld}, i. e. ($\varepsilon_l = \varepsilon_{ls} + \varepsilon_{ld}$). There is very limited information available on stagnant liquid hold up, ε_{ls}, however, Zai-Sha *et. al*,[34] reported experimental data from which ε_{ls}, was found to be 0.05. The total liquid hold up, ε_l, was evaluated from the correlation proposed by Sato *et. al.* (Table 4.3)[30]. The dynamic liquid hold up (ε_{ld}) can be evaluated from the difference between the total liquid hold up (ε_l) and the static liquid hold up (ε_{ls}). Thus the wetted fraction f_s and f_d are given as

$$f_d = \frac{f_w}{\left(1+\varepsilon_{ls}/\varepsilon_{ld}\right)} \qquad 4.41$$

$$f_s = f_w - f_d \qquad 4.42$$

Equations 4.41 and 4.42 indicate that with the knowledge of total wetted fraction, and from the dynamic and static liquid hold ups it would be possible to calculate the wetted fractions in the two zones separately. The total wetted fraction was calculated from the correlation proposed by Aldahan (Table 4.3)[32] under the reaction conditions considered.

For a gas-liquid-solid reaction in a trickle bed reactor under conditions of stagnant liquid pockets, it has been shown by Sicardi *et. al.*[35] and Colombo *et. al.*[36] that the liquid-solid mass transfer in the stagnant zone (k_{ss}) can be as much as 20-100 times less than the liquid-solid mass transfer in the dynamic zone (k_{sd}) and as much as 20-30% of the total area of the catalyst can be covered by stagnant zones under certain conditions. For the present study, no significant variation in the performance of reactor was observed when k_{ss} varied in the range of 20-100 times less than the k_{sd} and hence, was assumed to be equal to 100 times less than k_{sd}.

4.2.3 Up-flow Reactor Model

The reaction kinetics and transport dynamics are closely interlinked and their effects on reactant conversion and products selectivity are inseparable. Therefore, the model equations described earlier for the down-flow reactor can also be used for the up-flow reactor with the appropriate modifications of mass transfer and hydrodynamic parameters.[37] These parameters include the degree of catalyst wetting, mixing and flow pattern of the fluids, axial dispersion coefficient, and the liquid hold up. The selection of hydrodynamic conditions depends not only on the processing requirement, but also on the contacting pattern. As shown in Figure 4.3, the nature of multiphase contacting in various flow modes (cocurrent downflow or upflow) is distinct.[38]

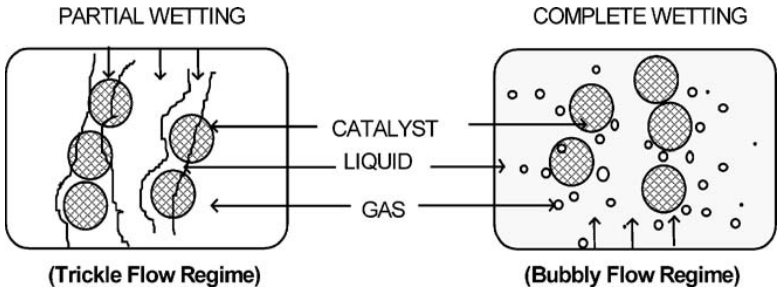

Figure 4.3. Contacting pattern in trickle flow and bubble flow regimes

When the bed is operated in trickle flow regime under partial wetting conditions for the catalyst pellets, gas phase is the continuous phase and liquid phase is the dispersed phase. However, the packed bubble column (i.e. FBR with upflow mode) operates in bubbly flow regime with fully wetted catalyst pellets. In this regime, the solid particles are completely wetted by the continuous liquid phase, whereas the gas phase is dispersed as bubbles flowing through the packing channels. The key differences in modeling downflow and upflow modes are the values of the mass transfer parameters and the catalyst wetting efficiency. Since, the upflow operation is characterized by high liquid hold up, it was assumed the catalyst wetting is complete. Hence, the wetting efficiency was taken as unity. The correlations used for the evaluation of mass transfer and hydrodynamic parameters for the up-flow mode are presented in Table 4.4. These parameters were used for the simulation of results under wide range of operating conditions.

Table 4.4. Correlations Used for Upflow Modeling

Parameter	Correlation	Reference
Gas-liquid mass-transfer coefficient	$k_L a_B = 5.48\times10^{-3}\left[u_l \delta_{gl}\right]^{0.5}$	39
Liquid-solid mass transfer coefficient, k_s	$k_s = \left(0.48\ln\left(\frac{\mathrm{R}_{e_G}}{\mathrm{R}_{e_L}}\times10^2\right) - 0.03\left[\ln\left(\frac{\mathrm{R}_{e_G}}{\mathrm{R}_{e_L}}\times10^2\right)\right]^2 - 0.3\right)\frac{DSh_0}{d_p}$	40
Pressure drop per unit length of reactor, δ_{gl}	$\left[\delta gl\right]^{0.5} = \frac{2 f_{gl} u_g{}^2 \rho_g}{d_{p_e}}$	41
Liquid hold up	$\varepsilon_l = \in_B 1.47\,\mathrm{R}_{e_L}{}^{0.11}\,\mathrm{R}_{e_G}{}^{-0.19}\left(a_p d_p\right)^{-0.41}$	42
Axial dispersion coefficient	$\frac{u_l d_p}{D_{EL}} = 0.128\times\varepsilon_l\times\mathrm{R}_{eL}{}^{0.245}\times\mathrm{R}_{eG}{}^{-0.16}\left(a_p d_p\right)^{0.53}$	42

4.3 SLURRY REACTOR MODEL

4.3.1 Bubble Column Slurry Reactor (BCSR)

The BCSR model developed in Chapter-3, Section 3.2, was used to evaluate the reactor performance at some specific reaction conditions for the purpose of comparison with the fixed bed reactor. The model was based on the mixing cell approach and further extended by including a liquid backflow stream from all but the bottom most mixing cell. CFD model was used to estimate the extent of backflow among the mixing cells. The model incorporates the contributions of gas-liquid, liquid-solid mass transfer, heat effects and the intrinsic kinetics. In Chapter-3, the comparison of BCSR with and without consideration of backmixing within the reactor was discussed. In this chapter, this model is used to compare the reactor performance with FBR model for the reaction system considered in this work.

4.3.2 Continuous Stirred Tank Reactor (CSTR)

The BCSR model can also be used to develop CSTR model with the following modifications:

- Number of cells (N) = 1, corresponds to the case of complete backmixing, and hence, the temperature and liquid concentration throughout the reactor are assumed to be constant and equal to the outlet conditions
- The correlations for the evaluation of hydrodynamic and mass transfer parameters as shown in Table 4.5
- Non-isothermal model: For CSTR, the total heat capacity of the contents of the reactor was added in the non-isothermal model of BCSR to account for the heat effects as follows:

$$\left\{\begin{bmatrix} L\varepsilon_g\rho_g C_{pg}+L\left(1-\varepsilon_g-w/\rho_p\right) \\ +LwCp_s \end{bmatrix}\left(T-T_0\right)\right\} = \tau\left\{\begin{matrix} \left(-\Delta H_1\right)R_A+(-\Delta H_2)R_1+(-\Delta H_3)R_2 \\ +(-\Delta H_4)R_4-\dfrac{4U_w\left(T_b-T_w\right)}{d_T} \end{matrix}\right\} \qquad 4.43$$

$$+\tau\left(u_l\rho_l C_{pl}+u_g\rho_g C_{pg}\right)\left(T-T_0\right)$$

The final dimensionless form of non-isothermal model for CSTR can be written as

$$\theta = 1+\frac{\beta_6\alpha_{R5}}{N q_B}\left[\frac{\left(d_l+k_{85}f_l+k_{95}h_l\right)\sqrt{a_s}}{1+k_a\sqrt{a_s}}\right]+\beta_7\left[\alpha_{R1}b_l-\alpha_{R2}d_l\,c_{H_2O}\right] \qquad 4.44$$

$$+\beta_8\left[\alpha_{R3}d_l-\alpha_{R4}f_l\,c_{H_2O}\right]+\beta_9\left[\alpha_{R6}g_l-\alpha_{R7}h_l\,c_{H_2O}\right]-\beta_{10}\left(\theta-\theta_w\right)$$

The dimensionless parameters used in the model are given in Table 4.2.

Table 4.5. Correlations Used for CSTR Modeling

Parameter	Correlation	Reference
Gas-liquid mass-transfer coefficient	$k_L a_B = 0.01099 \times N_r^{1.16} \times d_I^{1.979} \times u_g^{0.32} \times V_L^{-0.521}$	43
Liquid-solid mass transfer coefficient, k_s	$\frac{k_s d_p}{D_m F_c} = 2 + 0.4\left[\frac{e d_p^4 \rho_l^3}{\mu_l^3}\right]^{0.25}\left[\frac{\mu_l}{\rho_l D_m}\right]^{1/3}$	44
Power Consumption	$\frac{P}{p_o} = 0.497\left[\frac{Q_g}{N_r d_I^3}\right]^{-0.38}\left[\frac{N_r^2 d_I^3 \rho_l}{S_T}\right]^{-0.18}$	45
Diffusivity coefficient	$D_m = 7.4 \times 10^{-8} \frac{(\phi M_w)^{1/2} T}{\mu_l \upsilon_m^{0.6}}$	26
Gas hold up	$\varepsilon_g = 0.011 u_g^{0.36} S_T^{-0.36} \mu_l^{-0.056}\left[\frac{P}{V_L} + \frac{P_g}{V_L}\right]^{0.27}$	46

4.4 NUMERICAL SIMULATIONS

PPDA is a solid reactant and has low solubility in MEK. Hence, the intrinsic kinetics for reductive alkylation of PPDA with MEK using 3% Pt/Al_2O_3 catalyst was studied after reaching the equilibrium among PPDA, M-imine and Di-imine (Chapter-2: Part-A) i.e. the complete homogeneous liquid mixture. Also, it was already observed that the equilibrium reaction was not affected either by catalyst or by hydrogen. Hence, the numerical simulations for all the reactors (FBR-upflow and downflow, BCSR, CSTR) considered in this work were carried out under the assumption of equilibrium mixture (PPDA, M-imine and Di-imine) entering into the reactor and conversion and selectivities to the products were evaluated based on the total initial concentration of PPDA. The boundary conditions used for the fixed bed and slurry reactor models are given in the following sections.

4.4.1 Fixed Bed Reactor (FBR)

The performance of FBR has been investigated using the axial dispersion model (ADM) and plug flow model.

4.4.1.1 Axial Dispersion Model

The axial dispersion model (equations 4.19-4.29) was solved as two point boundary value problem (BVP) using the function 'BVP4C' for second order differential equations and 'FSOLVE' for non-linear equations in MATLAB 7, 2004.[47] The following boundary conditions were used to investigate the effect of axial dispersion on reactor performance,

$$At\ z = 0, \quad \frac{1}{P_e}\left(\frac{dx_{ld}}{dz}\right) = x_l - x_{li}$$

$$where, x = a_{ld}, b_{ld}, d_{ld}, f_{ld}, g_{ld}, h_{ld}, p_{ld} \qquad 4.46$$

$$At\ z = 1, \quad \frac{dx_l}{dz} = 0$$

$$where, x = a_{ld}, b_{ld}, d_{ld}, f_{ld}, g_{ld}, h_{ld}, p_{ld}$$

4.4.1.2 Plug Flow Model

The axial dispersion model can be reduced to the plug flow model by considering negligible axial dispersion and therefore the calculations can be markedly simplified. The two point boundary value problem can be eliminated. Therefore, for solving the plug flow model, equations 4.19-4.28 were first reduced to first order differential equations by eliminating the second order differential term. The plug flow model (Equations 4.19-4.29 combined with Equation 4.39) was then solved as initial value problem (IVP) using the functions 'ODE45' and 'FSOLVE', differential and non-linear equation solver respectively, in MATLAB 7, 2004.[47] The following initial conditions were used for all the plug flow model simulations

At $z = 0$, b_l, d_l, f_l = Dimensiónless equilibrium concentrations; and

$$a_l = 1;\ g_l = h_l = p_l = 0;\ \theta = 1; \qquad 4.45$$

4.4.2 Slurry Reactor

The slurry reactor models (BCSR and CSTR) were solved using the function 'FSOLVE', non-linear equation solver in MATLAB 7, 2004[47] with the following initial conditions,

At $z = 0$, b_l, d_l, f_l = Dimensiónless equilibrium concentrations; and

$a_l = 1$; $g_l = h_l = p_l = 0$; $\theta = 1$;

For any given set of inlet boundary conditions of fixed bed and slurry reactor models, the concentrations of reactant/product species and temperature were calculated along the length of the reactor and at the exit of the reactor. At any given length of the reactor, the fractional conversion of PPDA was calculated as

$$X_B = 1 - b_l \tag{4.47}$$

The global rate of hydrogenation taking into account all the hydrogenation reaction steps involved in the overall reaction sequence (Figure 4.1) was calculated as

$$R_{H2} = \tau'\left(g_{lj} + h_{lj} + 2p_{lj}\right)B_{li} \tag{4.48}$$

In equation 4.48, τ' is the mean residence time of the liquid in the reactor ($\tau' = u_l / L$), u_l is the liquid velocity, L is the length of the reactor, g_l, h_l, and p_l are the dimensionless concentrations of M-amine, Intermediate and Di-amine respectively, at any length of the reactor.

The productivity of Di-amine can be defined as follows on the basis of constant catalyst loading (Equation 4.49) and constant reactor volume (Equation 4.50) for the comparison of different reactors considered in this work

$$Productivity\ of\ the\ diamine\left[\frac{kg\ Di-amine}{(kg\ catalyst)(hr)}\right] = \frac{u_l \times A_R \times conc.of\ diamine \times M_w}{weight\ of\ the\ catalyst} \times 3600 \tag{4.49}$$

$$Productivity\ of\ the\ diamine\left[\frac{kg}{m^3 hr}\right] = \left(u_l / L\right) \times conc.of\ diamine \times M_w \times 3600 \tag{4.50}$$

The selectivity to M-imine, Di-imine, M-amine, Intermediate and Di-amine was evaluated using the following relationships:

$$S_{m-imine} = \frac{d_l}{1-b_l} \times 100 \quad 4.51$$

$$S_{di-imine} = \frac{f_l}{1-b_l} \times 100 \quad 4.52$$

$$S_{m-amine} = \frac{g_l}{1-b_l} \times 100 \quad 4.53$$

$$S_{intermediate} = \frac{h_l}{1-b_l} \times 100 \quad 4.54$$

$$S_{di-amine} = \frac{p_l}{1-b_l} \times 100 \quad 4.55$$

The maximum temperature rise was calculated as

$$\Delta T_{max} = T - T_i \quad 4.56$$

where T represents the actual temperature calculated from non-isothermal model and T_i represents the initial temperature.

4.5 RESULTS AND DISCUSSION

4.5.1 Comparison of FBR Performance for Downflow and Upflow Modes

The model equations developed in earlier section (Section 4.2) allow prediction of the conversion of PPDA (X_B), global rate of hydrogenation (R_{H2}), selectivity to products and the maximum temperature rise (ΔT_{max}) for a given set of inlet conditions. The performance of the FBR (Downflow and upflow) is compared in terms of the conversion and selectivity towards the products at identical volumetric nominal space times (defined as reactor length/superficial liquid velocity) and identical reactant feed concentration. This is the proper scale up variable, when the catalyst beds for upflow and downflow operations are identically packed (i.e. bed voidage is constant).[48] Further, in order to understand the effect of various operating parameters on the performance of FBR, simulations were performed

for the range of operating conditions presented in Table 4.6 unless stated explicitly. The plug flow model of FBR was first simulated to understand the effect of different operating conditions on the reactor performance. The effect of axial dispersion on the reactor performance is discussed in a separate section.

Table 4.6. Operating Conditions for Fixed Bed Reactor

Catalyst weight, kg	0.024-0.084
Initial PPDA conc., kmol/m^3	0.5-1.5
Temperature, K	373-413
Total pressure, MPa	2-6
Liquid velocity, u_l, m/s	$0.1\text{-}10.5 \times 10^{-4}$
Gas Velocity, u_g, m/s	2×10^{-5} — 5×10^{-2}
Reactor diameter, m	0.019
Diameter of catalyst particle, m	0.001
Density of catalyst particle, kg/m^3	1.26×10^{-3}
Bed voidage	0.5
Porosity of catalyst,ε	0.3
Tortuosity of catalyst, τ	7.5

4.5.1.1 Effect of Liquid Velocity

The effect of liquid velocity on conversion of PPDA at different temperatures for FBR with downflow and upflow modes of operation is shown in Figure 4.4. The conversion was found to decrease with an increase in liquid velocity and increase with increase in temperature. Figure 4.5 shows the effect of liquid velocity on global rate of hydrogenation, selectivity to M-amine and Di-amine and temperature rise at operating temperature of 413K for the FBR with downflow and upflow modes of operation. The global rate of hydrogenation was observed to increase with increase in the liquid velocity for both the modes of operation. For the downflow mode (TBR), with increase in liquid velocity, one expects increase in wetted fraction of the catalyst as well as an increase in gas-liquid and liquid-solid mass transfer coefficients. At lower liquid velocity, catalyst particles are partially wetted, and under these conditions, it is expected that rate increases due to direct

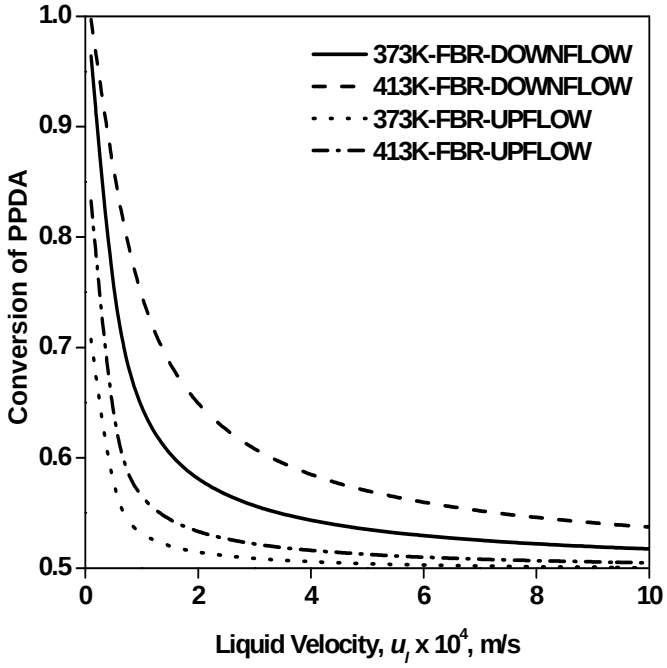

Figure 4.4. Effect of liquid velocity on conversion of PPDA at different temperatures
Reaction conditions: P = 6 MPa, B_{li} = 1 kmol/m^3, w = 0.058 kg = 854.3 kg/m^3, u_g = 5 ×10^{-2} m/s

mass transfer of gas phase reactant to the catalyst surface (already wetted internally due to capillary forces). Hence, with an increase in liquid velocity, an increase in wetted fraction is expected to retard the rate of reaction to some extent, while an increase in external mass transfer coefficients will enhance the rate resulting in opposite effects. The result is higher conversion (~100% and 83%) and selectivity to Di-amine (~68% and 34%) in downflow mode as compared to upflow mode of operation respectively. Whereas, in case of upflow, the catalyst is completely wetted; the access of gaseous reactant to catalyst site is limited to that through liquid film only. This provides an additional resistance to the mass transfer of gaseous reactant to the catalyst surface; this effect is increased at high space times due to low gas-liquid mass transfer coefficient and results in conversion lower than that obtained in downflow mode.

The temperature rise was observed to be higher with increase in the liquid velocity, but not very significant for both the trickle bed and upflow modes of operation under the reaction conditions studied (Figure 4.5). This might due to the equilibrium steps involved in the overall reaction scheme and the compensation to the effect of wetting and the increase in external mass transfer coefficients. For upflow mode slightly lower temperature

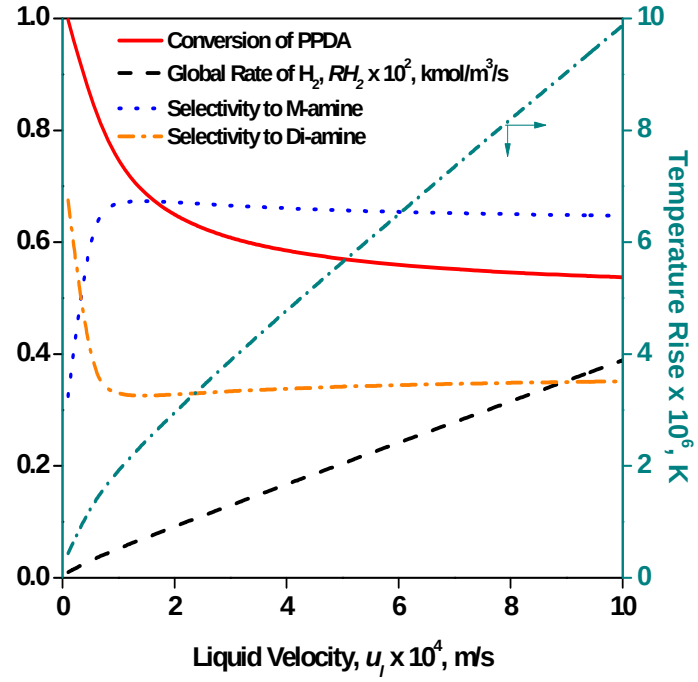

(A) FBR-DOWNFLOW

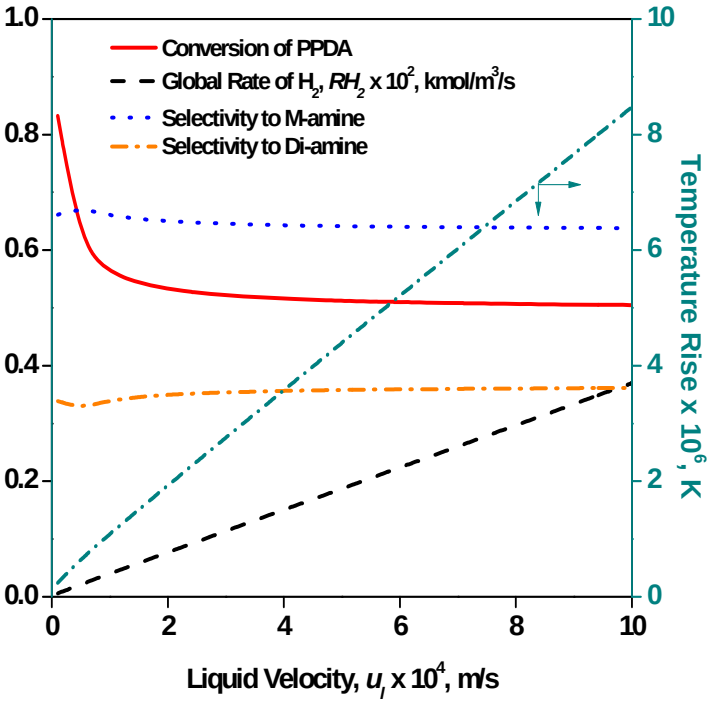

(B) FBR-UPFLOW

Figure 4.5. Effect of liquid velocity on conversion of PPDA, global rate of hydrogenation, and selectivity to M-amine and Di-amine

Reaction conditions: T = 413K, P = 6 Mpa, B_{li} = 1 kmol/m^3, w = 0.058 kg = 854.3 kg/m^3, u_g = 5×0^{-2} m/s

rise was observed than trickle bed due to the efficient heat removal capacity of upflow mode. Therefore, it can be concluded that the non-isothermal effects for the reductive alkylation of PPDA are not significant for both the modes of operation.

For the downflow case, it can be observed from Figure 4.5 that with increase in liquid velocity, selectivity to the final desired product Di-amine decreases and selectivity to M-amine increases, but only up to the liquid velocity of 1×10^{-4} m/s. After this velocity, the selectivity to both M-amine and Di-amine remains almost constant. Whereas in upflow case, the selectivity to M-amine and Di-amine remains almost constant with increase in the liquid velocity. This is due to the decreasing space time with increase in liquid velocity and hence all the consecutive and parallel reaction steps involved in the overall reaction could not occur simultaneously. This phenomenon is explained in Figures 4.6-A and 4.6-B, which shows the concentration of various species involved in the overall reaction as a function of space time in the reactor. Also, the kinetic modeling data presented in Table 4.1 clearly indicates this phenomenon. As the equilibrium mixture (PPDA, M-imine and Di-imine) enters the reactor, first the M-imine and Di-imine in the equilibrium reaction mixture immediately hydrogenate to M-amine and Intermediate respectively because of the higher hydrogenation rates (Table 4.1). In case of downflow mode, as the equilibrium mixture flows down the reactor, H_2 will be the driving force for the equilibrium reaction to proceed. Hence, as the space time increases (i.e. liquid velocity decreases), PPDA as well as M-imine concentration decreases and hence M-amine concentration increases initially and decreases further. M-amine then transforms to Intermediate by equilibrium reaction (Figure 4.1). As the kinetic modeling data (Table 4.1) clearly indicates the slow hydrogenation rate for the Intermediate to Di-amine, in the continuous reactor, the results presented in Figures 4.4, 4.5 and 4.6 for downflow mode were expected.

On the contrary, in upflow mode, the concentrations of M-amine and Di-amine increase with increase in the space time (Figure 4.6-B). In upflow mode, the catalyst particles are completely wetted, and the entire catalyst surface can be utilized completely. Also, the mass and heat transfer efficiencies in upflow mode are higher than those for downflow mode. But with increase in liquid velocity, the space time decreases and liquid hold up increases. Hence, as the overall reaction scheme involves the combination of homogeneous

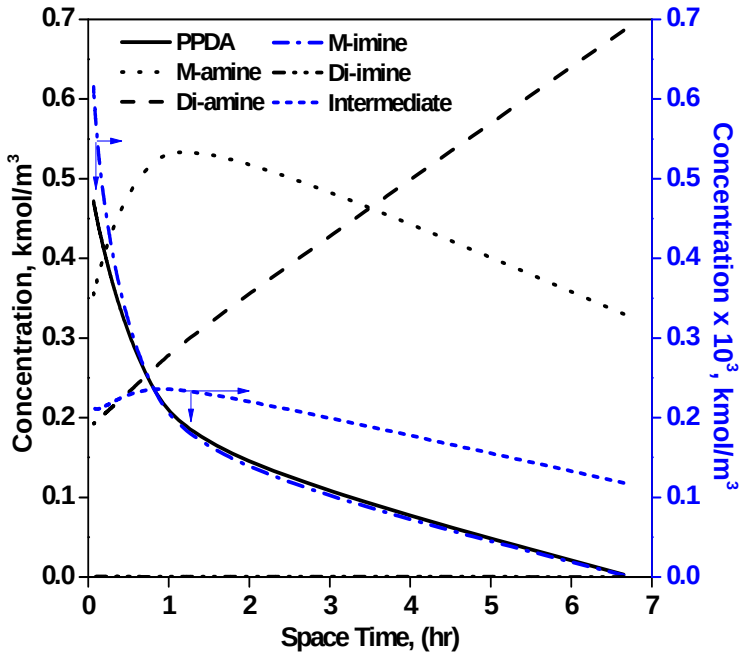

(A) FBR-DOWNFLOW

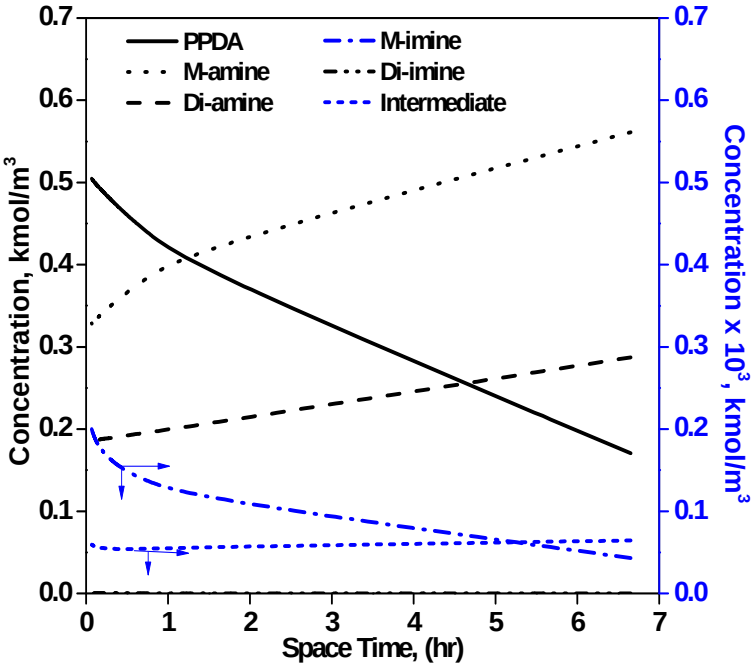

(B) FBR-UPFLOW

Figure 4.6. Effect of liquid velocity on the concentrations of various species involved in the reaction

Reaction conditions: T = 413K, P = 6 Mpa, B_{li} = 1 kmol/m^3, w = 0.058 kg = 854.3 kg/m^3, u_g = 5 ×10^{-2} m/s

non-catalytic as well as heterogeneous catalytic steps, homogeneous reactions occur more significantly in the liquid. Also, it was observed that the intraparticle diffusional resistance is significant in upflow mode as compared to downflow mode. This reduces the upflow mode efficiency. With increase in the space time, the concentrations of M-amine and Di-amine increases slowly as compared to the downflow mode, while concentration of M-imine decreases, but the concentration of Intermediate is almost constant and the reaction could not proceed effectively. Therefore, it clearly indicates that the higher space time is necessary for the upflow mode as compared to downflow mode to improve the reactor performance.

The phenomena will be clearer from Figures 4.7-4.9, which shows the results along the length of the reactor. Figure 4.7 shows the global rate of hydrogenation along the length of the reactor at fixed space time. It clearly indicates that the global rate of hydrogenation was almost 40% greater in downflow mode of operation than upflow mode. Therefore, it can be concluded that the heterogeneous catalytic steps involved in the overall reaction could proceed better in downflow mode as compared to the upflow mode of operation.

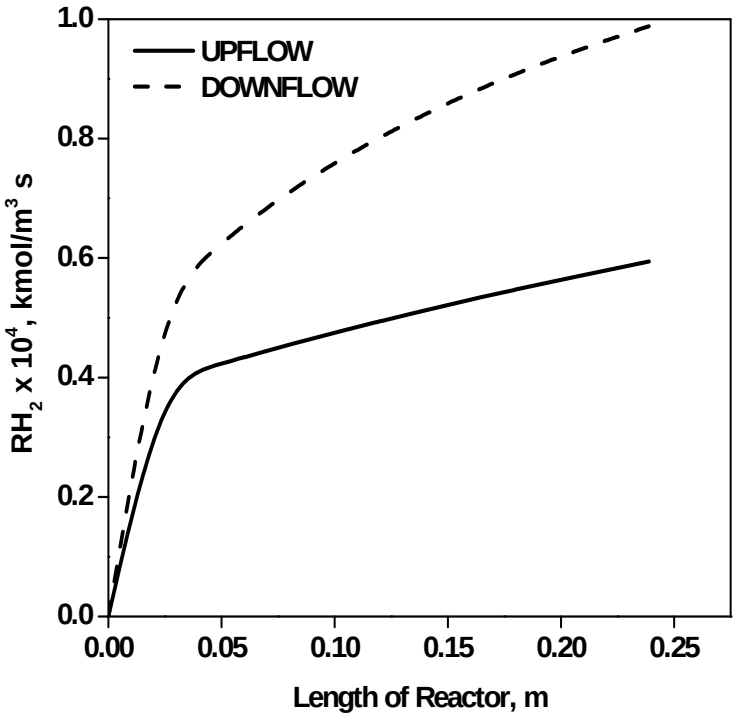

Figure 4.7. Global rate of hydrogenation along the length of reactor
Reaction conditions: u_l = 0.1 ×10^{-4} m/s, u_g = 5 ×10^{-2} m/s, w = 0.058 kg, T=413K, P=6 Mpa, B_{li}=1 kmol/m^3

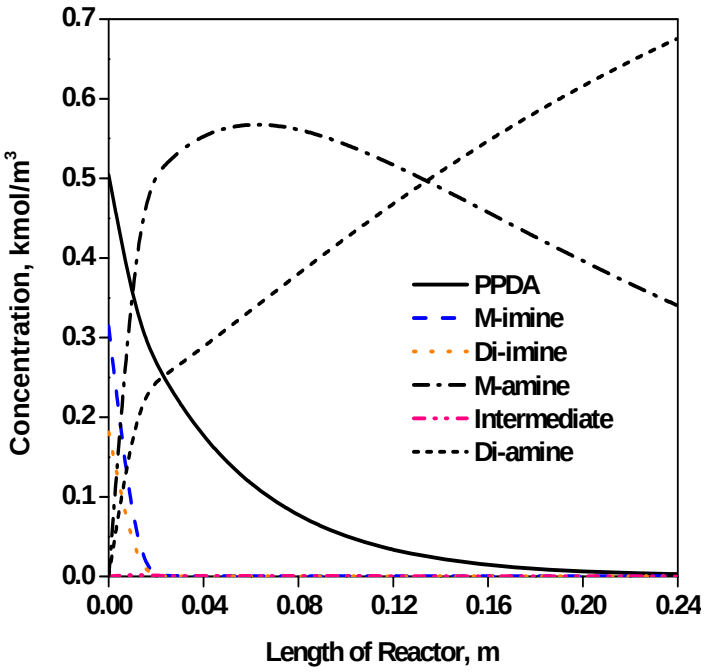

(A) FBR-DOWNFLOW

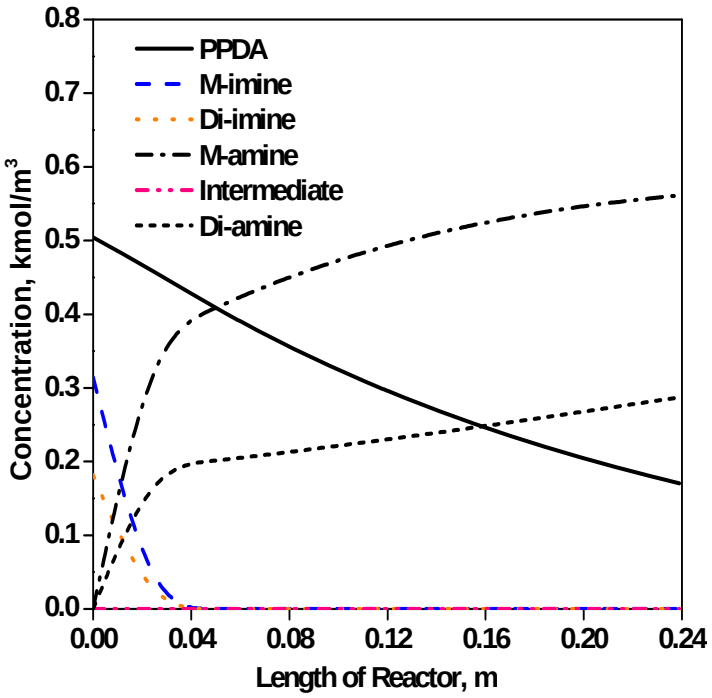

(B) FBR-UPFLOW

Figure 4.8. Species concentration profile along the length of reactor at minimum liquid velocity

Reaction conditions: T = 413K, P = 6 MPa, B_{li} = 1 kmol/m^3, w = 0.058 kg, u_l = 0.1 ×10^{-4} m/s, u_g = 5 ×10^{-2} m/s.

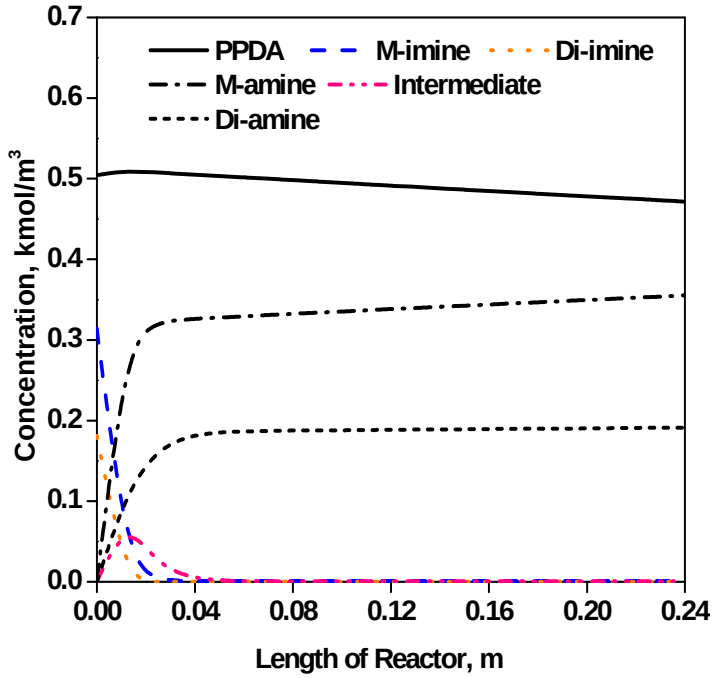

(A) FBR-DOWNFLOW

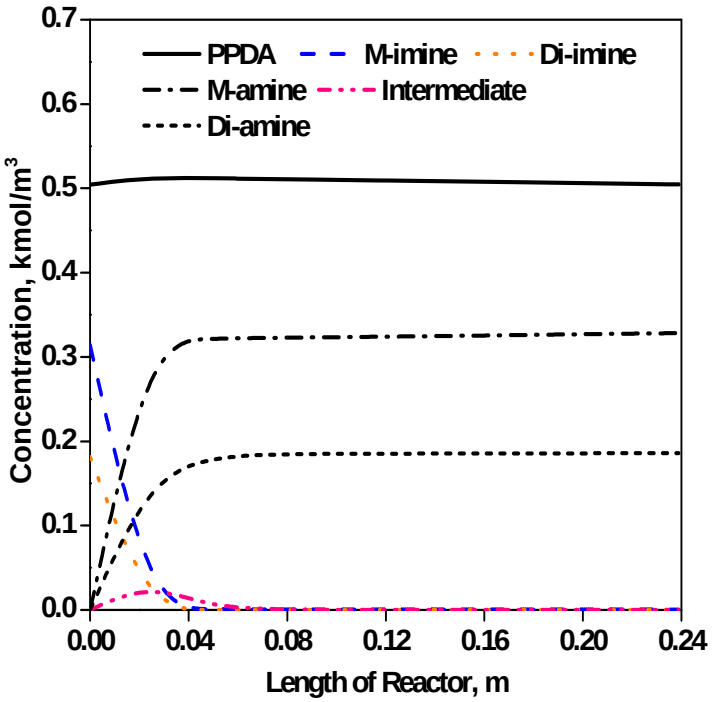

(B) FBR-UPFLOW

Figure 4.9. Species concentration profile along the length of reactor at maximum liquid velocity

Reaction conditions: T = 413K, P = 6 MPa, B_{li} = 1 kmol/m^3, w = 0.058 kg, u_l = 10 ×10^{-4} m/s, u_g = 5 ×10^{-2} m/s.

Figure 4.8 and Figure 4.9 shows the concentration of various species involved in the overall reaction along the length of the reactor at minimum and maximum liquid velocity considered in this work for FBR with downflow and upflow mode respectively. It was observed from Figure 4.8 that at lower liquid velocity (Figure 4.8-A and 4.8-B) for downflow mode, the reaction continues even after the complete conversion of PPDA for the conversion of M-amine to Di-amine, with high selectivity to Di-amine. On the contrary, in upflow mode, the reaction could not proceed up to the complete conversion of PPDA itself. At higher liquid velocity (i.e. lower space time), the downflow performance approaches upflow due to the catalyst wetting efficiency approaching that of upflow (Figure 4.9-A and 4.9-B).

Based on these studies, it can be concluded that the FBR with downflow mode outperforms upflow mode for the reaction system considered in this work, under the reaction conditions studied. Further the lower liquid velocity (0.1×10^{-4} m/s) and higher temperature (413K) was considered to understand the effect of various operating parameters on the overall reaction.3

4.5.1.2 Effect of Inlet PPDA Concentration

The effect of inlet concentration of PPDA on the selectivity to products in downflow and upflow modes of operation is shown in Figure 4.10. The selectivity to M-imine, Di-imine and Intermediate was observed to be very small and the trends are shown in Figure 4.10 to understand the effect more clearly within the reactor. With increase in inlet PPDA concentration, the selectivity to M-amine and Di-amine changes marginally in downflow mode as compared to the upflow mode. The high selectivity to Di-amine was observed in downflow mode (70%) as compared to upflow mode (42%). This difference is mainly due to the partial wetting of catalyst particles in the downflow mode, which is known to enhance the overall rate as discussed earlier.

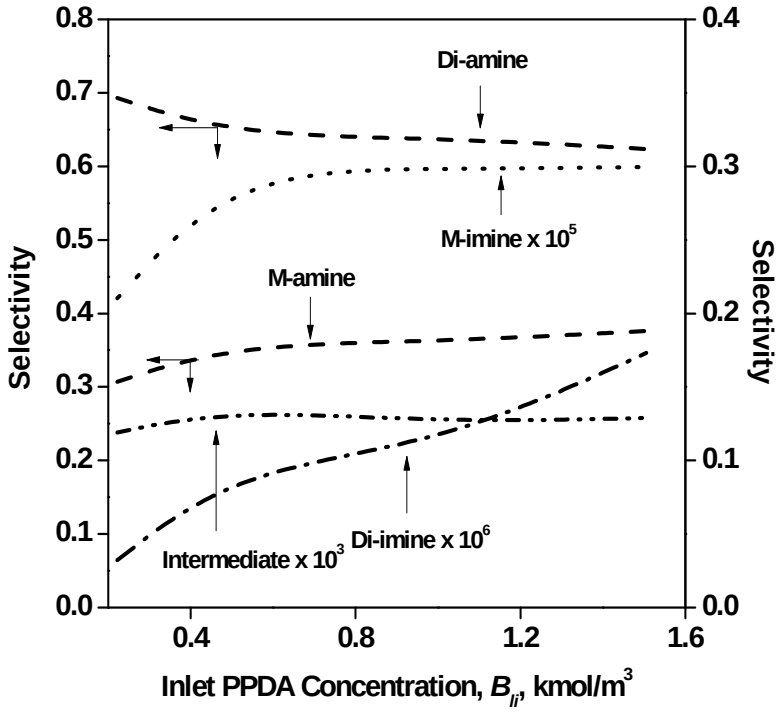

(A) FBR-DOWNFLOW

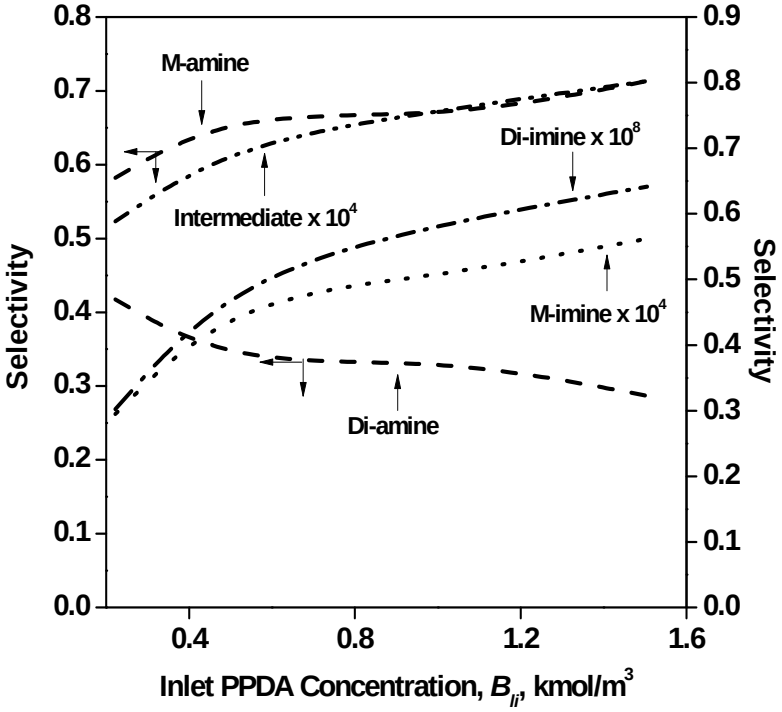

(B) FBR-UPFLOW

Figure 4.10. Selectivity to products as a function of inlet PPDA concentration
Reaction conditions: u_l = 0.1 ×10^{-4} m/s, u_g = 5 ×10^{-2} m/s, T = 413K, P = 6 Mpa, w = 0.058 kg

4.5.1.3 Effect of Catalyst Loading

Figure 4.11 shows the selectivity to products as a function of catalyst loading for downflow and upflow mode of operation. For the downflow mode with increase in the catalyst loading, the selectivity to M-imine, Di-imine, M-amine and Intermediate decreases, and the selectivity to final desired product Di-amine increases, whereas for upflow mode the selectivity to products remains almost constant. Also, the complete conversion of PPDA and maximum of 80% selectivity to Di-amine was found in downflow mode whereas about 90% conversion and 40% selectivity to Di-amine was found in upflow mode of operation. It should be noted here that for the upflow mode, the selectivity toward the hydrogenation products is not much dependent on the catalyst loading, whereas for downflow mode it increases continuously with increase in the catalyst loading. This is because the intraparticle diffusional resistance was found to be significant in upflow mode (0.72) as compared to the downflow mode (0.98). Also, with increase in catalyst loading, the catalyst bed length increases, which in turn increases the space time and hence all the consecutive and parallel reactions involved in the overall reaction can precede well simultaneously in downflow mode as compared to the upflow mode of operation.

4.5.1.4 Effect of Hydrogen Pressure

Figure 4.12 shows the selectivity to products as a function of hydrogen pressure for both downflow and upflow mode of operation. No significant change was observed in selectivity to products with increase in hydrogen pressure for both downflow and upflow modes of operation. The selectivity to Di-amine was observed to be 69% for downflow operation whereas it is 38% in upflow mode of operation under the reaction conditions studied. Therefore, it can be concluded that the effect of hydrogen pressure on selectivity to products is not significant for the reaction system considered in this work and downflow operation outperforms the upflow mode of operation under the reaction conditions studied.

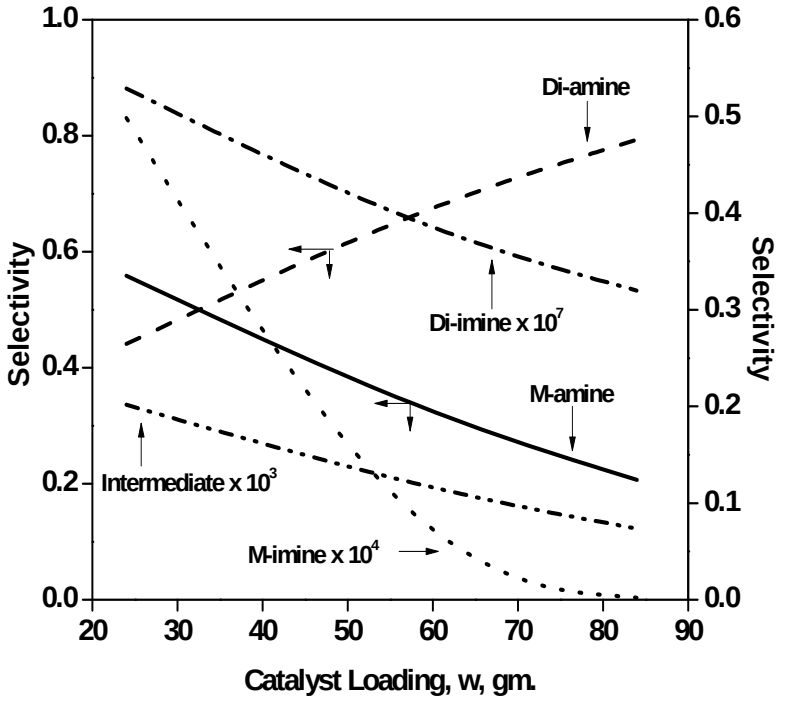

(A) FBR-DOWNFLOW

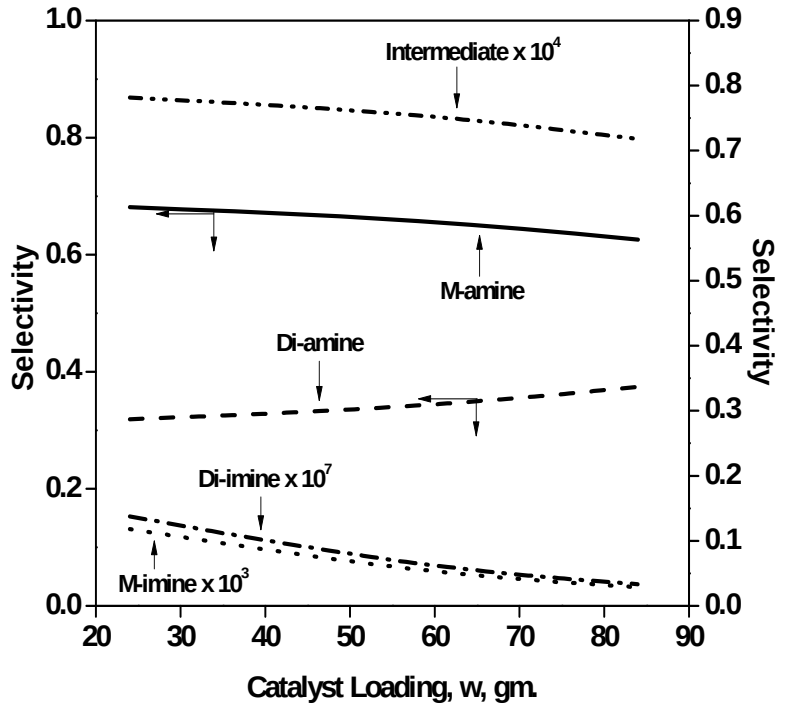

(B) FBR-UPFLOW

Figure 4.11. Selectivity to products as a function of catalyst loading
Reaction conditions: u_l = 0.1 ×10^{-4} m/s, u_g = 5 ×10^{-2} m/s, T = 413K, P = 6 Mpa, B_{li} = 1 kmol/m^3

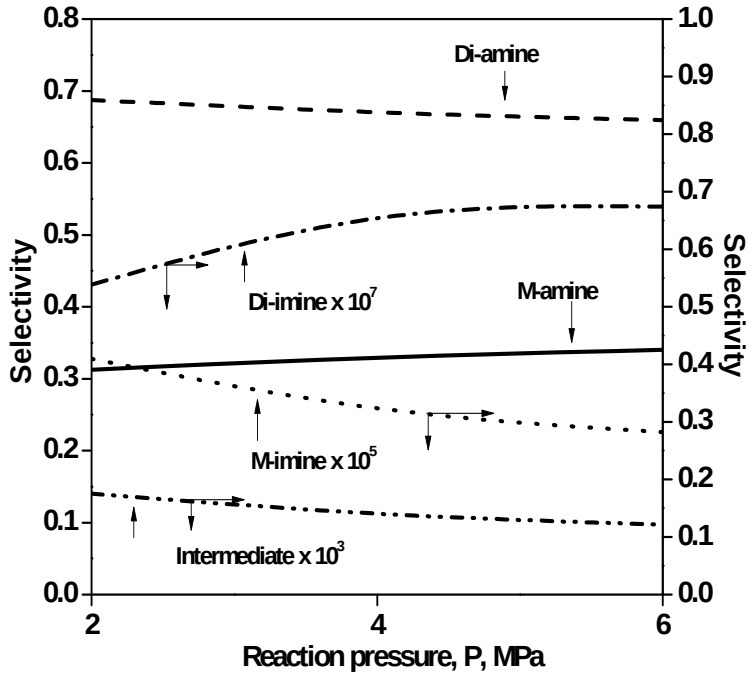

(A) FBR-DOWNFLOW

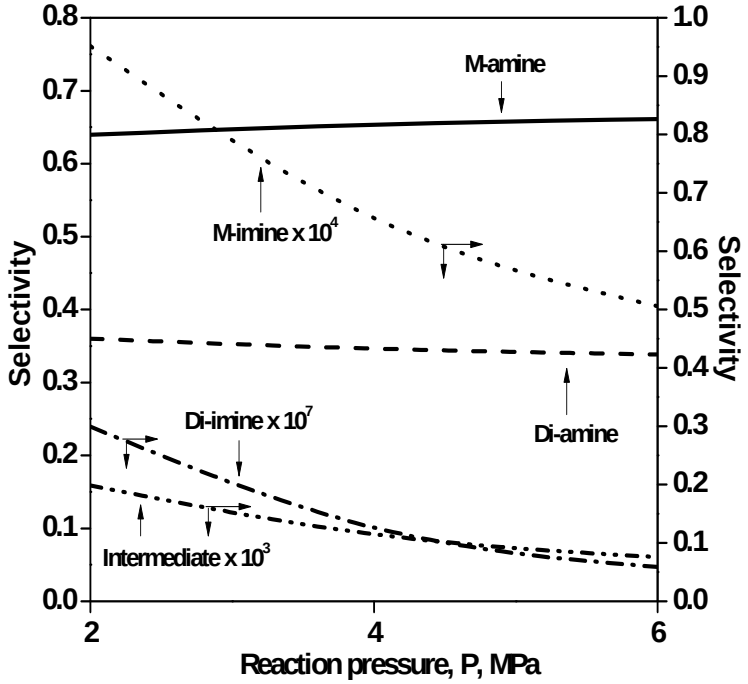

(B) FBR-UPFLOW

Figure 4.12. Selectivity to products as a function of partial pressure of hydrogen
Reaction conditions: u_l = 0.1 ×10^{-4} m/s, u_g = 5 ×10^{-2} m/s, T = 413K, w = 0.058 kg B_{li} = 1 kmol/m^3

4.5.1.5 Effect of Gas Velocity

The effect of gas velocity on the selectivity to hydrogenation products M-amine and Di-amine is shown in Figure 4.13 for the downflow and upflow mode of operation. It was observed that with increase in gas velocity, the selectivity to M-amine increases and Di-amine decreases for both downflow and upflow mode reactor. This may be because with increase in gas velocity at a fixed liquid velocity, the liquid hold up in the reactor decreases and hence the selectivity to M-amine increases and Di-amine decreases. Also, the downflow outperforms the upflow mode of operation because of the partial wetting effect in trickle bed mode. It must be noted here that at the lower gas velocity (u_g = 0.2 × 10^{-4} m/s), about 97 % selectivity to Di-amine can be achieved in downflow mode, whereas it is 83 % in upflow mode. Therefore, the gas velocity is an important parameter to optimize the reactor performance.

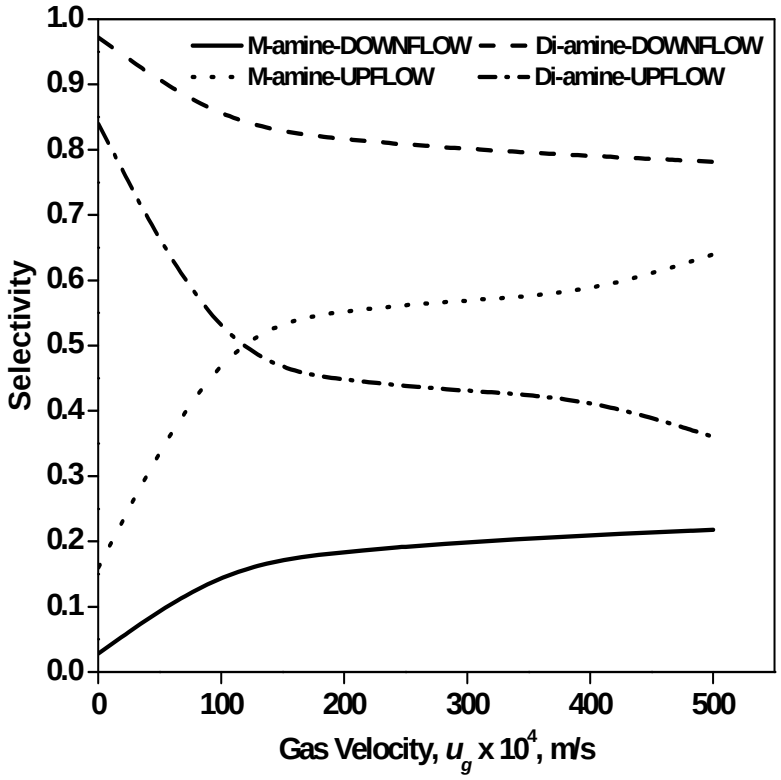

Figure 4.13. Selectivity to M-amine and Di-amine as a function of gas velocity
Reaction conditions: u_l = 0.1 ×10^{-4} m/s, w = 0.084 kg, T = 413K, P = 6 MPa, B_{li} = 1 kmol/m^3

4.5.1.6 Effect of Axial Dispersion

The liquid phase backmixing is accounted for by including an axial dispersion coefficient, D_{EL}, for the reactants and products in liquid phase. Axial dispersion can be severe in trickle flow or bubbly flow reactors with increasing conversion such as when conversion reaches around 90% for a laboratory scale TBR of 0.3m in length.[49] The axial dispersion coefficient is defined as dimensionless Peclet number (P_e) as shown in Table 4.2, in which the reactor length features as characteristic dimension. Therefore, when $P_e \rightarrow \infty$, the model reduces to the case of plug flow of the liquid phase and $P_e \rightarrow 0$ represents the situation where liquid phase is completely back mixed.[1]

In order to check the accuracy of the axial dispersion model, the conversion of PPDA as a function of space time was predicted for various peclet number values for both downflow and upflow modes of operation (Figure 4.14). It can be seen that with increasing peclet number, the axial dispersion model reduces to the case of plug flow model. The plug flow prevails in the reactor for P_e > 10. Also, it was observed that the deviation of axial dispersion model (ADM) from plug flow is not more than 15% for both the downflow and upflow modes of operation at high space times under the reaction conditions studied.

4.5.1.6.1 Criterion For Negligible Axial Dispersion

Several criteria have been proposed in the literature for appraising the significance of the axial dispersion effect. An early one was developed by Mears[49] for liquid limiting reactions based on the minimum bed length required to neglect the axial dispersion effect. Cassanello *et. al.* [50,51,52] demonstrated that the Mears criteria apply only for liquid limiting reactions. Hence, he has formulated another criterion for liquid or gaseous limited reactions, based on general approximation to the solution of the axial dispersion model, to establish the conditions under which the liquid axial dispersion affects the behavior of three phase FBRs for both downflow and upflow operations. This criterion implies that the deviation of ADM with respect to the plug flow model should not be larger than 5%. Hence, it must be verified that

$$P_{eL} \geq -\left(21-20R_{CM}\right)+\left[\left(21-20R_{CM}\right)^2-21+20R_{CM}\right]^{0.5} \qquad 4.57$$

where, R_{CM} is the ratio of reactant concentrations at the reactor outlet calculated according the completely backmixed ($P_e \to 0$) and plug flow models ($P_e \to \infty$). This criterion is valid for any type of kinetics and very useful, when geometrical characteristics and operating conditions of the reactor are defined. Therefore, the criterion presented by Cassanello *et. al.*[51] (i.e. equation 4.57) was applied to the conditions used for the reaction system considered in this work. For this purpose the dimensionless Peclet number was predicted using the literature correlations shown in Tables 4.2 and 4.3 for downflow and upflow modes respectively and the reactant outlet concentrations were evaluated. Figure 4.15 shows the comparison between the Peclet number predicted by literature correlation and equation 4.57 as a function of space time. It clearly indicates that for space time > 0.7 hr. and the space time > 3 hr., the axial dispersion may be significant for downflow and upflow modes of operation respectively under the reaction conditions studied.

Figure 4.16 shows the conversion of PPDA as a function of space time using the Peclet number predicted by the correlations (Table 4.2 and 4.3) for both downflow and upflow modes. It was observed that the deviation of ADM from plug flow model for the predicted conversion of PPDA is less than 5% for both downflow and upflow modes. This gives rise to the implication that the axial dispersion does not play an important role under the reaction condition studied. Therefore, the criterion may be used for the reactor design purposes by determining the operating conditions and geometric features in order to ensure the negligible axial dispersion effect, based on the assumption that the deviation of ADM with respect to plug flow should not be larger than 5%.

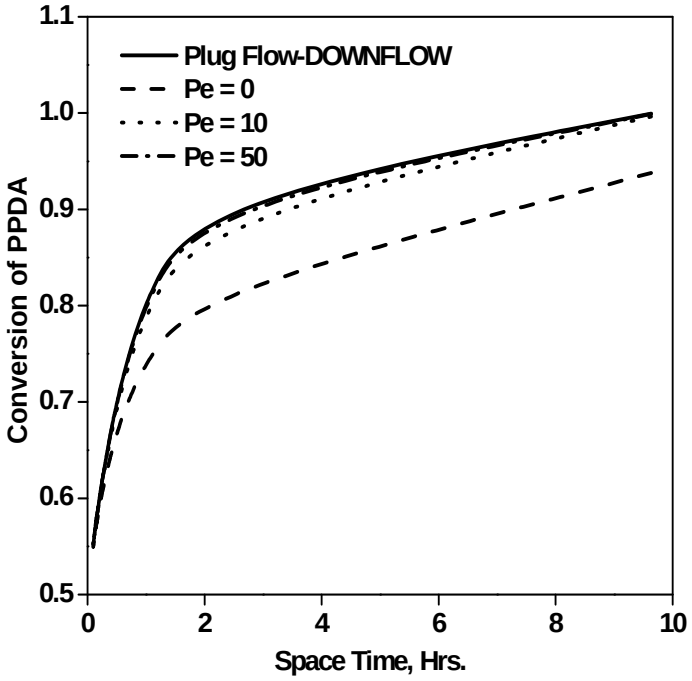

(A) FBR-DOWNFLOW

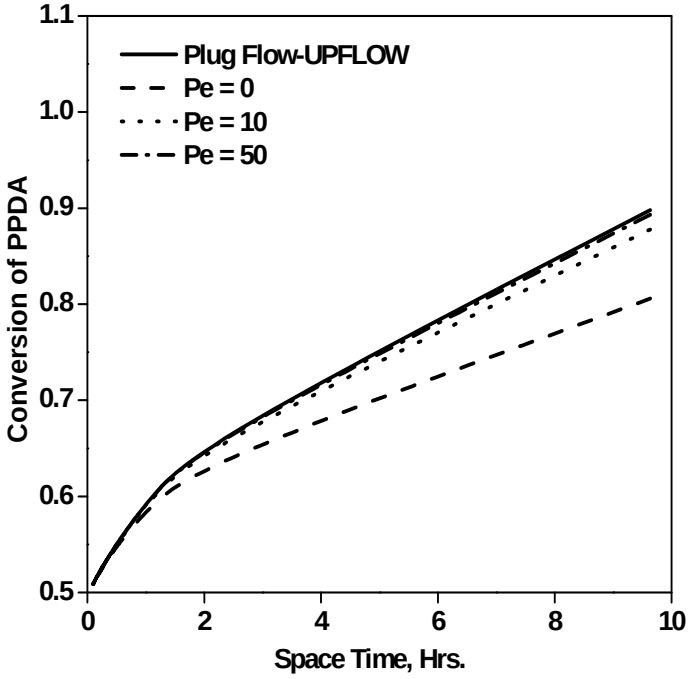

(B) FBR-UPFLOW

Figure 4.14. Effect of axial dispersion on conversion of PPDA
Reaction conditions: u_g = 5 ×10^{-2} m/s, T = 413K, P = 6MPa, w = 0.084 kg, B_{li} = 1 kmol/m^3

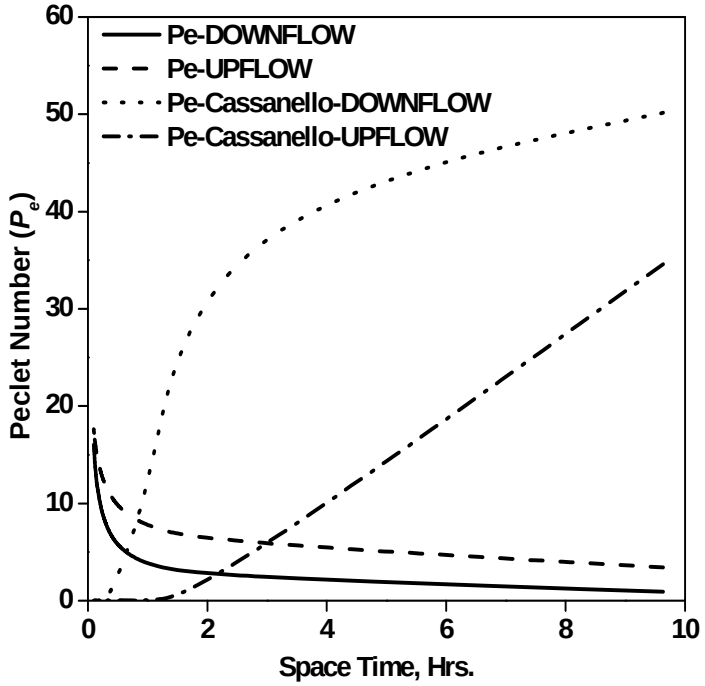

Figure 4.15. Peclet number as a function of space time
Reaction conditions: $u_g = 5 \times 10^{-2}$ m/s, $w = 0.084$ kg, $T = 413$K, $P = 6$ MPa, $B_{li} = 1$ kmol/m^3

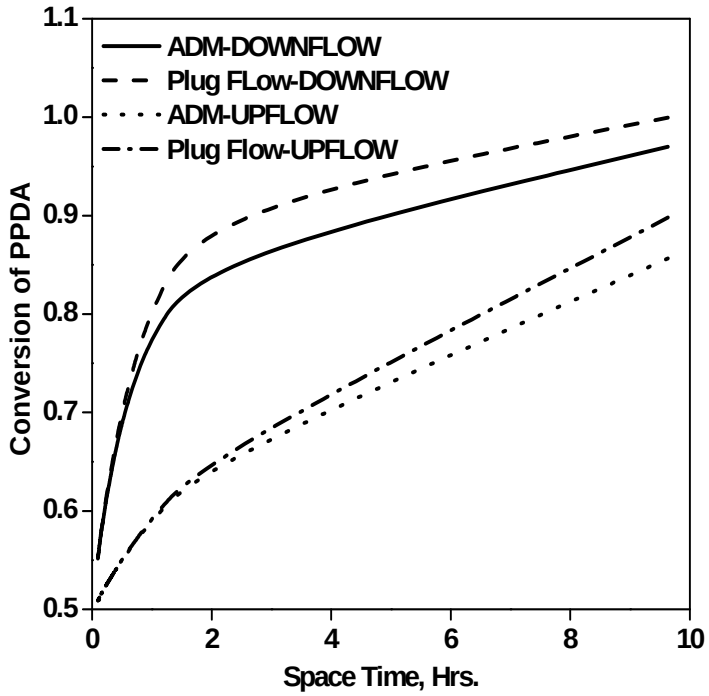

Figure 4.16. Conversion of PPDA as a function of space time

Reaction conditions: $u_g = 5 \times 10^{-2}$ m/s, $w = 0.084$ kg, $T = 413$K, $P = 6$ MPa, $B_{li} = 1$ kmol/m^3

4.5.2 Comparison of Fixed Bed Reactor Vs Slurry Reactor Performance

The comparison of fixed bed (downflow and upflow) and slurry reactors (BCSR and CSTR) has been made on the basis of constant catalyst loading and the constant total volume of the reactor.

4.5.2.1 Comparison Based on Constant Catalyst Loading

The fixed bed and slurry reactors were simulated for the identical feed concentration and reaction conditions with same weight of the catalyst, but the reactor volumes are different. The BCSR was simulated for both with and without consideration of back mixing. The extent of back mixing in BCSR was evaluated using the CFD model as discussed in Chapter-3, Section 3.2.5, and the estimated value was taken from Table 3.5 for the reaction conditions considered for the comparison. A comparison of performances among FBR and slurry reactors is shown in Figure 4.17 in terms of productivity of Di-amine per unit weight of the catalyst per hour. It clearly indicates that the BCSR without backmixing is the best choice among other reactor configurations considered, but BCSR with consideration of backmixing reduces the performance of BCSR significantly and the performance of BCSR is almost equal to CSTR. Therefore, slurry reactor (BCSR or CSTR) can be considered as the best choice among other reactor configurations studied when constant catalyst loading is taken as basis for the comparison, under the reaction conditions studied. Also, it is useful to evaluate possible ways to control and manipulate the degree of back mixing in the BCSR. Hence, the use of radial baffles for reducing backmixing in the BCSR as proposed by Khare *et. al.*[53] may be the useful approach to optimize the BCSR performance.

4.5.2.2 Comparison Based on Constant Volume Reactor

The fixed bed and slurry reactors were simulated under the conditions of constant volume reactor by keeping the length to diameter ratio same. For this purpose, the operating conditions were kept same for all the reactors, except the catalyst loading. The catalyst loading is high in FBR as compared to slurry reactors. The superficial liquid and gas velocity considered was very small as 1×10^{-5} m/s and 2×10^{-5} m/s respectively. Therefore, for BCSR, it was assumed that the superficial gas velocity will not influence the

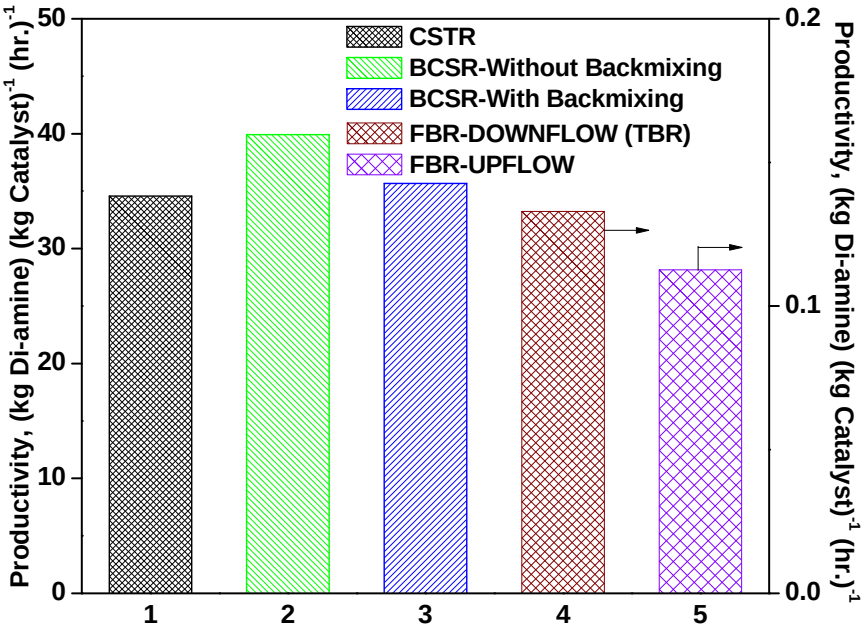

Figure 4.17. Comparison of fixed bed and slurry reactor performances in terms of productivity based on constant catalyst loading

Reaction conditions: u_l = 2 ×10^{-4} m/s, u_g = 2 ×10^{-2} m/s, w = 0.084 kg, T = 413K, P = 6 MPa, B_{li} = 1 kmol/m^3

Reactor dimensions: Slurry Reactors (BCSR and CSTR):- d_T = 0.25m, L = 4m

FBR (Downflow and Upflow):- d_T = 0.01985m, L = 0.3176m

internal liquid circulation within the column and hence, the case of BCSR-with backmixing was not considered for the comparison. Figure 4.18 shows the comparison of the reactor performance in terms of productivity of Di-amine per unit weight of catalyst per hour (Figure 4.18-A), productivity of Di-amine per unit volume of reactor per hour (Figure 4.18-B) and selectivity towards M-amine and Di-amine (Figure 4.18-C). Figure 4.18 clearly indicates the BCSR is the best choice when constant catalyst loading is taken as basis for comparison and TBR is the best choice when constant volume of the reactor is considered as basis for comparison. This is because the catalyst loading is higher in FBR and hence the rate of hydrogenation is higher and the maximum selectivity towards the desired product Di-amine can be achieved in FBR (96%) as compared to slurry reactor (80%).

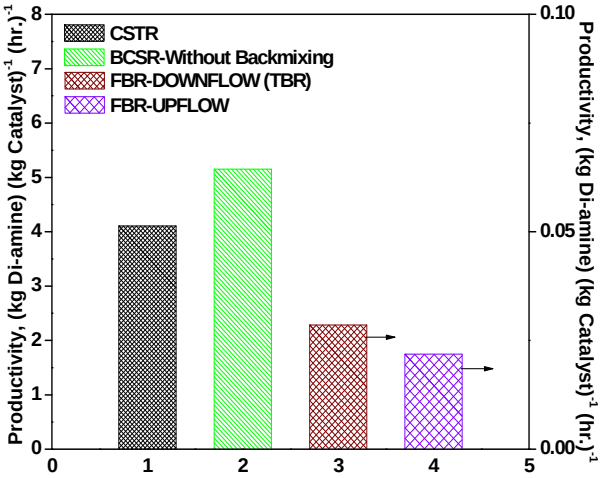

(A) Productivity of Di-amine per unit weight of catalyst per hour

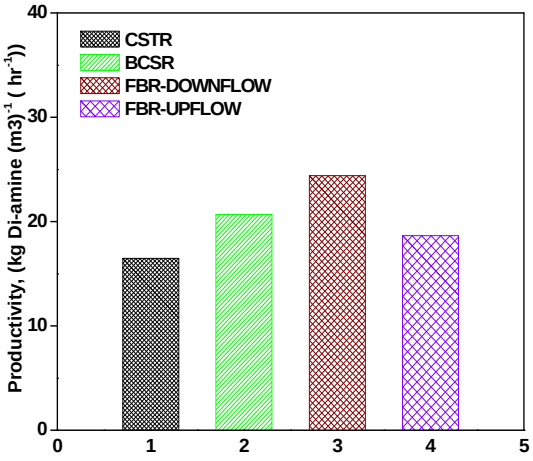

(B) Productivity of Di-amine per unit volume of reactor per hour

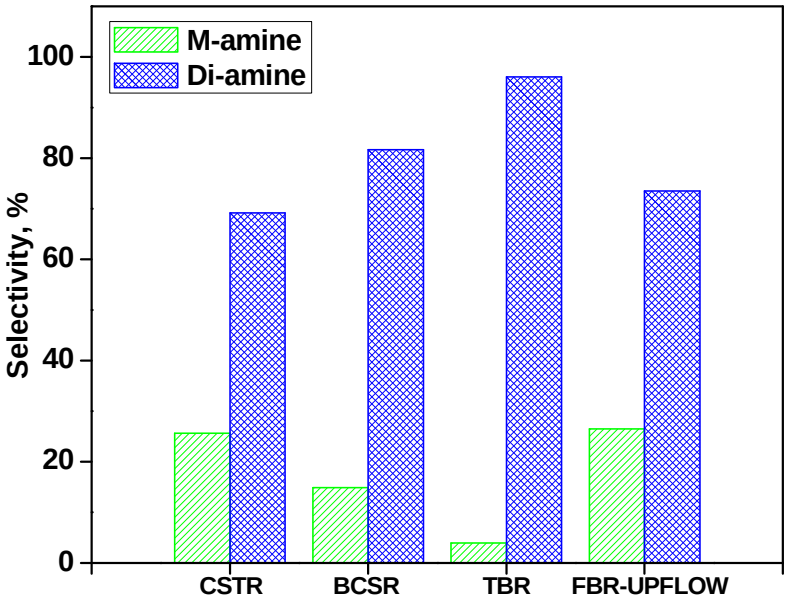

(C) Selectivity

Figure 4.18. Comparison of fixed bed and slurry reactor performances based on constant volume reactor

Reaction conditions: u_l = 0.1 ×10^{-4} m/s, u_g = 0.2 ×10^{-4} m/s, T = 413K, P = 6 MPa, B_{li} = 1 kmol/m^3, and N = 16 for BCSR

Catalyst loading: FBR: w = 0.084 kg = 854.3 kg/m^3, BCSR: w = 0.00039 kg = 4 kg/m^3

Reactor dimensions: d_T = 0.01985 m, L = 0.3176, hence L/D = 16 for both Slurry and FBR

4.6 CONCLUSIONS

A fixed bed reactor model with downflow and upflow modes of operation has been developed incorporating the contributions of partial wetting and stagnant liquid holdup effects in addition to the external and intraparticle mass transfer resistances and heat effects for reductive alkylation of PPDA. The comparison between the two modes of FBR was evaluated theoretically. It was found that the FBR with downflow outperforms the upflow mode for all the reaction conditions studied. Further, the comparison between slurry (BCSR and CSTR) Vs FBR (Downflow and Upflow) is made in terms of productivity and selectivity. It was found that BCSR is the best choice when constant catalyst loading was taken as basis for comparison and the FBR with downflow operation is the best choice when constant volume of the reactor was considered as basis for comparison. The reactor models developed could be useful to optimize the overall performance of multiphase reactors considered and will enhance our understanding to recommend a suitable reactor based on true intrinsic kinetics for the reaction system considered.

APPENDIX-B

The detailed derivations of axial dispersion model are given below. The axial dispersion model can be reduced to the plug flow model by considering the negligible axial dispersion. The dimensionless parameters used in the following equations are defined in Table 4.2 and are not repeated in this section.

B.1 Mass balance of hydrogen in liquid phase

The mass balance of hydrogen in dimensionless form can be written as

$$D_{EL}\frac{d^2A_{ld}}{dx^2}-u_l\frac{dA_{ld}}{dx}+k_La_B\left(A^*-A_{ld}\right)=f_dk_{sd}a_p\left(A_{ld}-A_{s_d}\right)+K_{ex}\varepsilon_{ls}\left(A_{ld}-A_{l_s}\right)$$

In dimensionless form

$$\frac{1}{P_e}\frac{d^2a_{ld}}{dz^2}-\frac{da_{ld}}{dz}+\alpha_{gl}\left(1-a_{ld}\right)=f_d\alpha_{lsd}\left(a_{ld}-a_{sd}\right)+\frac{L\,K_{ex}\varepsilon_{ls}}{u_l}\left(a_{ld}-a_{ls}\right) \qquad \text{B.1}$$

To solve the above second order differential equation, equation B.1 can be converted into the two first order differential equations as follows:

Let, $a=\dfrac{da_{ld}}{dz}$ $\qquad \therefore \dfrac{da}{dz}=\dfrac{d^2a_{ld}}{dz^2}$

Hence equation A.1 can be written as

$$\frac{1}{P_e}\frac{da}{dz}-a+\alpha_{gl}\left(1-a_{ld}\right) \;=\; f_d\alpha_{lsd}\left(a_{ld}-a_{sd}\right) \;+\; \frac{L\,K_{ex}\varepsilon_{ls}}{u_l}\left(a_{ld}-a_{ls}\right) \qquad \text{B.2}$$

The derivations for concentration of hydrogen on the catalyst surface in dynamic, stagnant and dry zones can be found in section 4.2.2.3 and are not repeated here.

B.2 Mass balance of PPDA

The mass balance of PPDA can be written as

$$D_{EL}\frac{d^2B_{ld}}{dx^2}-u_l\frac{dB_{ld}}{dx}+\varepsilon_l\left[k_{eq1}B_l-k_{eq2}D_l\left(D_l+2F_l+G_l+2H_l+2P_l\right)\right]=0 \qquad \text{B.3}$$

In dimensionless form

$$\frac{1}{P_e}\frac{d^2 b_{ld}}{dz^2} - \frac{db_{ld}}{dz} - \varepsilon_l \left[\alpha_{R1} b_l - \alpha_{R2} d_l c_{H_2O} \right] = 0 \qquad \text{B.4}$$

To solve the equation A.4, it can be converted to two first order differential equations as follows:

$$b = \frac{db_{ld}}{dz} \qquad \therefore \frac{db}{dz} = \frac{d^2 b_{ld}}{dz^2}$$

$$\therefore \quad \frac{1}{P_e}\frac{db}{dz} - b = \varepsilon_l \left[\alpha_{R1} b_l - \alpha_{R2} d_l \left(d_l + 2f_l + g_l + 2h_l + 2p_l \right) \right] \qquad \text{B.5}$$

Similarly, the mass balance of other liquid species can be solved by converting the second order differential equations into two first order differential equations respectively. The initial and final forms of equations for the other reactants/products species can be written as follows:

B.3 Mass balance of M-imine

$$\begin{aligned} &D_{EL}\frac{d^2 D_{ld}}{dx^2} - u_l \frac{dD_{ld}}{dx} + \varepsilon_l \left[k_{eq1} B_l - k_{eq2} D_l \left(D_l + 2F_l + G_l + 2H_l + 2P_l \right) \right] \\ &-\varepsilon_l \left[k_{eq3} D_l - k_{eq4} F_l \left(D_l + 2F_l + G_l + 2H_l + 2P_l \right) \right] - \frac{\eta_c w k_5 D_l \sqrt{A_S}}{1 + K_A \sqrt{A_S}} = 0 \end{aligned} \qquad \text{B.6}$$

In dimensionless form,

$$\begin{aligned} &\frac{1}{P_e}\frac{d^2 d_{ld}}{dz^2} - \frac{dd_{ld}}{dz} + \varepsilon_l \left[\alpha_{R1} b_l - \alpha_{R2} d_l \left(d_l + 2f_l + g_l + 2h_l + 2p_l \right) \right] \\ &-\varepsilon_l \left[\alpha_{R3} d_l - \alpha_{R4} f_l \left(d_l + 2f_l + g_l + 2h_l + 2p_l \right) \right] \\ &-\frac{\eta_c \alpha_{R5} d_l}{q_B} \left[\frac{f_d \sqrt{a_{sd}}}{1 + k_a \sqrt{a_{sd}}} + \frac{f_s \sqrt{a_{ss}}}{1 + k_a \sqrt{a_{ss}}} + \frac{(1 - f_d - f_s)\sqrt{a_{sg}}}{1 + k_a \sqrt{a_{sg}}} \right] = 0 \end{aligned} \qquad \text{B.7}$$

B.4 Mass balance of Di-imine

$$D_{EL}\frac{d^2 F_{ld}}{dx^2} - u_l \frac{dF_{ld}}{dx} + \varepsilon_l \left[k_{eq3} D_l - k_{eq4} F_l \left(D_l + 2F_l + G_l + 2H_l + 2P_l \right) \right] - \frac{\eta_c w k_8 F_l \sqrt{A_S}}{1 + K_A \sqrt{A_S}} = 0 \qquad \text{B.8}$$

In dimensionless form

$$\frac{1}{P_e}\frac{d^2 f_{ld}}{dz^2}-\frac{df_{ld}}{dz}+\varepsilon_l\left[\alpha_{R3}d_l-\alpha_{R4}f_l\left(d_l+2f_l+g_l+2h_l+2p_l\right)\right]$$
$$-\frac{\eta_c\alpha_{R8}f_l}{q_B}\left[\frac{f_d\sqrt{a_{sd}}}{1+k_a\sqrt{a_{sd}}}+\frac{f_s\sqrt{a_{ss}}}{1+k_a\sqrt{a_{ss}}}+\frac{(1-f_d-f_s)\sqrt{a_{sg}}}{1+k_a\sqrt{a_{sg}}}\right]=0 \quad \text{B.9}$$

B.5 Mass balance of M-amine

$$D_{EL}\frac{d^2G_{ld}}{dx^2}-u_l\frac{dG_{ld}}{dx}+\frac{\eta_c wk_5 D_l\sqrt{A_S}}{1+K_A\sqrt{A_S}}$$
$$-\varepsilon_l\left[k_{eq6}G_l-k_{eq7}H_l\left(D_l+2F_l+G_l+2H_l+2P_l\right)\right]=0 \quad \text{B.10}$$

In dimensionless form,

$$\frac{1}{P_e}\frac{d^2g_{ld}}{dz^2}-\frac{dg_{ld}}{dz}+\frac{\eta_c\alpha_{R5}d_l}{q_B}\left[\frac{f_d\sqrt{a_{sd}}}{1+k_a\sqrt{a_{sd}}}+\frac{f_s\sqrt{a_{ss}}}{1+k_a\sqrt{a_{ss}}}+\frac{(1-f_d-f_s)\sqrt{a_{sg}}}{1+k_a\sqrt{a_{sg}}}\right]$$
$$-\varepsilon_l\left[\alpha_{R6}g_l-\alpha_{R7}h_l\left(d_l+2f_l+g_l+2h_l+2p_l\right)\right]=0 \quad \text{B.11}$$

B.6 Mass balance of Intermediate

$$D_{EL}\frac{d^2H_{ld}}{dx^2}-u_l\frac{dH_{ld}}{dx}+\varepsilon_l\left[k_{eq6}G_l-k_{eq7}H_l\left(D_l+2F_l+G_l+2H_l+2P_l\right)\right]$$
$$-\frac{\eta_c wk_8F_l\sqrt{A_S}}{1+K_A\sqrt{A_S}}-\frac{\eta_c wk_9H_l\sqrt{A_S}}{1+K_A\sqrt{A_S}}=0 \quad \text{B.12}$$

In dimensionless form,

$$\frac{1}{P_e}\frac{d^2h_{ld}}{dz^2}-\frac{dh_{ld}}{dz}+\varepsilon_l\left[\alpha_{R6}g_l-\alpha_{R7}h_l\left(d_l+2f_l+g_l+2h_l+2p_l\right)\right]$$
$$-\frac{\eta_c\left(\alpha_{R8}f_l-\alpha_{R9}h_l\right)}{q_B}\left[\frac{f_d\sqrt{a_{sd}}}{1+k_a\sqrt{a_{sd}}}+\frac{f_s\sqrt{a_{ss}}}{1+k_a\sqrt{a_{ss}}}+\frac{(1-f_d-f_s)\sqrt{a_{sg}}}{1+k_a\sqrt{a_{sg}}}\right]=0 \quad \text{B.13}$$

B.7 Mass balance of Di-amine

$$D_{EL}\frac{d^2P_{ld}}{dx^2}-u_l\frac{dP_{ld}}{dx}+\frac{\eta_c w k_9 H_l\sqrt{A_S}}{1+K_A\sqrt{A_S}}=0 \qquad \text{B.14}$$

In dimensionless form,

$$\frac{1}{P_e}\frac{d^2p_{ld}}{dz^2}-\frac{dp_{ld}}{dz}+\frac{\eta_c\alpha_{R9}h_l}{q_B}\left[\frac{f_d\sqrt{a_{sd}}}{1+k_a\sqrt{a_{sd}}}+\frac{f_s\sqrt{a_{ss}}}{1+k_a\sqrt{a_{ss}}}+\frac{(1-f_d-f_s)\sqrt{a_{sg}}}{1+k_a\sqrt{a_{sg}}}\right]=0 \qquad \text{B.15}$$

NOMENCLATURE

a_B = gas-liquid interfacial area, m^2/m^3

a_p = external surface area of the pellet, $[6w/\rho_p d_p]$, m^{-1}

A^* = saturation solubility of hydrogen, $kmol/m^3$

a_l = dimensionless concentration of hydrogen in the liquid phase

A_l = concentration of hydrogen in the liquid phase, $kmol/m^3$

a_s = dimensionless concentration of hydrogen on catalyst surface

A_s = concentration of hydrogen on the catalyst surface, $kmol/m^3$

A_R = area of reactor, m^2

b_l = dimensionless concentration of PPDA in the liquid phase, (B_l/B_{li})

B_l = concentration of PPDA in the liquid phase, $kmol/m^3$

B_{li} = initial concentration of PPDA in the liquid phase, $kmol/m^3$

C_m = concentration of MEK, $kmol/m^3$

C_{H2O} = concentration of water, $kmol/m^3$

c_{H2O} = dimensionless concentration of water

C_{pl} = heat capacity of liquid, kJ/kg/K

C_{pg} = heat capacity of gas, kJ/kg/K

C_{ps} = heat capacity of solid catalyst, kJ/kg/K

d_l = dimensionless concentration of M-imine in liquid phase, (D_l/B_{li})

D_l = concentration of M-imine in the liquid phase, $kmol/m^3$

D_e = effective diffusivity, m^2/s

D_m = molecular diffusivity, m^2/s

d_p = particle diameter, m

d_T = reactor diameter, m

d_I = diameter of the impeller, m

D_{EL} = liquid phase axial dispersion coefficient, m^2/s

E_i = activation energy for hydrogenation step *i*, kJ/mol

e = energy supplied by the agitator to the liquid per unit mass, m^2/s^3

f_l = dimensionless concentration of di-imine in liquid phase, (F_l/ B_{li})

F_l = concentration of di-imine in liquid phase, $kmol/m^3$

f_d = fraction of catalyst wetted by dynamic liquid

f_s = fraction of catalyst wetted by stagnant liquid

f_w = wetted fraction

F_r = froude number, ($u_g^2 / (g \times d_p)$)

F_c = shape factor of the catalyst

f_{gl} = friction factor for gas-liquid flow in packed beds

g_l = dimensionless concentration of M-amine in liquid phase, (G_l/ B_{li})

G_l = concentration of M-amine in liquid phase, $kmol/m^3$

g = acceleration due to gravity, m/s^2

G_{aL} = galileo number, ($d_p^3 \, g \, \rho_l^2/\mu_l^2$)

h_l = dimensionless concentration of Intermediate in liquid phase, (H_l/ B_{li})

H_l = concentration of intermediate in liquid phase, $kmol/m^3$

H_e = henry's constant of solubility for H_2, $kmol/m^3/atm$

H_A = solubility coefficient of hydrogen, ($L/H_e/R_g/T$)

k_5, k_8 *and* k_9 = reaction rate constants, $(m^3/kg)(m^3/kmol)^{0.5}s^{-1}$

k_{85} = dimensionless rate constant, (k_8/k_5)

k_{95} = dimensionless rate constant, (k_9/k_5)

k_a = dimensionless adsorption equilibrium constant, ($K_A\sqrt{A^*}$)

K_A = adsorption equilibrium constant, m^3/kmol

$k_L a_B$ = gas-liquid mass transfer coefficient, s^{-1}

k_s = liquid-solid mass transfer coefficient, s^{-1}

k_{gs} = coefficient of direct mass transfer from gas-to-solid surface, cm/s

K_{ex} = exchange coefficient between dynamic and stagnant liquid, s^{-1}

L = length of reactor, m

M_w = molecular weight

N = number of cells

N_r = speed of agitation, s^{-1}

p_l = dimensionless concentration of di-imine in liquid phase, (P_l/ B_{li})

P_l = concentration of D-amine in liquid phase, kmol/m^3

P_r = prandtl number, ($C_{pl}\ \mu_{ls}/\lambda$)

P_v = vapor pressure of solvent, MPa

P_e = dimensionless Peclet number, (u_l L / D_{EL})

P = power consumption for agitation for an aerated liquid, W

P_o = power consumption for agitation of a gas free liquid, W

P_g = power supplied to the liquid by gas phase

$\Delta P/Z$ = pressure drop per unit bed length, N/m^3

Q_g = volumetric flow rate of gas, m^3/s

Q_l = volumetric flow rate of liquid, m^3/s

q_B = stoichiometric ratio ($B_{li}/A_{go}/H_A$)

R_1 to R_6 = reaction rates for individual reaction steps, (kmol/m^3/s)

R = radius of catalyst pellet, m

R_{eL} = reynolds number for liquid, ($d_p u_l \rho_l / \mu_l$)

R_{eG} = reynolds number for gas, ($d_p u_g \rho_g / \mu_g$)

R_A = overall rate of hydrogenation, kmol/m^3/s

R_{H2} = global rate of hydrogenation, kmol/m^3/s

R_g = universal gas constant, kJ/kmol/K

S_{h0} = sherwood number

S_{TW} = surface tension of water, dyne/cm

S_T = surface tension of liquid, dyne/cm

S_c = schimdt number, ($\mu_l / \rho_l / D_m$)

$S_{m\text{-}imine}$ = selectivity to M-imine

$S_{di\text{-}imine}$ = selectivity to Di-imine

$S_{m\text{-}amine}$ = selectivity to M-amine

$S_{intermediate}$ = selectivity to Intermediate

$S_{di\text{-}amine}$ = selectivity to Di-amine

T_i = inlet temperature, K

T = outlet temperature, K

T_w = wall temperature, K

ΔT_{max} = maximum temperature rise, K

U_w = bed-to-wall heat transfer coefficient, kJ/m^2/K/s

u_g = gas velocity, m/s

u_l = liquid velocity, m/s

V_R = reactor volume, m^3

V_L = volume of the liquid in the reactor, m^3

w = catalyst loading, kg/m^3

z = dimensionless reactor length

Greek letters

η_c = overall catalytic effectiveness factor

α_A = dimensionless gas-liquid mass transfer coefficient

α_{ls} = dimensionless liquid-solid mass transfer coefficient

$\alpha_{R1}, \alpha_{R3}, \alpha_{R6}$ = dimensionless forward reaction rate constants

$\alpha_{R2}, \alpha_{R4}, \alpha_{R7}$ = dimensionless backward reaction rate constants

$\alpha_{R5}, \alpha_{R8}, \alpha_{R9}$ = dimensionless reaction rate constant

β_1-β_4, & β_6-β_9 = dimensionless thermicity parameters

β_5 & β_{10} = dimensionless heat transfer parameters

ΔH_1 = heat of reaction for catalytic hydrogenation steps, kJ/kmol

ΔH_2, ΔH_3, ΔH_4 = heat of reaction for equilibrium reaction steps R_1, R_2 and R_4 respectively, kJ/kmol

ε_g = gas hold up

ε_l, ε_{ld}, ε_{ls} = liquid hold up, total, dynamic and stagnant respectively

ε = Porosity

$\in_B$ = bed porosity

τ = tortuosity

δ_{gl} = pressure drop per unit bed height in a fixed bed reactor, $dyne/cm^2$

θ = dimensionless exit temperature, (T/T_i)

θ_w = dimensionless wall temperature, (T_w/T_i)

θ_b = dimensionless bed temperature, (T_b/T_i)

$\lambda_{eff.}$ = effective thermal conductivity, kJ/s.m.°C

ρ_l = density of the liquid, kg/m^3

ρ_g = density of gas, kg/m^3

ρ_p = density of catalyst particle, kg/m^3

μ_l = viscosity of the liquid, kg/m/s

μ_g = viscosity of the gas, kg/m/s

υ_m = molar volume of the solute

λ_L = thermal conductivity of liquid phase, J/m/s/K

ϕ = thiele parameter

ϕ_o = dimensionless parameter defined by equation 4.12

χ = parameter defined by equation 4.29

Subscripts

d = dynamic zone

g = dry zone

s = stagnant zone

l = liquid phase

REFERENCES

1. Ramachandran, P. A.; Chaudhari, R. V. *Three Phase Catalytic Reactors*. Gordon & Breach: New York, **1983**.
2. Duducovic, M. P.; Larachi, F.; Mills, P.L. Multiphase Catalytic Reactors: A perspective on current knowledge and future trends. *Catalysis Reviews*, **2002**, *44 (1)*, 123.
3. Chaudhari, R.V.; Mills, P.L. Multiphase catalysis and reaction engineering for emerging pharmaceutical processes. *Chem. Eng. Sci.*, **2004**, *59*, 5337.
4. Schembecker, G.; Droge, T.; Westhaus, U.; Simmrock, K.H. A Heuristic-Numeric Consulting System for the Choice of Chemical Reactors. *Proc. Found. Computer-Aided Proc. Des*., AIChE Symp. Series, No. 304, **1995**, *91*, 336.
5. Mehta, V. L.; Kokossis, A. Development of a Novel Multiphase Reactor Using a Systematic Design Procedure. *Comput. Chem. Eng*., **1997**, *21* Suppl., S325.
6. Mehta, V. L.; Kokossis, A. New Generation Tools for Multiphase Reaction Systems: A Validated and Systematic Methodology for Novelty and Design Automation. *Computers Chem. Eng*., **1998**, *22* Suppl., S119..
7. Kelkar, V. V.; Ng,, K.M. Screening Procedure for Synthesizing Isothermal Multiphase Reactors. *A.I.Ch. E. Journal*, **1998**, *44*, 1563
8. Chaudhari, R.V.; Mills, P.L. Multiphase reactors for fine chemicals and pharmaceuticals. *La Chemica e I'Industria*, **2000**, *82*, 539.
9. Krishna, R.; Sie, S.T. Strategies for Multiphase Reactor Selection. *Chem. Eng. Sci*., **1994**, *49*, 4029.
10. Doraiswamy, L. K.; Sharma, M. M. Heterogeneous reactions, Analysis, examples and reactor design. *Fluid--fluid-solid reactions,* Vol. 2. Wiley, New York, U.S.A, **1984**.
11. Westerterp, K. R.; xan Swaaij, W. P. M.; Bcenackcrs, A. A. C. M. Chemical reactor design and application.. Wilcy, New York, U.S.A., **1984**.
12. Joshi, J. B.; Shertukde, P. V.;Godbole, S. P. Modelling of three phase sparged catalytic reactors. *Rev. Chem. Eng.*, **1988**, *5(I 4)*, 71
13. Wild, G.; Larachi, F.; Charpcntier, J. C. Heat and mass transfer in gas-liquid solid fixed bed reactors. In Heat and mass transfer in porous beds. M. Quintard and M. Todorovic. Elsevier. Amsterdam, pp. 616-632, **1992**.
14. Chaudhari, R.V.; Ramachandran, P..A. Modeling of catalytic trickle bed reactors. In Heat and mass transfer in porous. Eds. M. Quintard and M. Todorovic. Elsevier, Amsterdam, The Netherlands, **1992**.
15. Goto, S.; Smith, J. M. Trickle bed reactor performance Part II: reaction studies. *A.I.Ch.E.Journal,* **1975**, 21, 706.
16 Levec, J.; Smith, J. M. Oxidation of acetic acid solutions in a trickle-bed reactor. *A.I.Ch.E.J.*, **1976**, *22*, 159.
17. Herskovitz, M. Modeling of a trickle-bed reactor: the hydrogenation of xylose to xylitol, *Chem.Eng. Sci.*, **1985**, *40*, 1309.
18. Beaudry, E. G.; Dudukovic, M. P.; Mills, P. L. Trickle-bed reactors: liquid diffusional effects in a gas limited reaction. *A.I.Ch.E.Journal.*, **1987**, *33*, 1435.
19. Bergault, I.; Rajashekharam, M. V.; Chaudhari, R. V.; Schweich, D. Delmas, H. Modeling of comparison of acetophenone hydrogenation in trickle-bed and slurry airlift reactors,'' *Chem. Eng. Sci.*,**1997**, *52*, 4033.
20. Guettel, R.; Turek, T. Comparison of different reactor types for low temperature fischer-tropsch synthesis: A simulation study. *Chem.Eng. Sci.*, **2009**, *64*, 955.
21 Rajashekharam, M. V.; Jaganathan, R.; Chaudhari, R.V. A trickle-bed reactor model for hydrogenation of 2, 4 Dinitrotoluene: Experimental verification. *Chem. Eng. Sci.***, 1998**, *53*, 787.
22. Tan, C. S.; Smith, J. M. Catalyst particle effectiveness with unsymmetrical boundary conditions. *Chem. Eng. Sci.,* **1980**, *35*, 1601.
23..Chaudhari, R.V.; Ramachandran, P.A. Mass transfer in trickle bed reactors. Heat & Mass Transfer in porous Media (Eng)., Edited by Q. Michel; A. Marija S. Elsevier (Amsterdam), Netherlands**, 1993**, p.633.
24. Bischoff, K. B. Effectiveness factors for general reaction rate forms. *A.I.Ch.E. Journal.*, **1965**, *11*, 351.
25. Hochmann, J. M.; Effron, E. Two phase cocurrent downflow in packed beds. *Ind. Eng. Chem. Fundam.***1969**, *8*, 63.
26. Wilke, C. R.; Chang, P. Correlation for diffusion coefficients in dilute solutions. *A.I.Ch.E.Journal,* **1955**, *1*, 264.

27. Goto, S.; Smith, J. M. Trickle bed reactor performance Part II: reaction studies. *A.I.Ch.E.Journal,* **1975***,* 21, 706.
28. Satterfield, C. N.; Vab Eek, M. W.; Bliss, G. S. Liquid-solid mass transfer in packed beds with down flow cocurrent gas-liquid flow. *A.I.Ch.E.Journal*, **1978***, 24*, 709.
29. Duducovic A.; Milosevic, V.; Pjanovic, R. Gas-solid and gas-liquid mass transfer coefficients. *A.I.Ch.E. Journal*, **1996**, *42*, 269.
30. Sato, Y.; Hiros, T.; Takahashi, F.; Toda, M. Pressure loss and liquid holdup in packed bed reactor with cocurrent gas-liquid flow. *J. Chem. Eng. Japan,* **1973**, 6, 147.
31. Baldi, G. In *Multiphase Chemical Reactors, Vol.* II *Design Methods,* eds, A. E. Rodrigues, J. M. Cole and N, M. Sweed, Sithoff and Noorldhoff, USA, **1981**, p. 307.
32. Al-Dahhan, M. H.; Larachi, F.; Dudukovic, M. P.; Laurent, A. High-pressure trickle-bed reactors: A Review,'' *Ind. Eng. Chem. Res.*, **1997**, *36*, 3292.
33. Michell, R.W.; Furzer, I.A. Mixing in trickle flow through packed beds. *Chem. Eng. J.*, **1972**, *4*, 53.
34. Zai-Sha, M.; Tian-Ying, X.; Chen, J. Theoretical predictions of static liquid hold up in trickle bed reactors and comparison with experimental results. *Chem. Eng. Sci.*, **1993**, *48*, 2697.
35. Sicardi, S.; Baldi, G.; Gianetto, A.; Specchia, V. (1980) Catalyst area wetted by flowing liquid and semi stagnant liquid in trickle bed reactors. *Chem. Eng. Sci.*,**1980**, *35*, 67.
36. Colombo, A. J.; Baldi, G.; Sicardi, S. Solid-liquid contacting effectiveness in trickle bed reactors. *Chem. Eng. Sci.* **1976**, *31*, 1101.
37. Chaudhari, R.V.; Jaganathan, R.; Mathew, S.P.; Julcour, C.; Delmas, H. Hydrogenation of 1,5,9-Cyclododecatriene in fixed bed reactors: down-Vs-upflow modes. *A.I.Ch.E. Journal*, **2002**, *48*, 110.
38. Guo, J.; Al-Dahhan, M. A sequential approach to modeling catalytic reactions in packed bed reactors. *Chem. Eng. Sci.*, **2004**, *59*, 2023.
39. Reiss, L. P. Cocurrent gas-liquid contacting in packed columns. *Ind. Eng. Chem. Proc. Des. Dev*., **1967**, *6*, 486.
40. Specchia, V.; Baldi, G.; Gianetto, A. Solid-liquid mass transfer in cocurrent two-phase flow through packed beds. *Ind. Eng. Chem. Proc. Des. Dev*., **1978**, 17, 362.
41. Turpin, J. L.; Huntington, R. L. Prediction of pressure drop for two phase, two component cocurrent flow in packed beds. *A.I.Ch.E. Journal.*, **1967**, *13*, 1196.
42. Steigel, G. J.; Shah, Y. T. Backmixing and liquid holdup in gas-liquid cocurrent upflow packed column. *Ind. Eng. Chem. Proc. Des. Dev.*, **1977**, *16*, 37.
43. Bern, L.; Lidefelt, J.O.; Schoon, N.H. Mass transfer and scale up in fat hydrogenation. *J. Am. Oil. Chem. Soc.*, **1976**, *53*, 463.
44. Sano, Y.; Yamaguchi, N.; Adachi, T. Mass transfer coefficients for suspended particles in agitated vessels and bubble columns. *J. Chem. Eng. Japan*, **1974**, *7*, 255.
45. Luong, H. T.; Volesky, B. Mechanical power requirements of gas-liquid agitated systems. *A.I.Ch.E. Journal*, **1979**, *25*, 893.
46. Loiseau, B.; Midoux, N.; Charpentier, J.C. Some hydrodynamics and power input data in mechanically agitated gas-liquid contactors. *A.I.Ch.E. Journal*, **1977**, *23*, 931.
47. MATLAB 7, Release 14, The MathWorks, Inc., **2004**.
48. Khadilkar, M. R.; Wu, Y. X.; Al-Dahhan, M. H.; Dudukovic M.P. Comparison of Trickle Bed and Upflow Reactor Performance at High Pressure: Model prediction and experimental observations. *Chem. Eng. Sci.*, **1996**, *51*, 2139.
49. Mears, D.E. Tests for transport limitations in experimental catalytic reactors. *Ind. Eng. Chem.. Process Des. Dev.*, **1971**, *10*, 541.
50. Cassanello, M.C.; Martinez, O.M.; Cukierman, A.L. Effect of liquid axial dispersion on the behavior of fixed bed three phase reactors. *Chem. Eng. Sci.*, **1992**, *47*, 3331.
51. M.C. Cassanello, A.L. Cukierman, O.M. Martinez, Actas del V Congreso Latinoamericano de Transferencia de Calor y Materia, IID-5.1, **1994**.
52. Cassanello, M.C.; Cukierman A.L.; Martinez, O.M. General criteria to analyze the role of mass transfer and hydrodynamics in trickle bed reactors. *Chem. Eng. Technol.*, **1996**, *19*, 410.
53. Khare, A. S.; Dharwadkar, S.V.; Joshi, J.B.; Sharma, M. M. Liquid- and solid-Phase mixing in sectionalized bubble column slurry reactor. *Ind. Eng. Chem. Res.*, **1990**, *29*, 1503.

CHAPTER 5

CFD Modeling of Pulverized Biomass Combustion in an Entrained Flow Reactor

5.1 INTRODUCTION

Biomass being an important renewable energy source is attracting more attention in order to improve understanding of their process characteristics during mass to energy conversion. Their use in co-combustion plants is limited at present but represents a short time option for reducing CO_2 emissions.[1] The increase of biomass/coal ratio can be achieved by optimizing the operating conditions. To this purpose, data are required for conditions similar to large plants, which operate at high heating rate and short residence time. The basic mechanism (in combustion as well as gasification reactors) is a fast pyrolysis with release of volatile species. The behavior of biomass is much different as compared to fossil fuels and the effect of the operating conditions on pyrolysis parameters are known to be important.[2] Any rational attempt to design this type of application requires detailed knowledge of the rate laws describing the evolution of biomass particles (devolatilization and subsequent oxidation) under realistic conditions.[3]

The devolatilization and combustion rates of different types of biomass can be obtained from the well-defined experiments in the laboratory. The methods like fluid bed reactors,[4,5,6] thermogravimetric analysis,[7,8,9,10] entrained flow reactor (EFR),[11,12,13] wire mesh reactor,[14] and radiant heating techniques[15,16] are commonly employed to characterize the different types of fuels. Some of these studies reproduced the reaction conditions closer to those encountered in practical combustors and some of the experiments were not specifically designed to derive any reaction rate information. Furthermore only few studies were devoted to provide the kinetic parameters for high temperature processes. Most of the previous experimental research in this field concerns thermogravimetric tests performed at low heating rates and/or relatively low temperatures.[7] Some studies show the comparisons of the observed pyrolysis rates for big isolated particles with model predictions, but ultimately based, again, on the kinetics of the involved reactions determined by thermogravimetric analysis.[8, 9, 10] Therefore, thermogravimetric analysis can give only a fingerprint of the fuel, because the thermal conditions are far from those of practical applications. The pyrolysis kinetics changes substantially with varying the heating rate.[17] The EFR has short residence time (< 5 s), high heating rates (10^4-10^5 K/s) and varying O_2 concentration. EFR offers conditions similar to those in practical systems like pulverized fuel (pf) combustors and therefore is a better choice. However, only few experimental

works have been found in the open literature addressing the evolution of biomass particles under conditions representative of pf systems.[3,18,19,20,21] The biomass burnout data obtained from the EFR experiments is useful to obtain global/apparent kinetic rate parameters representing the devolatilization and char oxidation.

The devolatilization and subsequent oxidation rates are usually represented by Arrhenius-type rate expression. The associated kinetic parameters (pre-exponential factor and activation energy) can be obtained by the methods like Arrhenius plot method or development of plug flow model, which is fitted to experimental biomass burnout data along the length of EFR. [3,18,22,23] The Arrhenius plot method has several intrinsic drawbacks like the oxidation rate constant is based on single representative particle size and the values of kinetic parameters obtained are specific to the set of experimental measurements obtained.[24] Whereas, plug flow models can account for particle size distribution and complete devolatilization and combustion history of biomass particles along the length of EFR. These estimated kinetic parameters can be used as input parameters for combustion sub model in simulating large scale combustors that may be based on lumped model approach[25] or more recent computational fluid dynamic (CFD) models.[26,27,28]

Substantial progress has been made in the development and application of comprehensive multidimensional computational combustion models for fossil fuels. These models are now accessible as features in commercially available CFD computer codes.[29] Eaton *et. al.*[30] in an extensive review paper discussed the types of the data required to validate the predictions of combustion model and the current status of the combustion models and submodels. During the past years, few authors have used CFD tools to explore potential applications of biomass combustion in industrial pf combustors.[31,32] Invariably the kinetic data used in these models for both devolatilization and char oxidation are based on thermogravimetric analysis of the raw fuel or char prepared in the reactor, performed at low heating rates. As happens in case of coal combustion, the extrapolation of those results to the conditions found in the burners of pulverized biomass may entail severe uncertainties.[33] Brown *et. al.*[34] used CFD to model the gas and particles flow in a laminar EFR. The CFD model did not account for reactions on the particles, which were assumed to be nonreactive. In the procedure it was assumed that the impact of solid particles and

product gases on the flow and temperature of the bulk flow is negligible. This makes sense, when the flow of the solid fuel is significantly lower than that of the bulk flow. Marklund *et. al.*[35] investigated numerically through CFD an entrained flow gasifier with the fuel injections generating a swirl flow. The authors highlighted the complexity of the model and the need of validation with the experimental results. Meesri and Moghtaderi[13] evaluated the capability of a CFD code to predict sawdust combustion conversions. They developed a model introducing global kinetic parameters obtained through experiments. The agreement between predicted and experimental results was very good but the data were obtained only for very high conversions. Also there are few attempts to validate the devolatilization or char oxidation characteristics of pf biomass in EFR by using CFD models.[13, 36,37] Such studies have been reported for single operating conditions or at lower operating temperatures and concerns with CFD prediction validation focused on near complete devolatilization or char oxidation.

Recently, Jimenez *et. al.*[3] have done systematic experimental studies to characterize devolatilization and oxidation of pulverized biomass (*Cynara cardunculus*). The apparent kinetic rate parameters were derived by developing one dimensional (1D) plug flow model, which may be useful for the development of the detailed multidimensional CFD model for biomass combustion systems. The plug flow models are generally simple, can account for particle size distribution (PSD) and the complete combustion history of the biomass particles along the length of EFR. However plug flow model doesn't account for the radial variations in velocity, temperature, O_2 concentration, particle trajectory and effects of inlet configuration. These may have influence on the predictions of the burnout behavior, as the particles at the same axial distance can experience different oxygen and temperature history at various radial locations. In order to account these effects, it is required to develop multidimensional CFD model for EFR, which can handle multiple complex and simultaneous processes like fluid flow, heat transfer, particle trajectories and chemical reactions.

The present work attempts to develop a methodology for coupling CFD model and experimental measurements for providing valuable global kinetic parameters to large scale applications of biomass fuels (fast pyrolysis, co-combustion and gasification). For this purpose, the experimental results recently reported by Jimenez *et. al.*[3] were used. The 1D

plug flow model and two dimensional (2D) axisymmetric CFD model were developed based on the experimental results available in Jimenez *et. al*.[3] The comparison between the predictions of 1D plug flow model and 2D axisymmetric CFD model is discussed. The sensitivity study on various model parameters was performed and their role in prediction of the devolatilization and char oxidation characteristics of biomass has been discussed. The proximate and ultimate analyses of biomass are listed in Table 5.1. The details of CFD model equations are discussed in the following section.

Table 5.1. Biomass Composition[3]

Proximate analysis	Wt. %	Ultimate analysis	Wt. %
Moisture	12.26	C	38.57
Ash	6.57	H	5.33
Volatiles	70.6	N	0.55
Fixed carbon	10.57	S	0.1
		O (By difference)	36.62

5.2 CFD MODEL

5.2.1 Entrained Flow Reactor

The entrained flow reactor considered in this work[3] has internal tube diameter 78 mm and total tube length of 1600 mm. There are two inlets; first is for the injection of transportation air with the biomass particles at the center of the EFR and the second is for the coaxial entry for auxiliary air. When the biomass particles are injected into the reactor furnace, they quickly gets heated at a rate 10^4 K/s. The particle then undergoes four distinctive processes namely drying, volatile release, volatile combustion and char combustion. The schematic and detailed description of EFR can be found elsewhere[3] and is not repeated here. In the present work, CFD model has been developed to simulate experiments recently reported by Jimenez *et. al.*[3]

5.2.2 Model Assumptions

The following assumptions were made for the development of CFD model and that are same as Jimenez *et. al.*[3]

- The oxygen first reacts with carbon to form CO, which diffuses into gas phase and subsequently gets oxidized to CO_2
- During the combustion of biomass particles, the diameter of particle remains constant and the density of the particle changes
- The shape of the particle was assumed to be spherical

5.2.3 Mathematical Equations

As the dispersed phase was present in low volume fraction (< 1%), the Eulerian/Lagrangian approach was chosen to describe the gas phase and solid particles motion. The gas phase was solved in the Eulerian reference frame, by solving equations for mass conservation, chemical species transport, momentum transport and energy balance. The biomass particles were solved in the Lagrangian reference frame, by solving mass, force and energy balances on the particles. A fully coupled method is needed to take into account the interactions (through chemical species, momentum and heat) between the gas and solid phases. The gas phase in EFR was laminar (NR_e < 500). Radiation was taken into account through discrete ordinate (DO) model in the energy equation. The detailed description of mathematical equations involved in CFD model is given in the following section.

5.2.3.1 Multiphase Flow Governing Equations

5.2.3.1.1 Mass Balance

The entrained flow reactor was modeled with 2D axisymmetric computational domain as the combustion process is almost completed in the central core region of the EFR and the flow does not show any significant variation in the azimuthal direction.[38] The schematic of 2D axisymmetric model is shown in Figure 5.1-A. For steady state, 2D axisymmetric, continuity equations for continuous phase can be written as

$$\frac{1}{r}\frac{\partial}{\partial r}(\rho r U)+\frac{\partial}{\partial z}(\rho W) \quad = S_m \qquad 5.1$$

where, ρ is density of fluid, U and W are the fluid velocity in radial r and axial direction z respectively and the S_m is the source term for the total mass added from the discrete phase.

The species conservation equation can be written as

$$\frac{1}{r}\frac{\partial}{\partial r}\left(\rho r U m_k\right)+\frac{\partial}{\partial z}\left(\rho W m_k\right) = \frac{1}{r}\frac{\partial}{\partial r}\left(\rho D_{km} r \frac{\partial m_k}{\partial r}\right)+\frac{\partial}{\partial z}\left(\rho D_{km}\frac{\partial m_k}{\partial z}\right)+R_k+S_k \quad 5.2$$

where, m_k is mass fraction of species k, D_{km} is the diffusion coefficient for species k in the mixture, R_k is the net rate of production of species k by gas phase chemical reactions, S_k is the source of species k from dispersed phase. The net source of chemical species k due to reaction is computed as the sum of the Arrhenius reaction sources over the N_r reactions that the species participate in,

$$R_k = M_{w,k}\sum_{r=1}^{Nr} R_{k,r} \quad 5.3$$

$$R_{k,r} = \left(v'_{k,r} - v_{k,r}\right) K_r \prod_l \left[C_{l,r}\right]^{n_l,r} \quad 5.4$$

where, $C_{l,r}$ is the molar concentration of each reactant l^{th} species in reaction r, $\eta'_{l,r}$ exponent for each l^{th} reactant in reaction r, $v'_{k,r}$ and $v_{k,r}$ are stoichiometric coefficient for k^{th} species as product and reactant respectively, K_r is the kinetic rate constant.

The source term S_k from the dispersed phase is written as

$$S_k = \frac{\Delta\left(\dot{m}_{pk}\right)}{V} \quad 5.5$$

$$S_m = \sum_k S_k \quad 5.6$$

where, $\dot{m}_{pk}$ is the particle mass flow rate of component k corresponding to the number of particles that crosses the cell, Δ is the change in the property across that cell and V is the cell volume.

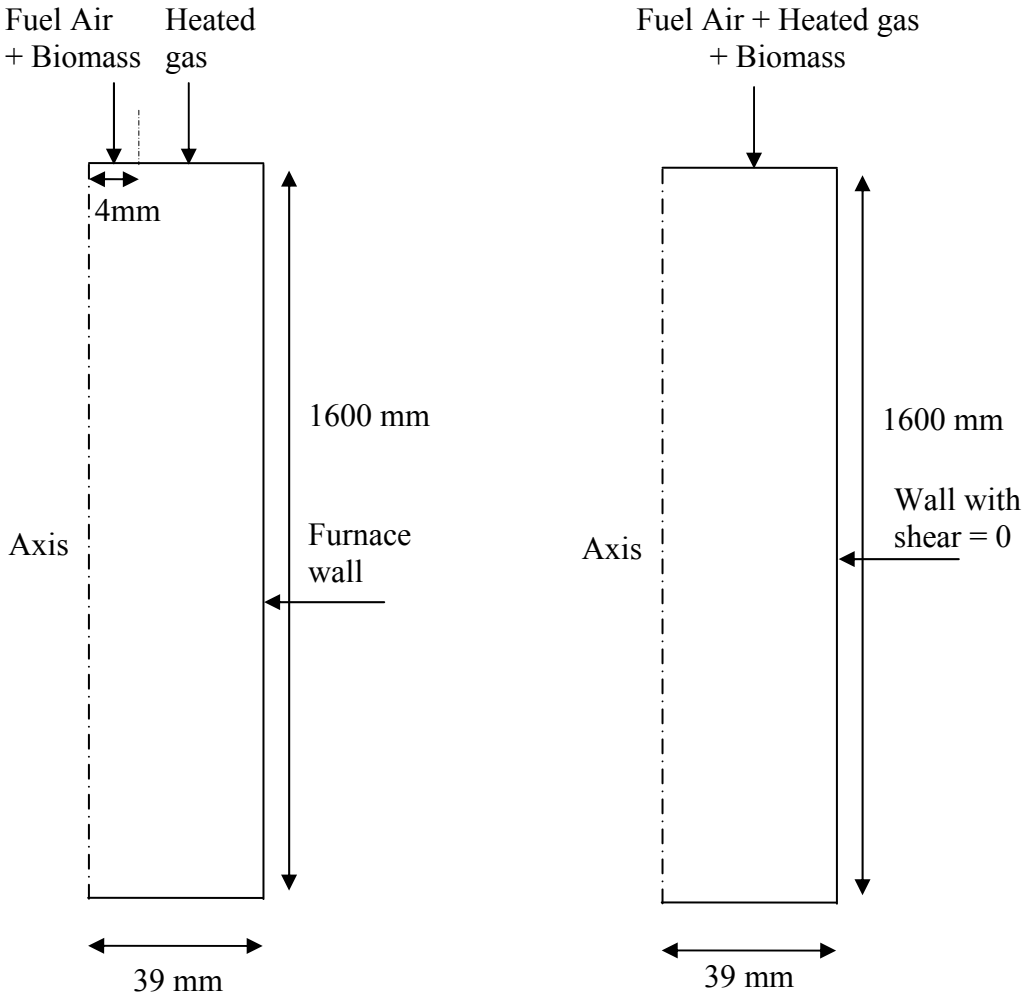

(A) 2D Axisymmetric Reactor (B) 1D Plug Flow Reactor

Figure 5.1. Computational domain of entrained flow reactor

5.2.3.1.2 Momentum Balance

The momentum equation for continuous phase in radial *r* and axial *z* direction can be written as

Radial momentum, *r*

$$\frac{1}{r}\frac{\partial}{\partial r}(\rho r U U)+\frac{\partial}{\partial z}(\rho W U) = \frac{1}{r}\frac{\partial}{\partial r}\left(\mu r\frac{\partial U}{\partial r}\right)+\frac{\partial}{\partial z}\left(\mu\frac{\partial U}{\partial z}\right)+F_z+S_U \qquad 5.7$$

Axial momentum, z

$$\frac{1}{r}\frac{\partial}{\partial r}(\rho r U W)+\frac{\partial}{\partial z}(\rho W W) = \frac{1}{r}\frac{\partial}{\partial r}\left(\mu r\frac{\partial W}{\partial r}\right)+\frac{\partial}{\partial z}\left(\mu\frac{\partial W}{\partial z}\right)+F_r+S_W \quad 5.8$$

Source term for r momentum $S_U=-\frac{\partial p}{\partial r}+\frac{1}{r}\frac{\partial}{\partial r}\left(\mu r\frac{\partial U}{\partial r}\right)+\frac{\partial}{\partial z}\left(\mu\frac{\partial W}{\partial r}\right)-\frac{2\mu U}{r^2}$

Source term for z momentum $S_W=-\frac{\partial p}{\partial z}+\frac{1}{r}\frac{\partial}{\partial r}\left(\mu r\frac{\partial U}{\partial z}\right)+\frac{\partial}{\partial z}\left(\mu\frac{\partial W}{\partial z}\right)$

The momentum source term F, for a particular cell is calculated from every particle trajectory j crossing that cell

$$F_i=\frac{\Delta\left(\dot{m}_{pk}\,u_{p,i}\right)}{V} \quad 5.9$$

where $u_{p,\,i}$ is the velocity components of the particle in i^{th} direction (r or z)

5.2.3.1.3 Energy Balance

The overall energy balance can be written as

$$\frac{1}{r}\frac{\partial}{\partial r}(\rho r U h)+\frac{\partial}{\partial z}(\rho W h) = \frac{1}{r}\frac{\partial}{\partial r}\left(k r\frac{\partial T}{\partial r}\right)+\frac{\partial}{\partial z}\left(k\frac{\partial T}{\partial z}\right)+S_h \quad 5.10$$

where, k is the thermal conductivity of gas, h is an enthalpy. The volumetric source term, S_h is sum of heat of gas phase chemical reactions ($S_{h\,rxn}$), heat added from discrete phase (S_Q) and radiation (S_R).

$$S_h = S_{h,rxn} + S_Q + S_R \quad 5.11$$

$$h=\sum_k m_k h_k \quad \because h_k=\int_{Tref}^{T} C_{pk}\,dT \quad 5.12$$

The heat released due to chemical reactions is

$$S_{h,rxn}=-\sum_k \frac{\left(h_k^0+\int_{Tref}^{T}\Delta C_{pk}\,dT\right)R_k}{M_k} \quad 5.13$$

where, R_k the volumetric rate of creation of species k, h_k^0 is the formation enthalpy of species k at the reference temperature T_{ref}

The heat added from the discrete phase is due to char oxidation

$$S_Q = \sum_j \frac{\left[(1 - f_{heat})\Delta(\dot{m}_c)H_c\right]_j}{V} \quad 5.14$$

The f_{heat} is the fraction of heat absorbed by the particle, H_c is heat released during char oxidation.

5.2.3.2 Particle Motion Equations

The discrete phase was modeled by using Lagrangian approach. The discrete phase momentum balance on single particle of size j, can be written as

$$\frac{du_{p,i,j}}{dt} = \sum F_{i,j} \quad 5.15$$

where, F_{ij} is the sum of the forces acting on the particle in i^{th} direction. If only gravity and drag force acting on particle of size j is considered, then F_{ij} can be written as

$$\sum F_{i,j} = \frac{(\rho_p - \rho_g)}{\rho_p} g + \frac{18\mu}{d_{p,j}{}^2 \rho_p} \frac{C_D \mathrm{Re}_p}{24} (u_{p,j,i} - v_i) \quad 5.16$$

where, ρ_P, d_p and $u_{p,i,j}$ are the density, diameter and velocity components of the particle of size j in i^{th} direction (r or z), μ is the viscosity of gas phase, g is gravitational constant and C_D is drag coefficient, v_i is the velocity component of gas phase (U or W). Morsi and Alexander [39] correlation was used to calculate C_D.

The trajectory of particles of size j in radial and axial direction can be calculated as

$$\frac{dx_{i,j}}{dt} = u_{p,i,j} \quad 5.17$$

Species conservation equations for single particle can be written as

$$\frac{d\left(M_{p0} m_k\right)}{dt} = S_{pk} \quad 5.18$$

The M_{p0} is the initial mass of biomass particle; m_k is the mass fraction of species k.

S_{pk} can be formulated by considering various particle level phenomena of interest such as devolatilization and surface reaction-char combustion. Hence the S_{pk} can be written as

$$S_{pk} = M_{p0}\left[\frac{dm_v}{dt} + \frac{dm_c}{dt}\right] \qquad 5.19$$

where, the m_v and m_c is mass fraction of volatile and char respectively.

5.2.3.3 Reaction Kinetics

The devolatilization was modeled using simple single step Arrhenius type kinetic rate model. The biomass devolatilization rate can be written as [40]

$$\frac{dm_v}{dt} = -A_v e^{(-Ev/RT_P)}\left(m_{v_0} - m_v\right) \qquad 5.20$$

where, m_{v0} indicates the total initial volatile mass fraction in the biomass and m_v is the fraction of volatile released from the biomass, A_v is the pre exponential factor for devolatilization, E_v is the activation energy for devolatilization, T_p is the temperature of the particle and R is the universal gas constant.

Char combustion rate was calculated by using kinetic/diffusion model of Baum and Street,[41] which is available in Fluent[42]. It was assumed that the char gets oxidized to CO by following reaction.

$C_{(s)}$ + 0.5 $O_{2\,(g)}$ => CO $_{(g)}$ (i)

This model is simple in implementation and needs apparent kinetic rate constant, which accounts for both chemical and internal pore diffusion resistance.

The rate of char oxidation for any particle can be written as, [41,43]

$$M_{p0}\frac{dm_c}{dt} = -A_p\frac{K_c K_d}{K_c + K_d}Y_{O_2}\frac{\rho_g R T_g}{MW_{O_2}} \qquad 5.21$$

where, the kinetic rate constant for char oxidation reaction is

$$K_c = A_C\, e^{(-E_C/RT_P)} \qquad 5.22$$

where, A_c is pre exponential factor and, E_c is the activation energy for char combustion.

The bulk gas phase diffusion coefficient for oxidant [43] can be given as,

$$K_d = \frac{5\times10^{-12}}{d_p}\left(\frac{T_g + T_p}{2}\right)^{0.75} \quad 5.23$$

U is unburnt fraction of biomass and can be written as

$$U = \frac{\sum_j N_{p,j} w_j \left(m_v + m_c\right)}{M_{v0} + M_{c0}} \quad 5.24$$

where, w_j is the initial mass of particle of size j, M_{v0} and M_{c0} are the initial mass of volatile and char respectively and $N_{p,j}$ is number of particle of size j and can be written as

$$N_{p,j} = \frac{w_j}{\left(\frac{\rho_p^0 \pi \left(d_{p,j}^0\right)^3}{6}\right)} \quad 5.25$$

The sources of inter-phase transport are

$$\Delta\left(\dot{m}_{pk}\right) = \sum_j N_{p,j}\, w_j \frac{d\left(m_k\right)}{dt} \quad 5.26$$

and

$$\Delta\left(\dot{m}_p\right) = \sum_k \Delta\left(\dot{m}_{pk}\right) \quad 5.27$$

The volatile material was represented by single species as VOL ($CH_{2.28}O_{0.98}$), which was estimated from proximate and ultimate analysis of biomass. Following two gas phase reactions were assumed:

$CO_{(g)}$ + $0.5\ O_{2\,(g)}$ => $CO_{2\,(g)}$ (ii)

$VOL_{(g)}$ + $1.08\ O_{2\,(g)}$ => $CO_{2\,(g)}$ + $1.14\ H_20_{\,(g)}$ (iii)

The rate of gas phase reactions of $CH_{2.28}O_{0.98}$ and CO resulting from the char combustion was determined by Arrhenius type rate expression[44,45]

$$K_r = A_r\, e^{(-E_r / RT)} \quad 5.28$$

5.2.3.4 Heat Transfer

The radiative heat transfer in EFR was modeled by using discrete ordinate (DO) model. DO is considered to be more suitable for systems having optical thickness (equal to characteristic dimension of EFR absorption coefficient) is less than 1.[38, 42] As the optical

thickness was found to be less than 0.06 [0.078 (m) * 0.77 (m^{-1})] for the EFR considered here, DO model was used to model the radiative heat transfer. DO model solves the transport equation of radiation intensity, I in the direction $\vec{s}$ and can be written as

$$\nabla \cdot (I\,\vec{s}) + \left(a + a_p + \sigma_p\right) I(\vec{r},\vec{s}) = an^2 \frac{\sigma T^4}{\pi} + E_p + \frac{\sigma_p}{4\pi} \int_{\Omega=0}^{4\pi} I(\vec{r},\vec{s}^{\,'})\,\phi\left(\vec{s},\vec{s}^{\,'}\right) d\Omega^{'} \qquad 5.29$$

where, I is radiant intensity, $\vec{r}$ is position vector, $\phi\left(\vec{s},\vec{s}^{\,'}\right)$ is scattering phase function, σ is Stefan Boltzmann constant, a is absorption coefficient of gas phase. Here, isotropic scattering (i.e., scattering that is equally likely in all directions) was assumed and for isotropic scattering $\phi\left(\vec{s},\vec{s}^{\,'}\right)$ =1.

a_p is the equivalent absorption coefficient due to the presence of particulates, and is defined as $a_p = \lim_{V\to 0} \sum_{n=1}^{N} \varepsilon_{pn} \frac{A_{pn}}{V}$ 5.30

The equivalent emission E_p is defined as,

$$E_p = \lim_{V\to 0} \sum_{n=1}^{N} \varepsilon_{pn} A_{pn} \frac{\sigma T_{pn}^{\,4}}{\pi V} \qquad 5.31$$

The equivalent particle scattering factor σ_p, is given as

$$\sigma_p = \lim_{V\to 0} \sum_{n=1}^{N} \left(1 - f_{pn}\right)\left(1 - \varepsilon_{pn}\right) \frac{A_{pn}}{V} \qquad 5.32$$

and it is computed during particle tracking. The f_{pn} is the particle scattering factor associated with the n^{th} particle.

The energy balance for the single particle can be calculated as

$$M_p Cp_P \frac{dT_P}{dt} = \left(f_{heat} M_{p,0} \frac{dm_c}{dt} H_c \right) + Q_{rad} + Q_{conv} \qquad 5.33$$

Here, M_p is mass of particle at any time, C_{pp}, Q_{rad} and Q_{conv} are the particle specific heat, radiative and convective heat transfer respectively.

The particle radiative heat transfer can be written as

$$Q_{rad} = \varepsilon_P \sigma A_p (T_R^{\,4} - T_P^{\,4}) \quad 5.34$$

And the convective heat transfer can be written as

$$Q_{conv} = hA_P (T_g - T_P) \quad 5.35$$

where, ε_P is the emissivity of particle, σ Stefan-Boltzmann constant ($=5.67\times10^{-8}\, W/m^2K^4$), T_R is the radiation temperature $=\left(\frac{I}{4\sigma}\right)^{1/4}$ and h is heat transfer coefficient.

5.3 BOUNDARY CONDITIONS

5.3.1 1D Plug Flow Model

The following boundary conditions for 1D plug flow model were used based on the experiments reported by Jimenez *et. al.*[3]

a) Single inlet was defined for Fuel Air (FA), Heated Gas (PA) and was specified as mass flow rate (Figure 1-B) and the outlet was specified as outlet vent.
b) Biomass particle inlet temperature was assumed as 298K
c) For devolatilization, the gas was assumed to be partially heated at the entrance of the reactor.[46] The gas and particle inlet operating conditions are specified in Table 5.2.
d) The wall material was specified as silicon carbide and free slip condition was assigned to wall.
e) The wall was operated under isothermal conditions by specifying the respective operating temperature with emissivity = 0.96.[47]
f) The gas velocity was calculated based on the operating conditions and the same was patched in the computational domain.
g) For discrete phase, the biomass particles were injected from gas inlet by specifying it as group injection. The reflect condition was specified for the particles at the wall

and escape condition was specified at the outlet. All other model parameters are listed in Table 5.5.

5.3.2 2D Axisymmetric Model

The following boundary conditions for 2D axisymmetric CFD model were used based on the experiments reported by Jimenez *et. al.*[3]

a) Two separate inlets were specified for FA and PA. The FA and biomass particles were injected from FA inlet and the coaxial entry of hot gas was introduced from PA inlet (Figure 1-A)
b) For devolatilization, the gas was assumed to be partially heated at the entrance of the reactor. The gas and particle inlet operating conditions are specified in Table 5.3.[46]
c) For combustion, the gas inlet temperature was assumed to be same as operating temperature of EFR. The gas and particle inlet operating conditions are specified in Table 5.4.[46]
d) The gas flow inlet was defined as mass flow rate; the outlet was specified as outlet vent.
e) The wall was operated under isothermal conditions by specifying the respective operating temperature with emissivity = 0.96.[48] No slip condition was specified to the wall.
f) For discrete phase, the biomass particles were injected from the FA inlet by specifying it as group injection. The reflect condition was specified for the particles at the wall and escape condition was specified at the outlet. All other model parameters are listed in Table 5.5.

Table 5.2. Operating Conditions for Biomass Devolatilization for 1D Plug Flow Model

	Fuel air + Heated Gas			
	1073 K	1203 K	1313 K	1448 K
Mass flow rate(kg/s)	7.47×10^{-4}	7.47×10^{-4}	7.47×10^{-4}	7.47×10^{-4}
Inlet gas stream temperature (K)	500	500	500	500
Wall temperature (K)	1073	1203	1313	1448
Biomass particle temperature (K)	298	298	298	298
Biomass flow rate (kg/s)	1.111×10^{-5}			

Table 5.3. Operating Conditions for Biomass Devolatilization for 2D Axisymmetric CFD Model

	Fuel Air	Heated Gas			
	N_2	1073K	1203K	1313K	1448K
Mass flow rate (kg/s)	7.95×10^{-5}	6.68×10^{-4}	6.68×10^{-4}	6.68×10^{-4}	6.68×10^{-4}
Inlet stream temperature (K)	298	523.85	523.85	523.85	523.85
Wall temperature (K)	Operating temperature				
Biomass particle inlet temperature (K)	500				
Biomass flow rate (kg/s)	1.111×10^{-5}				

Table 5.4. Operating Conditions for Biomass Combustion for 2D Axisymmetric Model

Inlets	Fuel Air	Auxiliary Air	Auxiliary Air
Gas	Air	Heated gas (For T = 1313K, 1448K, 1573K and O_2 at outlet = 4 mol %)	Heated gas (For T=1448K and O_2 at outlet = 8 mol %)
Mass flow rate(kg/s)	8.21×10^{-5}	3.9×10^{-4}	3.95×10^{-4}
Temperature (K)	298	Operating temperature of EFR	
Mass fraction			
O_2	0.233	0.028	0.086
CO_2	-	0.133	0.125
H_2O	-	0.109	0.102
Biomass particle input temperature (K)		500	
Biomass flow rate (kg/s)		1.111×10^{-5}	

Table 5.5. Model Parameters

Parameter	Value	Reference
Particle emissivity	0.9	32
Particle scattering factor (f_p)	0.6	32
Swelling factor (S_w)	1	
Heat fraction (f_{heat})	1	49
Particle density (ρ_p), kg/m^3	450	3
Particle heat capacity (Cp_p), J/kg K	2300	
Emissivity of wall (silicon carbide wall)	0.96	47

5.4 NUMERICAL SIMULATION

Commercial CFD solver, FLUENT 6.3 (of Ansys Inc., USA)[42] was used to solve the mass, energy and momentum governing equations. The kinetic parameters were taken from Jimenez *et. al.*[3] and are specified in Table 5.6 unless stated explicitly. The Particle size distribution (PSD) data was obtained from Jimenez *et. al*[46], which is shown in Figure 5.2. The Rosin-Rammler equation was fitted to the PSD of the biomass particles and the model parameters were obtained as mean particle diameter = 640 μm and spread parameter = 2.877.

Table 5.6. Kinetic Parameters[3]

Devolatilization		Char oxidation	
A_v (s^{-1})	E_v (J/kmol)	A_c (kg/m^2sPa)	E_c (J/kmol)
47.17	11×10^6	0.00046	63×10^6

The influence of number of computational cells on prediction of biomass burnout was studied by performing simulations on uniform grid of size 5340 (20 x 267) to 83148 (78 x 1066). It was observed that the use of 20787 (39 x 533) cells were adequate to capture the burnout profile. Hence 20787 cells were used in all the subsequent simulations.

Preliminary numerical experiments were carried out to evaluate different discretization schemes and based on this second order accurate discretization scheme was used for all the subsequent simulations. Velocity and pressure coupling was handled by SIMPLE algorithm. For 1D plug flow model, the simulations were performed without solving flow whereas for the 2D axisymmetric model, the flow was solved. The residuals of velocity components, species, energy, radiation were monitored. Various criteria like insignificant change (<1%) in velocity, species, temperature and combustion profiles at various location of the EFR were used to decide appropriate level of convergence.

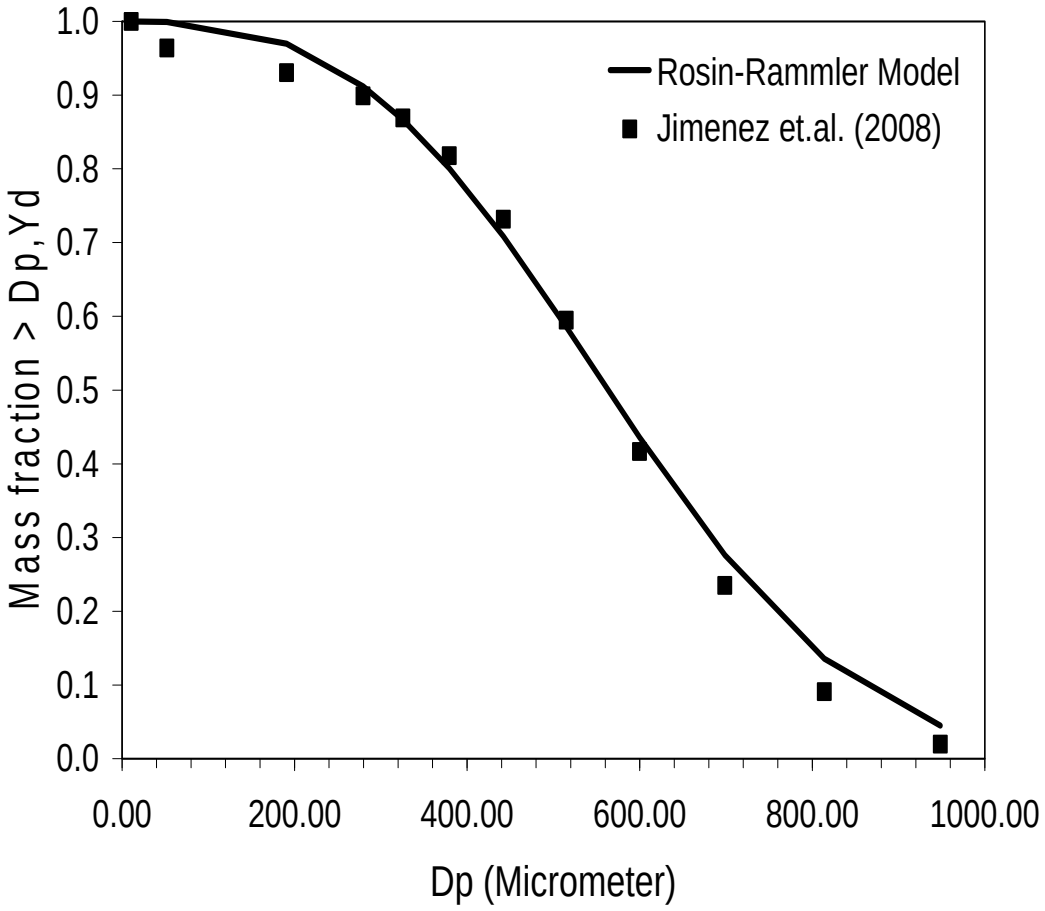

Figure 5.2. Rosin-Rammler fit to particle size distribution (PSD) data[3]

5.5 RESULTS AND DISCUSSION

Numerical investigation of the devolatilization and combustion characteristic of pulverized biomass in an EFR has been performed. Two types of models (1D plug flow model and 2D axisymmetric CFD model) were developed and used to simulate the experimental measurements reported recently by Jimenez *et. al.*[3] along the length of the EFR. It should be noted here that all the experimental data points of unburnt fraction of biomass presented in this work were taken from the paper of Jimenez *et. al.*[3] Simulation results obtained are discussed in the following section.

5.5.1 Biomass Devolatilization

5.5.1.1 1D Plug Flow Model

Numerical simulation of 1D Plug flow model of EFR was simulated to predict the biomass burnout. The optimized kinetic parameters reported by Jimenez *et. al.*[3] were used in this simulation (Table 5.6). In devolatilization series experiments, [46] the N_2 was injected through the same lines to the pre-burner chamber, and then passes across the honeycomb. Since both were hot, and there was a good contact, especially at the honeycomb, it was expected that the gases to be partially heated at the entrance of the EFR. Hence, the sensitivity of inlet gas stream temperature (T_g) was studied for all the operating temperatures in the range of 298K to respective operating temperature. Based on this study, the inlet gas stream temperature of 500K was found to be suitable to quantitatively capture the burnout behavior of biomass. Figure 5.3 clearly indicates that the 1D plug flow model developed in FLUENT shows a good agreement with the devolatilization experimental measurements with the kinetic parameters reported by Jimenez *et. al.*[3] This gives confidence in the CFD model developed in FLUENT. Hence, further 2D axisymmetric CFD model simulations were carried out with the T_g of 500K.

5.5.1.2 2D Axisymmetric CFD Model

The 2D axisymmetric model of EFR was simulated by specifying two separate inlets for FA and PA (Figure 1-A). The inlet FA temperature was taken as 298K and PA temperature was adjusted in such a way that overall T_g will be 500K. The kinetic parameters and particle inlet temperature (T_p) were similar to those used in 1D plug flow model studies. Figure 5.4 represents the comparison between experimental measurements and 2D axisymmetric CFD model predictions for all operating temperatures. Result shows that 2D axisymmetric model under predicts the devolatilization profile significantly. Therefore, it is necessary to check the sensitivity of predicted results with respect to various model parameters. First, the sensitivity studies were performed by varying the pre-exponential factor (A_v) in the range of 47.17 to 200 s^{-1}, keeping the activation energy at fixed value, for the operating temperatures of 1073K and 1448K. It was observed that the model could not capture the experimental measurements at lower temperature (1073K) in the initial period of devolatilization.

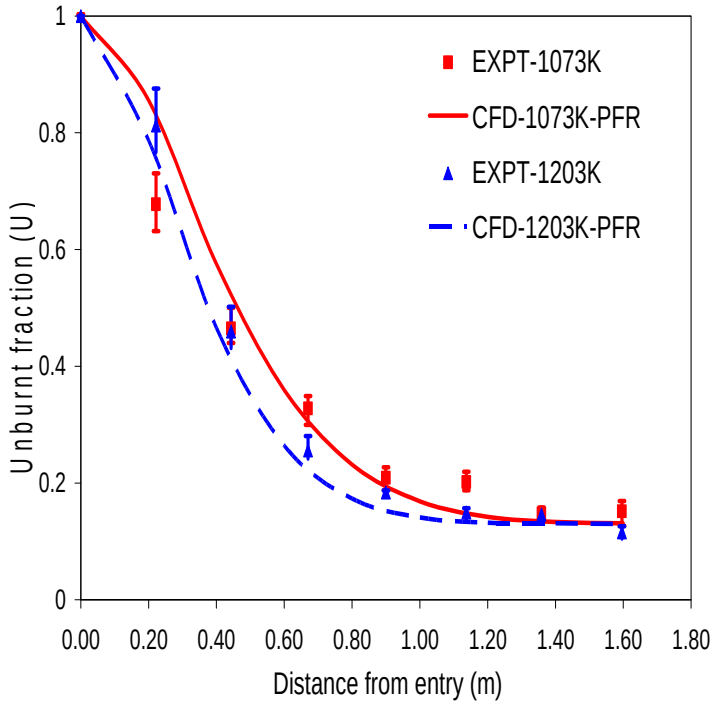

(A) 1073K and 1203K

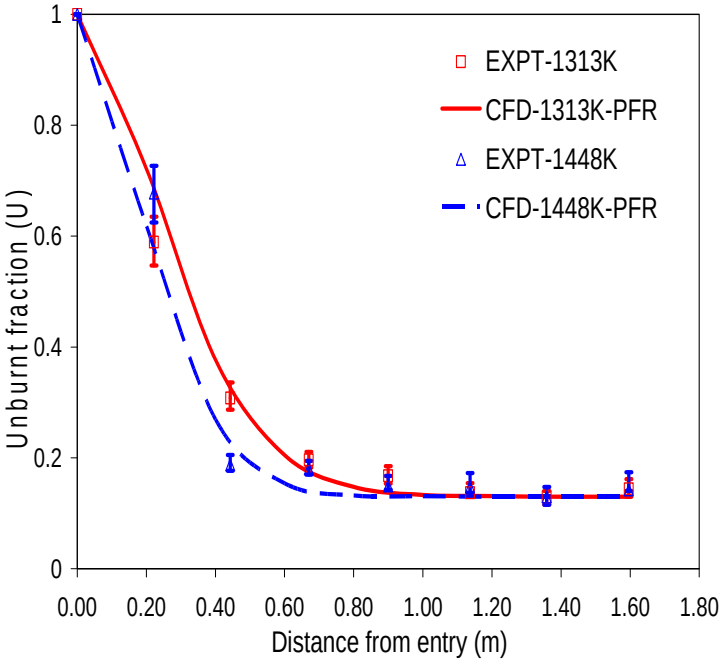

(B) 1313K and 1448K

Figure 5.3. Comparison of experimental results with 1D plug flow model predictions at various operating temperatures for inlet gas stream temperature of 500K

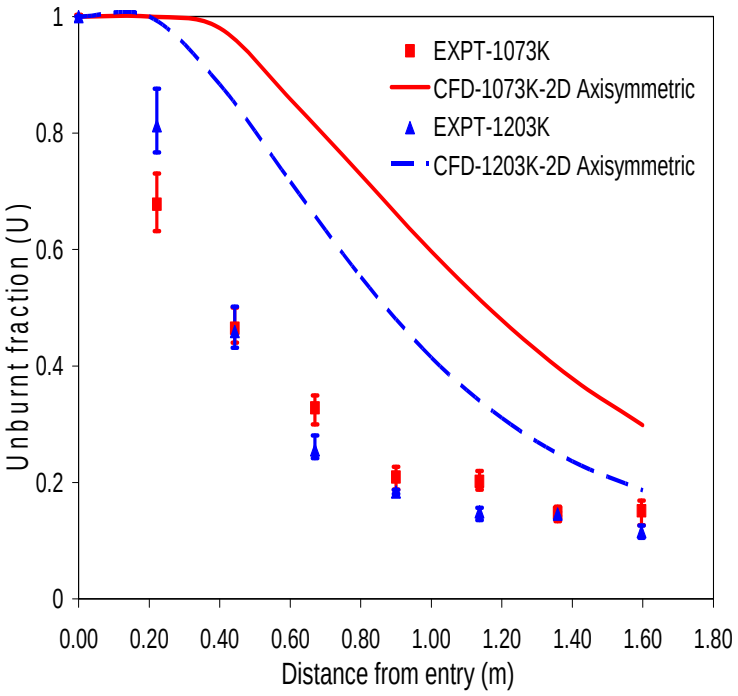

(A) 1073K and 1203 K

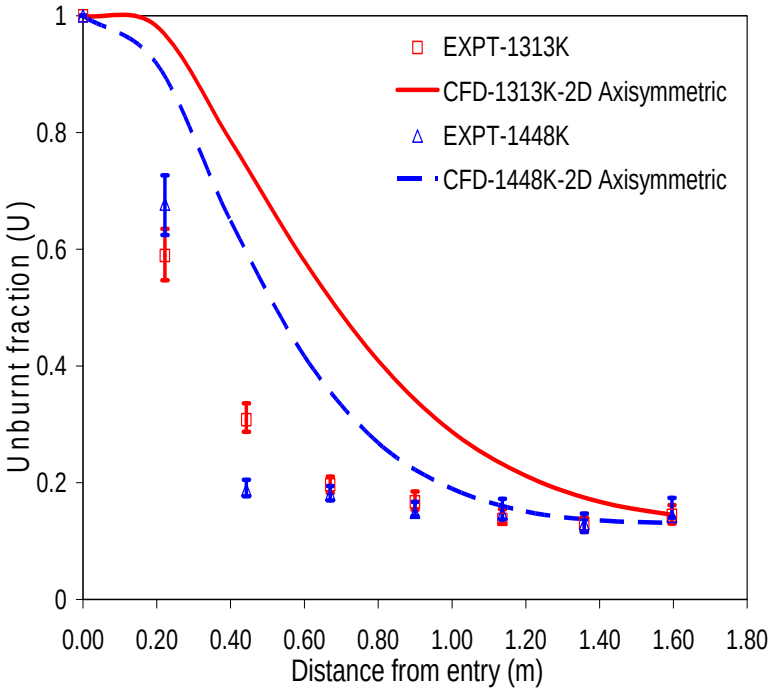

(B) 1313K and 1448K

Figure 5.4. Comparison between experimental measurements and 2D axisymmetric CFD model predictions

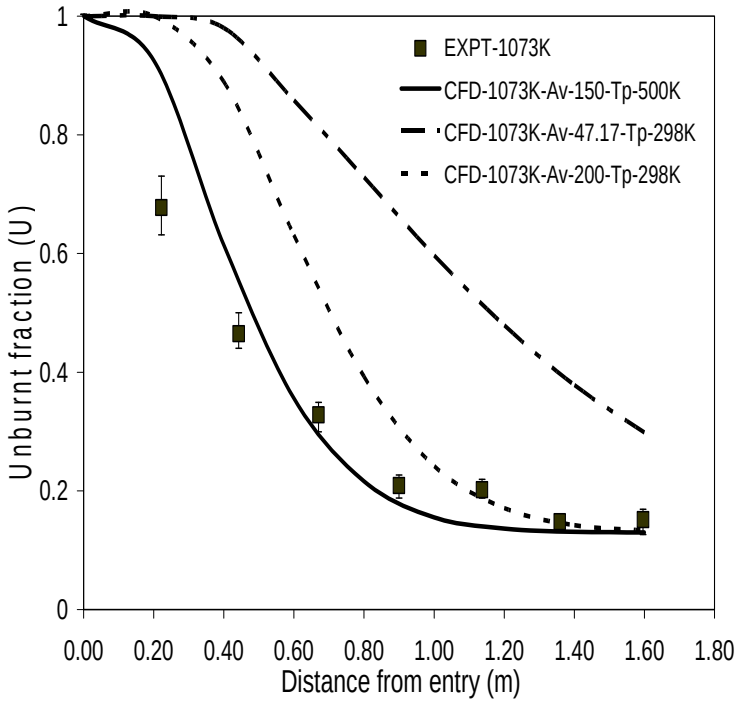

(A) 1073K

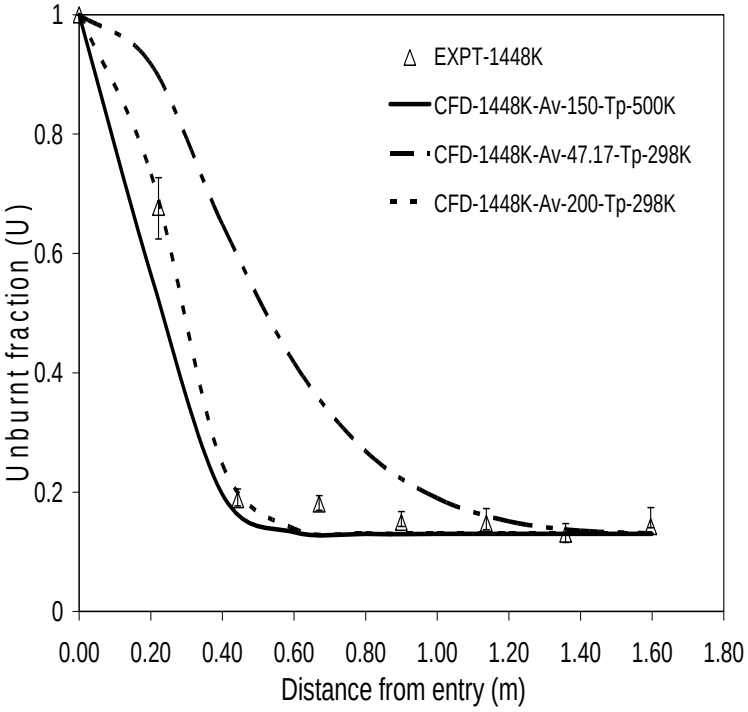

(B) 1448K

Figure 5.5. Comparison between experimental measurements and 2D axisymmetric CFD model predictions: Sensitivity of kinetic parameter A_v and particle inlet temperature T_p.

The model shows good agreement with the experimental measurements for higher temperature condition (1448K) for the high A_v value (A_v = 200 s^{-1}). Hence, the sensitivity studies were performed by varying T_p in the range of 298K to 500K and A_v in the range of 47.17 to 150 s^{-1}. The good agreement was observed between the experimental measurements and CFD model predictions with A_v = 150 s^{-1} and E_v = 1.1 $\times 10^7$ J/kmol. Simulation results in Figure 5.5 were shown for two temperatures 1073K and 1448K and similar observation was found for all other operating temperatures (see Figure 5.6).

It should be noted here that in 1D plug flow model studies, T_p and T_g were taken as 298K and 500K respectively. Whereas in 2D axisymmetric CFD model, T_p needs to be fine tuned to capture the burnout behavior of biomass. This is because in devolatilization series experiments[46], the fuel injection gun was located as low as possible to allow the co-flow gases to heat up along the upper half of the reactor. Hence, as FA and biomass particles were injected from FA inlet, it was expected that the gas and particles are partially heated at the entrance of the EFR. This phenomenon could not be captured in 1D plug flow model. To ensure this, 1D plug flow model was also simulated with the T_p of 500K, and observed that the model over predicts the experimental measurements. Hence, these input boundary conditions of 2D axisymmetric CFD model were used for the further simulations (Table 5.3).

Subsequently, the simulations were performed by varying the activation energy in the range of $0.1\times10^{+7}$ to $1.1\times10^{+7}$ J/kmol, keeping the pre-exponential factor (A_v = 47.17 s^{-1}) constant. Again the good agreement was observed between CFD model predictions and the experimental measurements with $E_v = 0.6\times10^{+7}$ J/kmol (Figure 5.6). This clearly shows that the devolatilization kinetic parameters play significant role in the prediction of burnout behavior.

The above sensitivity studies had given the range in which the A_v and E_v can be varied to capture the experimental burnout data. Simulations were performed with A_v = 98.58 s^{-1} and then the value of E_v was tuned to fit the experimental burnout data. It was observed that

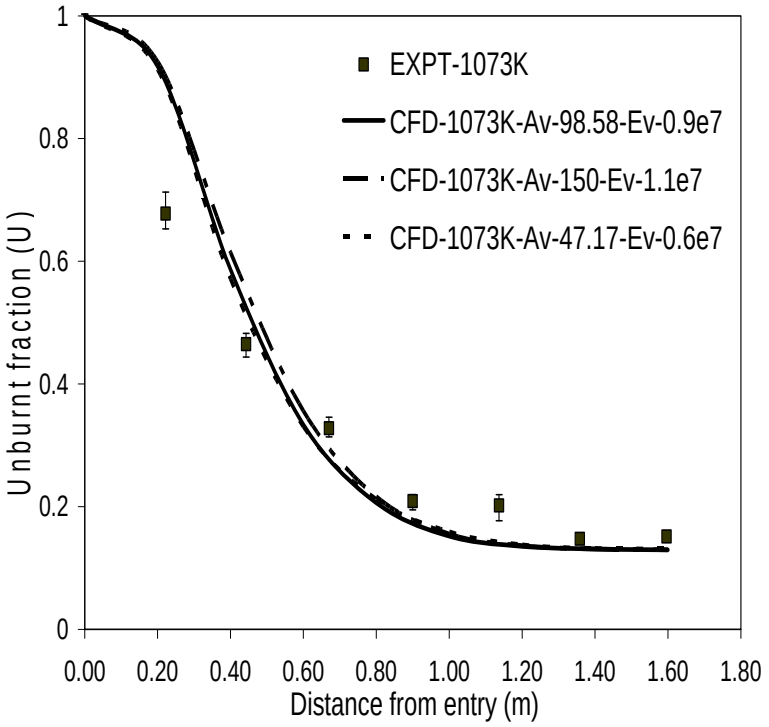

(A) 1073K

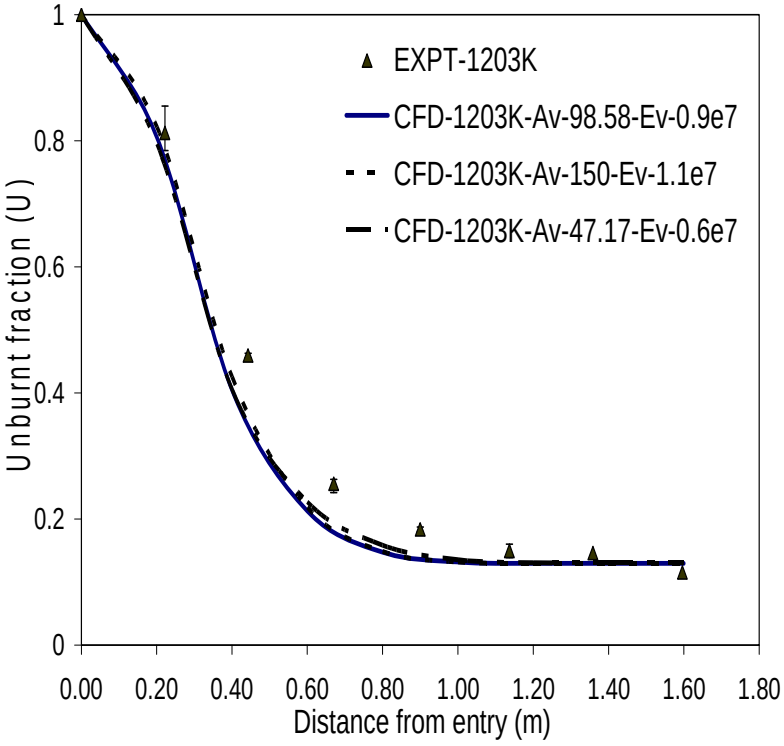

(B) 1203K

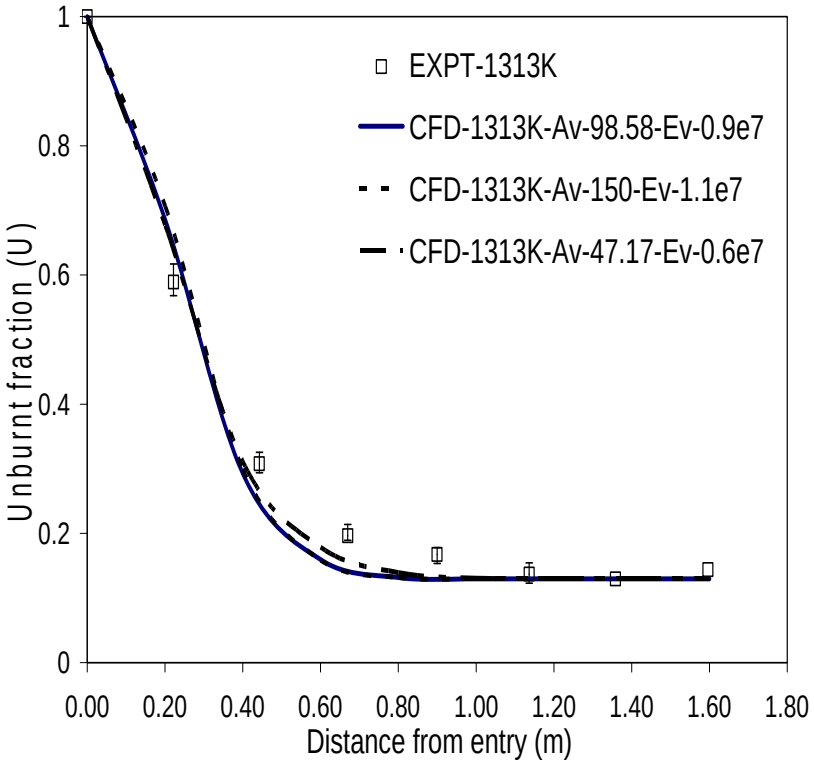

(C) 1313K

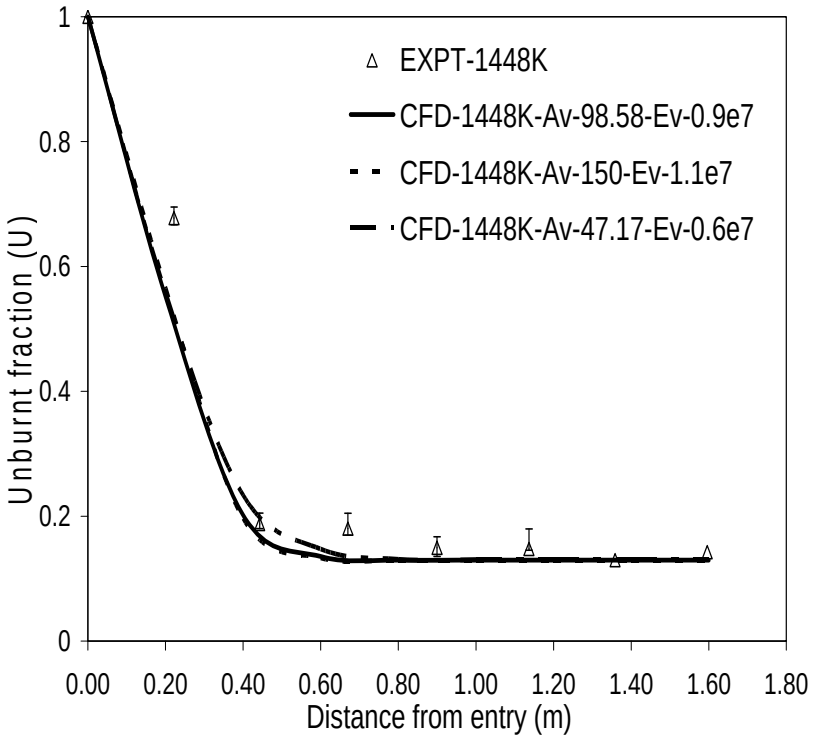

(D) 1448K

Figure 5.6. 2D axisymmetric model predictions with three sets of fine tuned kinetic parameters for biomass devolatilization case

with E_v = 0.9 $\times 10^{+7}$ J/kmol shows good fit to the experimental burnout data (Figure 5.6). Comparison of the model predictions for these three sets of kinetic parameters at 1073K-1448K is shown in Figure 5.6, which shows no significant difference in burnout predictions. Hence one set of devolatilization kinetic parameters (A_v = 150s^{-1}, E_v = 1.1$\times 10^{+7}$ J/kmol) were used to simulate the 2D axisymmetric CFD model for further biomass combustion study.

5.5.2 Biomass Combustion

5.5.2.1 2D Axisymmetric CFD Model

In biomass combustion experiments, roughly half of the total burnout time is devoted to the release of volatiles because of the high volatile content of biomass (~70%).[3] Therefore, devolatilization plays an important role in the overall process. For combustion study, first the CFD model was simulated with the kinetic parameters reported by Jimenez *et. al.*[3] [Table 5.6], which are based on their 1D plug flow model studies. The gas and particle boundary conditions are shown in Table 5.4. Figure 5.7-A shows the comparison between experimental measurements and CFD model predictions at 1313K and 1573K. Result shows that the model under predicts the experimental data significantly. This was the similar observation as observed in 2D axisymmetric devolatilization case. Hence, subsequently, the simulations were performed with the kinetic parameters derived from 2D axisymmetric devolatilization case (A_v = 150s^{-1}, E_v = 1.1$\times 10^{+7}$ J/kmol). Figure 5.7-B shows the comparison between experimental measurements and CFD model predictions. It was observed that the CFD model could capture the experimental profile qualitatively in the initial period of devolatilization (up to 0.6m distance from the entry of EFR), but it under predicts the char combustion profile. Hence it is necessary to fine tune the char combustion kinetic parameters to capture the complete combustion profile of biomass. Simulation results in Figure 5.7 were shown for two temperatures and similar observation was found for other operating conditions.

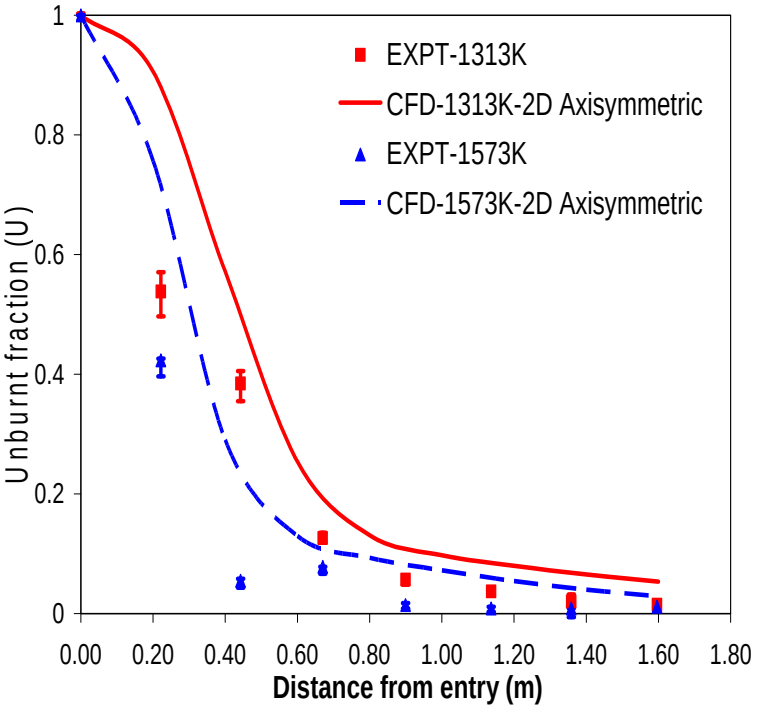

(A) $A_v = 47.17\ s^{-1}$, $E_v = 1.1\times10^{+7}$ J/kmol

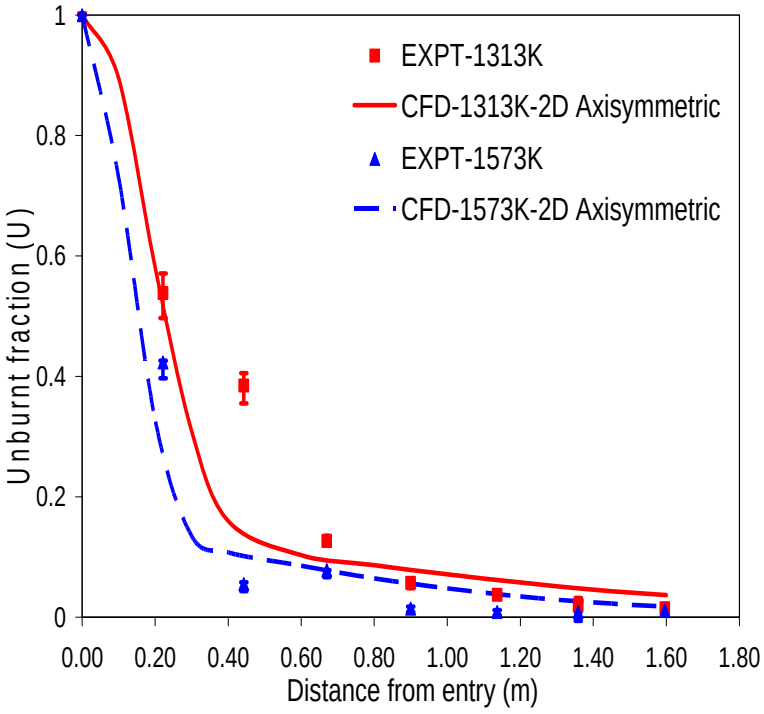

(B) $A_v = 150 s^{-1}$, $E_v = 1.1\times10^{+7}$ J/kmol

Figure 5.7. Comparison between experimental measurements and 2D axisymmetric CFD model predictions

For the purpose of fine tuning the char combustion kinetic parameters, the sensitivity study was performed by varying the pre-exponential factor (A_c) in the range of 0.46×10^{-3} kg/m^{2}sPa to 3.5×10^{-3} kg/m^{2}sPa, keeping the activation energy same ($E_c = 6.3 \times 10^7$ J/kmol). Figure 5.8 shows the comparison between experimental measurements and CFD model predictions for char combustion part only (0.6m to 1.6m distance from the entry of the EFR) at 1313K and 1448K. It was observed that the CFD model could capture the char combustion profile qualitatively with $A_c = 3.5 \times 10^{-3}$ kg/m^{2}sPa. Simulations were also performed at different oxygen concentration to understand the applicability of these evaluated parameters at various operating conditions. The operating conditions were adjusted such that the oxygen concentration at the exit of the EFR is 8 mol %. Figure 5.9 shows that the CFD model was able to capture the qualitative trend of combustion profile for all the operating conditions. It is important to note here that the gas velocities for devolatilization and combustions tests are different. Since the calculation of combustion curves relies greatly on the kinetic parameters for the devolatilization of the particles, the correct reproduction of combustion series observed in Figure 5.7-B by 2D axisymmetric CFD model can be regarded as a proof of robustness for the method followed.

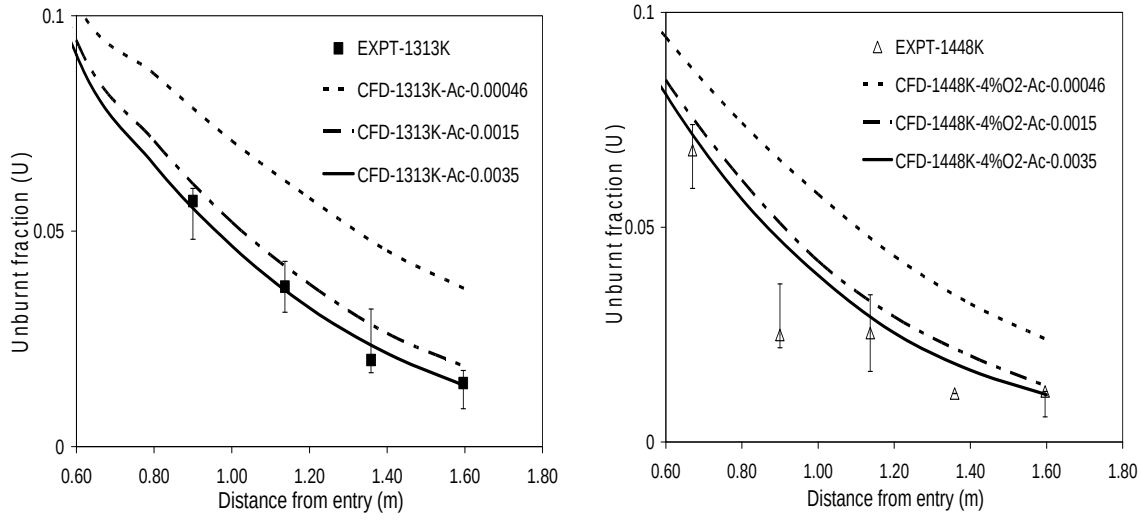

(A) 1313K (B) 1448K

Figure 5.8. Comparison between experimental measurements and 2D axisymmetric CFD model predictions: Sensitivity of char combustion kinetic parameters (A_c and E_c).

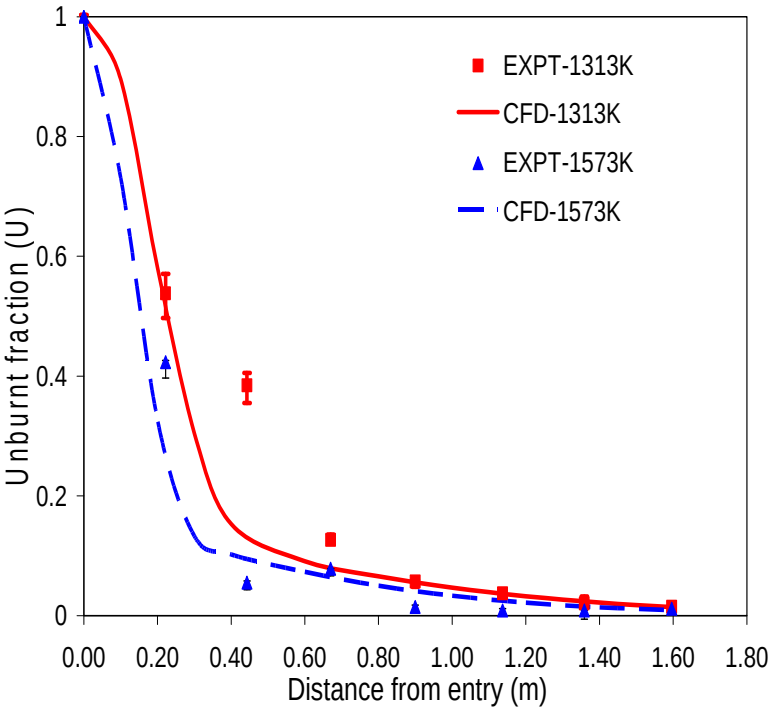

(A) 1313K and 1573K (4 mol % O_2 at exit of EFR)

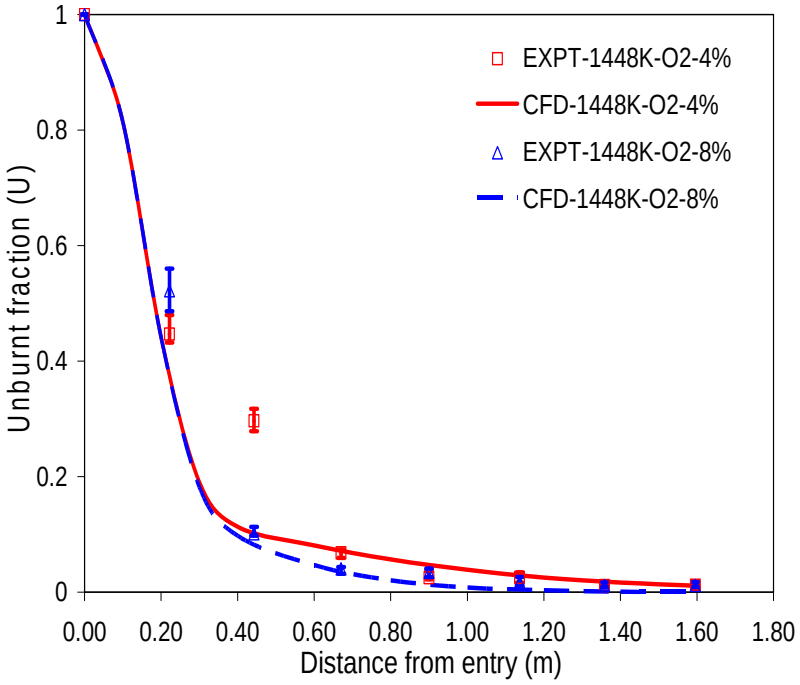

(B) 1448K (4 mol % and 8 mol% O_2 at exit of EFR)

Figure 5.9. CFD model prediction for biomass burnout for $A_c = 3.5 \times 10^{-3}$ kg/m^{2}sPa

5.6 IMPORTANCE OF 2D AXISYMMETRIC CFD MODEL FOR EFR

In order to simulate 1D plug flow behavior, the velocity was patched in the computational domain and the flow equation was not solved. The biomass particles were injected from all over the cross sectional areas of inlet face of EFR, but in experiments, the particles were introduced from the central inlet with Fuel/pneumatic air. From the contour plot of rate of biomass burnout of 2D axisymmetric CFD model of devolatilization case (Figure 5.10-A), it is evident that most of the particles travel along the axis after injection into the EFR. Figure 6-A shows that the gas velocity along the axis is around 2 m/s to 2.8 m/s and around 0.1 m/s near to the wall region, where as for 1D plug flow model, the average velocity profile was ~ 0.73 m/s (Figure 5.10-B).

The residence time distribution (RTD) of particles depends upon the particle trajectory that it follows after injection. The residence time distributions (RTD) of particles obtained from 2D axisymmetric CFD and 1D plug flow model simulations are shown in Figure 5.11. The mean residence time for 1D plug flow model was 1.6821 s with standard deviation = 0.3659 s. For 2D axisymmetric CFD model the mean residence time was observed to be 0.6239 s with standard deviation = 0.0628 s. The ratio of mean residence time of 1D plug flow model to 2D axisymmetric CFD model was ~ 2.69, which is greater than the ratio of maximum velocity in laminar flow and superficial velocity (2). This may be because of high velocity jets considered in the 2D axisymmetric CFD model. In 1D plug flow model, the biomass particles were injected from all over the cross sectional areas of inlet face of EFR. With 2D axisymmetric CFD model, actual inlet configuration was considered and the biomass particles were injected from the central FA inlet jet of EFR. The high FA inlet jet velocity of biomass particles (1.381 m/s at FA inlet and 0.123 m/s at PA inlet at 298K) leads to significant reduction in average residence time compared to the 1D plug flow model. Because of the lower effective residence time, when the kinetic parameters based on the 1D plug flow model were implemented in the 2D axisymmetric CFD model, the results under predicted the biomass burnout profile.

Therefore the kinetic parameters cannot be obtained with the plug flow assumption. The flow profile inside the EFR needs to be computed and the kinetic parameters should be evaluated based on this realistic information. The influence of inlet configuration on the flow profile is significant in EFR and hence any modeling effort should account the non-

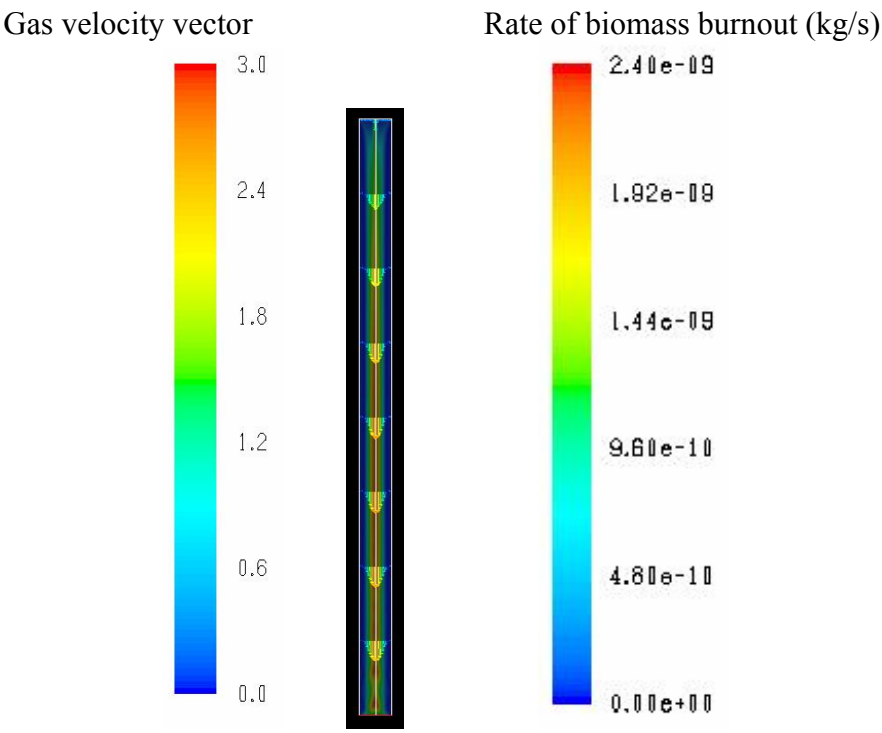

(A) 2D axisymmetric model (1448K)

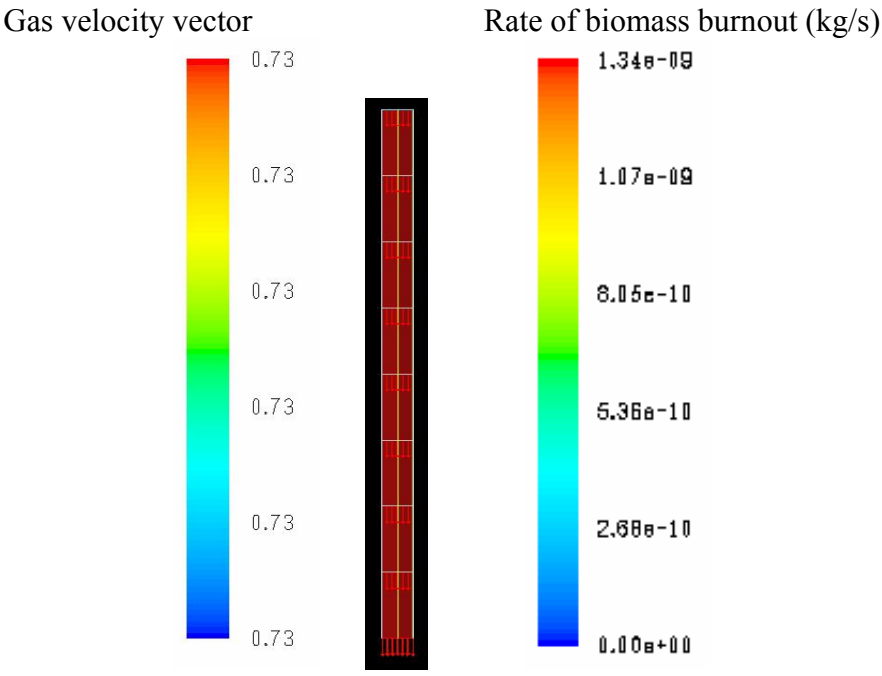

(B) 1D plug flow model (1448K)

Figure 5.10. Contour plot of biomass burnout superimposed with velocity magnitude vector for devolatilization case

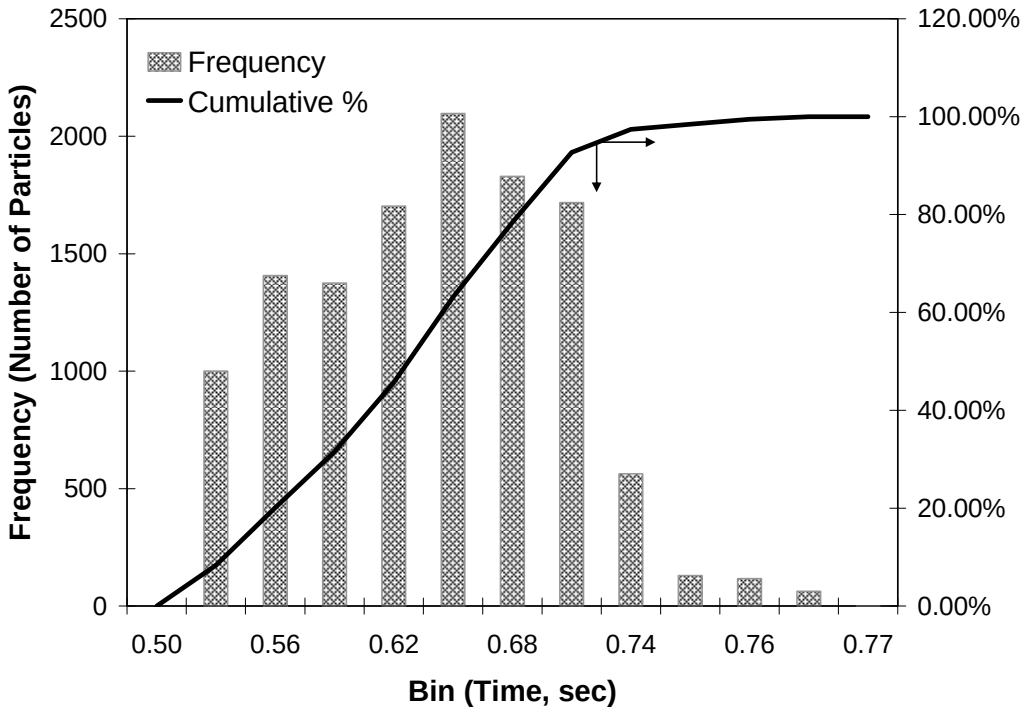

(A) 2D axisymmetric model

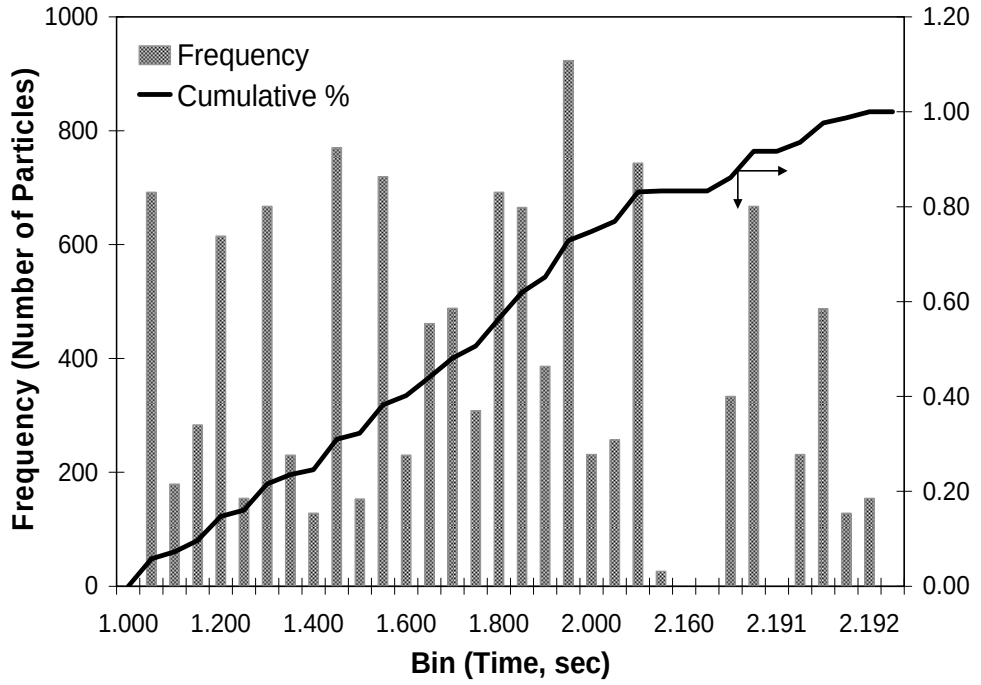

(B) 1D plug flow model

Figure 5.11. Residence time distribution of poly dispersed particles (operating temperature 1448K)

uniformity at the inlet region and its effect on the flow profile. The kinetic parameters based on 2D axisymmetric CFD model studies are given in Table 5.7.

Table 5.7. Kinetic Parameters based on 2D axisymmetric CFD model

Devolatilization		Char oxidation	
A_v (s^{-1})	E_v (J/kmol)	A_c (kg/m^2sPa)	E_c (J/kmol)
150	11×10^6	0.0035	63×10^6

5.7 CONCLUSIONS

1D plug flow model and 2D axisymmetric CFD model of a laminar flow EFR were developed. The models were used to assess the influence of the kinetic parameters and operating conditions on the burning characteristic of biomass (*cynara cardunculus*). The comparison between the 1D plug flow model and 2D axisymmetric CFD model predictions with the experimental data reported by Jimenez *et. al.*[3] is discussed. It was observed that the estimation of kinetic parameters were sensitive to various assumption made while simplifying the model. The major observations and conclusions are listed below:

- 1D Plug flow model of devolatilization case with the kinetic parameters reported by Jimenez *et. al.*[3] captures the quantitative burnout profile at inlet gas stream temperature of 500K
- 2D axisymmetric CFD model with the kinetic parameters derived from 1D plug flow model under predicts the biomass burnout profile significantly for both devolatilization and combustion cases
- The 2D axisymmetric CFD model studies shows that the rates of devolatilization and char combustion are 3-4 times and 7-8 times greater than the rates found in 1D plug flow model studies respectively
- 2D axisymmetric CFD simulations show that the nature of gas flow was developing laminar flow rather than ideal plug flow. As particles were injected from central injection, most of the particles travel along the axis of the EFR with maximum velocity, which leads to shorter residence time of the particle as compared to plug

flow model. This leads to under prediction of the burnout profile with kinetic parameters proposed by Jimenez *et. al.*[3] Hence, it is important to simulate the gas flow, particle flow and inlet configuration of EFR. Therefore, the biomass devolatilization and combustion kinetic parameters can be more realistic if they are estimated from the detailed multidimensional CFD model. It is then possible to more confidently extrapolate the information to large scale biomass combustors and gasifiers.

NOMENCLATURE

A	absorption coefficient of gas	m^{-1}
a_p	equivalent absorption coefficient due to the presence of particulates	m^{-1}
A_{pn}	projected area of particle	m^2
A_c	pre exponential factor for char oxidation	s^{-1}
A_v	pre exponential factor for devolatilization	kg m^{-2} s^{-1} Pa^{-1}
C_D	drag coefficient	
$C_{l,\,r}$	molar concentration of each reactant l^{th} species in reaction r	kmol m^{-3}
C_p	heat capacity	$Jkg^{-1}K^{-1}$
D_{km}	diffusion coefficient for species k in the mixture	m^2 s^{-1}
d_p	particle diameter	m
E_p	equivalent emission	W m^{-3}
E_c	activation energy for char oxidation	J $kmol^{-1}$
E_v	activation energy for devolatilization	J $kmol^{-1}$
F	momentum source term	Kg m^{-2} s^{-2}
f_{heat}	fraction of char oxidation heat absorbed by the particle	
f_{pn}	particle scattering factor associated with the n^{th} particle	
g	gravitational constant	m^2 s^{-1}
h	gas enthalpy	J kg^{-1}
h_k^0	enthalpy of formation of species k at the reference temperature, T_{ref}	J kg^{-1}
h	heat transfer coefficient	$Wm^{-2}K^{-1}$
H_c	heat released during char oxidation	Jkg^{-1}
I	radiant intensity	Wm^{-2}
k	thermal conductivity of gas	$Wm^{-1}K^{-1}$
K_c	char oxidation kinetic rate constant	kg m^{-2} s^{-1} Pa^{-1}
K_v	devolatilization kinetic rate constant	s^{-1}

K_d	gas phase diffusion coefficient for oxygen	kg m^{-2} s^{-1} Pa^{-1}
m_k	mass fraction of species k	--
M_p	mass of particle	kg
m_v , m_c	mass fraction of volatile and char respectively	--
$\dot{m}_{pk}$	particle mass flow rate of component k	kg s^{-1}
MW	molecular weight	kg $kmol^{-1}$
Q_{conv}	heat flow towards the particle by Convection	W
Q_{rad}	heat flow towards the particle by Radiation	W
r	radial direction	--
R	gas constant	J mol^{-1} K^{-1}
R_k	net rate of production of species k by chemical reaction	kg $s^{-1}m^{-3}$
$R_{k,r}$	volumetric rate of creation of species k in r^{th} reaction	kmol $s^{-1}m^{-3}$
$S_{h,rxn}$	source term for heat of gas phase chemical reactions	Wm^{-3}
S_Q	source term for heat added from discrete phase	W m^{-3}
S_k	source of species k from dispersed phase	kg $s^{-1}m^{-3}$
S_m	source term for the total mass added from the discrete phase	kg $s^{-1}m^{-3}$
t	time after injection	s
T_p	particle temperature	K
T_R	radiation temperature $=\left(\frac{I}{4\sigma}\right)^{1/4}$	K
U	fluid velocity in radial direction r	m s^{-1}
U	unburnt fraction of biomass	
$u_{p,i}$	particle velocity in i^{th} direction (r or z)	m s^{-1}
v_i	gas velocity in i^{th} direction (U or W)	m s^{-1}
V	volume of computational cell	m^3
W	fluid velocity in axial direction z	m s^{-1}
w	initial mass of particle	kg
x	distance in axial or radial direction	m
Y	mass fraction	

Greek letters

$\eta'_{l,r}$	exponent for each l^{th} reactant in reaction r	
$\phi(\vec{s},\vec{s}')$	scattering phase function	
σ	stefan Boltzmann constant $= 5.67 \times 10^{-8}$	W m^{-2} K^{-4}
ε_{pn}	emissivity of particle	
σ_p	equivalent particle scattering factor	
$v'_{k,r}$ *and* $v_{k,r}$	stoichiometric coefficient for k^{th} species as product and reactant respectively	
μ	viscosity of gas phase	kg m^{-1} s^{-1}
□	density	kg m^{-3}

Subscripts

db	dry basis
g	gas
i	direction
j	particle size
p	particle
O_2	oxygen

REFERENCES

1. Sami, M.; Annamalai, K.; Wooldridge, M. Co-firing of coal and biomass fuel blends. *Prog. Energy Combust. Sci.*, **2001**, *27*, 171.
2. Guerreo, M.; Ruiz, MP; Alzueta, MU; Bilbao, R.; Millera, A. Pyrolysis of eucalyptus at different heating rates: Studies of char characterization and oxidative reactivity. *J. Anal. Appl. Pyrolysis*, **2005**, *74*, 307.
3. Jimenez, S.; Remacha, P.; Ballesteros, J. C.; Gimenez, A.; Ballester, J. Kinetics of Devolatilization and Oxidation of a Pulverized Biomass in and Entrained flow Reactor under Realistic Combustion Conditions. *Combust. Flame*, **2008**, *152*, 588.
4. Scott, DS; Piskorz, J.; Radlein, D. Liquid products from the continuous flash pyrolysis of biomass. *Ind. Eng. Chem. Process Des. Dev.*, **1985**, *24*, 581.
5. Gary, M.R.; Corcoran, W.H.; Gavalas, G.R. Pyrolysis of a wood-derived material, Effects of moisture and ash content. *Ind. Eng. Chem. Process Des. Dev.*, **1985**, *24*, 646.
6. Jiang, H.; Morey, R.V. Air Gasification of Corn Cobs at Fluidization. *Biomass Bioenergy*, **1992**, *3*, 87.
7. Jenkins, B.M.; Baxter, L.L.; Miles, T.R. Jr.; Miles, T.R. Combustion Properties of biomass. *Fuel Process. Technol.*, **1998**, *54*, 17.
8. Di Blasi, C. Modeling and simulation of combustion processses of charring and non- charring solid fuels. *Prog. Energy Combust. Sci.*, **1993**, *19*, 71
9. Gronli, M.G.; Melaaen, M.C. Mathematical model for wood pyrolysis: Comparison of experimental measurements with model predictions. *Energy Fuels*, **2000**, *14*, 791.
10. Bryden, K.M.; Hagge, M.J. Modeling the combined impact of moisture and char shrinkage on the pyrolysis of biomass particle. *Fuel*, 2003, 82, 1633.
11. Wagenaar B.M.; Heyvel, Van Den EJMT. Cocombustion of *Miscanthus* in a pulverized coal combustor: Experiments in a drop tube furnace. *Biomass Bioenergy*, **1997**, *12*, 185.
12. Jae, G.L.; Jae, H.K.; Hyo, J.L.; Jun, P.; Kim, S.D. Characteristics of entrained flow coal gasification in a drop tube reactor. *Fuel*, **1996**, *75(9)*,1035
13. Meesri, C.; Moghtaderi, B. Experimental and Numerical Analysis of Sawdust Char Combustion Reactivity in a Drop Tube Reactor. *Combust. Sci. and Tech.*, **2003**, *175*, 793.
14. Kawser, J.; Hayashi, J.; Li, C. Z. Pyrolysis of Victorian Brown Coal and Gasification of Nascent Char in CO2 atmosphere in a Wire Mesh Reactor. *Fuel*, **2004**, *83*, 833.
15. Mario, L.; Colomba D.B. Pyrolysis kinetics of wheat and corn straw. *J. Anal. Appl. Pyrolysis*, **1998,** *44*,181.
16. Colomba, D.B.; Carmen, B.; Antonio, S.; Raul, APB. Weight Loss Dynamics of Wood Chips under Fast Radiative Heating. *J. Anal. Appl. Pyrolysis*, **2001**, *57*, 77.
17. Wiktorsson, LP; Wanzl, W. Kinetic parameters for coal pyrolysis at low and highheating rates – a comparison of data from different laboratory equipment. *Fuel*, **2000**, *79,* 701.
18. Wornat, M.J.; Hurt, R.H.; Davis, K.A.; Yang, N.Y.C. Single particle combustion of two biomass chars. *Proc. Combust. Inst.*, **1996**, *26*, 3075.
19. Hurt, R.H.; Mitchell, R.E. On the combustion kinetics of heterogeneous char particle populations. *Proc. Combust. Inst.*, **1992**, *24*, 1233.
20. Zolin, A.; Jensen, A.; Jensen, P.A.; Frandsen, F.; Dam-Johansen, K. The influence of inorganic materials on the thermal deactivation of fuel chars. *Energy Fuels*, **2001**, *15*, 1110.
21. Bharadwaj, A.; Baxter, L. L.; Robinson, A.L. Effects of Intraparticle Heat and Mass Transfer on Biomass Devolatilization: Experimental Results and Model Predictions. *Energy Fuels*, **2004**, *18*, 1021.
22. Smith, I. W. Combustion rate of bituminous coal char in the temperature range 800K-1700K, *Fuel*, **1973**, 52.
23. Field, M.A. Rate of combustion of size graded fractions of char from a low-rank coal between 1200K and 2000K, Combustion and Flame, **1969**, *13*, 237.
24. Ballester, J.; Jimenez, S. Kinetic parameters for the oxidation of pulverized coal as measured from drop tube tests, *Combust. Flame*, **2005**, *142*, 210.
25. Lockwood, F.C. Combustion Chambers and Furnaces, E.T.S.I.I., University of Zaragoza, **1986**.
26. Díez, L. I.; Cortés, C.; Campo A. Modeling of pulverized coal boilers: review and validation of on-line simulation techniques. *Applied Thermal Engineering*, **2004**, *25(10)*, 1516.
27. Fan, J.; Qian, L.; Ma,Y.; Sun, P.; Cen, K. Computational modeling of pulverized coal combustion processes in tangentially fired furnaces. *Chem. Eng. J.*, **2001**, *81(1)*, 261.

28. Yin, C.; Caillat, S.; Harion, J; Baudoin, B.; Perez, E. Investigation of the flow, combustion, heat-transfer and emissions from a 609 MW utility tangentially fired pulverized-coal. *Fuel*, **2002**, *81(8)*, 997.
29. Rostami, A.A.; Hajaligol, M.R.; Wrenn, S. E. A Biomass Pyrolysis Submodel for CFD Applications. *Fuel*, **2004**, *83*, 1519.
30. Eaton, AM; Smoot, LD; Hill, SC; Eatough, CN. Components, formulations, solutions, evaluation, and application of comprehensive combustion models. Prog. Energy Combust. Sci., **1999**, *25*, 387.
31. Gera, D.; Mathur, M.P.; Freeman, M.C.; Robinson, A. Effect of large aspect ratio of biomass particles on carbon burnout in utility boiler. *Energy Fuels*, **2002**, *16*, 1523.
32. Backreedy, R.I.; Fletcher, L.M.; Jones, J.M.; Ma, L.; Pourkashanian, M.; Williams, A. Co-firing Pulverized Coal and biomass: A Modeling Approach. *Proc. Combust. Inst.*, **2005**, *30 (2)*, 2955.
33. Carpenter, A.N.; Skorupska N. M. Coal Combustion –Analysis and Testing, IEACR/64, IEA Coal Research, London, **1993**.
34. Brown, AL; Dayton, DC; Nimlos, MR; Daily, JW. Design and characterization of entrained flow reactor for the study of biomass pyrolysis chemistry at high heating rates. *Energy Fuels*, **2001**, *15*, 1276.
35. Mrklund, M.; Gebart, R.; Fletchet, D.F. CFD model for optimization of an entrained flow gasifier for black liquor. In: Proceedings of colloquium on black liquor combustion and gasification. Park city, USA, **2003**.
36. Xiu, S.; Wang, N.; Yi, W.; Li, B.; Shahbazi, G. Validation of Kinetic Parameter Values for Prediction of Pyrolysis Behavior of Corn Stalks in a Horizontal Entrained Flow Reactor. *Biosystems Engineering*, **2008**, *100*, 79.
37. Jones, J.M.; Pourkashanian, M.; Williams, A.; Hainsworth, D. A Comprehensive biomass Combustion Model. Renewable Energy, **2000**. *19*, 229.
38. Sheng, C.; Moghtaderi, B.; Gupta, R.; Wall, T. F. A computational fluid dynamics based study of the combustion characteristics of coal blends in pulverized coal-fired furnace, *Fuel*, **2004**, *83*, 1543
39. Morsi, S.A.; Alexander, A.J. An Investigation of Particle Trajectories in Two-Phase Flow Systems. *J. Fluid Mech*, **1972**, *55(2)*, 193
40. Badzioch, S.; Hawksley, P. G. W. Kinetics of Thermal Decomposition of Pulverized Coal Particles. *Ind. Eng. Chem. Process Des. Dev.*, **1970**, *9*, 521
41. Baum, M.M.; Street P.J. Predicting the combustion behavior of coal particles. *Combust. Sci. and Tech.*, **1971**, *3(5)*, 231
42. Ansys Fluent 6.3, Fluent Inc., 10 Cavendish Court, Lebanon, NH03766, U.S.A.
43. Field, M.A. Rate of combustion of size graded fractions of char from a low-rank coal between 1200K and 2000K. *Combust. Flame*, **1969**, *3*, 237
44. Siminski, V.J.; Wright, F.J.; Edelman, R.B.; Economos, C.; Fortune, O.F. Research on methods of improving the combustion characteristics of liquid hydrocarbon fuels. AFAPL TR, **1972**, *72*, Vols. II and Air Force Aeropropulsion Laboratory, Wright Patterson Air Force Base, OH, I.
45. Kim, Y.J.; Lee J.M.; Kim S. D. Modeling of coal gasification in an internally circulating fluidized bed reactor with draught tube. *Fuel*, **2000**, *79*, 69.
46. Jimenez et al., LITEC-CSIC (Spanish Council for Scientific Research), María de Luna 10, 50018 Zaragoza, Spain, personal communication.
47. Modest, M. F. Radiative heat transfer, Academic press. **2003**.
48. Modest, M. F. Radiative heat transfer, Academic press. **2003**.
49. Boyd, R. K.; Kent, J.H. Three-dimensional furnace computer modeling, In 21st Symp. (Int'l) on combustion, *The Combust. Inst.*, **1986**, 265.

Publications & Symposia

Published Papers

1. Kinetics of Reductive Alkylation of *p*-Phenylenediamine with Methyl Ethyl Ketone Using 3% Pt/Al_2O_3 Catalyst in a Slurry Reactor
   Narendra G. Patil, Debdut Roy, **Amit S. Chaudhari**, Raghunath V. Chaudhari
   Ind. Eng. Chem. Res., 2007, 46, 3243-3254

2. Modeling of Bubble Column Slurry Reactor for Reductive Alkylation of *p*-Phenylenediamne
   Amit S. Chaudhari, Mohan R. Rampure, Vivek V. Ranade, Rengaswamy Jaganathan, Raghunath V. Chaudhari
   Chemical Engineering Science, 2007, 62, 7290-7304

3. Kinetics of Reductive Alkylations of Phenylenediamines: Influence of Substrates Isomeric Structure
   D. Roy, **Amit S. Chaudhari**, R. V. Chaudhari
   Chemical Engineering Science, 2010, 65, 232-239

4. CFD Modeling of Pulverized Biomass Combustion in an Entrained Flow Reactor
   Amit S. Chaudhari, Devkumar F. Gupta, V. V. Ranade, Raghunath V. Chaudhari
   Communicated to "*Ind. Eng. Chem. Res.*"

Presentations in National & International Symposiums

1. Reductive Alkylation of *p*-Phenylenediamine with Methyl Ethyl Ketone Using 3% Pt/Al_2O_3: Kinetics and Modeling of a semibatch Slurry Reactor
   Amit S. Chaudhari, Debdut Roy, Narendra G. Patil, Raghunath V. Chaudhari
   Poster Presentation at International Conference **CAMURE-6-ISMR-5**, National Chemical Laboratory, Pune, INDIA. January 14-17, 2007

2. Modeling of Bubble Column Slurry Reactor for Reductive Alkylation of *p*-Phenylenediamne

Amit S. Chaudhari, Mohan R. Rampure, Vivek V. Ranade, Rengaswamy Jaganathan, Raghunath V. Chaudhari

Oral presentation at **GLS-8** (8^{th} International Symposium on Gas-Liquid-Solid Reactor Engineering), New Delhi, INDIA, December 16-19, 2007

3. Kinetics of Reductive Alkylations of Phenylenediamines: Influence of Substrates Isomeric Structure

   Amit S. Chaudhari, D. Roy, R. V. Chaudhari

   Oral Presentation at **ISCRE-20** (20^{th} International Symposium on Chemical Reaction Engineering), Kyoto, JAPAN, September 7-10, 2008

4. Comparative Study on Modeling of Multiphase Reactors for Reductive Alkylation of *p*-Phenylenediamine

   Amit S. Chaudhari, R. Jaganathan, Vivek V. Ranade, Raghunath. V. Chaudhari

   Poster presentation at **ACEPT-2009** (Advances in Chemical Engineering and Process Technology), National Chemical Laboratory, Pune, INDIA, June 4-6, 2009

5. CFD Modeling of Pulverized Biomass Combustion in an Entrained Flow Reactor

   Amit S. Chaudhari, Devkumar F. Gupta, V. V. Ranade, Raghunath V. Chaudhari

   Oral presentation at **CAMURE-7-ISMR-6**, Montreal, Quebec, Canada, August 23-27, 2009